

VECTOR2 & FORMWORKS USER'S MANUAL

SECOND EDITION

P. S. Wong

F.J. Vecchio

H. Trommels

August, 2013

Abstract

VecTor2 © is a program based on the Modified Compression Field Theory for nonlinear finite element analysis of reinforced concrete membrane structures. Considering the inherent intricacies of nonlinear finite element analysis and VecTor2, user facilities are imperative to their rational and convenient application.

Program documentation for VecTor2 and a new preprocessor software entitled FormWorks © are presented in this report. The program documentation describes the theoretical basis of VecTor2, the finite element library and the constitutive models for concrete, reinforcement and bond materials. This documentation and the FormWorks manual provide guidance for modeling and data input.

FormWorks is a graphics-based preprocessor program for the Windows © environment. FormWorks includes facilities for data visualization and input, bandwidth reduction and automatic mesh generation. The latter requires only economical user input, permits a high degree of user control over mesh topology and generates mixed element type meshes for reinforced concrete structures.

Table of Contents

| | |
|--------------------------------------------------------|-------------|
| Abstract | ii |
| List of Figures | xiv |
| List of Appendices | xxi |
| Notation | xxii |
| | |
| 1 Introduction | 1 |
| 1.1 Background | 1 |
| 1.2 The VecTor2 Program | 2 |
| 1.3 Research Objectives | 3 |
| 1.4 Organization | 4 |
| | |
| 2 Part I: VecTor2 | 5 |
| 2.1 Introduction | 5 |
| 2.2 Modified Compression Field Theory (MCFT) | 5 |
| 2.2.1 Assumptions | 6 |
| 2.2.2 Compatibility Relationships | 7 |
| 2.2.3 Equilibrium Relationships | 8 |
| 2.2.4 Constitutive Relationships | 9 |
| 2.2.5 Consideration of Local Crack Conditions | 10 |
| 2.2.6 Consideration of Local Crack Conditions with FRC | 12 |
| 2.3 Disturbed Stress Field Model (DSFM) | 14 |
| 2.3.1 Compatibility Relationships | 14 |
| 2.3.2 Equilibrium Relationships | 16 |
| 2.3.3 Constitutive Relationships | 17 |
| 2.3.4 Shear Slip Relationships | 20 |
| 2.4 Finite Element Implementation | 21 |
| 2.4.1 Composite Material Stiffness Matrix | 23 |

| | | |
|----------|-------------------------------------------------------------------|----|
| 2.4.2 | Element Stiffness Matrices | 26 |
| 2.4.3 | Pseudo Nodal Loads | 26 |
| 2.4.4 | Total Load Iterative Secant Stiffness Solution | 28 |
| 2.5 | Augmented Analysis Features | 29 |
| 2.5.1 | Modeling of Lateral Expansion Effect | 29 |
| 2.5.2 | Modeling of Triaxial Stresses | 31 |
| 2.5.3 | Analysis of Cyclically Loaded Structures | 32 |
| 2.5.4 | Analysis of Construction and Loading Chronology | 34 |
| 2.5.5 | Bond-Slip Mechanisms | 35 |
| 2.5.6 | Dynamic Analysis | 36 |
| 2.5.6.1 | Introduction | 36 |
| 2.5.6.2 | Newmark Direct Integration Method: Newmark Beta and Gamma Factors | 37 |
| 2.5.6.3 | Damping | 37 |
| 2.5.6.4 | Ground Acceleration | 38 |
| 2.5.7 | Accounting for Strain History | 38 |
| 2.5.8 | Accounting for Strain Rate Effects | 38 |
| 2.5.9 | Structural Damping | 41 |
| 2.5.9.1 | Rayleigh Damping | 41 |
| 2.5.9.2 | Alternative Damping | 42 |
| 2.5.10 | Geometric Nonlinearity | 43 |
| 2.5.11 | Crack Allocation | 43 |
| 2.5.11.1 | Uniform Crack Allocation (Deluce, Lee, and Vecchio, 2012) | 43 |
| 2.5.11.2 | Variable Crack Allocation (Sato 2002) | 44 |
| 2.5.12 | Additional Analysis Parameters | 45 |
| 2.5.12.1 | Concrete Aggregate Type | 45 |
| 2.5.12.2 | Concrete Conductivity | 45 |
| 2.5.12.3 | Concrete Fracture Energy | 45 |

| | |
|-------------------------------------------------------|-----------|
| | v |
| 2.5.12.4 Prestressing Friction and Wobble Coefficient | 46 |
| 2.5.12.5 Thermal Time-Stepping Factor | 47 |
| 2.5.12.6 Material Resistance/Creep Factors | 47 |
| 3 Element Library | 48 |
| 3.1 Reinforced Concrete Elements | 48 |
| 3.1.1 Constant Strain Triangle | 48 |
| 3.1.2 Plane Stress Rectangle | 50 |
| 3.1.3 Quadrilateral | 51 |
| 3.1.3.1 Isoparametric Quadrilateral Elements | 52 |
| 3.1.3.2 Degenerate Quadrilateral Elements | 52 |
| 3.2 Reinforcement Elements | 53 |
| 3.2.1 Truss Bar | 53 |
| 3.3 Bond – Slip Elements | 54 |
| 3.3.1 Link | 55 |
| 3.3.2 Contact | 56 |
| 4 Models for Concrete Materials | 59 |
| 4.1 Compression Pre-Peak Response | 59 |
| 4.1.1 Linear | 60 |
| 4.1.2 Popovics | 61 |
| 4.1.3 Hognestad (Parabola) | 62 |
| 4.1.4 Popovics (High Strength) | 62 |
| 4.1.5 Hoshikuma et al. | 64 |
| 4.1.6 Smith-Young | 65 |
| 4.1.7 Lee et al 2012 (FRC) (Lee et al, 2012) | 65 |
| 4.2 Compression Post-Peak Response | 66 |
| 4.2.1 Pre-Peak Base Curve | 68 |
| 4.2.2 Modified Park-Kent | 68 |

| | |
|-------|----------------------------------------------------|
| | vi |
| 4.2.3 | Popovics / Mander 69 |
| 4.2.4 | Hoshikuma et al. 70 |
| 4.2.5 | Saenz / Spacone 71 |
| 4.2.6 | Montoya 2003 73 |
| 4.2.7 | Lee et al 2012 (FRC) 74 |
| 4.3 | Compression Softening 74 |
| 4.3.1 | No compression softening 76 |
| 4.3.2 | Vecchio 1992-A (ϵ_1/ϵ_2 -Form) 76 |
| 4.3.3 | Vecchio 1992-B (ϵ_1/ϵ_0 -Form) 77 |
| 4.3.4 | Vecchio-Collins 1982 78 |
| 4.3.5 | Vecchio-Collins 1986 79 |
| 4.4 | Tension Stress-Strain Response 79 |
| 4.4.1 | No Tension Stiffening 80 |
| 4.4.2 | Modified Bentz 2003 81 |
| 4.4.3 | Vecchio 1982 81 |
| 4.4.4 | Collins-Mitchell 1987 82 |
| 4.4.5 | Bentz 1999 82 |
| 4.4.6 | Izumo, Maekawa Et Al. 83 |
| 4.4.7 | Tension Chord Model (Kaufmann) 84 |
| 4.4.8 | Lee 2011 (w/ Post Yield) (Lee et al. 2011) 85 |
| 4.5 | Tension Softening 87 |
| 4.5.1 | Not Considered 88 |
| 4.5.2 | Linear 89 |
| 4.5.3 | Bilinear 89 |
| 4.5.4 | Nonlinear (Yamamoto 1999 – No residual) 91 |
| 4.5.5 | Nonlinear (Hordijk) 92 |
| 4.5.6 | Exponential 94 |

| | | |
|-------|----------------------------------------------------|-----|
| 4.5.7 | Custom Input-Strain Based | 94 |
| 4.5.8 | Custom Input-Crack Based | 95 |
| 4.5.9 | FRC (fib Model Code 2010) | 95 |
| 4.6 | FRC Tension | 96 |
| 4.6.1 | Not Considered | 96 |
| 4.6.2 | SDEM-Monotonic (Lee et al 2012) | 96 |
| 4.6.3 | SDEM-Cyclic | 98 |
| 4.6.4 | Diverse Embedment Model (DEM, Lee et al 2011) | 99 |
| 4.6.5 | Variable Engagement Model (VEM: Voo & Foster 2003) | 100 |
| 4.6.6 | fib Model Code 2010 | 101 |
| 4.7 | Lateral Expansion | 101 |
| 4.7.1 | Constant Poisson's ratio | 101 |
| 4.7.2 | Variable Poisson's Ratio – Kupfer | 102 |
| 4.7.3 | Variable Poisson's Ratio – Montoya | 102 |
| 4.7.4 | Variable Montoya With Limit | 104 |
| 4.8 | Confinement Strength | 104 |
| 4.8.1 | Strength Enhancement Neglected | 104 |
| 4.8.2 | Kupfer / Richart Model | 104 |
| 4.8.3 | Selby Model | 105 |
| 4.8.4 | Montoya / Ottosen | 106 |
| 4.9 | Cracking Criterion | 107 |
| 4.9.1 | Uniaxial cracking stress | 108 |
| 4.9.2 | Mohr-Coulomb (Stress) | 108 |
| 4.9.3 | Mohr-Coulomb (Strain) | 110 |
| 4.9.4 | CEB-FIP Model | 110 |
| 4.9.5 | Gupta 1998 Model | 110 |
| 4.10 | Crack Stress Check | 111 |

| | | |
|------------------------------------------|------------------------------------------------------------|------------|
| 4.10.1 | Crack Stress Calc Omitted | 111 |
| 4.10.2 | Basic (DSFM/MCFT) | 111 |
| 4.10.3 | Advanced (Lee 2009) | 112 |
| 4.11 | Crack Width Check | 112 |
| 4.12 | Crack Slip Calculation | 114 |
| 4.12.1 | Not considered | 115 |
| 4.12.2 | Vecchio-Lai (Cyclic) [maybe don't include] | 115 |
| 4.12.3 | Maekawa (Monotonic) | 116 |
| 4.12.4 | Stress Model (Walraven) | 116 |
| 4.12.5 | Hybrid-I, II, and III Models | 116 |
| 4.13 | Creep and Relaxation | 117 |
| 4.14 | Hysteretic Response | 117 |
| 4.14.1 | No Plastic Offsets | 117 |
| 4.14.2 | Plastic offsets; linear loading/unloading | 118 |
| 4.14.3 | Plastic offsets; nonlinear loading/unloading | 120 |
| 4.14.4 | Plastic offsets; nonlinear w/ cyclic decay (Palermo Model) | 121 |
| 5 Models for other material types | | 126 |
| 5.1 | Structural Steel | 126 |
| 5.2 | Masonry | 127 |
| 5.2.1 | Introduction | 127 |
| 5.2.2 | Compressive Behavior | 128 |
| 5.2.3 | Tensile Behavior | 131 |
| 5.2.4 | Slip Along the Joints | 132 |
| 5.3 | Wood (Fixed Orthotropic) | 133 |
| 5.4 | Concrete-Steel Laminate | 134 |
| 5.5 | Concrete-SFRC Laminate and Masonry-SFRC Laminate | 135 |
| 5.6 | Concrete-Ortho Laminate | 136 |

| | |
|-------------------------------------------------------------------|------------|
| 6 Models for Reinforcement Materials | 137 |
| 6.1 Stress-Strain Response | 137 |
| 6.1.1 Ductile Steel Reinforcement | 137 |
| 6.1.2 Prestressing Steel | 139 |
| 6.1.3 Tension Only Reinforcement | 140 |
| 6.1.4 Compression Only Reinforcement | 140 |
| 6.1.5 Externally Bonded FRP Reinforcement | 140 |
| 6.2 Hysteretic Response | 140 |
| 6.2.1 Linear | 140 |
| 6.2.2 Seckin Model w/ Bauschinger Effect | 141 |
| 6.2.3 Menegotto-Pinto Model w/ Bauschinger Effect | 142 |
| 6.2.4 Elastic Hardening (Curvilinear) | 144 |
| 6.2.5 Elastic-Hardening (Trilinear) | 144 |
| 6.2.6 Elastic Plastic (Bilinear) | 145 |
| 6.3 Dowel Action | 145 |
| 6.3.1 Not considered | 145 |
| 6.3.2 Tassios Model | 146 |
| 6.4 Reinforcement Buckling | 147 |
| 6.4.1 Dhakal-Maekawa Model 2002 (DM) Model | 148 |
| 6.4.2 Refined Dhakal-Maekawa (RDM) Model | 149 |
| 6.4.3 RDM and DM buckling models for hysteretic response | 152 |
| 6.4.4 Determination of the Unsupported Length Ratio ($b/t=L/D$) | 153 |
| 6.4.5 Asatsu Model | 156 |
| 6.5 Steel Fibre Reinforced Concrete | 156 |
| 6.5.1 Introduction | 156 |
| 6.5.2 Stress-Strain Behavior of SFRC | 157 |
| 6.6 Laminates | 159 |

| | | |
|----------|----------------------------------------------------------------|------------|
| 6.7 | Shape Memory Alloy Type 1 and Type 2 | 160 |
| 6.7.1 | Shape Memory Alloy 1 (SMA 1) | 160 |
| 6.7.2 | Shape Memory Alloy 2 (SMA 2) | 161 |
| 7 | Models for Bond | 162 |
| 7.1 | Bond Stress-Slip Models for Embedded Bars | 162 |
| 7.1.1 | Perfect bond | 163 |
| 7.1.2 | Eligehausen Model | 163 |
| 7.1.3 | Gan Model | 166 |
| 7.1.4 | Harajli Model | 167 |
| 7.1.5 | Fujii Model | 169 |
| 7.1.6 | Eligehausen and Gan Models with No Cyclic Damage | 171 |
| 7.2 | Bond Stress-Slip Models for Externally Bonded Plates or Sheets | 172 |
| 7.2.1 | Perfect bond | 172 |
| 7.2.2 | Other models | 172 |
| 8 | Part II: FormWorks | 174 |
| 8.1 | Introduction | 174 |
| 8.2 | Installing FormWorks | 174 |
| 8.3 | An Overview of the FormWorks Modeling Process | 175 |
| 8.3.1 | Before Using FormWorks | 176 |
| 8.3.2 | VecTor2 Input and Output Files | 176 |
| 8.4 | FormWorks Basics | 178 |
| 8.4.1 | The FormWorks Interface | 178 |
| 8.4.2 | Creating a New Workspace | 179 |
| 8.4.3 | Saving the Workspace | 180 |
| 8.4.4 | Opening a Saved Workspace File | 181 |
| 8.5 | Viewing and Printing the Workspace | 181 |
| 8.5.1 | Manipulating the View | 181 |

| | | |
|-----------|-----------------------------------|------------|
| 8.5.1.1 | Horizontal and Vertical Scaling | 181 |
| 8.5.1.2 | Changing Display Limits | 181 |
| 8.5.1.3 | Zooming and Panning | 182 |
| 8.5.1.4 | Selecting Display Options | 183 |
| 8.5.2 | Printing the Workspace | 186 |
| 9 | The Job Data | 187 |
| 9.1 | The Job Control Page | 187 |
| 9.1.1 | Job Data Group | 188 |
| 9.1.2 | Structure Data Group | 188 |
| 9.1.3 | Load Data Group | 188 |
| 9.1.3.1 | Static Analysis | 188 |
| 9.1.3.2 | Dynamic Analysis | 192 |
| 9.1.4 | Analysis Parameters Group | 193 |
| 9.2 | The Model Page | 194 |
| 9.2.1 | Concrete Models | 195 |
| 9.2.2 | Reinforcement Models | 197 |
| 9.2.3 | Bond Models | 197 |
| 9.2.4 | Analysis Models | 197 |
| 9.3 | The Auxiliary Input Page | 199 |
| 9.3.1 | General | 200 |
| 9.3.2 | Dynamic Analysis Options | 201 |
| 9.3.3 | Tension Softening Options | 202 |
| 9.3.4 | Masonry Structures Data | 203 |
| 9.3.5 | Material Resistance/Creep Factors | 205 |
| 10 | The Structure Data | 207 |
| 10.1 | Preliminary considerations | 207 |
| 10.2 | Structure Limits | 208 |

| | | |
|-----------|------------------------------------|------------|
| 10.3 | Structure Information | 209 |
| 10.4 | Specifying Material Types | 209 |
| 10.4.1 | Reinforced Concrete Material Types | 210 |
| 10.4.1.1 | Reinforced Concrete | 211 |
| 10.4.1.2 | Structural Steel | 216 |
| 10.4.1.3 | Masonry | 218 |
| 10.4.1.4 | Wood-Orthotropic | 220 |
| 10.4.1.5 | Modeling Composite Materials | 222 |
| 10.4.2 | Reinforcement Material Types | 229 |
| 10.4.2.1 | Bond Types | 230 |
| 10.4.3 | Defining Nodes | 232 |
| 10.4.4 | Defining Elements | 233 |
| 10.4.4.1 | Viewing Elements Attributes | 238 |
| 10.4.4.2 | Viewing Multiple Element Layers | 239 |
| 10.4.5 | Assigning Material Types | 239 |
| 10.4.6 | Restraining the Structure | 241 |
| 10.4.7 | Automatic Method | 243 |
| 10.4.7.1 | Reinforced Concrete Regions | 243 |
| 10.4.7.2 | Reinforcement | 252 |
| 10.4.7.3 | Voids | 257 |
| 10.4.7.4 | Line Constraints | 259 |
| 10.4.7.5 | Point Constraints | 260 |
| 10.4.7.6 | Generating the Mesh | 262 |
| 11 | The Load Case Data | 265 |
| 11.1 | Load Limits | 265 |
| 11.2 | Selecting the Load Case | 265 |
| 11.3 | Load Information | 265 |

| | | |
|-----------|--------------------------------------------------------------|------------|
| | | xiii |
| 11.4 | Nodal Loads | 266 |
| 11.5 | Support Displacements | 268 |
| 11.6 | Gravity Loads | 269 |
| 11.7 | Temperature Loads | 271 |
| 11.8 | Concrete Prestrains | 272 |
| 11.9 | Ingress Pressures | 273 |
| 11.10 | Nodal Thermal Loads | 273 |
| 11.11 | Lumped Masses | 276 |
| 11.12 | Impulse Forces | 278 |
| 11.13 | Ground Acceleration Loads | 280 |
| 12 | Running VecTor2 | 283 |
| 12.1 | Starting the Analysis | 283 |
| 12.2 | Example 1: Simply Supported Beam | 285 |
| 12.3 | Example 2: SW22 | 289 |
| 13 | Summary & Recommendations | 293 |
| 13.1 | Summary | 293 |
| 13.2 | Recommendations | 293 |
| | References | 295 |
| | Appendix A – VecTor2 Input Files for Sample Problem 1 | 305 |
| | VecTor.JOB | 306 |
| | Appendix B – VecTor2 Input Files for Sample Problem 2 | 311 |

List of Figures

| | |
|--------------------------------------------------------------------------------------------------------------------------------------------|----|
| Figure 1: Reinforced concrete membrane element subject to in-plane stresses | 5 |
| Figure 2: Average concrete strains due to average stress-strain response of concrete | 7 |
| Figure 3 Free body diagram of reinforced concrete element showing average stresses | 8 |
| Figure 4 Comparison of average and local stresses at a crack | 11 |
| Figure 5: Comparison of average and local stresses at a crack (a) average stresses between crack; (b) local stresses at crack free surface | 13 |
| Figure 6: Deformation due to crack shear slip | 15 |
| Figure 7 VecTor2 nonlinear finite element analysis algorithm | 22 |
| Figure 8: Definition of secant moduli for a) concrete b) reinforcement | 25 |
| Figure 9: Rayleigh Damping (Chopra, 2007) | 42 |
| Figure 10: Prestressing Wobble and Friction Coefficients | 46 |
| Figure 11: Constant strain triangle element | 49 |
| Figure 12: Plane stress rectangle element | 50 |
| Figure 13: a) Quadrilateral element b) Decomposition of quadrilateral element into two constant strain triangle elements | 51 |
| Figure 14: Degenerate Quadrilateral Element (Li, 2004) | 52 |
| Figure 15: Truss bar element | 53 |
| Figure 16 Link element | 55 |
| Figure 17: Contact element | 57 |
| Figure 18: Linear pre- and post-peak concrete compression response | 60 |
| Figure 19 Popovics pre- and post-peak concrete compression response | 61 |
| Figure 20: Hognestad parabolic pre- and post-peak concrete compression response | 62 |
| Figure 21: Popovics high strength pre- and post-peak concrete compression response | 63 |
| Figure 22: Hoshikuma et al. concrete compressive pre-peak response | 64 |
| Figure 23: Smith-Young concrete compressive pre-peak response | 65 |
| Figure 24: Smith-Young concrete compression post-peak response for $f_p \leq f_c$ | 68 |

| | |
|---------------------------------------------------------------------------------------------|-----|
| Figure 25: Modified Park-Kent post-peak concrete compression response | 69 |
| Figure 26: Hoshikuma et al. concrete compressive post-peak response | 71 |
| Figure 27: Saenz/Spacone concrete compressive post-peak response | 72 |
| Figure 28: Montoya concrete compressive post-peak response | 73 |
| Figure 29: Strength and strain-softened compression response | 75 |
| Figure 30: Strength-only softened compression response | 76 |
| Figure 31: Vecchio 1992-A compression softening model | 77 |
| Figure 32: Vecchio 1982 compression softening model | 78 |
| Figure 33: Vecchio 1982 and Collins-Mitchell tension stiffening response | 82 |
| Figure 34: Izumo, Maekawa et al. tensions stiffening response | 83 |
| Figure 35: Tension chord model | 85 |
| Figure 36: Lee 2010 stress-strain response | 86 |
| Figure 37: Linear tension softening response with and without residual | 89 |
| Figure 38: CEB-FIP tension softening curve (CEB-FIP, 1990) | 90 |
| Figure 39: Bilinear Tension softening model implemented in VecTor2 | 91 |
| Figure 40: Yamamoto tension softening response with and without residual | 92 |
| Figure 41: Envelope curves for normal and light-weight concrete (Cornelissen et al, 1986) | 92 |
| Figure 42: Stress-crack opening relationships (Cornelissen et al., 1986) | 93 |
| Figure 43: Custom input-strain based tension softening in VecTor2 | 94 |
| Figure 44 tension-crack opening relationship in fib model code 2010 (fib, 2010) | 96 |
| Figure 45: Stiffness for the re- and unloading response of FRC in cyclic tension | 98 |
| Figure 46: Kupfer variable Poisson's ratio model | 102 |
| Figure 47: Lateral strain-axial strain curves for Imran-Pantazopoulou tests (Montoya, 2003) | 103 |
| Figure 48: Mohr-Coulomb (Stress) cracking criterion | 109 |
| Figure 49: Shear across with crack through aggregate interlock | 111 |
| Figure 50: Maximum crack width check including effect of element size | 113 |
| Figure 51: Palermo model of concrete hysteretic response in compression | 124 |

| | |
|-------------------------------------------------------------------------------------------------------------------------------------------------------------------------------------------------|-----|
| Figure 52: Palermo model of concrete hysteretic response in tension | 125 |
| Figure 53: Stress-strain behavior of structural steel in VecTor2 | 126 |
| Figure 54: Masonry joints | 127 |
| Figure 55: Ganz failure criterion implemented in VecTor2 (Ganz, 1985) | 128 |
| Figure 56: Masonry compressive stress-strain behavior | 130 |
| Figure 57: Variation in masonry elastic modulus | 131 |
| Figure 58: Masonry Joint Slip | 132 |
| Figure 59: Concrete-steel laminate element (Vecchio and McQuade, 2011) | 134 |
| Figure 60: Ductile steel reinforcement stress-strain response [left(a): Linear strain-hardening (Trilinear); right (b): Nonlinear strain-hardening (HP4)] | 138 |
| Figure 61: Prestressing steel reinforcement stress-strain response | 140 |
| Figure 62: Seckin model of ductile steel reinforcement for hysteretic response [left (a): Seckin w/ Bauschinger-Trilinear; right (b): Seckin w/ Bauschinger-HP4] | 141 |
| Figure 63: Menegotto-Pinto model of ductile steel reinforcement for hysteretic response [left (a): Menegotto-Pinto w/ Bauschinger-Trilinear ; right (b): Menegotto-Pinto w/ Bauschinger-HP4] | 143 |
| Figure 64: curvilinear strain hardening | 144 |
| Figure 65: Trilinear stress-strain response | 144 |
| Figure 66: Elastic-plastic stress-strain response | 145 |
| Figure 67: Dowel resistance mechanism | 147 |
| Figure 68: Compressive stress-strain relationships (Dhakai and Maekawa, 2002a, b) | 148 |
| Figure 69: Compressive stress-strain relationships (Akkaya et al., 2013) | 150 |
| Figure 70: Hysteretic models for ductile reinforcement including buckling [left (a): Seckin; right (b): Menegotto-Pinto] | 152 |
| Figure 71: Values of n_b and n_l for common reinforcement | 154 |
| Figure 72: Tensile stress-strain response of FRC for low and high fibre volume contents (Susetyo, 2009) | 158 |

| | |
|--------------------------------------------------------------------------------------------------------------------------------|-----|
| Figure 73: Compressive stress-strain curve of SFRC, illustrating a) fibre content and b) fibre aspect ratio (Susetyo, 2009) | 159 |
| Figure 74: Stress-strain response for SMA 1 | 160 |
| Figure 75: Stress-strain response for SMA2 | 161 |
| Figure 76: Eligehausen bond stress-slip response | 165 |
| Figure 77: Gan bond stress-slip response | 167 |
| Figure 78: Harajli bond stress-slip response | 169 |
| Figure 79: Eligehausen cyclic bond stress-slip relationship | 171 |
| Figure 80: Bond stress-slip response for externally bonded plates or sheets | 173 |
| Figure 81: Input and output files for VecTor2 analysis | 176 |
| Figure 82: FormWorks application window | 179 |
| Figure 83: Creating new Workspace windows | 180 |
| Figure 84: Display Limits dialog box | 182 |
| Figure 85: Display Options dialog box | 184 |
| Figure 86: Job Control property page | 187 |
| Figure 87: Monotonic type loading | 189 |
| Figure 88: Cyclic type loading | 189 |
| Figure 89: Reversed cyclic type loading | 190 |
| Figure 90: The Models page | 195 |
| Figure 91: The Auxiliary Input Page | 199 |
| Figure 92: Masonry joints | 203 |
| Figure 93: Masonry joint shear strength ratio | 204 |
| Figure 94: Structure Limits dialog box | 208 |
| Figure 95: Structure Information dialog box | 209 |
| Figure 96: Reinforced Concrete Materials Properties Dialog Box | 211 |
| Figure 97: Define Reinforced Concrete Properties Dialog Box: Structural Steel | 216 |
| Figure 98: Define Reinforced Concrete Properties: Masonry | 218 |

| | |
|------------------------------------------------------------------------------------|-----|
| Figure 99: Define Reinforced Concrete Properties: Wood-Orthotropic | 220 |
| Figure 100: Define Reinforced Concrete Properties: Concrete-Steel Laminate | 222 |
| Figure 101: Define Reinforced Concrete Properties: Concrete-SFRC Laminate | 224 |
| Figure 102: Define Reinforced Concrete Properties: Masonry-SFRC Laminate | 226 |
| Figure 103: Define Reinforced Concrete Properties: Concrete-Ortho Laminate | 227 |
| Figure 104: Reinforcement Materials Properties Dialog Box | 229 |
| Figure 105: Bond Properties Dialog Box | 230 |
| Figure 106: Create Nodes Dialog Box | 232 |
| Figure 107: Example of node creation entry | 233 |
| Figure 108: Create Rectangular Elements Dialog Box | 234 |
| Figure 109: Example of rectangular element creation entry | 235 |
| Figure 110: Example of link element creation entry | 236 |
| Figure 111: Example of contact element creation entry | 237 |
| Figure 112: Element attributes dialog | 238 |
| Figure 113: Assign Material types dialog box | 240 |
| Figure 114: Selecting elements for material type assignment with the mouse | 241 |
| Figure 115: Create Support Restraints Dialog Box | 241 |
| Figure 116: Selecting nodes for restraints with the mouse | 242 |
| Figure 117: Examples of legal and illegal region definitions and intersections | 244 |
| Figure 118: RC Regions Property Page | 245 |
| Figure 119: Example of reinforced concrete region creation | 246 |
| Figure 120: Hybrid Discretization | 247 |
| Figure 121: Grid Superposition Discretization | 248 |
| Figure 122: Division Point Insertion Discretization | 248 |
| Figure 123: Hybrid Discretization with Rectangle Option | 249 |
| Figure 124: Division Point Insertion Discretization with Quadrilateral Option | 249 |
| Figure 125: Division Point Insertion Discretization with Smoothed Triangles Option | 250 |

| | |
|------------------------------------------------------------------------|-----|
| Figure 126: Reinforcement Page | 253 |
| Figure 127: Example of reinforcement path creation | 255 |
| Figure 128: Voids and Constraints | 258 |
| Figure 129: Example of point constraint creation | 262 |
| Figure 130: Mesh Creation Page | 263 |
| Figure 131: Load Limits Dialog Box | 265 |
| Figure 132: Load Information Dialog Box | 266 |
| Figure 133: Apply Nodal Loads Dialog Box | 267 |
| Figure 134: Apply Support Displacements Dialog Box | 268 |
| Figure 135: Apply Gravity Loads Dialog Box | 269 |
| Figure 136: Apply Temperature Loads Dialog | 271 |
| Figure 137: Apply Concrete Prestraints Dialog Box | 272 |
| Figure 138: Apply Ingress Pressures Dialog Box | 273 |
| Figure 139: Thermal profiles in VecTor2 (Zhou, 2004) | 274 |
| Figure 140: Apply Nodal Thermal Loads Dialog Box | 275 |
| Figure 141: Apply Lumped Masses Dialog Box | 276 |
| Figure 142: Impulse forces in VecTor2 | 278 |
| Figure 143: Apply Impulse Forces Dialog Box | 279 |
| Figure 144: Apply Ground Acceleration Load Dialog | 280 |
| Figure 145: input file format of VECTOR.EQR file | 281 |
| Figure 146: Bandwidth Reduction Dialog Box | 283 |
| Figure 147: VecTor2 Analysis Proceeding | 285 |
| Figure 148: Reinforced Concrete Beam | 286 |
| Figure 150: Load versus midspan deflection of reinforced concrete beam | 287 |
| Figure 149: FormWorks Model | 287 |
| Figure 151: Crack pattern of reinforced concrete beam at ultimate load | 288 |
| Figure 152: SW22 | 289 |

| | |
|--------------------------------------------------------------|-----|
| Figure 153: FormWorks Model for SW22 | 290 |
| Figure 154: Models used for SW22 | 291 |
| Figure 155: Load-displacement response for SW22 | 291 |
| Figure 156: Deflected Shape and Final Crack Pattern for SW22 | 292 |

List of Appendices

| | |
|-------------------------------------------------------|-----|
| Appendix A – VecTor2 Input Files for Sample Problem 1 | 296 |
| Appendix B – VecTor2 Input Files for Sample Problem 2 | 302 |

Notation

| | |
|----------------|---------------------------------------------------------------------------------------------|
| a | = maximum aggregate size |
| A_{ce} | = effective cross-sectional area of concrete |
| c | = convergence averaging factor |
| c | = cohesion of the mortar bed joint interface (masonry) |
| c_t | = compression softening coefficient |
| $[B]$ | = element strain-displacement matrix |
| d_b | = diameter of reinforcing bar |
| $[D]$ | = composite material stiffness matrix |
| $[D_c]$ | = concrete material stiffness matrix relative to x,y axes |
| $[D_c]'$ | = concrete material stiffness matrix relative to principal axes |
| $[D_f]'$ | = fibre stiffness matrix relative to the direction of the tensile stress attained by fibres |
| $[D_s]$ | = reinforcement material stiffness matrix relative to x,y axes |
| $[D_s]'$ | = reinforcement material stiffness matrix relative to principal axes |
| C_d | = compression softening, strain softening factor |
| C_s | = compression softening, shear slip factor |
| $CMOD_i$ | = crack mouth opening displacement |
| d_f | = fibre diameter |
| E_c | = initial tangent stiffness of concrete |
| $E_{c,d}$ | = dynamic modulus of elasticity of concrete |
| \bar{E}_{c1} | = secant modulus of concrete in the principal tensile direction |
| \bar{E}_{c2} | = secant modulus of concrete in the principal compressive direction |
| E_{eh} | = un- and re-loading stiffness due to mechanical anchorage effect of fibres |
| \bar{E}_{f1} | = fibre stiffness matrix relative to the direction of the tensile stress attained by fibres |
| E_{mx} | = minimum modulus |

| | |
|-------------|--------------------------------------------------------------------------------|
| $E_{m,y}$ | = maximum modulus of elasticity |
| E_s | = initial tangent stiffness of reinforcement |
| \bar{E}_s | = secant modulus of reinforcement |
| E_{st} | = un- and re-loading stiffness due to frictional bond behavior of fibres |
| f'_c | = concrete cylinder uniaxial compressive strength |
| f_{cd} | = dynamic compressive strength of concrete |
| f_{cc} | = concrete cube strength |
| f_{cs} | = static compressive strength of concrete |
| f_{cx} | = average concrete axial stress in the x-direction |
| f_{cy} | = average concrete axial stress in the y-direction |
| f_{eh} | = tensile stress attained by fibres due to the mechanical anchorage effect |
| f_f | = tensile stress due to fibres at a crack |
| f_{fts} | = residual tensile stress at an initial crack opening |
| f_{it} | = intermediate stress |
| f_{mx} | = compressive strength in the x- direction with bed joint aligned horizontally |
| f_{my} | = compressive strength in the y-direction with bed joint aligned horizontally |
| f_p | = peak concrete compressive stress |
| $f_{r1,3}$ | = residual stresses input by user |
| f_{st} | = tensile stress attained by fibres due to the frictional bond behavior |
| f_{sx} | = average stress of reinforcement parallel to the x-direction |
| f_{sy} | = average stress of reinforcement parallel to the y-direction |
| f_{scrx} | = local stress at a crack of reinforcement parallel to the x-direction |
| f_{scry} | = local stress at a crack of reinforcement parallel to the y-direction |
| f_{yield} | = yield strength of reinforcement |
| f'_t | = concrete cracking strength |
| f_{td} | = dynamic tensile strength of concrete |

- f_{ts} = static tensile strength of concrete
- f'_{ty} = tensile strength of the mortar bed joint interface in the x-direction (perpendicular to the bed joints)
- $f_{w,cr,avg}$ = tensile stress attained by fibres, which is evaluated for the average crack width
- $f_{w,cr,max}$ = tensile stress attained by fibres, which is evaluated for the maximum crack width
- $[F^*]$ = pseudo nodal load vector
- $[F]$ = applied external nodal load vector
- $[F^o]$ = total nodal load vector
- \bar{G}_c = secant shear modulus of concrete
- G_f = fracture energy parameter
- h = element thickness
- k = post-peak decay parameter for stress-strain response of concrete in compression
- k = stiffness matrix (**for dynamic analyses**)
- k_d = shape factor based on post-peak compression stress-strain curve steepness
- k_r = spring stiffness of link element radial to reinforcement direction
- k_t = spring stiffness of link element tangential to reinforcement direction
- $[k]$ = element stiffness matrix
- $[k_c]$ = element stiffness matrix contribution from concrete
- $[k_s]$ = element stiffness matrix contribution from reinforcement
- $[K]$ = structure stiffness matrix
- K_d = damage factor or fibre efficiency factor
- K_{eh} = factors to represent the average pull-out stresses of a fiber due to the mechanical anchorage effect
- K_f = factor to account for fibre orientation and engagement
- K_{st} = factors to represent the average pull-out stresses of a fiber due to frictional bond behaviour
- $l_{a,crit}$ = critical fibre length for fibre fracture

- l_f = fibre length
 L/D = unsupported length to diameter ratio for steel reinforcing bars
 L_r = characteristic length
 m = mass matrix
 n = curve fitting parameter for stress-strain response of concrete in compression
 $[r]$ = nodal displacement vector
 R = ratio of principal stresses
 s = average crack spacing
 s_{eh} = slip at maximum tensile force due to the mechanical anchorage of a fiber with the inclination angle of 0 degree to the normal of the crack surface
 s_f = slip at the frictional bond strength for a fibre with the inclination angle of zero degree
 s_{mx} = average crack spacing in the x-direction
 s_{my} = average crack spacing in the y-direction
 sp_i = joint spacing
 s_0 = average crack spacing perpendicular to the crack
 th_i = thickness of joints
 $[T]$ = coordinate transformation matrix
 ν_{12}, ν_{21} = Poisson's ratios of concrete in the principal directions
 ν_{12}^e = elastic component of Poisson's ratio
 ν_{12}^* = residual component of Poisson's ratio
 ν_{cxy} = average concrete shear stress
 ν_{ci} = local concrete shear stress at a crack
 V_f = volumetric fibre ratio
 w = average crack width
 $w_{cr,avg}$ = average crack width
 $w_{cr,exp}$ = maximum experienced crack width

$w_{cr,max}$ = maximum crack width

α = orientation of reinforcement relative to positive x-axis

α = fibre engagement factor (**for FRC Tension calculations**)

α = direction of principal axes with respect to the direction of horizontal joints (**masonry**)

α_f = fibre orientation factor

β = Newmark beta factor (**for dynamic analyses**)

β = angle between principal axes and axes of orthotropy (**masonry**)

β_{cr} = crack width check crack coefficient

β_{eh} = coefficients to consider the effect of a fiber slip on the longer embedment side on the mechanical anchorage effect

β_d = compression softening reduction factor

β_f = coefficients to consider the effect of a fiber slip on the longer embedment side on the frictional behavior

β_l = confinement strength enhancement factor

$\Delta\theta_\epsilon$ = post-cracking rotation of principal total strain field

$\Delta\theta_\sigma$ = post-cracking rotation of the principal stress field

$\dot{\epsilon}_c$ = strain rate (compression)

$\dot{\epsilon}_{ct}$ = tensile strain rate of concrete

ϵ_{c1} = average net concrete axial strain, in the principal tensile 1-direction

ϵ_{c2} = average net concrete axial strain, in the principal compressive 2-direction

ϵ_{c80i} = post-peak strain at 80% of peak stress

ϵ_{cf} = average net concrete tensile strain, in the direction of the tensile stress attained by fibres

ϵ_{ch} = characteristic strain for concrete in tension

ϵ_{cr} = concrete cracking strain

ϵ_{cx} = average net concrete axial strain, in the x-direction

ϵ_{cy} = average net concrete axial strain, in the y-direction

- ε_c^o = elastic strain offsets in concrete
 ε_c^p = plastic strain offsets in concrete
 ε_{cmx} = maximum concrete compressive strain
 ε_{tmx} = maximum concrete tensile strain
 ε_i = intermediate strain
 ε_o = concrete compressive strain corresponding to f'_c
 ε_p = concrete compressive strain corresponding to f'_p
 ε_{sh} = reinforcement strain at onset of strain hardening
 ε_{sx} = average strain of reinforcement parallel to the x-direction
 ε_{sy} = average strain of reinforcement parallel to the y-direction
 ε_{syield} = yield strain of reinforcement
 ε_s^o = elastic strain offsets in reinforcement
 ε_s^p = plastic strain offsets in reinforcement
 ε_{ts} = terminal strain in concrete tension softening response
 ε_u = ultimate strain of reinforcement
 ε_x = total axial strain in the x-direction
 ε_y = total axial strain in the y-direction
 ε_x^s = average axial strain in the x-direction, due to shear slip
 ε_y^s = average axial strain in the y-direction, due to shear slip
 ξ = damping ratio
 γ = Newmark gamma factor
 γ_{cxy} = average net concrete shear strain
 γ_{xy} = total shear strain
 γ_{xy}^s = average shear strain due to shear slip

- μ = the reduction coefficient for the strength f_{mx}
- ω = natural frequency
- ω_m = ratio between the tensile strength in the x-direction (for $\alpha = 0$) and compressive strength f_{my}
- Ψ_s = bonded area per unit length
- ϕ_n = mode shape
- φ = friction angle of the mortar bed joint interface
- θ = orientation of principal net concrete strain field, measured counter-clockwise from x-axis
- θ_{crit} = critical fibre inclination angle which cause a fibre engagement for a given crack width
- θ_f = fibre inclination angle from axis perpendicular to the crack surface
- θ_{ic} = orientation of principal strain and stress field at initial cracking
- θ^l = rotation lag between orientation of principal strain and principal stress fields in concrete
- θ_n = angle between normal to crack surface and longitudinal axis of reinforcement
- θ_ϵ = orientation of principal total strain field, measured counter-clockwise from x-axis
- θ_σ = orientation of principal stress field, measured counter-clockwise from x-axis
- ρ = reinforcement ratio
- ρ_e = effective reinforcement ratio of steel bars
- ρ_F = effective reinforcement ratio for FRP sheets
- $\sigma_{f,cr,avg}$ = average fibre tensile stress at a crack
- σ_{fu} = fibre tensile strength
- σ_x = applied axial stress in the x-direction
- σ_y = applied axial stress in the y-direction
- $[\sigma^0]$ = pseudo prestress vector
- τ_b = fibre bond strength
- τ_{b0} = max average bond stress in steel bars
- $\tau_{eh,max}$ = pull-out strength due to the mechanical anchorage of an end-hooked fiber
- $\tau_{f,max}$ = frictional bond strength

τ_{xy} = applied shear stress

ψ = transformation angle between principal direction and positive x-axis

1 Introduction

1.1 Background

VecTor © is a suite of computer programs dedicated to nonlinear finite element analysis of reinforced concrete (NLFEARC). These programs have been developed at the University of Toronto by researchers studying reinforced concrete behavior and applications of the finite element method over the last two decades. By combining a variety of realistic nonlinear models for reinforced concrete with the powerful analytical capabilities of finite element analysis, these programs permit more accurate assessments of structural performance (strength, post-peak behavior, failure mode, deflections and cracking) than can be achieved by linear-elastic methods. At the same time, the finite element method allows analysts to address the composite nature of reinforced concrete material, changing material properties due to progressive cracking, challenging geometries and loadings – complexities which might thwart conventional analysis techniques.

As the results of NLFEARC have become increasingly reliable and modern digital computers advance in performance, NLFEARC has evolved from the research domain to a practical design tool. However, the capabilities that make these NLFEARC programs so remarkable, pose potential difficulties to the non-specialist user. While the reinforced concrete models are critical to the efficacy of the analysis, they may also be obscure to its users. Without an understanding of the theoretical basis of programs and their operation, the impressive output of the programs cannot be regarded with confidence. As such, the rational and effective use of NLFEARC programs requires guidance and user experience.

Moreover, generating input for finite element analysis requires knowledge of the finite element method itself. In order to idealize a structure to a valid mathematical model, users must exercise their discretion regarding the mesh topology, material selection, boundary conditions, load representation and computational efficiency. Lacking preprocessor facilities, the time-consuming and error-prone nature of data input may discourage the practical application of NLFEARC.

The availability of user facilities must be regarded as necessary for progress in the practical application of NLFEARC. It is the objective of this report to address this need by developing program documentation and preprocessor software and for the nonlinear finite element program VecTor2.

1.2 The VecTor2 Program

VecTor2 is a nonlinear finite element program for the analysis of two-dimensional reinforced concrete membrane structures. The program has been developed at University of Toronto since 1990, when its original version was known as TRIX ©. This development has coincided with experimental tests to corroborate the ability of VecTor2 to predict the load-deformation response of a variety of reinforced concrete structures exhibiting well-distributed cracking when subject to short-term static monotonic, cyclic and reverse cyclic loading.

The theoretical bases of VecTor2 are the Modified Compression Field Theory (Vecchio and Collins, 1986) and the Disturbed Stress Field Model (Vecchio, 2000) – analytical models for predicting the response of reinforced concrete elements subject to in-plane normal and shear stresses. VecTor2 models cracked concrete as an orthotropic material with smeared, rotating cracks. The program utilizes an incremental total load, iterative secant stiffness algorithm to produce an efficient and robust nonlinear solution.

Originally, VecTor2 employed the constitutive relationships of the MCFT. Subsequent developments have incorporated alternative constitutive models for a variety of second-order effects including compression softening, tension stiffening, tension softening, and tension splitting. Also, the capabilities of the VecTor2 have been augmented to model concrete expansion and confinement, cyclic loading and hysteretic response, construction and loading chronology for repair applications, bond slip, crack shear slip deformations, reinforcement dowel action, reinforcement buckling, and crack allocation processes.

Finite element models constructed for VecTor2 use a fine mesh of low-powered elements. This methodology has advantages of computational efficiency and numerical stability. It is also well suited to reinforced concrete structures, which require a relatively fine mesh to model reinforcement detailing and

local crack patterns. The element library includes a three-node constant strain triangle, a four-node plane stress rectangular element and a four-node quadrilateral element for modeling concrete with smeared reinforcement; a two-node truss-bar for modeling discrete reinforcement; and a two-node link and a four-node contact element for modeling bond-slip mechanisms.

VecTor2 reads ASCII text files for input and outputs binary and ASCII text files for analysis results. The software Augustus © provides graphical post-processing capabilities for the analysis results of VecTor2.

1.3 Research Objectives

The objective of this research is to make NLFEARC with VecTor2 more amenable to practical application for the non-specialist user. The strategy to meet these objectives is to develop documentation for VecTor2 and a new preprocessor software program, called FormWorks ©.

The purpose of the program documentation is to provide guidance for the rational usage of VecTor2. In a descriptive treatment, the documentation encompasses the following topics in relation to VecTor2:

- the Modified Compression Field Theory and Disturbed Stress Field Model
- the finite element formulation
- the element library
- the material models.

The FormWorks preprocessor software and its accompanying manual address the ease of use of VecTor2 as an analytical tool, by decreasing the potential for input error and expediting the modeling process. To fulfill this function, the FormWorks preprocessor includes the following amenities:

- an instructive manual for using FormWorks and VecTor2
- a graphical interface for data input and visualization in the Windows environment
- input data checking and editing capabilities
- a bandwidth reduction algorithm for improving computational efficiency
- an automatic mesh-generator.

Specific criteria for the automatic mesh-generator are as follows:

- accommodation of multiply connected regions and arbitrary material delineations
- generation of mixed element-type meshes using the VecTor2 element library
- preferential generation of isothetic rectangular elements for computational accuracy
- good computational characteristics of the mesh
- efficient and robust mesh generation algorithm
- high degree of user control over mesh topology
- aesthetically pleasing mesh topology for ease of result interpretation
- economical demands on human input effort.

1.4 Organization

The report is subdivided into the following parts and chapters.

Part I, which includes Chapters 2 through 7, pertains to the program VecTor2. Chapter 2 presents the theory and implementation of VecTor2. The Modified Compression Field Theory and Disturbed Stress Field Model are described as the theoretical bases of the VecTor2 analysis. The chapter subsequently discusses the implementation of these theories in the finite element algorithm and incorporation of advanced analysis features. Chapter 3 presents the VecTor2 finite element library and the role of elements in modeling reinforced concrete and reinforcement materials and bond-slip. Chapters 4, 5, 6 and 7 describe constitutive and behavioral models pertaining to concrete materials, models for other material types, reinforcement materials, and bond slip, respectively.

Part II, which includes chapters 8 through 12, serves as a user manual for the preprocessor program FormWorks. These chapters describe the user-interface and the finite element modeling process.

Chapter 13 summarizes this research and provides recommendations for further developments.

2 Part I: VecTor2

2.1 Introduction

This chapter begins with a review of the Modified Compression Field Theory and Disturbed Stress Field Model – the theoretical bases of VecTor2 analyses. The discussion subsequently focuses on the finite element implementation of these theories for monotonically loaded structures. Finally, consideration is given to the implementation of augmented analysis features for modeling lateral expansion, triaxial stresses, cyclic loading, construction and loading chronology, and bond-slip. Dynamic analysis in VecTor2 is also discussed, including an overview of damping and strain rate effects.

2.2 Modified Compression Field Theory (MCFT)

The MCFT (Vecchio and Collins 1986) is an analytical model for predicting the load-deformation response of reinforced concrete membrane elements subjected to shear and normal stresses, as shown in Figure 1. The MCFT determines the average and local strains and stresses of the concrete and reinforcement, and the widths and orientation of cracks throughout the load-deformation response of the element. Based on this information, the failure mode of the element can also be determined.

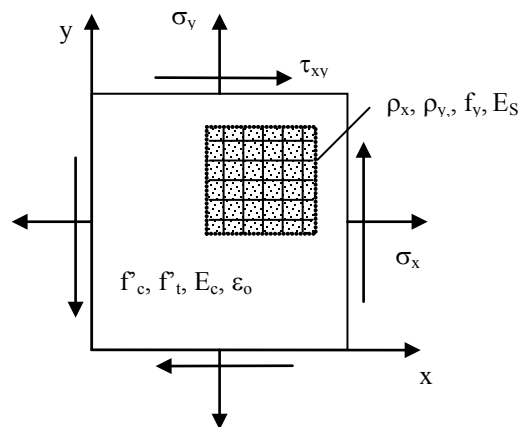


Figure 1: Reinforced concrete membrane element subject to in-plane stresses

The MCFT models cracked concrete as an orthotropic material using a smeared rotating crack approach. Cracked concrete is treated as a solid continuum with cracks distributed over the membrane element, as opposed to a solid interrupted by discrete physical discontinuities. The smeared cracks freely reorient, remaining coaxial with the changing direction of the principal concrete compressive stress field. As well as being computationally convenient, the smeared rotating crack approach is consistent with the distributed and meandering crack patterns observed in many reinforced concrete structures.

The theory is comprised of three sets of relationships: compatibility relationships for concrete and reinforcement average strains; equilibrium relationships involving average stresses in the concrete and reinforcement; and constitutive relationships for cracked concrete and reinforcement. The constitutive relationships for cracked concrete result from tests of reinforced concrete panels using a purpose-built Panel Element Tester at the University of Toronto. As such, the formulation of the MCFT incorporates realistic constitutive models for concrete based on experimentally observed phenomena. While cracks are smeared and the relationships are formulated in terms of average stresses and strains, a critical aspect of the MCFT is the consideration of local strain and stress conditions at cracks.

2.2.1 Assumptions

The MCFT utilizes the following assumptions:

- uniformly distributed reinforcement
- uniformly distributed and rotating cracks
- uniformly applied shear and normal stresses
- unique stress state for each strain state, without consideration of strain history
- strains and stresses are average over a distances including several cracks
- orientations of principal strain, θ_ϵ , and orientations of principal stress, θ_σ , are the same
- perfect bond between reinforcement and concrete
- independent constitutive relationships for concrete and reinforcement
- negligible shear stresses in reinforcement.

2.2.2 Compatibility Relationships

The compatibility relationships pertain to the average strains in the concrete and reinforcement components as shown in Figure 2.

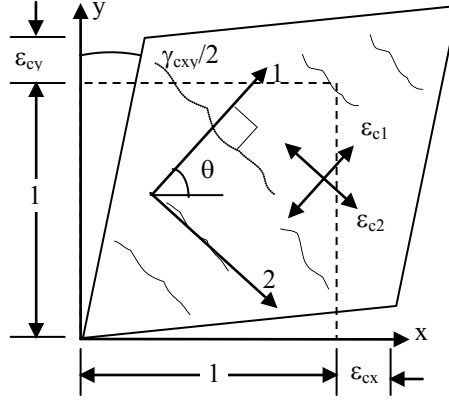


Figure 2: Average concrete strains due to average stress-strain response of concrete

With the perfect bond assumption, it follows that average strains experienced by the concrete are equally experienced by the reinforcement. Therefore, for non-prestressed reinforcement, the average strains in the concrete, ϵ_c , and reinforcement, ϵ_s , will be the same. Although the MCFT can address any number of reinforcement components and orientations, consider the orthogonally reinforced membrane element of Figure 1. The strains of the reinforcement parallel to the x and y directions are denoted by ϵ_{sx} and ϵ_{sy} , respectively. The compatibility relationships are expressed by the following equations:

$$\epsilon_x = \epsilon_{cx} = \epsilon_{sy} \quad (2.2.2.1)$$

$$\epsilon_y = \epsilon_{cy} = \epsilon_{sx} \quad (2.2.2.2)$$

With a value for the shear strain, γ_{xy} , relationships from Mohr's circle of strain determine the average principal concrete tensile strain, ϵ_{c1} , and the average principal concrete compressive strain, ϵ_{c2} as follows:

$$\epsilon_{c1}, \epsilon_{c2} = \frac{1}{2}(\epsilon_x + \epsilon_y) \pm \frac{1}{2} \left[(\epsilon_x - \epsilon_y)^2 + \gamma_{xy}^2 \right]^{\frac{1}{2}} \quad (2.2.2.3)$$

Relationships from Mohr's circle also determine the orientations of the average principal tensile strain axis, θ_ε , and stress axis, θ_σ , with respect to the x-axis:

$$\theta = \theta_\varepsilon = \theta_\sigma = \frac{1}{2} \tan^{-1} \left(\frac{\gamma_{xy}}{\varepsilon_x - \varepsilon_y} \right) \quad (2.2.2.4)$$

2.2.3 Equilibrium Relationships

Consider the free body diagram of the membrane element, in Figure 3.

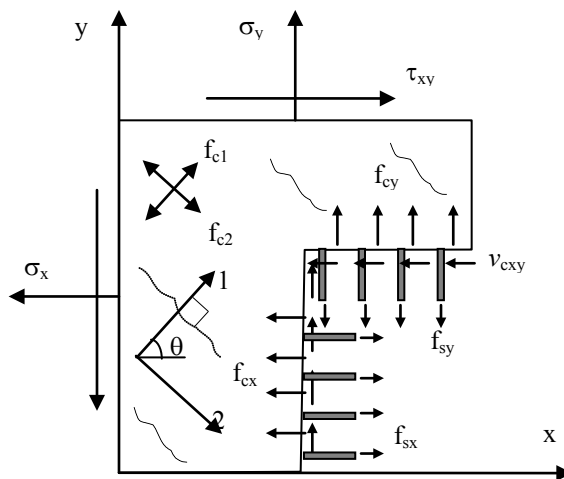


Figure 3 Free body diagram of reinforced concrete element showing average stresses

Equilibrium of forces in the x and y-directions requires that the resultants of the applied normal stresses, σ_x and σ_y , be balanced by the resultants of the average concrete stresses, f_{cx} and f_{cy} , and the reinforcement stresses f_{sx} and f_{sy} . Equilibrium of moments requires that the applied shear stresses, τ_{xy} , are entirely resisted by average shear stresses in the concrete, v_{cxy} , (assuming the reinforcement does not exhibit dowel action).

These equilibrium relationships for average stresses may be summarized as follows:

$$\sigma_x = f_{cx} + \rho_{sx} f_{sx} \quad (2.2.3.1)$$

$$\sigma_y = f_{cy} + \rho_{sy} f_{sy} \quad (2.2.3.2)$$

$$\tau_{xy} = v_{cxy} \quad (2.2.3.3)$$

where ρ_{sx} and ρ_{sy} are the reinforcement ratios in the x and y directions, respectively.

As cracked concrete is orthotropic with respect to the principal stress directions, Mohr's circle of stress can be used to relate the average concrete stresses, f_{cx} , and, f_{cy} , to the average principal concrete tensile stress, f_{c1} :

$$f_{cx} = f_{c1} - \nu_{cxy} \cdot \cot(90 - \theta_{\sigma}) \quad (2.2.3.4)$$

$$f_{cy} = f_{c1} - \nu_{cxy} \cdot \tan(90 - \theta_{\sigma}) \quad (2.2.3.5)$$

2.2.4 Constitutive Relationships

Constitutive models are necessary to relate the strains in the compatibility relationships with the stresses in the equilibrium relationships. As described by Vecchio and Collins (1986), thirty panels measuring 890x890x70mm were subject to in-plane stress conditions by the Panel Element Tester at the University of Toronto. The test results were analyzed to develop constitutive models for cracked concrete in compression and tension. It should be noted that other relationships have since been implemented in VecTor2.

With regards to concrete in compression, the constitutive relationship relates the principal compressive stress, f_{c2} , to the principal compressive strain, ϵ_{c2} . Panel test results indicate that the compressive strength and stiffness decrease as coexisting principal tensile strains, ϵ_{c1} , increase. This phenomenon, known as compression softening, is incorporated by softening the stress-strain response of concrete in uniaxial compression. The proposed relationship is as follows:

$$f_{c2} = \frac{f'_c \left[2(\epsilon_{c2}/\epsilon_o) - (\epsilon_{c2}/\epsilon_o)^2 \right]}{0.8 - 0.34(\epsilon_{c1}/\epsilon_o)} \quad (2.2.4.1)$$

The term in the numerator is the Hognestad parabolic relationship for concrete in uniaxial compression, often used for normal strength concretes. The value ϵ_o is the concrete cylinder strain (a negative value) corresponding to the peak compressive stress, f'_c , as determined from uniaxial compression tests of concrete cylinders. The term in the denominator reflects the softening effect of principal tensile strains.

With regards to concrete in tension, the constitutive relationship relates the principal tensile stress, f_{c1} , to the principal tensile strain, ϵ_{c1} . It is first necessary to determine the uniaxial cracking

strength, f'_t , and corresponding cracking strain, ε_{cr} . In the absence of information, they may be estimated as follows:

$$f'_t = 0.33\sqrt{f'_c} \quad (\text{in MPa}) \quad (2.2.4.2)$$

$$\varepsilon_{cr} = \frac{f'_t}{E_c} \quad (2.2.4.3)$$

where E_c is the initial tangent stiffness of the concrete, estimated as:

$$E_c = 5000\sqrt{f'_c} \quad (\text{in MPa}) \quad (2.2.4.4)$$

Before cracking, the concrete behaves linear-elastically in tension as follows:

$$f_{c1} = E_c \cdot \varepsilon_{c1} \quad \text{for } 0 < \varepsilon_{c1} < \varepsilon_{cr} \quad (2.2.4.5)$$

After cracking, tensile stresses may continue to exist in the concrete between cracks in reinforced concrete due to bond interactions between the concrete and reinforcement. To model this phenomenon, known as tension stiffening, the concrete tensile stress decays from the tensile strength as the principal concrete tensile strain increases. The MCFT proposed relationship is as follows:

$$f_{c1} = \frac{f'_t}{1 + \sqrt{200\varepsilon_{c1}}} \quad (2.2.4.6)$$

As for the reinforcement in compression and tension, the MCFT uses a bilinear relationship between the average stress, f_s and average strain, ε_s . An initial ascending linear-elastic branch is followed by a yield plateau, as described by the following equations:

$$f_{sx} = E_s \cdot \varepsilon_{sx} \leq f_{sxyield} \quad (2.2.4.7)$$

$$f_{sy} = E_s \cdot \varepsilon_{sy} \leq f_{syyield} \quad (2.2.4.8)$$

where E_s is the elastic modulus of the reinforcement, and $f_{sxyield}$ and $f_{syyield}$ are the yield stress of the reinforcement in the x and y-directions, respectively.

2.2.5 Consideration of Local Crack Conditions

Given a compatible average strain condition, the preceding relationships can determine the average stresses in the concrete and reinforcement and the applied shear and normal stresses that they equilibrate. However, it would be unconservative to disregard the possibility that the element response is

$$f_{c1} \leq \rho_x (f_{sxyield} - f_{s_x}) \cos^2 \theta_{nx} + \rho_y (f_{syyield} - f_{s_y}) \cos^2 \theta_{ny} \quad (2.2.5.2)$$

As a principal plane, shear stresses are absent from the section in Figure 4a. However, as the reinforcement generally crosses the crack at a skew angle, local shear stresses, v_{ci} , are present on the crack surface. Static equivalency of average and local stresses in the direction tangential to the crack determines the local shear stresses as follows:

$$v_{ci} = \rho_x (f_{s_{crx}} - f_{s_x}) \cos \theta_{nx} \cdot \sin \theta_{nx} + \rho_y (f_{s_{cry}} - f_{s_y}) \cos \theta_{ny} \cdot \sin \theta_{ny} \quad (2.2.5.3)$$

Independently of the above equation, local shear stresses can only become so large before sliding shear failure occurs. The shear stress is limited by aggregate interlock mechanisms, which decrease in efficacy as the crack width, w , increases and the maximum aggregate size, a , decreases. Based on the analysis of aggregate interlock by Walraven (1981), the MCFT limits the shear stress on the crack as follows:

$$v_{ci} \leq \frac{\sqrt{f'_c}}{0.31 + 24w/(a + 26)} \quad (\text{in mm, MPa}) \quad (2.2.5.4)$$

The average crack width, w , is the product of the principle concrete tensile strain and the average crack spacing perpendicular to the crack, s_θ :

$$w = \varepsilon_{c1} s_\theta \quad (2.2.5.5)$$

$$s_\theta = \frac{1}{\frac{\cos \theta}{s_{mx}} + \frac{\sin \theta}{s_{my}}} \quad (2.2.5.6)$$

The average crack spacing in the x-direction, s_{mx} , and y-direction, s_{my} , may be estimated from the bond properties and layout of the reinforcement. Refer to Collins and Mitchell, (1997).

If either the maximum permitted average concrete tensile stress or local shear stress at a crack is exceeded, then the strain state of the element is modified to result in a lower average concrete tensile stress.

2.2.6 Consideration of Local Crack Conditions with FRC

Where fibre reinforced concrete (FRC) is used, the fibres increase the maximum permissible tensile and shear stress at a crack. The following figure depicts the local stresses at the free surface of a crack.

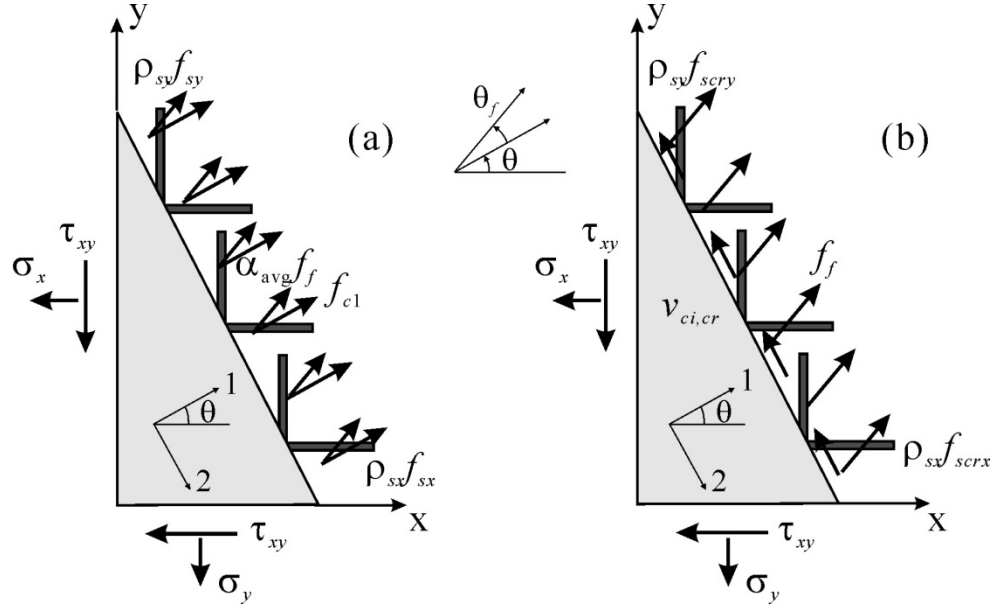


Figure 5: Comparison of average and local stresses at a crack
 (a) average stresses between crack; (b) local stresses at crack free surface

For equilibrium, from Figure 5 above:

$$f_{c1} \cos \theta + \rho_{sx} f_{sx} \cos \theta + \alpha_{avg} f_f \cos(\theta + \theta_f) = \rho_{sx} f_{scrx} \cos \theta - v_{ci,cr} \sin \theta + f_f \cos(\theta_{1n} + \theta_f) \quad (2.2.6.1)$$

$$f_{c1} \sin \theta + \rho_{sy} f_{sy} \sin \theta + \alpha_{avg} f_f \sin(\theta + \theta_f) = \rho_{sy} f_{scry} \sin \theta - v_{ci,cr} \cos \theta + f_f \sin(\theta + \theta_f) \quad (2.2.6.2)$$

where α_{avg} is the average fibre orientation factor, θ_f is the angle of the tensile stress attained by fibres from the axis perpendicular to the crack surface, f_f is the tensile stress due to fibres for a given crack width, and

$$\tan \theta_f = \frac{\delta_s}{w_{cr}} \quad (2.2.6.3)$$

Static equivalency of average and local stresses in the direction tangential to the crack determines the local shear stresses as follows:

$$\frac{v_{ci,cr}}{\cos \theta \sin \theta} = \rho_{sx} (f_{scrx} - f_{sx}) - \rho_{sy} (f_{scry} - f_{sy}) + (1 - \alpha_{avg}) f_f \left(\frac{\cos(\theta + \theta_f)}{\cos \theta} - \frac{\sin(\theta + \theta_f)}{\sin \theta} \right) \quad (2.2.6.4)$$

$$v_{ci,cr} = \sum_i \rho_{s,i} (f_{scr,i} - f_{s,i}) \sin \theta_{n,i} \cos \theta_{n,i} - (1 - \alpha_{avg}) f_f \sin \theta_f \quad (2.2.6.5)$$

2.3 Disturbed Stress Field Model (DSFM)

The DSFM (Vecchio, 2000) addresses systematic deficiencies of the MCFT in predicting the response of certain structures and loading scenarios. In lightly reinforced elements, where crack shear slip is significant, the rotation of the principal stress field tends to lag the greater rotation of the principal strain field. For such elements, the shear stiffness and strength is generally overestimated by the MCFT, which assumes the rotations are equal. Conversely, in elements that exhibit limited rotation of the principal stress and strain fields, the MCFT generally underestimates the shear stiffness and strength, partly because the concrete compression response calibrated for the MCFT is overly softened for the effect of principal tensile strains.

The DSFM is conceptually similar to the MCFT, but extends the MCFT in several respects. Most importantly, the DSFM augments the compatibility relationships of the MCFT to include crack shear slip deformations. The strains due to these deformations are distinguished from the strains of the concrete continuum due to stress. As such, the DSFM decouples the orientation of the principal stress field from that of the principal strain field, resulting in a smeared delayed rotating-crack model. Moreover, by explicitly calculating crack slip deformations, the DSFM eliminates the crack shear check as required by the MCFT. Constitutive relationships for concrete and reinforcement are also refined. The following discussion presents the compatibility, equilibrium and constitutive relationships of the DSFM, with an emphasis on differences from the MCFT.

2.3.1 Compatibility Relationships

While the MCFT assumes that principal strain and principal stress axes remain coaxial, panel tests results indicate that this assumption is not always true after the cracking. The evidence demonstrates the principal strain field generally changes inclination at a larger rate than the principal stress field, resulting in a differential lag between the principal strain and principal stress axes.

The phenomenon is attributable to the manner in which the strain and stress fields are determined. The measured strains are total strains, which are attributable to straining of the concrete continuum in response to applied stresses as shown in Figure 2 and discontinuous shear slip as shown in Figure 6.

Meanwhile, concrete stresses are attributable only to the continuum straining in response to applied stresses.

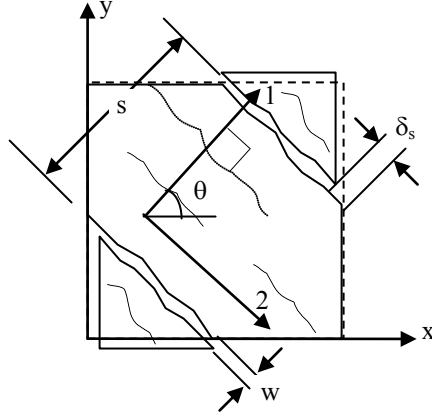


Figure 6: Deformation due to crack shear slip

To reconcile this behavior, the DSFM expresses the total strains, ϵ_x , ϵ_y , and γ_{xy} , as the sum of net concrete strains, ϵ_{cx} , ϵ_{cy} , and γ_{cxy} , and strain due to shear slip, ϵ_x^s , ϵ_y^s and γ_{xy}^s :

$$\epsilon_x = \epsilon_{cx} + \epsilon_x^s \quad (2.3.1.1)$$

$$\epsilon_y = \epsilon_{cy} + \epsilon_y^s \quad (2.3.1.2)$$

$$\gamma_{xy} = \gamma_{cxy} + \gamma_{xy}^s \quad (2.3.1.3)$$

Relationships from Mohr's circle determine the principal net concrete tensile strain, ϵ_{c1} , and the principal net concrete compressive strain, ϵ_{c2} , as follows:

$$\epsilon_{c1}, \epsilon_{c2} = \frac{1}{2}(\epsilon_{cx} + \epsilon_{cy}) \pm \frac{1}{2} \left[(\epsilon_{cx} - \epsilon_{cy})^2 + \gamma_{cxy}^2 \right]^{\frac{1}{2}} \quad (2.3.1.4)$$

The crack slip shear strain components, ϵ_x^s , ϵ_y^s and γ_{xy}^s , are calculated from the average crack slip shear strain γ_s . This quantity is defined as the crack slip, δ_s , divided by the average crack spacing, s , as follows:

$$\gamma_s = \frac{\delta_s}{s} \quad (2.3.1.5)$$

Relationships from Mohr's circle resolve γ_s into the components ϵ_x^s , ϵ_y^s and γ_{xy}^s :

$$\varepsilon_x^s = -\frac{1}{2}\gamma_s \sin(2\theta) \quad (2.3.1.6)$$

$$\varepsilon_y^s = \frac{1}{2}\gamma_s \sin(2\theta) \quad (2.3.1.7)$$

$$\gamma_{xy}^s = \gamma_s \cos(2\theta) \quad (2.3.1.8)$$

The orientation of the principal net concrete strains, θ , and orientation of principal concrete stresses, θ_σ , with respect to the x-axis are determined from Mohr's circle relationships involving the net concrete strain components as follows:

$$\theta = \theta_\sigma = \frac{1}{2} \tan^{-1} \left(\frac{\gamma_{cxy}}{\varepsilon_{cx} - \varepsilon_{cy}} \right) \quad (2.3.1.9)$$

Likewise, the orientation of the principal total strain field, θ_ε , is determined from the total strain components:

$$\theta_\varepsilon = \frac{1}{2} \tan^{-1} \left(\frac{\gamma_{xy}}{\varepsilon_x - \varepsilon_y} \right) \quad (2.3.1.10)$$

The difference between the orientation of total strains and the orientation of the principal concrete stresses defines the rotation lag, $\Delta\theta$:

$$\Delta\theta = \theta_\varepsilon - \theta_\sigma \quad (2.3.1.11)$$

Although the DSFM can address any number of reinforcement components and orientations, consider the orthogonally reinforced membrane element of Figure 1. Assuming perfect bond, the average strains of the reinforcement components in the x- and y-directions are equal to the total strains:

$$\varepsilon_{sx} = \varepsilon_x \quad (2.3.1.12)$$

$$\varepsilon_{sy} = \varepsilon_y \quad (2.3.1.13)$$

2.3.2 Equilibrium Relationships

Again, consider the orthogonally reinforced membrane element of Figure 1. The average stress equilibrium relationships of the DSFM are the same as those of the MCFT. They are summarized as follows:

$$\sigma_x = f_{cx} + \rho_{sx} f_{sx} \quad (2.3.2.1)$$

$$\sigma_y = f_{cy} + \rho_{sy} f_{sy} \quad (2.3.2.2)$$

$$\tau_{xy} = v_{cxy} \quad (2.3.2.3)$$

Additionally, the DSFM incorporates the equilibrium relationships for local stresses at the crack.

$$f_{cl} = \rho_x (f_{scrx} - f_{sx}) \cos^2 \theta_{nx} + \rho_y (f_{scry} - f_{sy}) \cos^2 \theta_{ny} \quad (2.3.2.4)$$

$$v_{ci} = \rho_x (f_{scrx} - f_{sx}) \cos \theta_{nx} \cdot \sin \theta_{nx} + \rho_y (f_{scry} - f_{sy}) \cos \theta_{ny} \cdot \sin \theta_{ny} \quad (2.3.2.5)$$

Equilibrium of stress resultants normal to the crack surface results in the following equations:

$$f_{cl} = \rho_x (f_{scrx} - f_{sx}) \cos^2 \theta_{nx} + \rho_y (f_{scry} - f_{sy}) \cos^2 \theta_{ny} \quad (2.3.2.6)$$

$$v_{ci} = \rho_x (f_{scrx} - f_{sx}) \cos \theta_{nx} \cdot \sin \theta_{nx} + \rho_y (f_{scry} - f_{sy}) \cos \theta_{ny} \cdot \sin \theta_{ny} \quad (2.3.2.7)$$

The average concrete tensile stress is subject to the limits of the yield strength of the reinforcement traversing the crack:

$$f_{cl} \leq \rho_x (f_{sxyield} - f_{sx}) \cos^2 \theta_{nx} + \rho_y (f_{syyield} - f_{sy}) \cos^2 \theta_{ny} \quad (2.3.2.8)$$

Unlike the MCFT, however, the tensile stress is not subject to the limitation of shear stresses at a crack, since the DSFM explicitly incorporates deformations due to shear slip rather than ascribing a limiting stress corresponding to shear slip failure.

2.3.3 Constitutive Relationships

Between the development of the MCFT and the DSFM, the constitutive models for cracked concrete were revised and refined. Although a variety of alternative models are available, the following discussion presents the models of the DSFM.

As previously discussed, the response of concrete in compression depends on both the principal compressive strain and coexisting principal tensile strain. Analyses of additional test panels (Vecchio and Collins, 1993) led to the reduction factor, β_d , to reflect the softening effect of the coexisting principal tensile strains:

$$\beta_d = \frac{1}{1 + C_s C_d} \leq 1.0 \quad (2.3.3.1)$$

The factor, C_d , accounts for the softening effect of transverse tensile strains:

$$C_d = 0.35(-\varepsilon_{c1}/\varepsilon_{c2} - 0.28)^{0.8} \quad (2.3.3.2)$$

The factor C_s recognizes whether or not the analysis accounts for element slip deformations. If the analysis couples the inherent softening effect of shear slippage with the softening effect due to tensile strains (as in the MCFT), then $C_s = 1.0$. Conversely, if the analysis considers elements slip distortion, as in the DSFM, then the softening effect appears to be less for the same value of $\varepsilon_{c1}/\varepsilon_{c2}$ since the softening effect is attributable only to the tensile strains. In this case, $C_s = 0.55$.

To soften the compressive strength and stiffness of the concrete, the concrete cylinder strength, f'_c , and corresponding peak strain, ε_o , are both reduced by the reduction factor to determine the peak compressive stress, f_p , and corresponding peak strain ε_p :

$$f_p = -\beta_d f'_c \quad (2.3.3.3)$$

$$\varepsilon_p = -\beta_d \varepsilon_o \quad (2.3.3.4)$$

Using the softened parameters, the following relationship determines the relationship between the principal concrete compressive stress, f_{c2} , and the principal net compressive strain, ε_{c2} :

$$f_{c2} = f_p \frac{n(\varepsilon_{c2}/\varepsilon_p)}{(n-1) + (\varepsilon_{c2}/\varepsilon_p)^{nk}} \quad (2.3.3.5)$$

where

$$n = 0.80 - f_p/17 \quad (\text{in MPa}) \quad (2.3.3.6)$$

$$k = \begin{cases} 1.0 & \text{for } \varepsilon_p < \varepsilon_{c2} < 0 \\ 0.67 - f_p/62 & \text{for } \varepsilon_{c2} < \varepsilon_p < 0 \end{cases} \quad (2.3.3.7)$$

With regards to concrete in tension, the response before cracking is linear-elastic, as follows:

$$f_{c1} = E_c \cdot \varepsilon_{c1} \quad \text{for } 0 \leq \varepsilon_{c1} \leq \varepsilon_{cr} \quad (2.3.3.8)$$

For cracked concrete, average concrete tensile stresses, f_{c1}^a , due to tension stiffening, can be generally be modeled by the nonlinearly decaying relationship (but must not exceed the bound imposed by equation 2.3.2.6):

$$f_{c1}^a = \frac{f_t}{1 + \sqrt{c_t \varepsilon_{c1}}} \quad \text{for } \varepsilon_{cr} < \varepsilon_{c1} \quad (2.3.3.9)$$

The coefficient, c_t , proposed by Bentz (1999) incorporates the influence of reinforcement bond characteristics and is computed as follows:

$$c_t = 2.2m \quad (2.3.3.10)$$

$$\frac{1}{m} = \sum_{i=1}^n \frac{4\rho_i}{d_{b_i}} |\cos \theta_{n_i}| \quad (\text{in mm}) \quad (2.3.3.11)$$

where d_{b_i} is the bar diameter and ρ_i is the reinforcement ratio of each of the n reinforcement components.

In addition to tension stiffening, post-cracking tensile stresses, f_{cl}^b , arise in plain concrete due to fracture mechanisms – a phenomenon known as tension softening. Tension softening effects may be significant in lightly reinforced concrete structures. The cracking tensile stress due to tension softening may be calculated by the following linear relationship:

$$f_{cl}^b = f_t \left[1 - \frac{(\varepsilon_{cl} - \varepsilon_{cr})}{(\varepsilon_{ts} - \varepsilon_{cr})} \right] \quad \text{for } \varepsilon_{cr} < \varepsilon_{cl} < \varepsilon_{ts} \quad (2.3.3.12)$$

The terminal strain, ε_{ts} , (the strain at which tensile stresses in plain concrete reduce to zero) is determined from the fracture energy parameter, G_f , (the area under the stress-strain curve of plain concrete, assumed to be 75 N/m), and the characteristic length, L_r , (assumed to be half the crack spacing):

$$\varepsilon_{ts} = 2.0 \frac{G_f}{f_t \cdot L_r} \quad (2.3.3.13)$$

Finally, the post-cracking principal tensile stress in the concrete is taken as the larger of the values predicted by the tension stiffening and tension softening phenomena:

$$f_{cl} = \max(f_{cl}^a, f_{cl}^b) \quad (2.3.3.14)$$

The DSFM constitutive model for reinforcement in tension or compression is trilinear to account for strain-hardening phenomenon:

$$f_s = \begin{cases} E_s \cdot \varepsilon_s & \text{for } 0 < \varepsilon_s < \varepsilon_{yield} \\ f_{yield} & \text{for } \varepsilon_{yield} < \varepsilon_s < \varepsilon_{sh} \\ f_{yield} + E_{sh}(\varepsilon_s - \varepsilon_{sh}) & \text{for } \varepsilon_{sh} < \varepsilon_s < \varepsilon_u \\ 0 & \text{for } \varepsilon_u < \varepsilon_s \end{cases} \quad (2.3.3.15)$$

where E_s is the elastic modulus of the reinforcement, $f_{s,yield}$ is the yield strength of the reinforcement, $\varepsilon_{s,yield}$ is the yield strain of the reinforcement, $\varepsilon_{s,h}$ is the strain at the onset of strain hardening, ε_u is the ultimate strain of the reinforcement.

2.3.4 Shear Slip Relationships

Having defined the compatibility, equilibrium and constitutive relationships, it remains necessary to model the crack slip, δ_s , to determine the crack slip shear strain, γ_s . One approach is to relate the crack slip to the local shear stresses, v_{ci} , at the crack. Based on the analysis of aggregate interlock by Walraven (1981), the following relationship may be used to determine the crack-slip and shear slip strain:

$$\delta_s^a = \frac{v_{ci}}{1.8w^{-0.8} + (0.234w^{-0.707} - 0.20) \cdot f_{cc}} \quad (2.3.4.1)$$

$$\gamma_s^a = \frac{\delta_s^a}{s} \quad (2.3.4.2)$$

where f_{cc} is the concrete cube strength, w is the average crack spacing and s is the average crack spacing.

However, the above approach is problematic in two respects. First, the equilibrium equation 2.3.2.5 predicts that the shear stress at a crack, and hence the crack slip, are always zero for unreinforced elements. This is equivalent to ignoring crack shear stresses arising from aggregate interlock – the sliding friction between the exposed aggregate and cement paste at the crack and the plastic deformation of the cement paste due to contact stresses. Secondly, the slip relationship does not account for the initial crack slip that occurs before contact areas develop between the rough crack surfaces.

To address these deficiencies, a second approach for modeling the shear slip is to specify a constant rotation lag, θ^l , between the inclination of the principal total strain axis, θ_ε and the inclination of the principal stress axis, θ_σ . Indeed, results of panel tests indicate that the lag is established soon after cracking, and generally falls in the range of 5° to 10° until the yielding of a reinforcement component, whereupon the lag increases. To implement this approach, it is necessary to define the post-cracking rotation, $\Delta\theta_\varepsilon$, of the principal total strain axis, relative to the orientation of the principal strains and stresses at initial cracking, θ_{ic} :

$$\Delta\theta_\varepsilon = \theta_\varepsilon - \theta_{ic}$$

(2.3.4.3)

The post-cracking rotation, $\Delta\theta_\sigma$, of the principal stress field is then related to $\Delta\theta_\varepsilon$, by the constant rotation lag is follows:

$$\Delta\theta_\sigma = \begin{cases} \Delta\theta_\varepsilon & \text{for } |\Delta\theta_\varepsilon| \leq \theta^l \\ (\Delta\theta_\varepsilon - \theta^l) & \text{for } |\Delta\theta_\varepsilon| > \theta^l \end{cases} \quad (2.3.4.4)$$

The orientation of the principal stress field is determined as the sum its orientation at initial cracking, and its post-cracking rotation:

$$\theta_\sigma = \theta_{ic} + \Delta\theta_\sigma \quad (2.3.4.5)$$

Finally, relationships from Mohr's circle determine the shear slip strain, γ_s^b :

$$\gamma_s^b = \gamma_{xy} \cdot \cos 2\theta_\sigma + (\varepsilon_y - \varepsilon_x) \cdot \sin 2\theta_\sigma \quad (2.3.4.6)$$

Further, it is possible to combine the two approaches in a hybrid model for shear slip. The shear slip strain is computed by both approaches and the larger of values is utilized:

$$\gamma_s = \max(\gamma_s^a, \gamma_s^b) \quad (2.3.4.7)$$

When the concrete element is unreinforced or when the local shear stress on the crack is small, the constant rotation lag governs the shear slip, reflecting the initial slip occurring prior to development of shear stresses at a crack. Conversely, when the shear stresses on the crack are large, the shear slip is predicted by the stress-based formulation. As such, using the both approaches collectively is consistent with the actual determinants of the shear slip.

2.4 Finite Element Implementation

Displacement-based finite element methods for structural analysis result in a system of equations relating unknown nodal displacements to specified forces by the structure stiffness matrix. The VecTor2 algorithm for nonlinear finite element analysis is summarized by the flow chart in Figure 7. The following discussion describes the details of some of these steps.

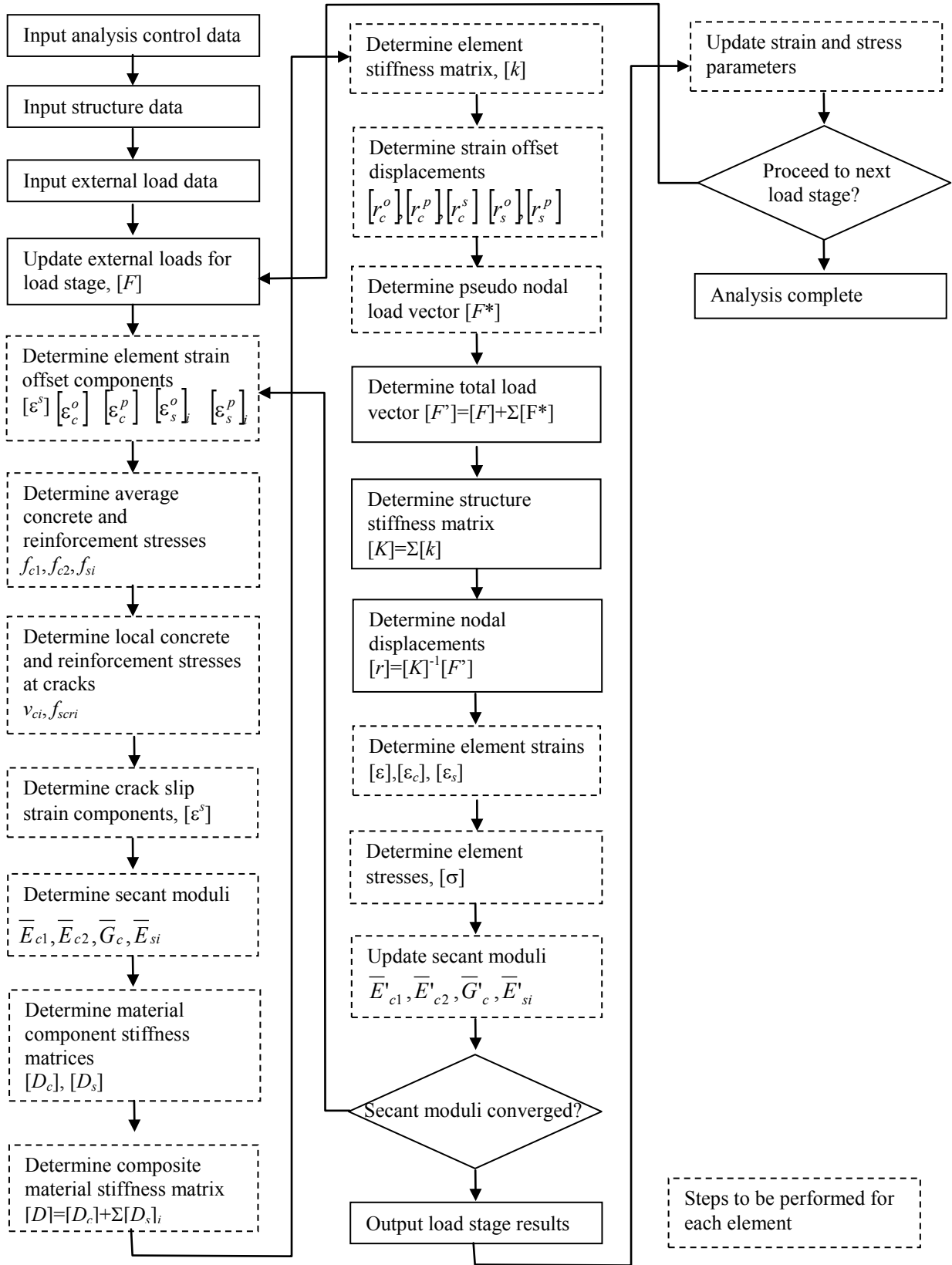


Figure 7 VecTor2 nonlinear finite element analysis algorithm

2.4.1 Composite Material Stiffness Matrix

In the most general case, total strains, $[\varepsilon] = [\varepsilon_x, \varepsilon_y, \gamma_{xy}]^T$, are comprised of net concrete strains $[\varepsilon_c]$, elastic strain offsets $[\varepsilon_c^o]$ (due to thermal, prestrains, shrinkage and lateral expansion effects), plastic strain offsets in the concrete, $[\varepsilon_c^p]$, (due to cyclic loading or damage), and strains due to crack shear slip, $[\varepsilon^s]$ (as considered by the DSFM).

$$[\varepsilon] = [\varepsilon_c] + [\varepsilon_c^o] + [\varepsilon_c^p] + [\varepsilon^s] \quad (2.4.1.1)$$

As well, compatibility relationships determine that the strain in the i^{th} smeared reinforcement component is the sum of the total strain, elastic strain offsets $[\varepsilon_s^o]$ (due to thermal and prestrain effects) and plastic strain offsets $[\varepsilon_s^p]$ (due to cyclic loading or damage):

$$[\varepsilon_s]_i = [\varepsilon] + [\varepsilon_s^o]_i + [\varepsilon_s^p]_i \quad (2.4.1.2)$$

At any point within the reinforced concrete continuum, the total strains are related to stresses $[\sigma]$ by the composite material stiffness matrix, $[D]$, as follows:

$$[\sigma] = [D][\varepsilon] - [\sigma^o] \quad (2.4.1.3)$$

The composite material stiffness matrix is the sum of the concrete material stiffness matrix, $[D_c]$, and the reinforcement component material stiffness matrices, $[D_s]_i$, as follows

$$[D] = [D_c] + \sum_{i=1}^n [D_s]_i \quad (2.4.1.4)$$

While the composite material stiffness matrix operates on total strains, element stresses can be directly related only to net strains of the concrete and reinforcement. Therefore, it is necessary to subtract the stress contribution of strain offsets and shear slip strains by use of the pseudo stress vector $[\sigma^o]$ calculated as follows:

$$[\sigma^o] = [D_c] \{ [\varepsilon_c^o] + [\varepsilon_c^p] + [\varepsilon^s] \} + \sum_{i=1}^n [D_s]_i \{ [\varepsilon_s^o]_i + [\varepsilon_s^p]_i \} \quad (2.4.1.5)$$

As the MCFT and DSFM model the reinforced concrete as an orthotropic material in the principal stress directions, it is necessary to formulate the concrete material stiffness matrix, $[D_c]'$, relative to these directions. If it is assumed that the Poisson's effect is negligible, then $[D_c]'$ is computed as follows:

$$[D_c]' = \begin{bmatrix} \bar{E}_{c1} & 0 & 0 \\ 0 & \bar{E}_{c2} & 0 \\ 0 & 0 & \bar{G}_c \end{bmatrix} \quad (2.4.1.6)$$

The secant moduli \bar{E}_{c1} , \bar{E}_{c2} , \bar{G}_c , as shown in Figure 8, are computed from the current values of the principal stresses, f_{c1} and f_{c2} , and the corresponding principal net concrete strains, ε_{c1} and ε_{c2} , as follows:

$$\bar{E}_{c1} = \frac{f_{c1}}{\varepsilon_{c1}}; \bar{E}_{c2} = \frac{f_{c2}}{\varepsilon_{c2}}; \bar{G}_c = \frac{\bar{E}_{c1} \cdot \bar{E}_{c2}}{\bar{E}_{c1} + \bar{E}_{c2}} \quad (2.4.1.7)$$

Likewise, material stiffness matrices $[D_s]_i'$ for each reinforcement component must first be determined relative to their longitudinal axes. As the reinforcement is assumed only to resist uniaxial stresses, $[D_s]_i'$ is computed as follows:

$$[D_s]_i' = \begin{bmatrix} \rho_i \bar{E}_{si} & 0 & 0 \\ 0 & 0 & 0 \\ 0 & 0 & 0 \end{bmatrix} \quad (2.4.1.8)$$

where ρ_i is the reinforcement ratio of the reinforcement component. The secant modulus \bar{E}_{si} , as shown in Figure 8, is computed from its current value of stress, f_{si} and the corresponding strain, ε_{si} as follows:

$$\bar{E}_{si} = \frac{f_{si}}{\varepsilon_{si}} \quad (2.4.1.9)$$

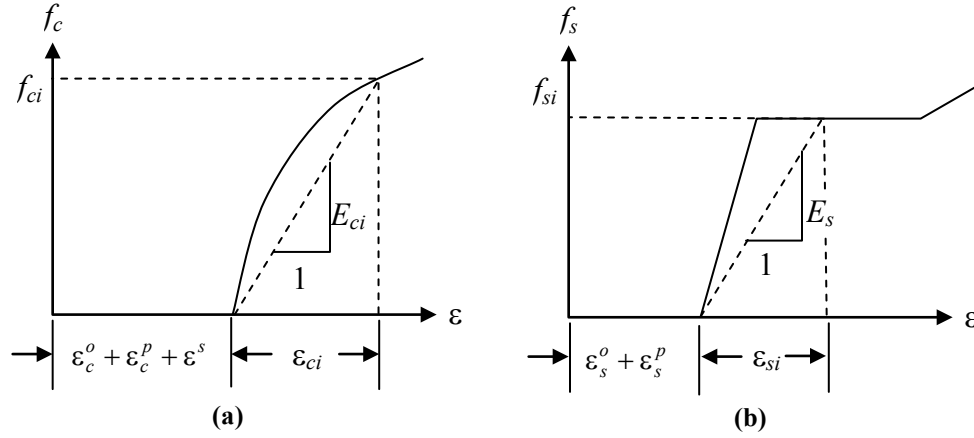


Figure 8: Definition of secant moduli for a) concrete b) reinforcement

Likewise, in the case of FRC, the material stiffness matrix for fibres can be determined based on the net strains in the direction of the crack. The fibre material stiffness matrix, $[D_f]'$, is computed as follows:

$$[D_f]' = \begin{bmatrix} \overline{E_{f1}} & 0 & 0 \\ 0 & 0 & 0 \\ 0 & 0 & 0 \end{bmatrix} \quad (2.4.1.10)$$

The secant modulus, $\overline{E_{f1}}$, is computed from the tensile stress attained by fibres which is averaged between cracks and from the strain:

$$\overline{E_{f1}} = \frac{\alpha_{avg} f_f}{\epsilon_{cf}} \quad (2.4.1.11)$$

$$\epsilon_{cf} = \frac{\epsilon_{c1} + \epsilon_{c2}}{2} + \frac{\epsilon_{c1} - \epsilon_{c2}}{2} \cos 2\theta_f \quad (2.4.1.12)$$

$$\theta_f = \tan^{-1} \frac{\delta_s}{w_{cr}} \quad (2.4.1.13)$$

The material stiffness matrices, $[D_c]'$, $[D_f]'$, and $[D_s]_i'$, are transformed from their respective principal axes to the x,y axes by means of the transformation matrix, $[T]$, as follows:

$$[D_c] = [T_c]^T [D_c]_i' [T_c] + [T_f]^T [D_f]_i' [T_f] \quad (2.4.1.14)$$

where $[T_c]$ is calculated using θ_σ , and $[T_f]$ is calculated using $\theta_\sigma + \theta_f$, and:

$$[D_s]_i = [T_s]_i^T [D_s]_i' [T_s]_i \quad (2.4.1.15)$$

$$[T] = \begin{bmatrix} \cos^2 \psi & \sin^2 \psi & \cos \psi \cdot \sin \psi \\ \sin^2 \psi & \cos^2 \psi & -\cos \psi \cdot \sin \psi \\ -2 \cos \psi \cdot \sin \psi & 2 \cos \psi \cdot \sin \psi & (\cos^2 \psi - \sin^2 \psi) \end{bmatrix} \quad (2.4.1.16)$$

For the concrete, the angle ψ is the inclination of the principal tensile stress axis, θ_σ , with respect to the positive x-axis. For the fibres, the angle ψ is the inclination of the principal tensile stress axis, $\theta_\sigma + \theta_f$ with respect to the positive x-axis. For the reinforcement, the angle ψ is the orientation, α_i , of each reinforcement component, with respect to the positive x-axis.

2.4.2 Element Stiffness Matrices

The element stiffness matrix, $[k]$ relates nodal forces to nodal displacements of the element. It is determined from the composite material stiffness matrix as follows:

$$[k] = \int_{vol} [B]^T [D] [B] dV \quad (2.4.2.1)$$

The strain-displacement matrix $[B]$, interpolates strains throughout the element continuum by operating on nodal displacements of the element. The form of the strain-displacement matrix depends on the type of the element, and the resulting value of the above integration will depend on the composite material stiffness matrix, the element geometry and the exactness of the integration method.

It is also possible to separate the element stiffness matrix into contributions from the stiffness of the concrete, $[k_c]$, and stiffness of the reinforcement components, $[k_s]_i$, by substituting the respective material stiffness matrix for the composite material stiffness matrix:

$$[k_c] = \int_{vol} [B]^T [D_c] [B] dV \quad (2.4.2.2)$$

$$[k_s]_i = \int_{vol} [B]^T [D_s]_i [B] dV \quad (2.4.2.3)$$

2.4.3 Pseudo Nodal Loads

The element stiffness matrix operates on total nodal displacements in a manner that is analogous to the material stiffness matrix operating on total strains. Like the use of the pseudo-stress vector, it is necessary to subtract the nodal force contributions of the nodal displacements due to strain offsets and crack shear slip by the use of a pseudo nodal load vector.

First, the offset and crack shear slip strains are resolved into components relative to the x,y axes.

For the concrete:

$$\begin{bmatrix} \varepsilon_c^o \end{bmatrix} = \begin{bmatrix} \varepsilon_c^o \\ \varepsilon_c^o \\ 0 \end{bmatrix}; \begin{bmatrix} \varepsilon_c^p \end{bmatrix} = \begin{bmatrix} \varepsilon_{cx}^p \\ \varepsilon_{cy}^p \\ \gamma_{cxy}^p \end{bmatrix}; \begin{bmatrix} \varepsilon_c^s \end{bmatrix} = \begin{bmatrix} \varepsilon_x^s \\ \varepsilon_y^s \\ \gamma_{xy}^s \end{bmatrix} \quad (2.4.3.1)$$

For the reinforcement components:

$$\begin{bmatrix} \varepsilon_s^o \end{bmatrix}_i = \begin{bmatrix} \varepsilon_{si}^o \cdot (1 + \cos 2\alpha_i)/2 \\ \varepsilon_{si}^o \cdot (1 - \cos 2\alpha_i)/2 \\ \varepsilon_{si}^o \cdot \sin 2\alpha_i \end{bmatrix}; \begin{bmatrix} \varepsilon_s^p \end{bmatrix}_i = \begin{bmatrix} \varepsilon_{si}^p \cdot (1 + \cos 2\alpha_i)/2 \\ \varepsilon_{si}^p \cdot (1 - \cos 2\alpha_i)/2 \\ \varepsilon_{si}^p \cdot \sin 2\alpha_i \end{bmatrix} \quad (2.4.3.2)$$

where α_i is the orientation of the reinforcement component relative to positive x-axis.

Integration of these strain components results in free nodal displacements $\begin{bmatrix} r_c^o \end{bmatrix}, \begin{bmatrix} r_c^p \end{bmatrix}, \begin{bmatrix} r_c^s \end{bmatrix}$, due to concrete offset strains and shear slip, and displacements $\begin{bmatrix} r_s^o \end{bmatrix}, \begin{bmatrix} r_s^p \end{bmatrix}$ due to reinforcement strain offsets, as follows:

$$\begin{bmatrix} r_c^o \end{bmatrix} = \int \begin{bmatrix} \varepsilon_c^o \end{bmatrix} dA; \begin{bmatrix} r_c^p \end{bmatrix} = \int \begin{bmatrix} \varepsilon_c^p \end{bmatrix} dA; \begin{bmatrix} r_c^s \end{bmatrix} = \int \begin{bmatrix} \varepsilon_c^s \end{bmatrix} dA \quad (2.4.3.3)$$

$$\begin{bmatrix} r_s^o \end{bmatrix} = \int \begin{bmatrix} \varepsilon_s^o \end{bmatrix} dA; \begin{bmatrix} r_s^p \end{bmatrix} = \int \begin{bmatrix} \varepsilon_s^p \end{bmatrix} dA \quad (2.4.3.4)$$

The pseudo nodal loads, $[F^*]$, required to produce equivalent nodal displacements for each element are determined by multiplying the free nodal displacements by the contributions of the concrete and reinforcement to the element stiffness matrix:

$$[F^*] = [k_c] \left\{ \begin{bmatrix} r_c^o \end{bmatrix} + \begin{bmatrix} r_c^p \end{bmatrix} + \begin{bmatrix} r_c^s \end{bmatrix} \right\} + \sum_{i=1}^n [k_s]_i \left\{ \begin{bmatrix} r_s^o \end{bmatrix} + \begin{bmatrix} r_s^p \end{bmatrix} \right\} \quad (2.4.3.5)$$

The pseudo nodal loads are added to the applied external loads, $[F]$, to determine the total nodal force vector, $[F']$:

$$[F'] = [F] + [F^*] \quad (2.4.3.6)$$

2.4.4 Total Load Iterative Secant Stiffness Solution

The global stiffness matrix, $[K]$, of the entire structure is assembled by the summation of all the element stiffness matrices:

$$[K] = \sum_{i=1}^m [k]_i \quad (2.4.4.1)$$

Having determined the global stiffness matrix and the total nodal load vector, the following system of equations results involving the unknown nodal displacements, $[r]$:

$$[F'] = [K][r] \quad (2.4.4.2)$$

Providing the structure is adequately restrained, the unknown nodal displacements are determined by pre-multiplying total nodal load vector by the inverse of the global stiffness matrix:

$$[r] = [K]^{-1} [F'] \quad (2.4.4.3)$$

The total element strains are determined from the nodal displacements, utilizing the strain-displacement matrix.

$$[\varepsilon] = [B][r] \quad (2.4.4.4)$$

The shear and normal stresses acting upon the element are determined by multiplying the element strains by the material stiffness matrices and subtracting the pseudo stress vector:

$$[\sigma] = [D_c] \{ [\varepsilon] - [\varepsilon_c^o] - [\varepsilon_c^p] - [\varepsilon^s] \} + [D_s] \{ [\varepsilon] - [\varepsilon_s^o] - [\varepsilon_p^o] \} \quad (2.4.4.5)$$

However, the secant moduli, \bar{E} , used to determine the structure stiffness matrix are only estimates that are initially based on the stress-strain state of the previous load step. Owing to the finite size of each load step, the stress-strain state corresponding to the current load step differs from that of the previous load step by a finite amount, resulting in an error in the computed nodal displacements. The error can be made arbitrarily small by an iterative refining the secant moduli. The secant moduli are recomputed as \bar{E}' for the calculated stress-strain state, and then averaged with the assumed values \bar{E} as follows:

$$\bar{E}_{(i+1)} = (1 - c) \cdot \bar{E}_i + c \cdot \bar{E}'_i \quad (2.4.4.6)$$

where c is a specified convergence averaging factor and i is the iteration number. When the secant moduli have acceptably converged or a specified number of iterations have been performed, VecTor2 concludes the analysis for the load step, stores the analysis results and proceeds to the next load step, if any.

2.5 Augmented Analysis Features

While the MCFT and DSFM form the basis for VecTor2, the program has been augmented to model the effects of lateral expansion, triaxial stresses, cyclic and reverse cyclic loading, construction and loading chronology, and bond slip. Each of these features is subsequently described.

2.5.1 Modeling of Lateral Expansion Effect

When reinforced concrete is uncracked or experiences relatively small tensile strains, lateral expansion may account for a significant portion of the total strains in the principal maximum strain direction. If these strains are incorrectly attributed to tensile straining due to stress, the compression softening effect may be overestimated. To address this potential inaccuracy, Vecchio (1992) implements concrete lateral expansion effects by modifying the formulation of the concrete material stiffness matrix.

For a linear-elastic material that is orthotropic in the principal directions, plane stresses

$[\sigma_1 \ \sigma_2 \ \tau_{12}]^T$ are related to plane strains $[\varepsilon_1 \ \varepsilon_2 \ \gamma_{12}]^T$, by the material stiffness matrix, $[D]$:

$$[D] = \frac{1}{1 - \nu_{12}\nu_{21}} \begin{bmatrix} E_1 & \nu_{12}E_1 & 0 \\ \nu_{21}E_2 & E_2 & 0 \\ 0 & 0 & (1 - \nu_{12}\nu_{21})G_{12} \end{bmatrix} \quad (2.5.1.1)$$

where, ν_{12} is the Poisson ratio relating ε_1 to σ_2 , and ν_{21} is the Poisson ratio relating ε_2 to σ_1 . The number of independent constants is reduced if the shear modulus, G_c , is approximated as follows:

$$G_{12} \approx \frac{E_1 E_2}{E_1(1 + \nu_{12}) + E_2(1 + \nu_{21})} \quad (2.5.1.2)$$

Further, the reciprocity requires that the strain energy of the element be independent of the sequence of loading. It follows that the remaining four constants are related as follows:

$$\nu_{12}E_1 = \nu_{21}E_2 \quad (2.5.1.3)$$

As the above terms are the off-diagonal elements of the $[D]$, the above condition is necessary for the symmetry of $[D]$. If it is assumed that the Poisson's ratio is zero, and the elastic moduli are replaced by secant moduli for concrete, the concrete material stiffness matrix of equation 2.4.1.5 results.

The response of concrete violates the above condition, such that the material stiffness matrix becomes unsymmetrical. As concrete is subjected to increasing compressive stress, progressive internal micro-cracking accelerates the rate of lateral expansion. The same mechanism is responsible for the softening of the compression stress-strain response. Therefore, it is generally true for $f_{c2} < f_{c1} < 0$, that $\nu_{12} > \nu_{21}$, $E_{c1} > E_{c2}$ and $\nu_{12}E_{c1} \neq \nu_{21}E_{c2}$.

This difficulty is circumvented by separating the lateral expansion effects into elastic and residual components. The elastic component is modeled by a symmetric concrete material stiffness matrix, while the residual component is modeled by elastic strain offsets, $[\varepsilon_c^o]$, as described in the preceding section. For the purpose of illustration, consider an element subject to biaxial compression such that $f_{c2} < f_{c1} < 0$. The strains in the principal directions due to the Poisson's effect are as follows:

$$\varepsilon_{c1} = -\nu_{12} \frac{f_{c2}}{\bar{E}_{c2}} \quad (2.5.1.4)$$

$$\varepsilon_{c2} = -\nu_{21} \frac{f_{c1}}{E_{c1}} \quad (2.5.1.5)$$

For the reasons stated above, suppose that the lateral expansion, ε_{c2} , is smaller than the lateral expansion ε_{c1} . The lateral expansion ε_{c2} is modeled entirely by the elastic component, while the lateral expansion ε_{c1} is modeled by both residual and elastic components. The elastic component of the Poisson's ratio, ν_{12}^e , is computed by the reciprocity condition:

$$\nu_{12}^e = \nu_{21} \frac{\bar{E}_{c2}}{E_{c1}} \quad (2.5.1.6)$$

The elastic components of the lateral expansion effects are implemented in the symmetric concrete material stiffness matrix, $[D_c]$ as follows:

$$[D_c] = \frac{1}{1 - \nu_{12}^e \nu_{21}^e} \begin{bmatrix} \bar{E}_{c1} & \nu_{12}^e \bar{E}_{c1} & 0 \\ \nu_{21}^e \bar{E}_{c2} & \bar{E}_{c2} & 0 \\ 0 & 0 & (1 - \nu_{12}^e \nu_{21}^e) \bar{G}_{c12} \end{bmatrix} \quad (2.5.1.7)$$

where,

$$\bar{G}_{c12} = \frac{\bar{E}_{c1} \bar{E}_{c2}}{\bar{E}_{c1}(1 + \nu_{12}^e) + \bar{E}_{c2}(1 + \nu_{21}^e)} \quad (2.5.1.8)$$

The residual component of the Poisson's ratio, ν_{12}^* , is the remaining portion of the expansion:

$$\nu_{12}^* = \nu_{12} - \nu_{12}^e \quad (2.5.1.9)$$

The residual component of the lateral expansion in the 1-direction is computed as an elastic strain offset using the residual component of the Poisson's ratio:

$$\varepsilon_{c1}^o = -\nu_{12}^* \frac{f_{c2}}{E_{c2}} \quad (2.5.1.10)$$

Models for determining the value of Poisson's ratio are described in subsequent sections.

2.5.2 Modeling of Triaxial Stresses

Although the MCFT is formulated for the plane stress state, VecTor2 accounts for out-of-plane stresses in the z-direction due to confinement of lateral expansion by out-of-plane reinforcement. The triaxial stress state is then utilized in computing the strength enhancement effects due to confinement. The out-of-plane concrete strain is computed as follows:

$$\varepsilon_{cz} = \frac{E_c}{E_c + \rho_z \cdot E_{sz}} \left(-\nu_{12} \frac{f_{c2}}{E_{c2}} - \nu_{21} \frac{f_{c1}}{E_{c1}} \right) \quad (2.5.2.1a)$$

where ρ_z is the reinforcement ratio of the out-of plane reinforcement. If however, the out-of-plane reinforcement has yielded, the out-of-plane concrete strain is computed as follows:

$$\varepsilon_{cz} = -\frac{\rho_z \cdot f_{z,yield}}{E_c} - \nu_{12} \frac{f_{c2}}{E_{c2}} - \nu_{21} \frac{f_{c1}}{E_{c1}} \quad (2.5.2.1b)$$

The stress, f_{sz} , in the out-of-plane reinforcement is determined as follows:

$$f_{sz} = E_s \varepsilon_{cz} \leq f_{z,yield} \quad (2.5.2.2)$$

where $f_{z,yield}$ is the yield strength of the out-of-plane reinforcement.

The resulting out-of-plane concrete compressive stress, f_{cz} , is determined from equilibrium as follows:

$$f_{cz} = -\rho_z \cdot f_{sz}$$

(2.5.2.3)

2.5.3 Analysis of Cyclically Loaded Structures

A simplifying assumption of the MCFT is ignoring the effect of strain history in determining the stress-strain response of the concrete and reinforcement components. Therefore, the constitutive relationships described so far correlate a unique stress value for any strain value. While this is adequate for monotonic loading, it is not adequate for cyclic loading due to the hysteretic response of concrete and reinforcement. When subjected to load reversals, these materials exhibit non-coincident stress-strain responses, which give rise to plastic strain offsets. Moreover, the hysteretic responses depend upon the plastic strain offset and maximum strains and stresses previously experienced by the materials. The hysteretic response of concrete and reinforcement are described as material models in subsequent sections. The following discussion describes how VecTor2 records the plastic strains and strain envelopes for the concrete.

When considering constitutive relationships for concrete, the pertinent strain directions are those parallel to the principal net concrete strains. However, these axes rotate as the load changes. As such, VecTor2 records concrete plastic strains and strain envelopes with respect to the x,y axes and transforms them to and from arbitrary orientations of the principal axes using relationships from Mohr's circle.

If the inclination of the principal net concrete strains is θ , then the following relationships transform plastic strains, $\varepsilon_{cx}^p, \varepsilon_{cy}^p, \gamma_{cxy}^p$, with respect to the X,Y axes to plastic strains, $\varepsilon_{c1}^p, \varepsilon_{c2}^p$, with respect to the principal 1,2 directions:

$$\varepsilon_{c1}^p = \frac{\varepsilon_{cx}^p + \varepsilon_{cy}^p}{2} + \frac{\varepsilon_{cx}^p - \varepsilon_{cy}^p}{2} \cdot \cos 2\theta + \gamma_{cxy}^p \cdot \sin 2\theta \quad (2.5.3.1)$$

$$\varepsilon_{c2}^p = \frac{\varepsilon_{cx}^p + \varepsilon_{cy}^p}{2} - \frac{\varepsilon_{cx}^p - \varepsilon_{cy}^p}{2} \cdot \cos 2\theta - \gamma_{cx}^p \cdot \sin 2\theta \quad (2.5.3.2)$$

In a given load step, the plastic strains change by the quantities $\Delta\varepsilon_{c1}^p$ and $\Delta\varepsilon_{c2}^p$, with respect to the principal 1 and 2 directions, respectively. The following relationships transform the plastic strain increments and add them to the previous plastic strains to update the plastic strains with respect to the x,y axes:

$$\varepsilon_{cx}^p' = \varepsilon_{cx}^p + \frac{\Delta\varepsilon_{c1}^p}{2} \cdot (1 + \cos 2\theta) + \frac{\Delta\varepsilon_{c2}^p}{2} \cdot (1 - \cos 2\theta) \quad (2.5.3.3)$$

$$\varepsilon_{cy}^p' = \varepsilon_{cy}^p + \frac{\Delta\varepsilon_{c2}^p}{2} \cdot (1 - \cos 2\theta) + \frac{\Delta\varepsilon_{c1}^p}{2} \cdot (1 + \cos 2\theta) \quad (2.5.3.4)$$

$$\gamma_{cxy}^p' = \gamma_{cxy}^p + \Delta\varepsilon_{c1}^p \cdot \sin 2\theta - \Delta\varepsilon_{c2}^p \cdot \sin 2\theta \quad (2.5.3.5)$$

Maximum concrete strains are defined by maximum compressive strains, ε_{cmx} , ε_{cmy} , and γ_{cmxy} , and maximum tensile strains ε_{tmx} , ε_{tmy} , and γ_{tmyx} , with respect to the X, Y directions. For brevity, the following discussion describes the treatment of the compressive strains only, but similar relationships result for the tensile strains. Although ε_{cmx} , ε_{cmy} , and γ_{cmxy} describe a compressive strain envelope, rather than a strain state, analogous relationships from Mohr's circle transform them to and from the principal and global axes.

The following relationships transform the maximum compressive strains, ε_{cmx} , ε_{cmy} , and γ_{cmxy} , with respect to the x,y axes to maximum compressive strains, strains ε_{cm1} and ε_{cm2} , with respect to the principal 1,2 directions:

$$\varepsilon_{cm1} = \frac{\varepsilon_{cmx} + \varepsilon_{cmy}}{2} + \frac{\varepsilon_{cmx} - \varepsilon_{cmy}}{2} \cdot \cos 2\theta + \gamma_{cmx} \cdot \sin 2\theta \quad (2.5.3.6)$$

$$\varepsilon_{cm2} = \frac{\varepsilon_{cmx} + \varepsilon_{cmy}}{2} - \frac{\varepsilon_{cmx} - \varepsilon_{cmy}}{2} \cdot \cos 2\theta - \gamma_{cmx} \cdot \sin 2\theta \quad (2.5.3.7)$$

In a given load step, the calculated principal net concrete strains are ε_{c1} and ε_{c2} . If these principal strains are more compressive than those described by ε_{cm1} and ε_{cm2} , then the envelope of compressive

strains must be updated. The incremental maximum compressive strains in the principal directions are defined as follows:

$$\Delta\varepsilon_{cm1} = \begin{cases} 0 & \text{if } \varepsilon_{c1} > \varepsilon_{cm1} \\ \varepsilon_{c1} - \varepsilon_{cm1} & \text{if } \varepsilon_{c1} < \varepsilon_{cm1} \end{cases} \quad (2.5.3.8)$$

$$\Delta\varepsilon_{cm2} = \begin{cases} 0 & \text{if } \varepsilon_{c2} > \varepsilon_{cm2} \\ \varepsilon_{c2} - \varepsilon_{cm2} & \text{if } \varepsilon_{c2} < \varepsilon_{cm2} \end{cases} \quad (2.5.3.9)$$

The following relationships transform the maximum compressive strain increments and add them to the previous maximum compressive strains to update the maximum compressive strains with respect to the x,y axes:

$$\varepsilon_{cmx}' = \varepsilon_{cmx} + \frac{\Delta\varepsilon_{cm1}}{2} \cdot (1 + \cos 2\theta) + \frac{\Delta\varepsilon_{cm2}}{2} \cdot (1 - \cos 2\theta) \quad (2.5.3.10)$$

$$\varepsilon_{cmy}' = \varepsilon_{cmy} + \frac{\Delta\varepsilon_{cm1}}{2} \cdot (1 - \cos 2\theta) + \frac{\Delta\varepsilon_{cm2}}{2} \cdot (1 + \cos 2\theta) \quad (2.5.3.11)$$

$$\gamma_{cmxy}' = \gamma_{cmxy} + \Delta\varepsilon_{cm1} \cdot \sin 2\theta - \Delta\varepsilon_{cm2} \cdot \sin 2\theta \quad (2.5.3.12)$$

Collectively, the plastic strains and strain envelopes and other stress envelope quantities allow VecTor2 to implement the hysteretic response models for the concrete. Likewise, VecTor2 records the strain and stress history of the reinforcement (without the additional complexity introduced by the transformations), to implement hysteretic response models for the reinforcement. The plastic strains resulting from the hysteretic response of both material components are treated by the pseudo nodal load approach described in the preceding section.

2.5.4 Analysis of Construction and Loading Chronology

Repaired reinforced concrete structures present an example where construction and loading chronologies significantly influence the load-deformation behavior. Initial loading of the original structure results in distress to the concrete and reinforcement materials. At some later time, possibly while still in service, the structure may be strengthened by casting of additional concrete, addition of reinforcing bars or the lay up of FRP composite materials. After repair, entirely new loads may be applied to the

repaired portions of the structure. The effectiveness of the repair procedure depends upon the load sharing between the original and newly added portions of the structure. In turn, this depends not only upon the final configuration of the structure and loads, but also the extent of damage prior to repair and the strain differentials between the original material and repair materials at the time of repair.

VecTor2 models construction and loading chronology by allowing elements to be engaged and disengaged during loading. Engaged elements represent portions of the structure that are currently present. They contribute to the strength and stiffness of the structure. Conversely, disengaged elements represent portions the structure that are currently absent. They do not contribute to the strength and stiffness of the structure. In cases where regions of a structure will be replaced by repair materials, engaged and disengaged elements occupy the same space in the mesh, resulting in a double meshed region.

At a given load stage, the total strains of disengaged elements, $[\varepsilon]$, are compatible with strains of the adjoining engaged elements. However, when disengaged elements are activated at a later load stage, the previously experienced total strains are recorded entirely as plastic strain offset strains, $[\varepsilon_c^p]$ and $[\varepsilon_s^p]$. Therefore, the newly engaged elements effectively behave as though they have been added in a zero elastic strain condition to previously engaged elements, which may be already distressed to some degree. At each load stage, the strain history of the elements are updated and recorded as necessary.

2.5.5 Bond-Slip Mechanisms

Bond action is the means by which stress transfers between the concrete and reinforcement and allows the two materials to behave compositely. As the concrete adjacent to reinforcement deforms, resisting bond stresses act tangentially to the reinforcement. In the case of embedded bar reinforcement, the bond stresses arise from chemical adhesion, friction and mechanical interlock with the concrete. In the case of externally bonded reinforcements, the bond stresses arise from the adhesive properties and shear resistance of materials adjoining the concrete and reinforcement. Bond action is critical in anchorage zones and near cracks, where high stress gradients in the reinforcement necessitate large bond stresses.

Perfect bond may exist in regions where bond stresses are sufficiently low. In this case, the change in reinforcement strain in response to loading is equal to the change in the total concrete strain. At higher levels of bond stress, damage to the bond results in imperfect bond action. Consequently, differential straining of the concrete and reinforcement occurs. This manifests as relative displacements or bond slip between the concrete and reinforcement. Among other factors, the bond stress is related to the extent of bond slip.

For many reinforced concrete structures subject to monotonic loading, proper reinforcement detailing ensures that the strength capacity is not governed by failure of bond action. The limited localized bond slip has minimal influence on the load-deformation response. For these structures, the perfect bond assumption of the MCFT is acceptable for modeling their behavior. In contrast, structures that are susceptible to bond failures may exhibit substantial bond slip that modifies the internal stress distribution and load-deformation response. As well, cyclically loaded structures experience a gradual degradation of bond that may significantly influence the hysteretic response.

VecTor2 models bond-slip mechanisms by use of the bond elements and bond stress-slip curves for embedded reinforcement and externally bonded reinforcement. The bond elements serve as deformable interfaces between concrete and discrete reinforcement elements, thereby removing the perfect bond relationship between the concrete and reinforcement materials. The stress-slip response of the bond elements is governed by the bond stress-slip curve. The bond stress-slip curves depend upon material properties, reinforcement layout and confining pressures.

2.5.6 Dynamic Analysis

2.5.6.1 Introduction

The structural modeling in FormWorks for dynamic analysis is much the same as for static analysis. The mesh generation and material model selection methods are identical for dynamic and static analysis. However, for certain dynamic analyses, parameters must be manually added to the analysis input files created by FormWorks.

2.5.6.2 Newmark Direct Integration Method: Newmark Beta and Gamma Factors

VecTor2 employs Newmark's method of direct integration to evaluate the dynamic response of structures. The iterative Newmark integration method was introduced in 1959 (Wilson, 2002).

$$u_t = u_{t-\Delta t} + \Delta t \dot{u}_{t-\Delta t} + \left(\frac{1}{2} - \beta\right) \Delta t^2 \ddot{u}_{t-\Delta t} + \beta \Delta t^2 \ddot{u}_t \quad (2.5.6.2.1)$$

$$\dot{u}_t = \dot{u}_{t-\Delta t} + (1 - \gamma) \Delta t \ddot{u}_{t-\Delta t} + \gamma \Delta t \ddot{u}_t \quad (2.5.6.2.2)$$

Updated in 1962 to eliminate the need for iteration and to introduce damping, the following equations resulted:

$$\ddot{u}_t = b_1(u_t - u_{t-\Delta t}) + b_2 \dot{u}_{t-\Delta t} + b_3 \ddot{u}_{t-\Delta t} \quad (2.5.6.2.3)$$

$$\dot{u}_t = b_4(u_t - u_{t-\Delta t}) + b_5 \dot{u}_{t-\Delta t} + b_6 \ddot{u}_{t-\Delta t} \quad (2.5.6.2.4)$$

where

$$b_1 = \frac{1}{\beta \Delta t^2}; \quad b_2 = \frac{1}{\beta \Delta t}; \quad b_3 = \beta - \frac{1}{2}; \quad b_4 = \gamma \Delta t b_1; \quad b_5 = 1 + \gamma \Delta t b_2; \quad b_6 = \Delta t(1 + \gamma b_3 - \gamma)$$

The Newmark Beta Factor, β , and Newmark Gamma Factor, γ , are the constants used in the method. The default value for γ in VecTor2 is 0.5; any other value will introduce artificial numerical damping to the solution (Saatci, 2007). The β factor determines how the acceleration changes within a time-step. A value of $\beta = 0.25$ is used in the integration when the acceleration is constant within a time-step (constant acceleration method), while $\beta = 1/6$ is typically used when the acceleration changes linearly through the time-step (linear acceleration method). The use of other values for β may greatly affect the accuracy and stability of the solution, and are therefore not often used. The constant acceleration method yielded the more stable results for the analyses found in Saatci (2007), and is the recommended method. Thus, the default value for β in VecTor2 is 0.25.

2.5.6.3 Damping

VecTor2 employs both Rayleigh and Alternative Damping. These two types of damping are discussed in more detail in Section 2.5.9.

2.5.6.4 Ground Acceleration

Ground acceleration can be used in dynamic modeling in VecTor2, and can be input in two ways. Ground acceleration may be specified in FormWorks or in a VECTOR.EQR file. The procedure for inputting this data is discussed in more detail in the FormWorks section of this manual.

2.5.7 **Accounting for Strain History**

Accounting for strain history is one of the analysis options in the *Model* tab of the *Define Job* dialog box. Accounting for strain history is the recommended option since it is important to consider previous loads, particularly when performing cyclic or reverse cyclic analyses. If previous loading is neglected, at the beginning of each new load stage, VecTor2 assumes that the structure is uncracked and not damaged in any way.

2.5.8 **Accounting for Strain Rate Effects**

Accounting for strain rate effects becomes important when modeling structures under impact loading or other high strain rate loading conditions. VecTor2 accounts for increased strain rates by calculating Dynamic Increase Factors (DIFs) for different material types and loading conditions. For concrete in tension and compression, the CEB-FIP 1990 Model Code DIFs are used. For both smeared and truss steel reinforcement, the CEB-FIP 1988 bulletin 187 DIF formulations are used. For structural steel, the DIFs are taken as 1 always.

In the following formulations, the DIF is equal to the ratio of the dynamic strength to the static strength, dynamic modulus to static modulus, or dynamic strain to static strain. The CEB-FIP 1990 Model Code provides the following formulations strain rate effects for concrete.

For concrete in compression, the following CEB-FIP formulations are valid for strain rates in the range of $30 \times 10^{-6} \text{s}^{-1} < |\dot{\epsilon}_c| < 3 \times 10^2 \text{s}^{-1}$ (CEB-FIP, 1990):

$$\frac{f_{cd}}{f_{cs}} = \begin{cases} \left(\frac{\dot{\epsilon}_c}{\dot{\epsilon}_0} \right)^{1.026\alpha} & \text{for } \dot{\epsilon}_c \leq 30 \text{ s}^{-1} \\ \gamma \left(\frac{\dot{\epsilon}_c}{\dot{\epsilon}_0} \right)^{\frac{1}{3}} & \text{for } \dot{\epsilon}_c > 30 \text{ s}^{-1} \end{cases} \quad (2.5.8.1)$$

where,

$$\alpha = \frac{1}{5+9\frac{f_{cs}}{f_{c0}}} \quad (2.5.8.2)$$

$$\gamma = 10^{6.156\alpha-2.0} \quad (2.5.8.3)$$

$$\dot{\varepsilon}_0 = 30 \times 10^{-6} \text{ s}^{-1}$$

$$f_{c0} = 10 \text{ MPa}$$

And $\dot{\varepsilon}_c$ is the strain rate, f_{cs} is the static compressive strength of concrete, f_{cd} is the dynamic compressive strength of concrete.

In VecTor2, the equation for γ is slightly different, and is calculated as follows:

$$\gamma = 10^{6.156\alpha-0.492} \quad (2.5.8.4)$$

For concrete in tension, for strain rates $3 \times 10^{-6} \text{ s}^{-1} < \dot{\varepsilon}_{ct} < 3 \times 10^2 \text{ s}^{-1}$, the following CEB-FIP formulations apply:

$$\frac{f_{td}}{f_{ts}} = \begin{cases} \left(\frac{\dot{\varepsilon}_{ct}}{\dot{\varepsilon}_0}\right)^{1.016\delta} & \text{for } \dot{\varepsilon}_{ct} \leq 30 \text{ s}^{-1} \\ \beta \left(\frac{\dot{\varepsilon}_{ct}}{\dot{\varepsilon}_0}\right)^{\frac{1}{3}} & \text{for } \dot{\varepsilon}_{ct} > 30 \text{ s}^{-1} \end{cases} \quad (2.5.8.5)$$

where,

$$\delta = \frac{1}{10+6\frac{f_{cs}}{f_{c0}}} \quad (2.5.8.6)$$

$$\beta = 10^{7.112\delta-2.33} \quad (2.5.8.7)$$

$$\dot{\varepsilon}_0 = 3 \times 10^{-6} \text{ s}^{-1}$$

$$f_{c0} = 10 \text{ MPa}$$

And f_{ts} is the static tensile strength of concrete, and f_{td} is the dynamic tensile strength of concrete. In VecTor2, the formulation for β is:

$$\beta = 10^{6.933\delta-0.492} \quad (2.5.8.8)$$

The CEB-FIP 1990 Model Code also provides a formulation for the effect of strain rate on the modulus of elasticity of concrete.

In compression, for compressive strain rates within the range of $30 \times 10^{-6} < |\dot{\varepsilon}| < 3 \times 10^2$:

$$\frac{E_{c,d}}{E_{c,i}} = \left(\frac{\dot{\varepsilon}_c}{\dot{\varepsilon}_{c0}}\right)^{0.026} \quad (2.5.8.9)$$

And in tension, for tensile strain rates within the range of $3 \times 10^{-6} \text{s}^{-1} < \dot{\varepsilon}_{ct} < 3 \times 10^2 \text{s}^{-1}$:

$$\frac{E_{c,d}}{E_{ci}} = \left(\frac{\dot{\varepsilon}_{ct}}{\dot{\varepsilon}_{ct0}} \right)^{0.016} \quad (2.5.8.10)$$

where,

$$\dot{\varepsilon}_{c0} = 30 \times 10^{-6} \text{s}^{-1} \text{ for compression}$$

$$\dot{\varepsilon}_{ct0} = 3 \times 10^{-6} \text{s}^{-1} \text{ for tension}$$

and $E_{c,d}$ is the dynamic modulus of elasticity, E_{ci} is the modulus of elasticity of concrete at 28 days, and $\dot{\varepsilon}_c$ is the strain rate.

The formulation employed in VecTor2 for peak strain at maximum load, valid for compressive strain rates of $30 \times 10^{-6} < |\dot{\varepsilon}| < 3 \times 10^2$ and tensile strains rates of $3 \times 10^{-6} \text{s}^{-1} < \dot{\varepsilon}_{ct} < 3 \times 10^2 \text{s}^{-1}$:

$$\frac{\varepsilon_{c1,d}}{\varepsilon_{c1}} = \left(\frac{\dot{\varepsilon}_c}{\dot{\varepsilon}_{c0}} \right)^{0.02} \quad (2.5.8.11)$$

where $\varepsilon_{c1,d}$ is the impact/dynamic strain at maximum load, ε_{c1} is the strain at maximum load for static loading, and $\dot{\varepsilon}_{c0}$ and $\dot{\varepsilon}_{ct0}$ have the same values as stated above.

For reinforcing steel, the CEB-FIP Bulletin 187 formulations are employed. The CEB-FIP formulations are valid for steel strain rates of $5 \times 10^{-5} \text{s}^{-1} \leq \dot{\varepsilon}_t \leq 10 \text{s}^{-1}$ for both smeared and truss bar reinforcement.

For the yield strength of reinforcement:

$$\frac{f_{y,d}}{f_y} = 1 + \frac{6}{f_y} \cdot \ln \left(\frac{\dot{\varepsilon}_t}{\dot{\varepsilon}_{t0}} \right) \quad (2.5.8.12)$$

And for ultimate strength of reinforcement steel:

$$\frac{f_{u,d}}{f_u} = 1 + \frac{7}{f_u} \cdot \ln \left(\frac{\dot{\varepsilon}_t}{\dot{\varepsilon}_{t0}} \right) \quad (2.5.8.13)$$

where

$$\dot{\varepsilon}_{t0} = 5 \times 10^{-5} \text{s}^{-1}$$

2.5.9 Structural Damping

Damping refers to the diminishing of the amplitude of the free vibration of a structure. The damping matrix for a given structure is determined from its modal damping ratios. VecTor2 offers two types of structural damping, Rayleigh Damping and Alternative Damping. In Rayleigh Damping, specifying the damping ratio for two damping modes defines the damping frequency for all modes. Alternative damping, consisting of the superposition of modal damping ratios, allows the user to specify zero viscous damping for the final damping modes.

2.5.9.1 Rayleigh Damping

One of the most common formulations for proportional damping is Rayleigh Damping. In Rayleigh Damping it is assumed that damping is proportional to both the mass and stiffness matrices (Chopra, 2007).

For mass-proportional damping, the generalized damping equation for the n th mode is

$$C_n = a_0 M_n \quad (2.5.9.1.1)$$

where the modal damping ratio is $\zeta_n = \frac{a_0}{2} \frac{1}{\omega_n}$.

To calculate a specific value of damping ratio for any one mode, the equation 11.4.3 can be modified as follows.

$$a_0 = 2\zeta_i \omega_i \quad (2.5.9.1.2)$$

Once a_0 is determined, the damping matrix and damping ratio for every other mode is determined.

Likewise, for stiffness-proportional damping, the coefficient a_1 is determined.

$$C_n = a_1 \omega_n^2 M_n \quad \text{and} \quad \zeta_n = \frac{a_1}{2} \omega_n; \quad a_1 = \frac{2\zeta_j}{\omega_j} \quad (2.5.9.1.3)$$

Combining both mass-proportional and stiffness-proportional damping, Rayleigh damping is defined as

$$c = a_0 m + a_1 k \quad (2.5.9.1.4)$$

Where the damping ratio is

$$\zeta_n = \frac{a_0}{2} \frac{1}{\omega_n} + \frac{a_1}{2} \omega_n \quad (2.5.9.1.5)$$

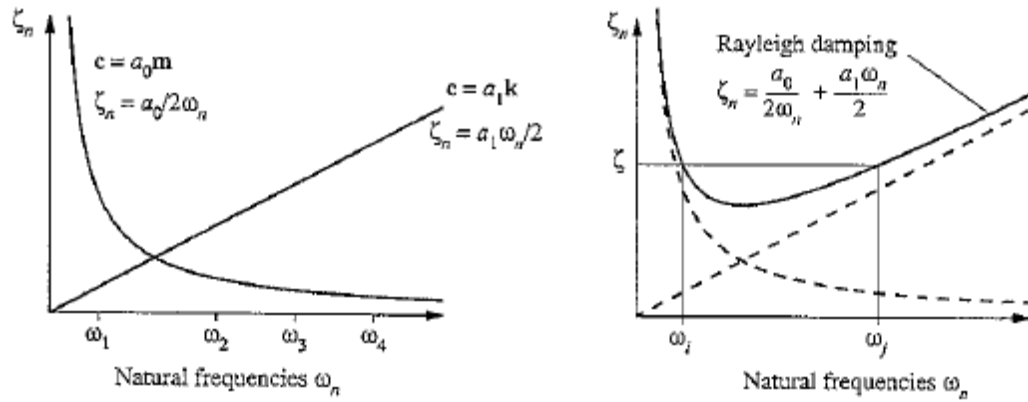


Figure 9: Rayleigh Damping (Chopra, 2007)

The coefficients a_0 and a_1 can be determined from the specific damping ratios ζ_i and ζ_j for the i th and j th modes.

$$\frac{1}{2} \begin{bmatrix} 1/\omega_i & \omega_i \\ 1/\omega_j & \omega_j \end{bmatrix} \begin{Bmatrix} a_0 \\ a_1 \end{Bmatrix} = \begin{Bmatrix} \zeta_i \\ \zeta_j \end{Bmatrix} \quad (2.5.9.1.6)$$

If the same damping ratio is assumed for both modes, a_1 and a_0 can be expressed as follows:

$$a_0 = \zeta \frac{2\omega_i\omega_j}{\omega_i + \omega_j} \quad \text{and} \quad a_1 = \zeta \frac{2}{\omega_i + \omega_j} \quad (2.5.9.1.7)$$

2.5.9.2 Alternative Damping

Alternative Damping allows for damping behavior for the first j modes and no viscous damping for the remaining modes.

The damping matrix for alternative damping is constructed as follows (Chopra, 2007):

$$c = m \left(\sum_{n=1}^N \frac{2\zeta_n\omega_n}{M_n} \phi_n \phi_n^T \right) m \quad (2.5.9.2.1)$$

where M_n is the generalized mass matrix, ϕ_n is the mode shape, m is the mass matrix, N is the total dynamic degrees of freedom.

The generalized mass for the n th mode is:

$$M_n = \phi_n^T \times m \times \phi_n \quad (2.5.9.2.2)$$

The n th term in the big equation is the contribution of the n th mode to the damping matrix. Only the first j modes in equation contribute to the damping response.

2.5.10 Geometric Nonlinearity

Geometric nonlinearity is used to consider secondary displacements and P-Delta effects and other large displacements.

2.5.11 Crack Allocation

Two crack allocation models are available in VecTor2, uniform and variable. The uniform crack allocation model is useful when determining crack widths and spacing for reinforced concrete with regular deformed reinforcing steel or fibre reinforced concrete; the DSFM is used to determine an average crack width and spacing. For concrete reinforced with FRP, the variable crack allocation model may be more appropriate.

2.5.11.1 Uniform Crack Allocation (Deluce, Lee, and Vecchio, 2012)

In normal reinforced concrete, an average crack width and spacing are calculated using the DSFM as follows (Vecchio, 2000):

$$w = \varepsilon_{c1} \cdot s \quad (2.5.11.1.1)$$

where w is the average crack width, and ε_{c1} is the average tensile strain.

Under biaxial conditions, the following crack spacing parameters are calculated with respect to the principal axis:

$$s = s_{cr} = 2 \left(c + \frac{s_b}{10} \right) k_3 + \frac{k_1 k_2}{s_m} \quad (2.5.11.1.2)$$

where,

$$s_b = \frac{1}{\sum_i \frac{\cos^2 \theta_i}{s_{b,i}}} \quad (2.5.11.1.3)$$

$$s_{b,i} = 0.5 \sqrt{\frac{\pi d_{b,i}^2}{\rho_{s,i}}} \quad (2.5.11.1.4)$$

$$s_m = \sum_i \frac{\rho_{s,i}}{d_{b,i}} \cos^2 \theta_i + \frac{\alpha_f V_f}{d_f} \cdot \max\left(\frac{l_f/d_f}{50}, 1.0\right) \quad (2.5.11.1.5)$$

$$k_1 = 0.4; \quad k_2 = 0.25; \quad k_3 = 1 - \frac{\min(V_f, 0.015)}{0.015} \cdot \left\{ 1 - \min\left(\frac{50}{l_f/d_f}, 1.0\right) \right\} \quad (2.5.11.1.6)$$

$$c = 1.5 a_{gg} \quad (2.5.11.1.7)$$

And a_{gg} is the maximum aggregate size, α is a fibre orientation factor (equal to 0.5 for an infinite element).

2.5.11.2 Variable Crack Allocation (Sato 2002)

The variable crack allocation model is well-suited for the estimation of crack widths in reinforced concrete members with fibre-reinforced polymer sheets.

To estimate the contribution of steel bars to crack formation, the stress at the final crack formation is (Sato and Vecchio, 2003):

$$f'_1 = \sum_{i=1}^n \frac{s_r \Psi_{s,i} \tau_{b0,i} \cos \theta_{s,i}}{2A_{ce}} \quad (2.5.11.2.1)$$

where s_r is the crack spacing, Ψ_s is the bonded area per unit length (mm^2/mm), τ_{b0} is the maximum average bond stress of the i^{th} steel bar, θ_s is the angle between the reinforcement and principle tensile concrete direction, and A_{ce} is the effective cross-sectional area of concrete.

The contribution of the FRP sheets to crack formation is as follows. Concrete stress reaches the tensile strength f'_t at the midpoint between cracks, and a new crack develops at this section.

For equilibrium at a new crack formation:

$$f'_t = \sum_{j=1}^n \frac{w_{F,j} t_{F,j} E_{F,j} \Delta \varepsilon_{F0,j} \cos^2 \theta_{F,j}}{A_{ce}} \quad (2.5.11.2.2)$$

However, the only term required to model crack formation is $t_F E_F \Delta \varepsilon_{F0}$:

$$t_F E_F \Delta \varepsilon_{F0max} = c_3 \times \min(1, s_r/220) \quad \text{N/mm} \quad (2.5.11.2.3)$$

where

$$c_3 = (15.8 + 1.34 \sqrt{t_F E_F}) \sqrt{G_F} \quad \text{N/mm} \quad (2.5.11.2.4)$$

When the average tensile stress in the cross-section of $R_{eF} \times w_F$ at the midpoint between two cracks approaches the tensile strength f'_t , a new crack develops.

Combining the two equations, equilibrium at the completion of new crack formation in reinforced concrete members with both steel bars and FRP sheets is expressed in the following equation.

$$f'_t = 2s_r \sum_{i=1}^m \frac{\rho_{e,i} \tau_{s0,i} \cos \theta_{s,i}}{d_{b,i}} + \sum_{j=1}^n (\rho_{F,j} E_{F,j} \Delta \varepsilon_{Fmax,j} \cos^2 \theta_{F,j}) \quad (2.5.11.2.5)$$

where ρ_e is the effective reinforcement ratio for steel bars, ρ_F is the effective reinforcement ratio for FRP sheets ($=t_F/R_{eF}$), i is the component (direction of steel bars), and j is the component of FRP sheets.

The crack spacing can be calculated as:

$$s = s_r = \begin{cases} \frac{f'_t}{2 \sum_{i=1}^m \frac{\rho_{c,i} \tau_{b0,i} \cos \theta_{s,i}}{d_{b,i}} + \frac{1}{220} \sum_{j=1}^n \frac{\rho_{F,j} c_{3,j} \cos^2 \theta_{F,j}}{t_{f,j}}} & \text{for } s_r \leq 220 \text{mm} \\ \frac{f'_t - \sum_{j=1}^m \frac{\rho_{f,j} c_{3,j} \cos^2 \theta_{F,j}}{t_{f,j}}}{2 \sum_{i=1}^n \frac{\rho_{e,i} \tau_{b0,i} \cos \theta_{s,i}}{d_{b,i}}} & \text{for } s_r > 220 \text{mm} \end{cases} \quad (2.5.11.2.6)$$

Details of the variable crack allocation model can be found in Sato (2003).

2.5.12 Additional Analysis Parameters

Different analysis options or material models available in VecTor2 require the user to specify additional parameters. These are discussed in this section. Additionally, it is possible for users to specify material resistance factors in FormWorks; this is discussed in this section and in the FormWorks section of the manual.

2.5.12.1 Concrete Aggregate Type

The type of aggregate is important when considering fire loads, due to the fact that siliceous and carbonate aggregates respond differently to elevated temperatures. Some characteristic properties, such as f'_c/f'_{c20} are found in (Zhou, 2005). The thermal strains also differ between siliceous and carbonate aggregate.

2.5.12.2 Concrete Conductivity

Concrete conductivity is important when determining thermal performance. In order to analyze the response of concrete under extreme thermal loading (ie. fire), this input is required.

2.5.12.3 Concrete Fracture Energy

In order to predict crack formation in reinforced concrete, the fracture energy is required. The fracture energy depends on the composite structure of the concrete and depends on the mechanical interaction of the aggregates and cement matrix (Wittman, 2002). The concrete fracture energy is lowest

for pure hardened cement paste and increases as the maximum aggregate size increases. One equation for determining the fracture energy is the following (Wittman, 2002):

$$G_f = a\Phi_{max}^n \quad \text{N/m} \quad (2.5.12.3.1)$$

Where $a = 80.6$ and $n = 0.32$.

Note that in VecTor2, the concrete fracture energy must be specified in units of kN/m. If a zero is entered in FormWorks for fracture energy, a default value of 0.075 kN/m is assigned in VecTor2.

2.5.12.4 Prestressing Friction and Wobble Coefficient

The pre-stressing friction coefficient, specified in units of /m, is dependent on the type of tendon and the radius of curvature of the tendon. Applicable to post-tensioned systems only, the range of friction coefficients recommended by ACI and CEB is summarized in Figure 10 below (Collins and Mitchell, 1997). Similar to the friction coefficient, the prestressing wobble coefficient is applied only to post-tensioned systems and is dependent on the type of tendon. Recommended values are also given in Figure 10.

Table 2-3 Representative friction values* recommended by CEB-FIP for tendons with radii of curvature not less than 6 m (20 ft). From Ref. 2-16.

| Type of Tendon | Curvature Coefficient, μ | Wobble Coefficient, K^\dagger | |
|----------------------------|------------------------------|---------------------------------|-----------|
| | | per foot | per meter |
| Cables in concrete ducts | 0.50 | 0.0015 | 0.0050 |
| Tendons in metal sheathing | | | |
| Drawn wires | 0.20 | 0.0006 | 0.0020 |
| Strand | 0.20 | 0.0006 | 0.0020 |
| Smooth rolled wires | 0.25 | 0.0008 | 0.0025 |
| Deformed wire | 0.30 | 0.0009 | 0.0030 |

*Multiply values by 0.90 if tendon is slightly lubricated.

\dagger In the CEB-FIP Model Code, K is expressed as 0.01μ per meter

Table 2-2 Range of friction coefficients recommended by ACI. From Ref. 2-15.

| Type of Tendon | Curvature Coefficient, μ | Wobble Coefficient, K | |
|----------------------------------------------------------|------------------------------|-------------------------|---------------|
| | | per foot | per meter |
| Tendons in flexible metal sheathing | | | |
| Wire tendons | 0.15–0.25 | 0.0010–0.0015 | 0.0033–0.0049 |
| 7-wire strand | 0.15–0.25 | 0.0005–0.0020 | 0.0016–0.0066 |
| High-strength bars | 0.08–0.30 | 0.0001–0.0006 | 0.0003–0.0020 |
| Tendons in rigid metal duct – 7-wire strand | 0.15–0.25 | 0.0002 | 0.00066 |
| Unbonded pregreased tendons – wires and 7-wire strand | 0.05–0.15 | 0.0003–0.0020 | 0.0010–0.0066 |
| Unbonded mastic-coated tendons – wires and 7-wire strand | 0.05–0.15 | 0.0010–0.0020 | 0.0033–0.0066 |

Figure 10: Prestressing Wobble and Friction Coefficients

2.5.12.5 Thermal Time-Stepping Factor

The thermal time stepping factor allows transient thermal loading (ie. fire loading) to be incorporated into VecTor2. The time step is used in the Crank-Nicolson Method, which is a finite difference numerical integration method implemented in VecTor2 for the analysis of transient thermal loading. Multiplying the thermal time stepping factor by the number of time steps gives the duration of each time step.

2.5.12.6 Material Resistance/Creep Factors

Material Resistance Factors are applied to decrease the strength of specified materials. The factored strength is equal to the input material strength multiplied by the material resistance factor. Information on how to input the resistance factors for concrete, rebar steel, prestressing steel, structural steel, masonry/mortar, and wood are provided in the FormWorks section of this manual. The concrete creep coefficient and prestressing steel relaxation coefficients are discussed in the Concrete Models section of this manual.

3 Element Library

The VecTor2 element library is subdivided into three element categories depending on the type of material the element models. The first category consists of planar triangular, rectangular and quadrilateral elements which model concrete with or without smeared reinforcement. The second category consists of the linear truss bar element which models discrete reinforcement. The third category consists of the non-dimensional link and contact elements, which model bond-slip.

All elements are simple and low powered, with minimal nodes, straight conforming boundaries, and linear displacement functions. Compared to higher powered elements, these lower powered elements are advantageous in two respects. First, VecTor2 explicitly calculates their stiffness coefficients without resorting to numerical integration. Second, low powered elements are not susceptible to spurious behaviors such as zero-energy modes. The following discussion describes the element type.

3.1 Reinforced Concrete Elements

Reinforced concrete elements are used to model plain concrete or concrete with smeared reinforcement, representing regions of a structure having well-distributed reinforcement. Owing to compatibility between the concrete and smeared reinforcement comprising the element, the concrete and reinforcement are perfectly bonded. The element stiffness matrices, $[k]$, are formulated with the composite material stiffness matrices by closed form evaluation of the following integral:

$$[k] = \int_{vol} [B]^T [D][B] dV \quad (3.1.1)$$

3.1.1 Constant Strain Triangle

The constant strain triangle, shown in Figure 11, is a three-noded element with uniform thickness, t . The element is defined by the three node numbers, in counterclockwise sequence i, j, k . As each node displaces in the x and y directions, the element has a total of six degrees of freedom. Although the triangle

may assume any orientation and shape, its accuracy degrades as the shape deviates from an equilateral triangle. As such, distorted and elongated triangles should be avoided.

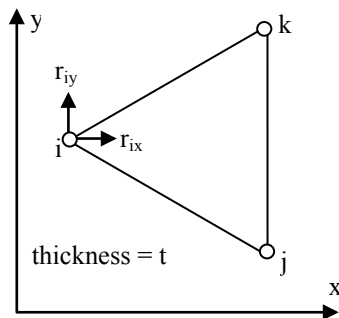


Figure 11: Constant strain triangle element

The displacement of any point in the element is expressed as a linear combination of the x and y coordinates. The element strains, $[\varepsilon]$, are related to the nodal displacements, $[r]$, by the strain-displacement matrix $[B]$ as follows:

$$[\varepsilon] = [B][r] \quad (3.1.1.1)$$

where

$$[\varepsilon] = [\varepsilon_x \quad \varepsilon_{xy} \quad \gamma_{xy}]^T \quad (3.1.1.2)$$

$$[r] = [r_{ix} \quad r_{iy} \quad r_{jx} \quad r_{jy} \quad r_{kx} \quad r_{ky}]^T \quad (3.1.1.3)$$

$$[B] = \frac{1}{2A} \begin{bmatrix} y_{jk} & 0 & y_{ki} & 0 & y_{ij} & 0 \\ 0 & x_{kj} & 0 & x_{ik} & 0 & x_{ji} \\ x_{kj} & y_{jk} & x_{ik} & y_{ki} & x_{ji} & y_{ij} \end{bmatrix} \quad (3.1.1.4)$$

$$x_{ij} = x_i - x_j \quad \text{and} \quad y_{ij} = y_i - y_j \quad (3.1.1.5)$$

Considering the terms of $[B]$, it is apparent that the strains and stresses are constant throughout the element. Consequently, the constant strain triangle behaves poorly in bending and a finer mesh is generally required to achieve the same accuracy as a mesh constructed with plane stress rectangles. For these reasons, use of the constant strain triangle should be limited to accommodating edges that are not parallel to the X or Y axes, and to make transitions in element size.

3.1.2 Plane Stress Rectangle

The plane stress rectangle, shown in Figure 12, is a four-noded element with uniform thickness, t . The element is defined by four node numbers in counterclockwise sequence, i, j, m, n . As each node translates in the x and y directions, the element has a total of eight degrees of freedom. The rectangle must be oriented isothetically, with its edges parallel to the x and y axes. Although the rectangle may assume any width and height, its accuracy degrades as the shape deviates from a square. As such, rectangles with aspect ratios exceeding 3:2 should be avoided.

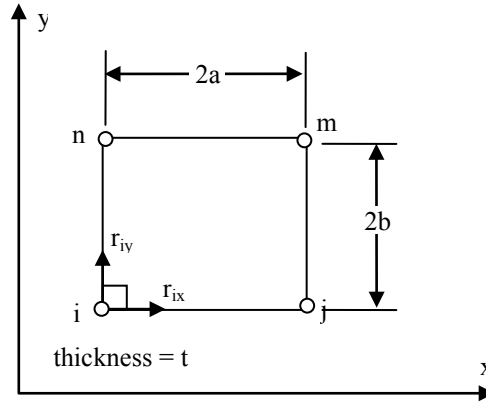


Figure 12: Plane stress rectangle element

The displacement of any point in the element is expressed as a bilinear combination of the x and y coordinates, including the mixed ‘ xy ’ term. The element strains, $[\varepsilon]$, are related to the nodal displacements, $[r]$, by the strain-displacement matrix, $[B]$, as follows:

$$[\varepsilon] = [B][r] \quad (3.1.2.1)$$

$$[\varepsilon] = [\varepsilon_x \quad \varepsilon_{xy} \quad \gamma_{xy}]^T \quad (3.1.2.2)$$

$$[r] = [r_{ix} \quad r_{iy} \quad r_{jx} \quad r_{jy} \quad r_{mx} \quad r_{my} \quad r_{nx} \quad r_{ny}]^T \quad (3.1.2.3)$$

$$[B] = \frac{1}{4ab} \begin{bmatrix} -(b-y) & 0 & (b-y) & 0 & (b+y) & 0 & -(b+y) & 0 \\ 0 & -(a-x) & 0 & -(a+x) & 0 & (a+x) & 0 & (a-x) \\ -(a-x) & -(b-y) & -(a+x) & (b-y) & (a+x) & (b+y) & (a-x) & -(b+y) \end{bmatrix} \quad (3.1.2.4)$$

Considering the terms of $[B]$, it is apparent that the plane stress rectangle can represent linear gradients of strains and stress across its width and height. Evaluation of strains at the center of the rectangular element avoids parasitic shear. Given that the plane stress rectangle is less overly stiff than the constant strain triangle, the plane stress rectangle is preferable for modeling reinforced concrete regions.

3.1.3 Quadrilateral

The quadrilateral, shown in Figure 13a, is a four-noded element with uniform thickness, t . The element is defined by four node numbers in counterclockwise sequence, i, j, m, n . As each node translates in the X and Y directions, the element has a total of eight degrees of freedom. The quadrilateral may assume any orientation and shape in the X, Y coordinate system. For accurate results, the quadrilaterals should be compact with approximately equal interior angles, and lacking in excessive skew, taper or warp.

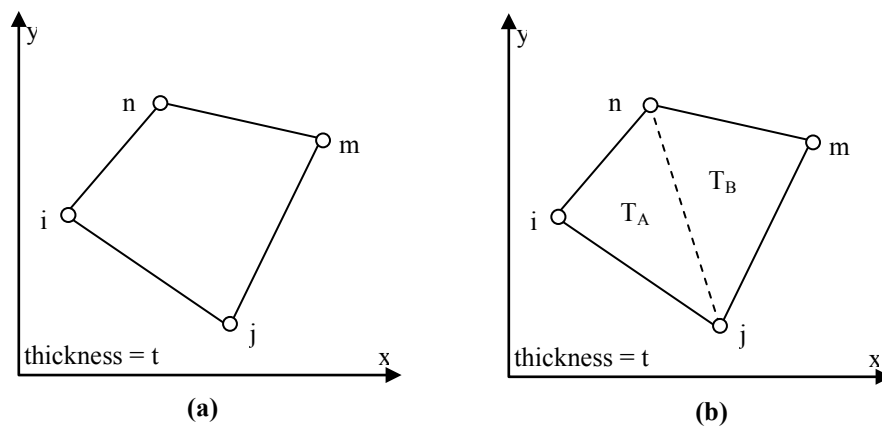


Figure 13: a) Quadrilateral element b) Decomposition of quadrilateral element into two constant strain triangle elements

VecTor2 divides the quadrilateral element into two constant strain triangles T_A and T_B , sharing the shortest diagonal as a common edge, as shown in Figure 13b. VecTor2 analyzes the two triangular elements separately, each with their own stiffness matrix. Having solved for the nodal displacements, VecTor2 computes the strains in the quadrilateral element as the area average of the strains in each triangular element. For the same reasons that apply to the constant strain triangles, the plane stress rectangle is preferable to the quadrilateral element. Use of the quadrilateral element should be limited to accommodating edges that are not parallel to the x or y axes, and to make transitions in element size.

Two different types of quadrilateral elements are available in VecTor2, isoparametric and degenerate. Both element types are discussed briefly below.

3.1.3.1 Isoparametric Quadrilateral Elements

For isoparametric elements, the same shape functions are used to represent the element geometry and determine the displacements. In this case, the quadrilateral coordinates are the parameters that define the shape functions, which are used to link the geometry and displacements.

3.1.3.2 Degenerate Quadrilateral Elements

Certain quadrilateral elements will degenerate into triangular elements. This is done by collapsing one of the sides of the quadrilateral. For a 4-node quadrilateral, degeneration results in a 3-node triangular element as illustrated in Figure 14..

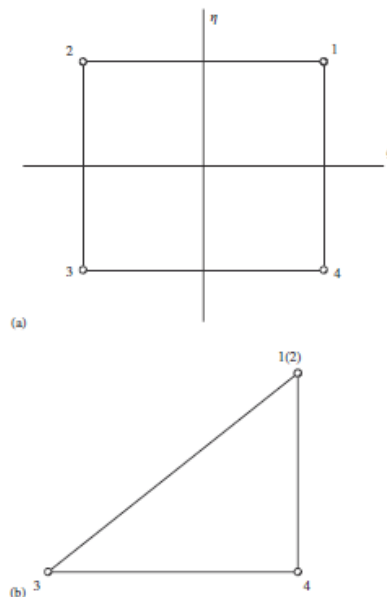


Figure 14: Degenerate Quadrilateral Element (Li, 2004)

Degenerate elements allow quadrilateral and triangular elements to both be used, which is convenient when dealing with complex structural geometry. Using degenerate elements, the shape functions of the quadrilateral elements are defined in terms of local coordinates and the shape functions for the triangular elements are defined in terms of global coordinates (Li, 2004).

3.2 Reinforcement Elements

Reinforcement elements are used to model reinforcement bars or FRP layers, or a lumped collection of them in close proximity relative to the surrounding element sizes. The stiffness matrix, $[k]$, of these elements are formulated with the reinforcement material stiffness matrix only. Use of the discrete reinforcement elements is required when either the behavior of individual bars or bond-slip mechanisms are of interest. Generally, as a matter of accuracy and computational economy, primary reinforcement is modeled by discrete reinforcement elements whereas well-distributed reinforcement is modeled by smeared reinforcement in the reinforced concrete elements.

3.2.1 Truss Bar

The truss bar, shown in Figure 15, is a two-noded element with uniform cross-sectional area, A . The element is defined by two node numbers, i, j . As each node displaces in the x and y directions, the element has a total of four degrees of freedom. The truss element may assume any orientation in the x, y coordinate system.

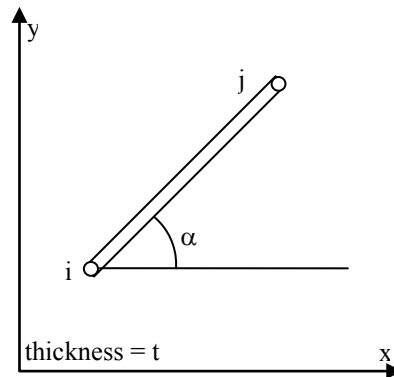


Figure 15: Truss bar element

The truss bar exhibits resistance only to elongation along its axis. The following equations relate the nodal forces, $[F]$, and nodal displacements, $[r]$, with the truss bar element stiffness matrix $[k]$:

$$[F] = [k][r] \quad (3.2.1.1)$$

where

$$[F] = [F_{ix} \quad F_{iy} \quad F_{jx} \quad F_{jy}]^T \quad (3.2.2.2)$$

$$[r] = [r_{ix} \quad r_{iy} \quad r_{jx} \quad r_{jy}]^T \quad (3.2.2.3)$$

$$[k] = \frac{AE}{L} \begin{bmatrix} \cos^2 \alpha & \cos \alpha \cdot \sin \alpha & -\cos^2 \alpha & -\cos \alpha \cdot \sin \alpha \\ \cos \alpha \cdot \sin \alpha & \sin^2 \alpha & -\cos \alpha \cdot \sin \alpha & -\sin^2 \alpha \\ \cos^2 \alpha & -\cos \alpha \cdot \sin \alpha & \cos^2 \alpha & \cos \alpha \cdot \sin \alpha \\ -\cos \alpha \cdot \sin \alpha & -\sin^2 \alpha & \cos \alpha \cdot \sin \alpha & \sin^2 \alpha \end{bmatrix} \quad (3.2.3.4)$$

3.3 Bond – Slip Elements

Without bond-slip elements, the reinforced concrete elements and discrete reinforcement elements are defined by common nodes. As such, the displacement of these elements is compatible, representing a condition of perfect bond between the concrete and discrete reinforcement elements.

Bond-slip elements serve as deformable interfaces between reinforced concrete elements and discrete reinforcement elements. Prior to slippage, bond-slip elements are defined by paired nodes having the same coordinates. A reinforced concrete element is attached to one of the nodes, and a discrete reinforcement element is attached to the other node. Increases of bond stresses are accompanied by bond slip, manifested by relative displacement of the paired nodes and the attached reinforced concrete and discrete reinforcement elements. VecTor2 includes two bond-slip elements: the link element and the contact element.

The accuracies of the link and contact element depend upon the variation in slip between successive nodes of the same discrete reinforcement elements. One measure of accuracy is the discrepancy between the theoretical strain energy and strain energy of bond elements to model given slip variations. As discussed by Keuser and Mehlhorn (1987), link elements model constant bond slips exactly, but provide poor accuracy for non-constant slip variations. Contact elements with a linear displacement function model constant and linear slip variations exactly, and provide good approximations of nonlinear slip variations. Nevertheless, it has been found that in practice (Gan, 2000, Wong, 2001) that both elements types provide similar and good accuracy when the mesh is sufficiently fine.

3.3.1 Link

The link element, (Ngo and Scordelis, 1967), shown in Figure 16, is a two-noded, non-dimensional element. The element is defined by two different node numbers, i and j . Prior to slippage, the paired nodes must have the same coordinate. One node must be incident to a reinforced concrete element, and the other node must be incident to a discrete reinforcement element. As each node displaces in the x and y directions, the element has a total of four degrees of freedom.

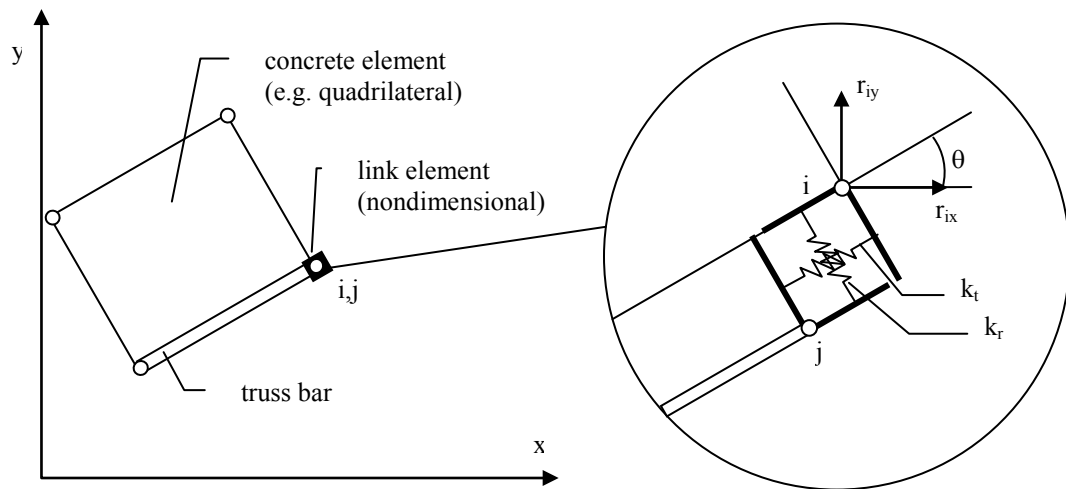


Figure 16 Link element

The link element may be conceptualized as two orthogonal springs, linking the reinforced concrete element and the discrete reinforcement element. One spring deforms tangentially to the discrete reinforcement element, representing bond slip and bond stresses. The other spring deforms radially to the discrete reinforcement element, representing radial displacements and stresses.

The nodal displacements of the elements in the x,y coordinate system, $[r]$, are transformed to deformations of the tangential spring (the bond slip), Δ_t , and the deformation of the radial spring, Δ_r , by the coordinate transformation matrix $[T]$:

$$[\Delta] = [T][r] \quad (3.3.1.1)$$

where,

$$[\Delta] = [\Delta_t \quad \Delta_r]^T \quad (3.3.1.2)$$

$$[r] = [r_{ix} \quad r_{iy} \quad r_{jx} \quad r_{jy}]^T \quad (3.3.1.3)$$

$$[T] = \begin{bmatrix} -\cos \theta & -\sin \theta & \cos \theta & \sin \theta \\ \sin \theta & -\cos \theta & -\sin \theta & \cos \theta \end{bmatrix} \quad (3.3.1.4)$$

The force in the tangential spring, F_t , is found by multiplying the bond slip, Δ_t , by the stiffness, k_t , and the bonded surface area tributary to the link, A . Likewise, the force in the radial spring, F_r , is found by multiplying the deformation of the radial spring, Δ_r , by the stiffness k_r , and the bonded surface areas, A , of embedded bars or external plates tributary to the link:

$$\begin{bmatrix} F_t \\ F_r \end{bmatrix} = A \begin{bmatrix} k_t & 0 \\ 0 & k_r \end{bmatrix} \begin{bmatrix} \Delta_t \\ \Delta_r \end{bmatrix} \quad (3.3.1.5)$$

The stiffness, k_t , relates to the bond stress to the bond slip and is determined from the bond-slip curve. In VecTor2, k_r is assigned a large value of $100 \cdot k_t$, to suppress the radial displacement of reinforcement element.

The nodal forces in the x,y directions, $[F]$, are determined by transforming the spring forces with transpose of the transformation matrix, $[T]^T$.

$$\begin{bmatrix} F_{ix} \\ F_{iy} \\ F_{jx} \\ F_{jy} \end{bmatrix} = [T]^T \begin{bmatrix} F_t \\ F_r \end{bmatrix} \quad (3.3.1.6)$$

Substituting equations 3.3.1.1 and 3.3.1.2 in equation 3.3.1.3, provides the stiffness relationship in the x,y coordinate system with the link element stiffness matrix $[k]$:

$$[F] = [k][r] \quad (3.3.1.7)$$

$$[k] = [T]^T A \begin{bmatrix} k_t & 0 \\ 0 & k_r \end{bmatrix} [T] \quad (3.3.1.8)$$

3.3.2 Contact

The contact element, shown in Figure 17, is a four-noded element, having only a linear dimension. The element is defined by four different node numbers in the sequence, j, k, m, n . Prior to

slippage, nodes, j and k must have the same coordinates. Either node j or node k must be attached to a reinforced concrete element. The other node must be attached to a discrete reinforcement element. The same condition applies to the nodes m and n . As each node displaces in the x and y directions, the element has a total of eight degrees of freedom. The contact element may assume any orientation in the x,y plane.

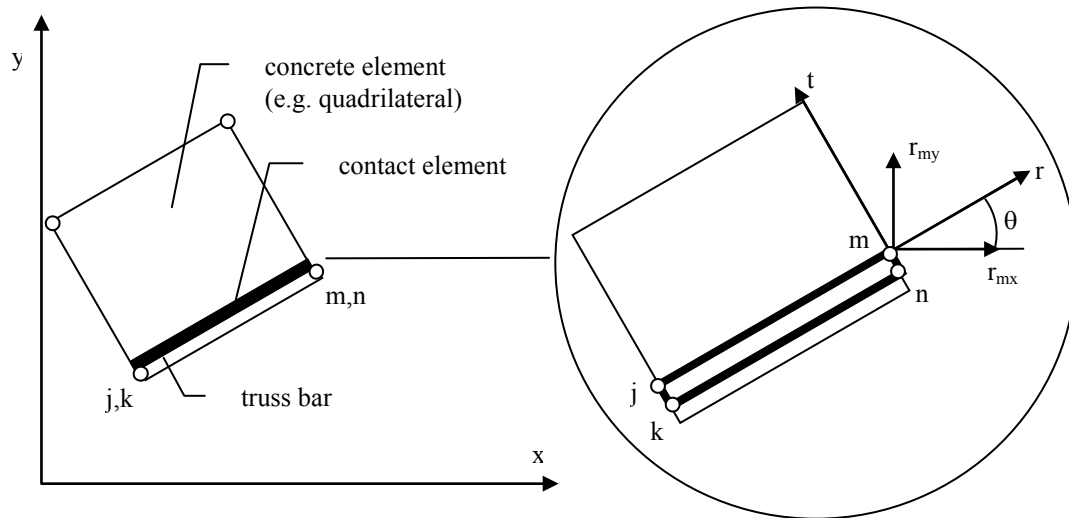


Figure 17: Contact element

The contact element models a continuous interface along the length of the discrete reinforcement element. With two node pairs defining the contact interface, the displacement of any point along the contact element is linearly interpolated from the nodal displacements to ensure conformal deformations with the reinforced concrete element and discrete reinforcement element. At any point, the bond stress, τ , is related to the tangential displacement, Δ_t , by the stiffness, k_t ; the radial stress, σ , is related to the radial displacement by the stiffness, k_r , as follows:

$$\begin{bmatrix} \tau \\ \sigma \end{bmatrix} = \begin{bmatrix} k_t & 0 \\ 0 & k_r \end{bmatrix} \begin{bmatrix} \Delta_t \\ \Delta_r \end{bmatrix} \quad (3.3.2.1)$$

The stiffness, k_t , relates to the bond stress to the bond slip and is determined from the bond-slip curve. In VecTor2, k_r is assigned a large value of $100 \cdot k_t$, to suppress the radial displacement of reinforcement element.

By minimizing of the potential energy of a loaded element, the following equilibrium relationship is found relating the nodal forces $[F]$ and displacements $[r]$ in the x,y coordinate system:

$$[F] = [k][r] \quad (3.3.2.2)$$

where

$$[F] = [F_{ix} \ F_{iy} \ F_{jx} \ F_{jy} \ F_{mx} \ F_{my} \ F_{nx} \ F_{ny}]^T \quad (3.3.2.3)$$

$$[r] = [r_{ix} \ r_{iy} \ r_{jx} \ r_{jy} \ r_{mx} \ r_{my} \ r_{nx} \ r_{ny}]^T \quad (3.3.2.4)$$

The contact element stiffness matrix, $[k]$, in the x,y coordinate system is found by transforming the contact element stiffness matrix, $[k]'$, in the local coordinate system with the transformation matrix $[T]$:

$$[k] = [T]^T [k]' [T] \quad (3.3.2.5)$$

where

$$[k]' = \frac{A}{6} \begin{bmatrix} 2k_t & 0 & -2k_t & 0 & k_t & 0 & -k_t & 0 \\ 0 & 2k_r & 0 & -2k_r & 0 & k_r & 0 & -k_r \\ -2k_t & 0 & 2k_t & 0 & -k_t & 0 & k_t & 0 \\ 0 & -2k_r & 0 & 2k_r & 0 & -k_r & 0 & k_r \\ \hline k_t & 0 & -k_t & 0 & 2k_t & 0 & -2k_t & 0 \\ 0 & k_r & 0 & -2k_r & 0 & 2k_r & 0 & -2k_r \\ -k_t & 0 & k_t & 0 & -2k_t & 0 & 2k_t & 0 \\ 0 & -k_r & 0 & k_r & 0 & -2k_r & 0 & 2k_r \end{bmatrix} \quad (3.3.2.6)$$

$$[T] = \begin{bmatrix} \cos \theta & \sin \theta & 0 & 0 & 0 & 0 & 0 & 0 \\ \sin \theta & \cos \theta & 0 & 0 & 0 & 0 & 0 & 0 \\ 0 & 0 & \cos \theta & \sin \theta & 0 & 0 & 0 & 0 \\ 0 & 0 & -\sin \theta & \cos \theta & 0 & 0 & 0 & 0 \\ \hline 0 & 0 & 0 & 0 & \cos \theta & \sin \theta & 0 & 0 \\ 0 & 0 & 0 & 0 & -\sin \theta & \cos \theta & 0 & 0 \\ 0 & 0 & 0 & 0 & 0 & 0 & \cos \theta & \sin \theta \\ 0 & 0 & 0 & 0 & 0 & 0 & -\sin \theta & \cos \theta \end{bmatrix} \quad (3.3.2.7)$$

and A is the bonded surface area tributary to the contact element.

4 Models for Concrete Materials

The concrete constitutive and behavioral models are paramount to the accuracy of the VecTor2 results. At each load step, the structure stiffness is determined from the stresses and strains calculated from the constitutive models. Further, the inclusion or omission of a model determines whether the effects of pertinent behaviors are included in the analysis, and the suitability of the results to the purpose of the analysis. Many of the models in VecTor2 include multiple options differing in degree and type, which may produce a divergence of results.

Regarding the constitutive relationships, VecTor2 utilizes Cauchy-type models, which describe the concrete response via nonlinear functions of stress and strain. This approach is amenable to concrete given that the combined behavior of aggregates, cement and reinforcement which that can often only be described by empirical relationships. These relationships typically involve mechanical properties determined from standard specimens under specific stress and strain conditions, rather than being inherent material properties. Bearing this in mind, it is necessary to select models judiciously for each analysis.

The following discussion describes the constitutive and behavioral models pertaining primarily to the response of the concrete material, although many models must be discussed in the context of reinforced concrete. First, the compressive stress-strain response is discussed followed by the associated models of compression softening. Second, the tensile stress-strain response is discussed followed by the associated models of tension softening, and FRC tension. Thirdly, confinement and lateral expansion models are described. Fourthly, cracking criterion, crack stress calculations, crack width models, and slip distortion models are considered. Finally, hysteretic response models are presented.

4.1 Compression Pre-Peak Response

The stress-strain response of concrete in uniaxial compression is nonlinear beyond low compressive stresses, despite the fact that the constituent cement paste and aggregates exhibit linear-elastic behavior in compression. The apparent contradiction is explained by the softening effect of internal microcracks that form as a result of stress concentrations at the interface of the cement paste and

aggregates. The ascending branch of the nonlinear stress-strain response is the subject of the subsequent discussion.

Compression pre-peak response models compute the principal compressive stress, f_{ci} , if the compressive principal strain, ε_{ci} , is less compressive than the strain, ε_p , corresponding to the peak compressive stress, f_p . The peak parameters are determined by adjusting the unconfined uniaxial concrete cylinder strength, f'_c , and the corresponding strain, ε_o , for compression softening due to transverse tensile strains, and strength enhancement due to confinement. Some of the following compression pre-peak response models are described by functions that extended into the post-peak range. In these cases, both the ascending and descending branches are presented.

4.1.1 Linear

The linear model, shown in Figure 18, is an elastic-plastic compression response curve, which is not normally used.

$$f_{ci} = \begin{cases} -\left(\frac{\varepsilon_{ci}}{\varepsilon_p}\right)f_p & \text{for } \varepsilon_p < \varepsilon_{ci} < 0 \\ -f_p & \text{for } \varepsilon_{ci} < \varepsilon_p < 0 \end{cases} \quad (4.1.1.1)$$

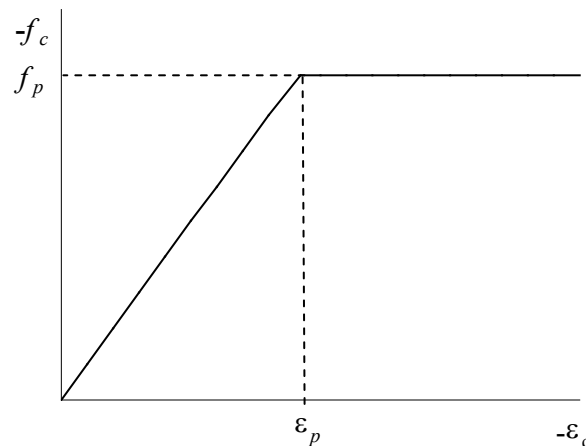


Figure 18: Linear pre- and post-peak concrete compression response

4.1.2 Popovics

Popovics (1973) presented stress-strain curves for a range of normal strength concretes. As shown in Figure 19, these curves reflect the greater stiffness and linearity of the ascending branch and the reduced ductility of concretes as the peak compressive stress increases.

The stress-strain curve is given by the following equation:

$$f_{ci} = -\left(\frac{\varepsilon_{ci}}{\varepsilon_p}\right) f_p \frac{n}{n-1 + \left(\varepsilon_{ci}/\varepsilon_p\right)^n} \quad \text{for } \varepsilon_{ci} < 0 \quad (4.1.2.1)$$

The long fraction represents the deviation from linear-elastic response. The curve fitting parameter, n , captures the greater linearity of higher strength concrete through the diminishing difference between the initial tangent stiffness E_c , and secant stiffness, E_{sec} . These values are computed as follows:

$$n = \frac{E_c}{E_c - E_{sec}} \quad (4.1.2.2)$$

$$E_{sec} = \frac{f_p}{|\varepsilon_p|} \quad (4.1.2.3)$$

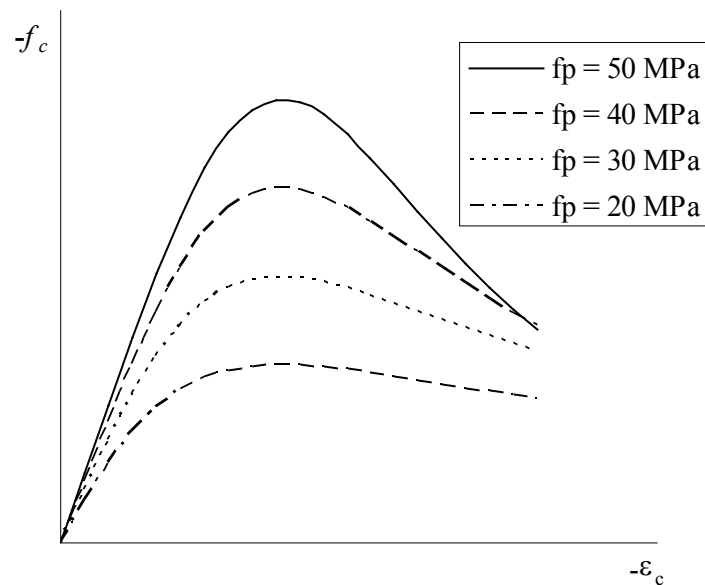


Figure 19 Popovics pre- and post-peak concrete compression response

4.1.3 Hognestad (Parabola)

The Hognestad parabola, as shown in Figure 20, is a simple compression response curve, suitable for normal concrete strengths (<40 MPa).

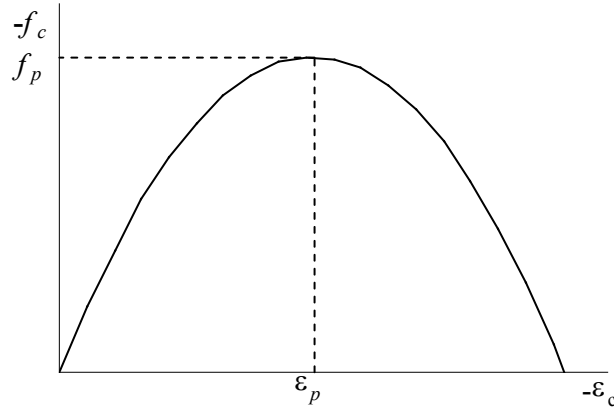


Figure 20: Hognestad parabolic pre- and post-peak concrete compression response

The stress-strain curve is described by the following relationship:

$$f_{ci} = -f_p \left\{ 2 \left(\frac{\epsilon_{ci}}{\epsilon_p} \right) - \left(\frac{\epsilon_{ci}}{\epsilon_p} \right)^2 \right\} < 0 \quad \text{for } \epsilon_{ci} < 0 \quad (4.1.3.1)$$

The stress-strain relationship is symmetric about ϵ_p , diminishing to zero stress at zero strain and $2\epsilon_p$. Note that the Hognestad parabola predefines the initial tangent stiffness, E_c , as follows:

$$E_c = 2f_p / |\epsilon_p| \quad (4.1.3.2)$$

4.1.4 Popovics (High Strength)

Collins and Porasz modified the stress-strain curve proposed by Thorenfeldt, Tomaszewicz, and Jensen (1987) and Popovics (1973) to accommodate the behavior of high strength concrete in compression. Experimental studies demonstrate that as the concrete strength increases, the response is linear to a greater percentage of the maximum compressive stress, the strain corresponding to the peak compressive stress increases, and the descending branch of the stress-strain curve declines more steeply. Also, intermediate high strength concretes exhibit a decreased ultimate compressive strain. The Popovics

– High Strength response curve, as shown in Figure 21, primarily differs from the Popovics response curve in the more rapid post-peak stress decay for higher strength concretes.

The stress-strain curve is given by the following equation:

$$f_{ci} = -\left(\frac{\varepsilon_{ci}}{\varepsilon_p}\right) f_p \frac{n}{n-1 + (\varepsilon_{ci}/\varepsilon_p)^{nk}} \quad \text{for } \varepsilon_{ci} < 0$$

(4.1.4.1)

The long fraction represents the deviation from linear-elastic response. The curve fitting parameter, n , captures the greater linearity of higher strength concrete through the diminishing difference between the initial tangent stiffness E_c , and secant stiffness E_{sec} . It is given by the following equation:

$$n = 0.80 + \frac{f_p}{17} \quad (f_p \text{ in MPa}) \quad (4.1.4.2)$$

The parameter, k , increases the post-peak decay in stress and is calculated as follows:

$$k = \begin{cases} 1.0 & \text{for } \varepsilon_p < \varepsilon_{ci} < 0 \\ 0.67 + \frac{f_p}{62} \geq 1.0 & \text{for } \varepsilon_{ci} < \varepsilon_p < 0 \quad (f_p \text{ in MPa}) \end{cases} \quad (4.1.4.3)$$

Note that the Popovics – High Strength relationship predefines the initial tangent stiffness, E_c , as follows:

$$E_c = \frac{f_p}{|\varepsilon_p|} \cdot \frac{n}{n-1} \quad (4.1.4.4)$$

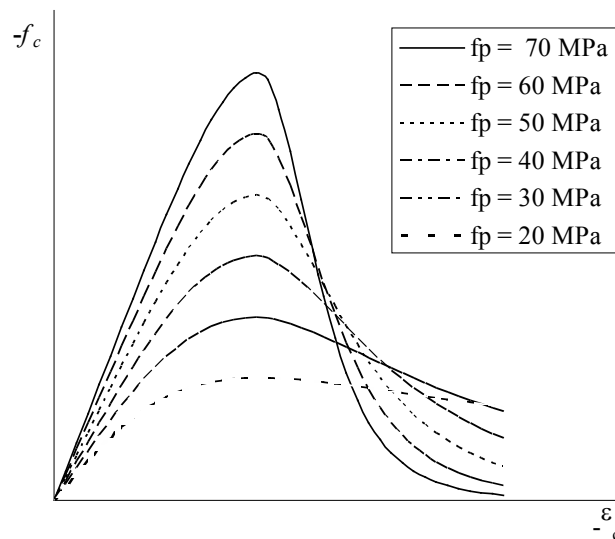


Figure 21: Popovics high strength pre- and post-peak concrete compression response

4.1.5 Hoshikuma et al.

In a study of confinement effects of reinforced concrete bridge piers with a variety of cross – sectional shapes, hoop reinforcement spacing and volumetric ratio, Hoshikuma, et al. (1997) proposed a stress-strain curve for concrete in compression, as shown in Figure 22. Experimental investigations indicated that the peak compressive stress, f_p , and corresponding strain, ε_p , depend upon the amount of hoop reinforcement, whereas the initial stiffness, E_c , does not. In this context, it is noted that Hognestad parabolic is deficient in that the initial stiffness is predetermined by equation. 4.1.3.2 in terms of the peak parameters, and is therefore an implicit function of the amount hoop reinforcement. To reconcile this inconsistency, the following relationship was proposed for the ascending branch of the compression stress-strain curve

$$f_{ci} = E_c \cdot \varepsilon_{ci} \left(1 - \frac{1}{n} \left(\frac{\varepsilon_{ci}}{\varepsilon_p} \right)^{n-1} \right) \quad \text{for } \varepsilon_p < \varepsilon_{ci} < 0 \quad (4.1.5.1)$$

The term in parentheses represents the deviation from linear-elastic response. The parameter, n , is expressed in term of the initial tangent stiffness E_c , and secant stiffness E_{sec} , as follows:

$$n = \frac{E_c}{E_c - E_{sec}} \quad (4.1.5.2)$$

$$E_{sec} = \frac{f_p}{|\varepsilon_p|} \quad (4.1.5.3)$$

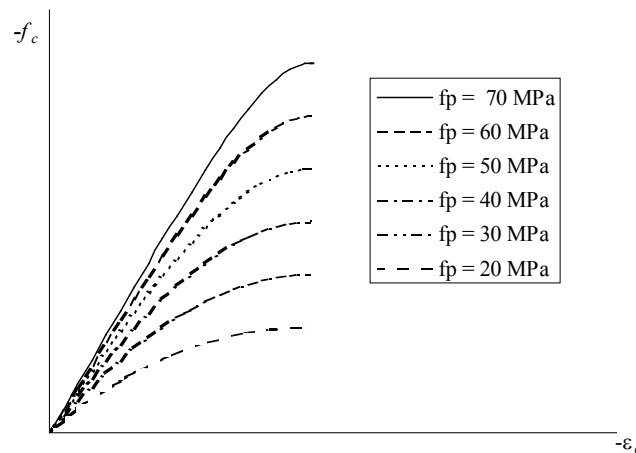


Figure 22: Hoshikuma et al. concrete compressive pre-peak response

The Hoshikuma et al. post-peak response is considered in the subsequent sections.

4.1.6 Smith-Young

Based on cylinder stress-strain curves, Smith and Young determined the following equation for the stress-strain behaviour of concrete (Smith and Young, 1956).

$$f_c = f'_c \left(\frac{\epsilon_c}{\epsilon_o} \right) \exp \left[1 - \left(\frac{\epsilon_c}{\epsilon_o} \right) \right] \quad (4.1.6.1)$$

The Smith-Young pre-peak curve is illustrated in Figure 23.

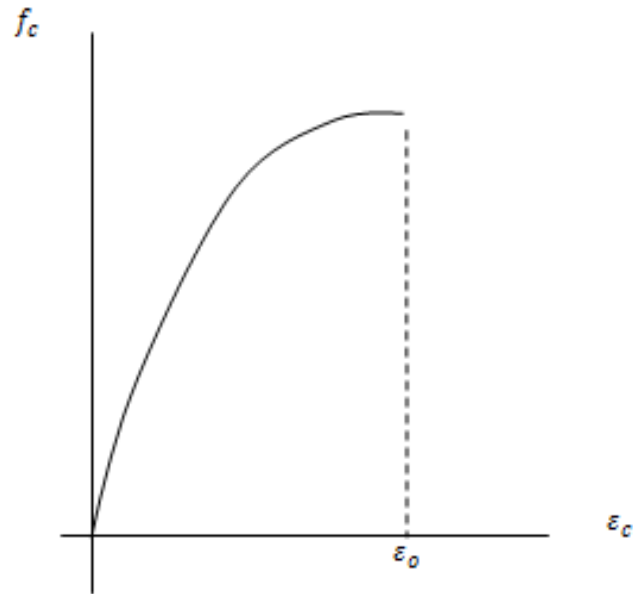


Figure 23: Smith-Young concrete compressive pre-peak response

4.1.7 Lee et al 2012 (FRC) (Lee et al, 2012)

For FRC in compression, the following stress-strain formulation is available in VecTor2:

$$f_c = f'_c \left[\frac{A(\epsilon_c/\epsilon_o)}{A-1+(\epsilon_c/\epsilon_o)^B} \right] \quad (4.1.7.1)$$

where A and B are the parameters considering the effect of fibres, which are evaluated for pre-and post-peak compressive behaviours, separately, as follows:

$$A = B = \frac{1}{1 - \left(\frac{f'_c}{\varepsilon_0 E_c}\right)^B} \quad \text{for } \varepsilon_c / \varepsilon_0 \leq 1 \quad (4.1.7.2)$$

$$A = 1 + 0.723 \left(V_f \frac{l_f}{d_f}\right)^{-0.957} \quad \text{for } \varepsilon_c / \varepsilon_0 > 1 \quad (4.1.7.3)$$

$$B = \left(\frac{f'_c}{50}\right)^{0.064} \left[1 + 0.882 \left(V_f \frac{l_f}{d_f}\right)^{-0.882}\right] \geq A \quad \text{for } \varepsilon_c / \varepsilon_0 > 1 \quad (4.1.7.4)$$

The strain at the compressive strength and elastic modulus of FRC can be calculated as follows:

$$\varepsilon_0 = \left(0.0003V_f \frac{l_f}{d_f} + 0.0018\right) f'_c{}^{0.12} \quad (4.1.7.5)$$

$$E_c = \left(-367V_f \frac{l_f}{d_f} + 5520\right) f'_c{}^{0.41} \quad (4.1.7.6)$$

4.2 Compression Post-Peak Response

Beyond the peak compressive stress, f_p , and corresponding strain, ε_p , concrete resists substantial compressive stress under continued compressive straining. Moreover, confinement of the concrete by transverse stresses enhances the strength and ductility of the concrete, transforming the failure in compression from brittle to ductile. This residual compressive strength and ductility may allow localized regions of a reinforced concrete structure to fail, but gradually unload so as to redistribute internal stresses and forestall total failure of the structure until additional deformation occurs. The effect of such post-peak behavior may be beneficial by allowing greater economy in design, or detrimental, should overstrength of the desired failure mode result in an undesirable failure mode. Post-peak behavior may also be significant in over-reinforced structures. As such, the selection of the compression post-peak response is significant to a realistic analysis of the load-deformation response.

Compression post-peak response models compute the principal compressive stress, f_{ci} , if the compressive principal compressive strain, ε_{ci} , is more compressive than the strain, ε_p , corresponding to the peak compressive stress, f_p . The peak parameters are determined by adjusting the unconfined uniaxial

concrete cylinder strength, f'_c , and the corresponding strain, ϵ_o , for compression softening due to transverse tensile strains, and strength enhancement due to confinement.

Of the following models presented, the Modified Park-Kent, Popovics/Mander, Hoshikuma et al. and Saenz/Spacone models are formulated in the context of confined concrete. If the Modified Park-Kent, Popovics/Mander, or Hoshikuma et al. models are selected and the concrete is not sufficiently confined, then an alternative formulation is necessary to compute the compression post-peak response. (The Saenz/Spacone is exempt from the following computation, owing to its inclusion of a control point on the post-peak stress-strain curve.) For these post-peak response models, the compression post-peak stress, f_{ci} , is computed as follows:

$$f_{ci} = (1 - c)f_{ci}^a + c \cdot f_{ci}^b \quad (4.2.1)$$

where

$$c = 4 \left(\frac{f_p - f'_c}{f'_c} \right), \quad 0 \leq c \leq 1 \quad (4.2.2)$$

$$f_{ci}^a = -f_p \left(\frac{\epsilon_{ci}}{\epsilon_p} \right) \cdot \exp \left\{ 1 - \left(\frac{\epsilon_{ci}}{\epsilon_p} \right) \right\} \quad (4.2.3)$$

$f_{ci}^b = \text{func}(\epsilon_{ci})$, as computed in the subsequent sections for confined concrete.

The stress computed as f_{ci}^a is the Smith-Young post-peak branch for unconfined concrete, as shown in Figure 24. The parameter, c , increases linearly from zero to one as f_p increases from f'_c to $1.25f'_c$. When used in equation 4.2.1, c effects a linear transition from the unconfined to confined compression post-peak response.

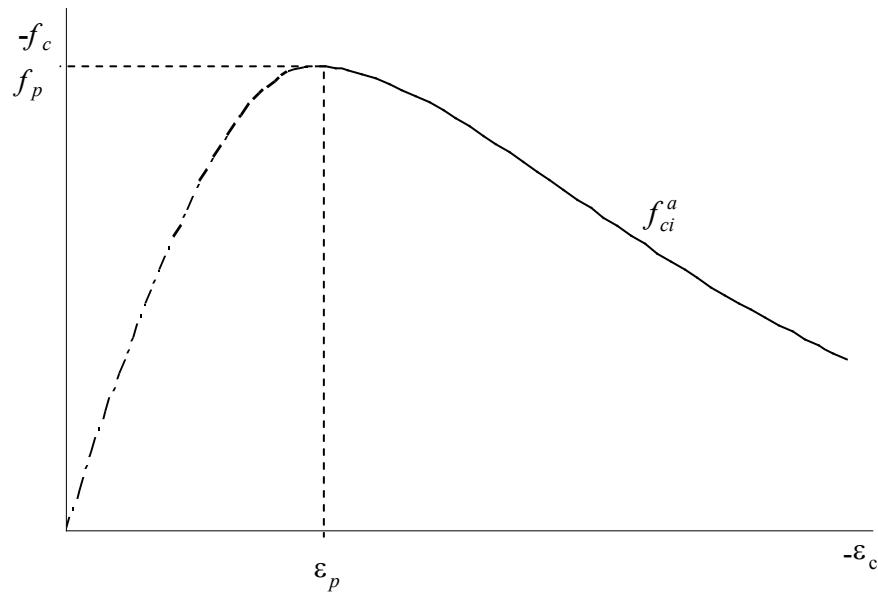


Figure 24: Smith-Young concrete compression post-peak response for $f_p \leq f'_c$

In addition, when the Modified Park-Kent, Popovics/Mander, Hoshikuma et al. and Saenz/Spacone models are selected, the post-peak response is assumed to have a sustaining branch equal to $0.2f_p$, whenever the concrete is sufficiently confined such that f_p exceeds f'_c .

$$f_{ci} = \text{func}(\varepsilon_{ci}) < -0.2f_p \quad \text{if } 0 < f'_c < f_p \quad (4.2.4)$$

4.2.1 Pre-Peak Base Curve

The Pre-Peak Base Curve option is a valid selection for the compression post-peak response if the Linear, Popovics, Hognestad (Parabola) or Popovics (High Strength) compression pre-peak response model is selected. The compression post-peak stress is computed using the equations presented in the previous section for the descending branch of the selected stress-strain curve.

4.2.2 Modified Park-Kent

Park, Priestly and Gill (1982) modified a stress-strain curve proposed by Kent and Park to account for the enhancement of concrete strength and ductility due to confinement. The stress-strain curve, as shown in Figure 25, was utilized to compute the flexural strength of reinforced concrete

columns confined by transverse hoop reinforcement. The linearly descending branch of the modified stress-strain curve is liberally adapted for VecTor2 as follows:

$$f_{ci}^b = -[f_p + Z_m f_p (\varepsilon_{ci} - \varepsilon_p)] < 0 \text{ or } -0.2f_p \quad \text{for } \varepsilon_{ci} < \varepsilon_p < 0 \quad (4.2.2.1)$$

where

$$Z_m = \frac{0.5}{\frac{3 + 0.29|f'_c|}{145|f'_c| - 1000} \cdot \left(\frac{\varepsilon_o}{-0.002}\right) + \left(\frac{|f_{lat}|}{170}\right)^{0.9} + \varepsilon_p} \quad (f'_c \text{ and } f_{lat} \text{ in MPa}) \quad (4.2.2.2)$$

and f_{lat} , is summation of principal stresses, acting transversely to the direction under consideration:

$$f_{lat} = f_{c1} + f_{c2} + f_{c3} - f_{ci} \leq 0 \quad i=1 \text{ or } 2 \quad (4.2.4.3)$$

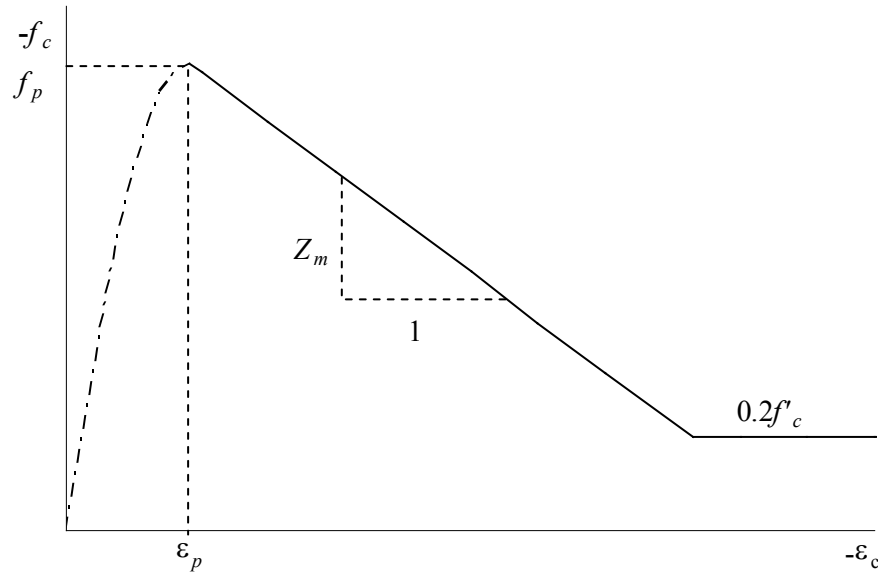


Figure 25: Modified Park-Kent post-peak concrete compression response

4.2.3 Popovics / Mander

Mander, Priestley and Park (1988), proposed a compression stress-strain curve for confined concrete with transverse hoop reinforcement. The form of stress-strain curve is the same as that proposed by Popovics (1973), except that the initial tangent stiffness, E_c , is assigned a particular value as follows:

$$f_{ci}^b = \left(\frac{\varepsilon_{ci}}{\varepsilon_p}\right) f_p \frac{n}{n-1 + \left(\frac{\varepsilon_{ci}}{\varepsilon_p}\right)^n} < 0.2f_p \quad \text{for } \varepsilon_{ci} < \varepsilon_p < 0 \quad (4.2.3.1)$$

where

$$n = \frac{E_c}{E_c - E_{sec}} \quad (4.2.3.3)$$

$$E_{sec} = \frac{f_p}{\epsilon_p} \quad (4.2.3.2)$$

$$E_c = 5000\sqrt{f'_c} \quad (4.2.3.4)$$

4.2.4 Hoshikuma et al.

In a study of confinement effects of reinforced concrete bridge piers with a variety of cross-sectional shapes, and transverse hoop reinforcement spacing and volumetric ratios, Hoshikuma et al. (1997) proposed a stress-strain curve for concrete in compression. Based on experimental investigations, the descending branch of the compression stress-strain curve, as shown in Figure 26, is idealized as a straight line given as follows:

$$f_{ci}^b = -[f_p + E_{des}(\epsilon_{ci} - \epsilon_p)] \leq -0.2f_p \quad \text{for } \epsilon_{ci} < \epsilon_p < 0 \quad (4.2.4.1)$$

where E_{des} is the deterioration rate of the descending branch. According to a regression analysis of experimental post-peak stress-strain curves for compressive stresses less than $|0.5f_p|$, Hoshikuma et al. proposed the following inverse relation between E_{des} and $\rho_s f_{yh}/f'_c{}^2$, where ρ_s is the volumetric ratio of hoop reinforcement, f_{yh} is the yield strength of hoop reinforcement and f'_c is the concrete cylinder strength:

$$E_{des} = \frac{11.2}{\rho_s f_{yh}/f'_c{}^2} \quad (4.2.4.2)$$

In VecTor2, the confining pressure, $\rho_s f_{yh}$, provided by the yielding of the hoop reinforcement is replaced by the mean lateral confining pressure, $f_{lat}/2$, and the deterioration rate is limited to half the initial tangent modulus as follows:

$$E_{des} = \frac{11.2}{(f_{lat}/2)/f'_c{}^2} \leq 0.5E_c \quad (4.2.4.3)$$

where f_{lats} is summation of principal stresses, acting transversely to the direction under consideration:

$$f_{lat} = f_{c1} + f_{c2} + f_{c3} - f_{ci} \leq 0 \quad i=1 \text{ or } 2 \quad (4.2.4.4)$$

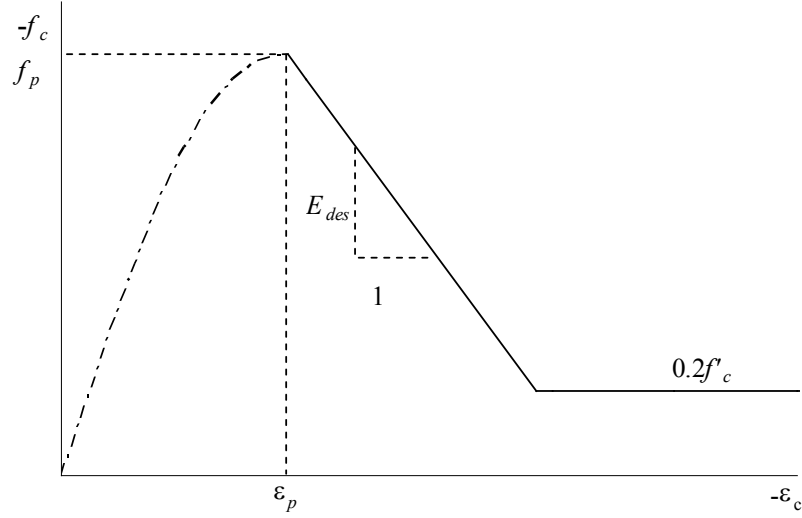


Figure 26: Hoshikuma et al. concrete compressive post-peak response

4.2.5 Saenz / Spacone

Saenz (1964) noted that higher strength concretes exhibit more rapidly descending compression post-peak responses. To reflect the shape of the descending branch, Saenz proposed that the compression stress-strain curve pass through a post-peak control point strain, ε_r , and corresponding stress, f_r , as well as satisfy stress and stiffness boundary conditions at zero stress and the peak compressive stress. The general form of such a curve, shown in Figure 27, is given as follows:

$$f_{ci} = \frac{K \cdot f_p \left(\frac{\varepsilon_{ci}}{\varepsilon_p} \right)}{1 + A \left(\frac{\varepsilon_{ci}}{\varepsilon_p} \right) + B \left(\frac{\varepsilon_{ci}}{\varepsilon_p} \right)^2 + C \left(\frac{\varepsilon_{ci}}{\varepsilon_p} \right)^3} \quad (4.2.5.1)$$

The parameters, A , B , C are expressed in terms of the stiffness ratio, strain ratio, and stress ratio,

K_σ , as follows:

$$A = C + K - 2 \quad (4.2.5.2)$$

$$B = 1 - 2C \quad (4.2.5.3)$$

$$C = K \frac{(K_\sigma - 1)}{(K_\varepsilon - 1)^2} - \frac{1}{K_\varepsilon} \quad (4.2.5.4)$$

where the stiffness ratio, K , compares the initial tangent stiffness, E_c , to the secant stiffness, E_{sec} :

$$K = \frac{E_c}{E_{\text{sec}}} \quad (4.2.5.5)$$

$$E_{\text{sec}} = \frac{f_p}{\varepsilon_p} \quad (4.2.5.6)$$

The strain ratio, K_ε , compares the post-peak control point strain, ε_r , and the strain corresponding to the peak stress, ε_p :

$$K_\varepsilon = \frac{\varepsilon_r}{\varepsilon_p} \quad (4.2.5.7)$$

and the stress ratio, K_σ , compares the peak compressive stress, f_p , to the post-peak control point stress, f_r :

$$K_\sigma = \frac{f_p}{f_r} \quad (4.2.5.8)$$

It remains necessary to specify the post-peak control point strain, ε_r , and corresponding stress, f_r .

Kwan and Spacone (2002) utilize the following empirical equation to determine the stress f_r , which increases as the confinement effect increases:

$$f_r = \frac{f_p f'_c}{5f'_c - f_p} \leq 1.4f_p \quad (4.2.5.9)$$

The strain, ε_r , is computed as four times the strain corresponding to peak compressive stress:

$$\varepsilon_r = 4\varepsilon_p \quad (4.2.5.10)$$

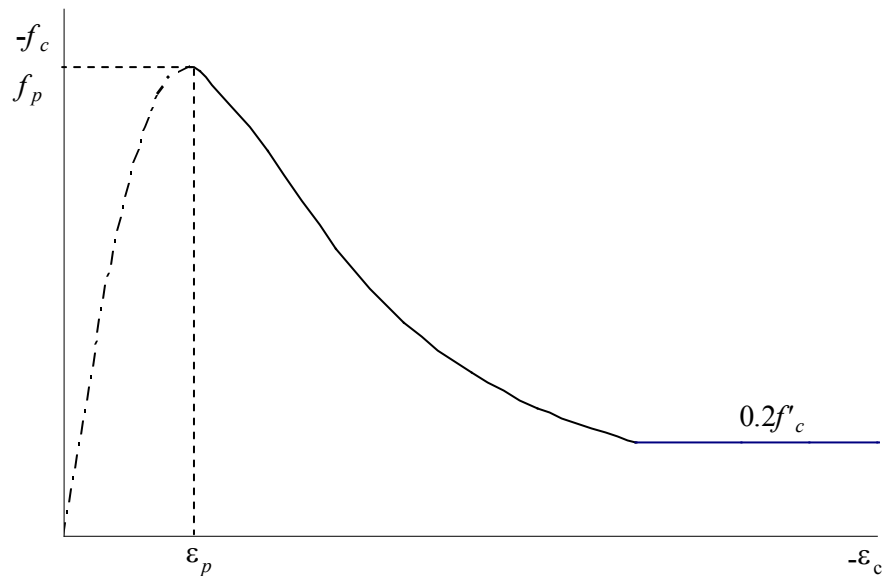


Figure 27: Saenz/Spacone concrete compressive post-peak response

4.2.6 Montoya 2003

Montoya proposed a post-peak model for steel and FRC confined concrete. This model includes a stress-strain curve which accounts for three-dimensional effects, concrete dilatation, strength enhancement, and post-peak softening or increased strain hardening. In formulating this model, varying concrete strengths, 20MPa to 100MPa, as well as confining pressure ratios, 0 to 100%, were studied. Note that the dilatation component of the model is discussed in a subsequent section of this user manual.

For post-peak compression, the following model is proposed (Montoya, 2004).

$$f_{ci} = \frac{f_{pi}}{A(\varepsilon_{ci}/f_{pi})^2 - B(\varepsilon_{ci}/f_{pi}) + C + 1.0} \quad (4.2.6.1)$$

where

$$A = k_d \quad (4.2.6.2)$$

$$B = 2 \frac{A}{E_{sec}} \quad (4.2.6.3)$$

$$C = \frac{A}{E_{sec}^2} \quad (4.2.6.4)$$

$$E_{sec} = \frac{f_{pi}}{\varepsilon_{pi}} \quad (4.2.6.5)$$

$$k_d = \frac{1}{4} \left(\frac{f_{pi}}{\varepsilon_{c80i} - \varepsilon_{pi}} \right)^2 \quad (4.2.6.6)$$

$$\frac{\varepsilon_{c80i}}{\varepsilon_{co}} = 1.5 + (89.5 - 0.60f'_c) \frac{f_{c1}}{f'_c} \quad (4.2.6.7)$$

And k_d is the shape factor which is a function of the post-peak curve's steepness, ε_{c80i} is the post-peak strain at 80% of the peak stress, E_{sec} is the secant Young's modulus. The compressive stress-strain curve is shown in Figure 28 below (Montoya, 2004).

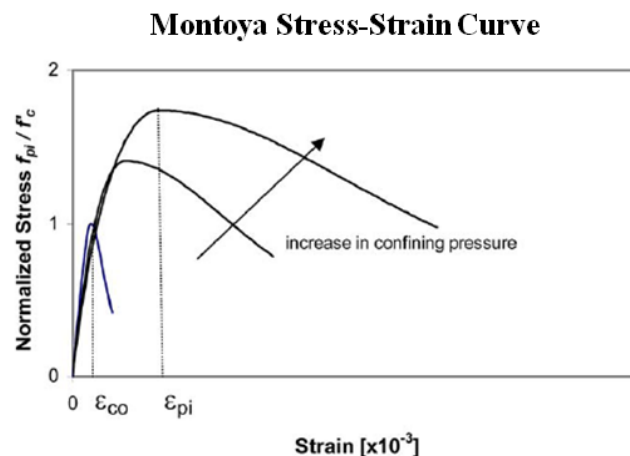


Figure 28: Montoya concrete compressive post-peak response

4.2.7 Lee et al 2012 (FRC)

The formulations implemented in VecTor2 for compressive behavior of FRC are outlined in the Lee et al 2011 (FRC) section 4.1.7.

4.3 Compression Softening

Compression softening in cracked concrete is the reduction of compressive strength and stiffness, relative to the uniaxial compressive strength, due to coexisting transverse cracking and tensile straining. This reduction can be substantial and have considerable effects on the load-deformation response of reinforced concrete structures, in terms of stiffness, ultimate strength capacity and ductility.

In VecTor2, the compression softening is effected by a softening parameter, β_d , with a value between zero and one, which is calculated by the compression softening models. These models are determined by statistical analysis of the stress-strain states of selected panel elements (890x890x70mm) and shell elements (1450x1450x350mm) tested at the University of Toronto (Vecchio and Collins, 1992). Depending on how the models calculate and apply β_d , the following compression softening models may be classified into two types: strength-and-strained softened and strength-only softened models.

Strength-and-strain softened models, as shown in Figure 29, use β_d to reduce both the uniaxial compressive strength, f'_c , and corresponding strain, ε_o , to determine the peak compressive strength, f_p , and corresponding strain, ε_p , used in the compression response models. The value of β_d is a function of $\varepsilon_{c1}/\varepsilon_{c2}$ – the ratio of the principal tensile strain to the principal compressive strain. In general, the calculation and application of strength-and-strained softened models is as follows:

$$\beta_d = \text{func}\left(\frac{\varepsilon_{c1}}{\varepsilon_{c2}}\right) \quad (4.3.1)$$

$$f_p = \beta_d \beta_l f'_c \quad (4.3.2)$$

$$\varepsilon_p = \beta_d \beta_l \varepsilon_o \quad (4.3.3a)$$

(The parameter, β_l , accounts for strength enhancement from confinement effects.)

However, if the compression softening is significant enough that $\varepsilon_p = \beta_d \beta_l \varepsilon_o$ is less compressive than ε_o , then a modification must be made to the calculation of ε_p so that the compression response ascends for strains up to ε_o and descends thereafter. When the compressive strain, ε_{c2} , is more compressive than $\beta_d \beta_l \varepsilon_o$, ε_p , is calculated as follows:

$$\varepsilon_p = \begin{cases} \varepsilon_{c2} & \text{if } \varepsilon_o < \varepsilon_{c2} < \beta_d \beta_l \varepsilon_o < 0 \\ \varepsilon_o & \text{if } \varepsilon_{c2} < \varepsilon_o < \beta_d \beta_l \varepsilon_o < 0 \end{cases} \quad (4.3.3b)$$

Further, for strains more compressive than ε_o , the softened response is computed by simply multiplying the base response by β_d .

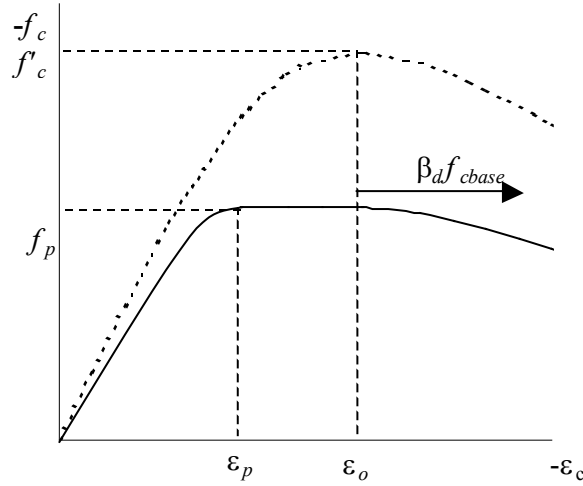


Figure 29: Strength and strain-softened compression response

Strength-only softened models, as shown in Figure 30, use β_d to reduce only the uniaxial compressive strength, f'_c , to determine the peak compressive strength, f_p , while the corresponding strain, ε_o , is unmodified for compression softening. The value of β_d is a function of $\varepsilon_{c1}/\varepsilon_o$ – the ratio of the principal tensile strain to the strain corresponding to the uniaxial compressive stress. As ε_{c2} is not considered as a variable, strength-only softened models are more amenable for manual calculation, but marginally weaker in correlation with experimental results and in accuracy.

$$\beta_d = \text{func} \left(\frac{\varepsilon_{c1}}{\varepsilon_o} \right) \quad (4.3.4)$$

$$f_p = \beta_d \beta_l f'_c \quad (4.3.5)$$

$$\varepsilon_p = \beta_l \varepsilon_o \quad (4.3.6)$$

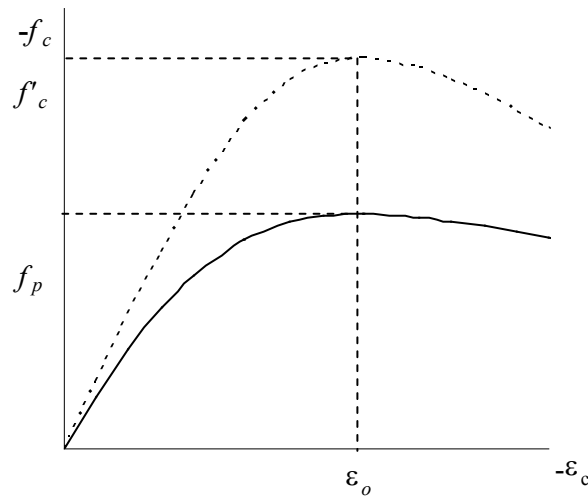


Figure 30: Strength-only softened compression response

It is assumed in the following discussion that the principal compressive strain ε_{c2} and the strain corresponding to peak stress, ε_o , are negative values while the principal tensile strain, ε_{c1} , is a positive value.

4.3.1 No compression softening

The compression response is independent of the coexisting tensile strains:

$$\beta_d = 1 \quad (4.3.1.1)$$

4.3.2 Vecchio 1992-A (e1/e2-Form)

The strength-and-strained softened model, shown in Figure 31, is based on the results of 116 panel and shell element tests. The ratio of the principal tensile strain to principal compressive stress is limited to 400 to avoid overestimation of the softening effect when the principal tensile strains are very large (e.g. when the reinforcement has yielded). The factor C_s recognizes whether shear slip deformations are considered (see discussion on DSFT). Both the uniaxial compressive strength and corresponding strain are softened. The model was originally developed for the Popovics (High Strength) compression stress-strain curve.

$$\beta_d = \frac{1}{1 + C_s \cdot C_d} \leq 1 \quad (4.3.2.1)$$

$$C_d = \begin{cases} 0 & \text{if } r < 0.28 \\ 0.35(r - 0.28)^{0.80} & \text{if } r > 0.28 \end{cases} \quad (4.3.2.2)$$

$$r = \frac{-\varepsilon_{c1}}{\varepsilon_{c2}} \leq 400 \quad (4.3.2.3)$$

$$C_s = \begin{cases} 0 & \text{if shear slip not considered} \\ 0.55 & \text{if shear slip considered} \end{cases} \quad (4.3.2.4)$$

$$f_p = \beta_d f'_c \quad (4.3.2.5)$$

$$\varepsilon_p = \beta_d \varepsilon_o \quad (4.3.2.6)$$

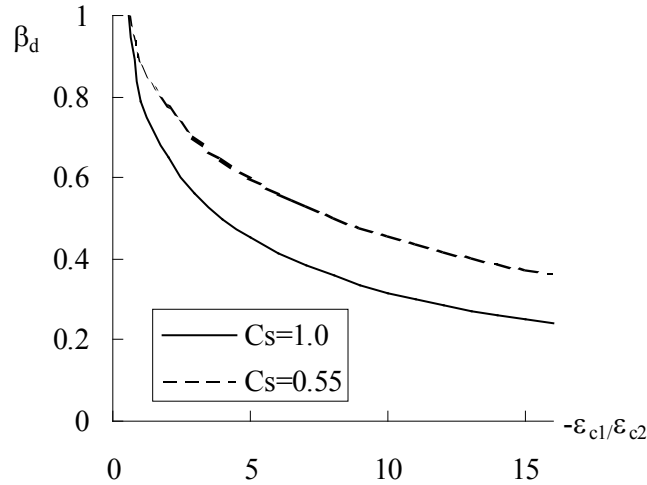


Figure 31: Vecchio 1992-A compression softening model

4.3.3 Vecchio 1992-B (e1/e0-Form)

The model is the strength-only softened version of the Vecchio 1992-A model. The factor C_s recognizes whether shear slip deformations are considered (see discussion on DSFT). The model was originally developed for the Popovics (High Strength) compression stress-strain curve.

$$\beta_d = \frac{1}{1 + C_s \cdot C_d} \leq 1 \quad (4.3.3.1)$$

$$C_d = 0.27 \left(\frac{-\varepsilon_{c1}}{\varepsilon_o} - 0.37 \right), \quad 0 \leq C_d \leq 50 \quad (4.3.3.2)$$

$$C_s = \begin{cases} 0 & \text{if shear slip not considered} \\ 0.55 & \text{if shear slip considered} \end{cases} \quad (4.3.3.3)$$

$$f_p = \beta_d f'_c \quad (4.3.3.4)$$

$$\varepsilon_p = \varepsilon_o \quad (4.3.3.5)$$

4.3.4 Vecchio-Collins 1982

The strength-and-strain softened model is based on the results of thirty panel tests. The model was originally developed for the Hognestad Parabola compression stress-strain curve. Note that this model does not recognize the softening effects of shear slip when they are included in the analysis.

$$\beta_d = \frac{1}{0.85 - 0.27 \left(\frac{\varepsilon_{c1}}{\varepsilon_{c2}} \right)} \leq 1 \quad (4.3.4.1)$$

$$f_p = \beta_d f'_c \quad (4.3.4.2)$$

$$\varepsilon_p = \beta_d \varepsilon_o \quad (4.3.4.3)$$

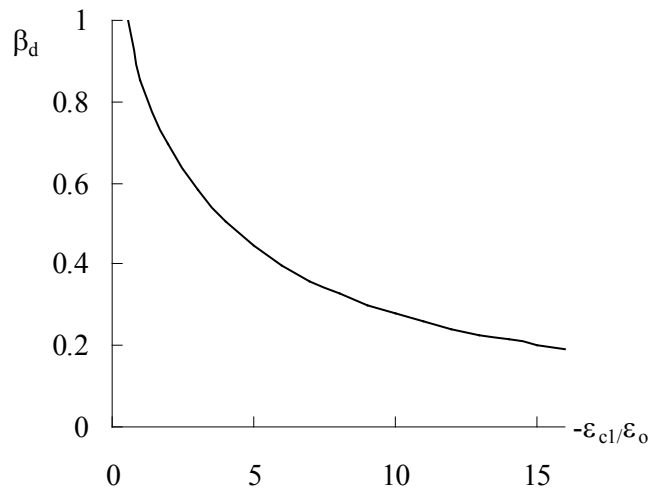


Figure 32: Vecchio 1982 compression softening model

4.3.5 Vecchio-Collins 1986

The model is strength-only softened version of the Vecchio-Collins 1982 model. The model was originally developed for the Hognestad Parabola compression stress-strain curve. Note that this model does not recognize the softening effects of shear slip when they are included in the analysis.

$$\beta_d = \frac{1}{0.8 - 0.34 \left(\frac{\varepsilon_{c1}}{\varepsilon_o} \right)} \leq 1 \quad (4.3.5.1)$$

$$f_p = \beta_d f'_c \quad (4.3.5.2)$$

$$\varepsilon_p = \varepsilon_o \quad (4.3.5.3)$$

4.4 Tension Stress-Strain Response

In tension, concrete is predominantly brittle and its response can be differentiated into uncracked and cracked response.

Prior to cracking the response is assumed to be linear-elastic, as follows:

$$f_{c1} = E_c \varepsilon_{c1} \quad \text{for } 0 < \varepsilon_{c1} < \varepsilon_{cr} \quad (4.4.1)$$

where,

$$\varepsilon_{cr} = \frac{f_{cr}}{E_c} \quad (4.4.2)$$

ε_{cr} is the cracking strain, E_c is the initial tangent stiffness of concrete, ε_{c1} is the principal tensile strain, and f_{cr} is the cracking stress of the concrete determined by the cracking criterion model.

After cracking in reinforced concrete structures, the concrete tensile stresses diminish virtually to zero at the free surface of cracks. However, owing to bond action with the reinforcement, average concrete tensile stresses continue to exist in the concrete between the cracks in the vicinity of the reinforcement. With additional tensile straining, cracks widen, the bond action degrades near the cracks and the average concrete tensile stresses gradually diminish to zero. While these average concrete tensile stresses must be less than f_{cr} (or else additional cracking ensues), they act over a relatively large tributary

area of the reinforcement. As such the stiffness of the reinforced concrete in tension is greater than that of the reinforcement alone. For this reason, the phenomenon is known as tension stiffening.

Tension stiffening is important to modeling the load-deformation behavior, particularly in the finite element context. If tension stiffening is neglected, the concrete tensile stress reduces immediately to zero upon cracking and the tensile stress must be redistributed entirely to the reinforcement. The discontinuous change in the stiffness may manifest as an unrealistic abrupt deviation in the load-deformation response and pose difficulties to the solution convergence for lightly reinforced structures.

The cracked concrete exhibiting tension stiffening must be within the tributary area of the reinforcement. In VecTor2, the tributary area of discrete reinforcement elements is delineated by a distance of 7.5 bar diameters from the discrete reinforcement element. (Note that in this manner, the tension stiffening effect depends somewhat on the coarseness of the finite element mesh). When the Tension Chord Model is selected, the tributary area of externally bonded FRP plates and sheets is based upon crack formation and bond considerations.

In VecTor2, the tension stiffening is effected by a gradually decreasing average stress-strain response of concrete in tension, as presented in the following discussion. The average concrete tensile stress determined is denoted by f_{c1}^a , to distinguish it from the average concrete tensile stress due to tension softening effects, denoted by f_{c1}^b . The magnitude, f_{c1}^a , is always limited by the yielding of the reinforcement of the crack, and additionally by the maximum shear stress at the crack when slip deformations are not included. The larger of the two tensile stresses is assumed to be the average post-cracking concrete tensile stress:

$$f_{c1} = \max(f_{c1}^a, f_{c1}^b) \quad (4.4.3)$$

4.4.1 No Tension Stiffening

The tension stiffening effect is ignored and the post-cracking concrete tensile stress is zero.

$$f_{c1}^a = 0 \quad \text{for } 0 < \varepsilon_{cr} < \varepsilon_{c1} \quad (4.4.1.1)$$

4.4.2 Modified Bentz 2003

The Bentz 2003 formulation for tension stiffening incorporates the percentage of reinforcement as well as bond characteristics; it is the default model in VecTor2. The formulation is as follows:

$$f_{c1} = \frac{f'_t}{1 + \sqrt{c_t \varepsilon_{c1}}} \quad \text{for } \varepsilon_{c1} > \varepsilon'_t \quad (4.4.2.1)$$

where

$$c_t = 3.6 t_d \cdot m \quad (4.4.2.2)$$

$$t_d = 0.6 \quad (4.4.2.3)$$

$$1/m = \sum_{i=1}^n 4\rho_i/d_{bi} \cdot |\cos(\theta - \alpha_i)| \quad (4.4.2.4)$$

And ρ_i is the reinforcement ratio, d_{bi} is the rebar diameter, θ is the inclination of the principle direction, and α_i is the inclination of reinforcement.

This formulation is modified when FRC is used (Lee et al. 2012). The following proposed tension stiffening model is incorporated into VecTor2:

$$f_{c1} = \frac{f_t}{1 + \sqrt{c_f \cdot 3.6 M \varepsilon_1}} \quad (4.4.2.5)$$

where

$$c_f = 0.6 + \frac{1}{0.034} \left(\frac{l_f}{d_f} \right) \frac{(100V_f)^{1.5}}{M^{0.8}} \quad \text{for hooked - end fibres} \quad (4.4.2.6)$$

$$c_f = 0.6 + \frac{1}{0.058} \left(\frac{l_f}{d_f} \right)^{0.9} \frac{V_f}{M^{0.8}} \quad \text{for straight fibres} \quad (4.4.2.7)$$

4.4.3 Vecchio 1982

This model, originally used in the Modified Compression Field Theory, is based upon tests conducted at the University of Toronto of thirty panel elements measuring 890x890x70mm with welded wire mesh reinforcement. Compared to the Collins-Mitchell 1987 model, this model is more appropriate for smaller scale elements and structures. The average concrete tensile stress-strain response is curve, shown in Figure 33, is determined as:

$$f_{c1}^a = \frac{f_{cr}}{1 + \sqrt{200\varepsilon_{c1}}} \quad \text{for } 0 < \varepsilon_{cr} < \varepsilon_{c1} \quad (4.4.3.1)$$

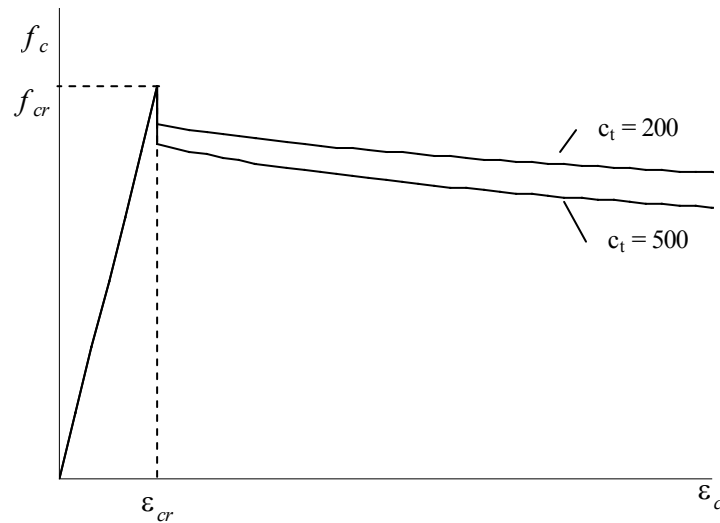


Figure 33: Vecchio 1982 and Collins-Mitchell tension stiffening response

4.4.4 Collins-Mitchell 1987

The model, a modification of the Vecchio 1982 model, is based upon the results of shell elements, measuring 1450x1450x350mm with reinforcing bars, tested at the University of Toronto. This model results in a more rapidly diminishing tension stiffening effect compared to the Vecchio 1982 model and is more appropriate for larger scale elements and structures. The average concrete tensile stress-strain response, shown in Figure 33, is curve is determined as:

$$f_{c1}^a = \frac{f_{cr}}{1 + \sqrt{500}\epsilon_{c1}} \quad \text{for } 0 < \epsilon_{cr} < \epsilon_{c1} \quad (4.4.4.1)$$

4.4.5 Bentz 1999

Bentz (1999) proposes a tension stiffening formulation that incorporates the bond characteristics of the reinforcement, given that the tension stiffening effect relies upon bond action. The model, originally formulated for sectional analysis of reinforced concrete members, has been adapted by Vecchio for VecTor2 to account for two dimensional stress conditions and the placement of smeared and discrete reinforcement. The average concrete tensile stress-strain response is curve is determined as:

$$f_{c1}^a = \frac{f_{cr}}{1 + \sqrt{3.6m} \cdot \epsilon_{c1}} \quad \text{for } 0 < \epsilon_{cr} < \epsilon_{c1} \quad (4.4.5.1)$$

In brief, the bond parameter, m reflects the ratio of the area of concrete to the bonded surface area of the reinforcement that is tributary to the concrete. For a constant area of reinforcement, the bond characteristics of numerous bars of smaller diameter are superior to those of fewer large diameter bars. As such, the former will have a smaller value of m and result in a larger tension stiffening effect.

4.4.6 Izumo, Maekawa Et Al.

Izumo et al. (1992) propose an analytical model for reinforced concrete panels subjected to in-plane stresses using a smeared crack approach. The model exhibits good accordance with the experimental results for seventeen of the Vecchio and Collins panels. The average concrete tensile stress-strain response curve, shown in Figure 34, is determined as:

$$f_{c1}^a = \begin{cases} f_{cr} & \text{for } 0 < \varepsilon_{cr} < \varepsilon_{c1} < 2\varepsilon_{cr} \\ f_{cr} \left(\frac{2\varepsilon_{cr}}{\varepsilon_{c1}} \right)^c & \text{for } 0 < 2\varepsilon_{cr} < \varepsilon_{c1} \end{cases} \quad (4.4.6.1)$$

The parameter, c , reflects the bond characteristics. In VecTor2, the model is implemented with $c = 0.4$, the recommended value for deformed reinforcing bars. Unlike the preceding models, the tensile stress remains at the cracking stress up to two times the cracking strain before descending nonlinearly.

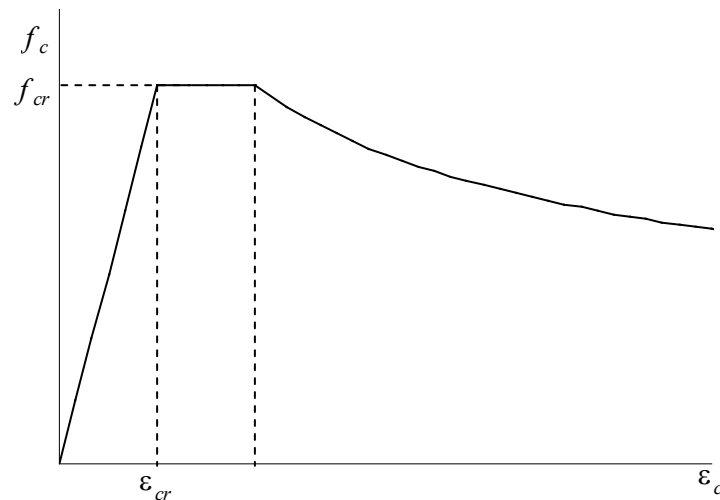


Figure 34: Izumo, Maekawa et al. tensions stiffening response

4.4.7 Tension Chord Model (Kaufmann)

The preceding tension stiffening models are empirical relationships based on investigations of concrete reinforced with embedded steel bars or wire, rather than externally bonded FRP plates or sheets. Considering the differences in dimensional and mechanical properties between the steel and FRP, and the more brittle bond between FRP and concrete, it follows that the preceding tension stiffening models are not ideal for determining tension stiffening effects due to FRP plate or sheet reinforcement.

To address crack spacing and tension stiffening effects in concrete reinforced with externally bonded FRP plates and sheets, as well as conventional reinforcement, Sato and Vecchio (2003) implemented the tension chord model (Kauffmann and Marti, 1998). This tension chord model considers a truss-like segment of reinforced concrete, as shown in Figure 35. The two ends of the chord represent two consecutive cracks, and the length of the chord is equal to the crack spacing. The chord is subject to tensile stresses along the longitudinal axis, which are resisted entirely by the reinforcement at the ends, and by a distribution of tensile reinforcement and concrete stresses between the two cracks. For a given value of tensile reinforcement stress at the ends of the chords, the tension chord model considers the bond stresses and slips between the concrete and reinforcement to determine the distribution of tensile stresses for the two materials between the cracks.

With its dependence on the crack spacing and bond stress-slip relationships, the tension chord model cannot be simply summarized as stress-strain relationship for concrete. While the complete description is beyond the scope of this discussion, the average concrete tensile stress is determined as follows:

$$f_{c1}^a = s_r \tau_{bo} \sum_{i=1}^m \left\{ \frac{\rho_{e,i} \cos \theta_{s,i}}{d_{b,i}} \cdot \min \left(1, \sqrt{\frac{\cos \theta_{s,i}}{s_r \varepsilon_s}} \right) \right\} + \sum_{j=1}^n \rho_{F,j} E_{F,j} \Delta \varepsilon_F \cos^2 \theta_{F,j} \quad (4.4.7.1)$$

The first term in the above equation represents the contribution of the steel reinforcement to tension stiffening. The value s_r is the crack spacing, τ_{bo} is the maximum average bond stress of the steel reinforcement, and ε_s is the average reinforcement strain. For the i th steel reinforcement, $\rho_{e,i}$ is the effective reinforcement ratio in its tributary area, $d_{b,i}$ is its diameter, and $\theta_{s,i}$ is the angle between principal

concrete tensile stress direction and the axis of the steel reinforcement. The second term in the above equation represents the contribution of the FRP reinforcement to tension stiffening. The value $\Delta\varepsilon_F$ is the average difference between the average FRP strains and the local FRP strains at a crack. For the j th FRP reinforcement, $\rho_{F,j}$ is the effective reinforcement ratio in its tributary area, $E_{F,j}$ is the elastic modulus of elasticity, $\Delta\theta_{F,j}$ is the angle between principal concrete tensile stress direction and the axis of the FRP reinforcement.

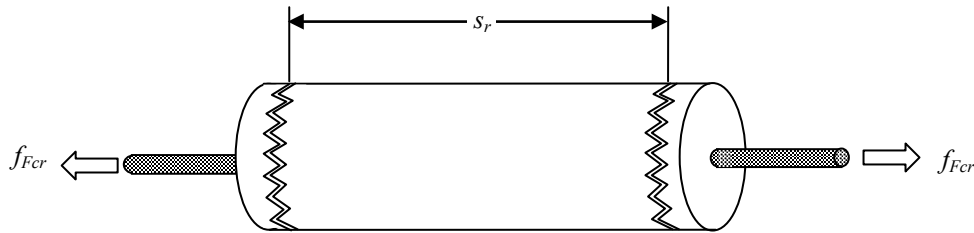


Figure 35: Tension chord model

4.4.8 Lee 2011 (w/ Post Yield) (Lee et al. 2011)

This model is based on the comparison of parametric studies with experimental results for uniaxial members, and includes a proposed model for the behaviour of reinforced concrete after yielding of reinforcement. The model allows VecTor2 to calculate the reinforcement stresses at crack locations, and makes it possible to determine the average strain conditions that will result in the rupture of reinforcement. Thus, the ductility of reinforced concrete members can be more accurately predicted. Also, improved estimates of strength and deformation capacity for concrete members with nonductile reinforcement can be made with this model.

Figure 36 shows the variation of the average tensile stress in concrete up to failure.

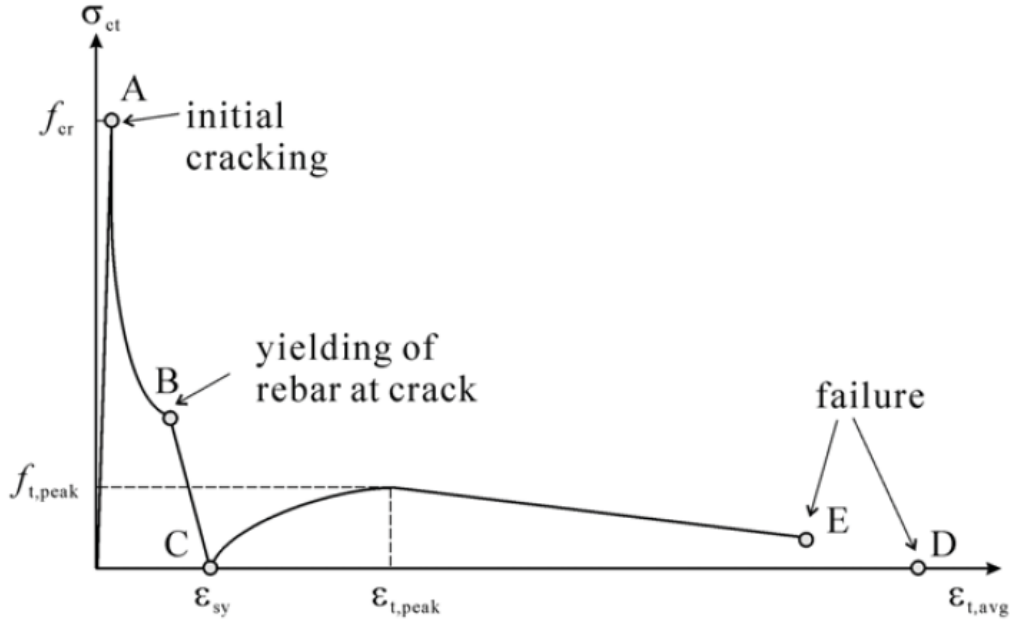


Figure 36: Lee 2010 stress-strain response

The proposed tension stiffening model for the stress-strain relationship of concrete after yielding of the reinforcement is:

$$f_{ct,avg} = \begin{cases} f_{ct,peak} - f_{ct,peak} \left(\frac{\varepsilon_{t,peak} - \varepsilon_{t,avg}}{\varepsilon_{t,peak} - \varepsilon_{sy}} \right)^2 & \text{for } \varepsilon_{sy} \leq \varepsilon_{t,avg} \leq \varepsilon_{t,peak} \\ f_{ct,peak} - \frac{f_{ct,peak} - 0.5f_{ct,peak,\rho_{min}}}{0.1 - \varepsilon_{t,peak}} (\varepsilon_{t,avg} - \varepsilon_{t,peak}) \geq 0.5f_{ct,peak,\rho_{min}} & \text{for } \varepsilon_{t,avg} \geq \varepsilon_{t,peak} \end{cases} \quad (4.4.8.1)$$

where

$$\rho_{min} = \frac{\varepsilon_{cr} \cdot E_c}{f_{sy} - \varepsilon_{cr} \cdot E_s} \quad (4.4.8.2)$$

$$\varepsilon_{t,peak} = 0.01 + 0.001 \cdot \max(15 - d_b, 0) \geq \varepsilon_{sh} \quad (4.4.8.3)$$

$$f_{ct,peak} = a \sqrt{f'_c} \quad (4.4.8.4)$$

$$a = -0.0313 \rho_s^{0.57} d_b + 3.3881 \rho_s^{0.76} \quad (4.4.8.5)$$

In this proposed model, the steel stress at the location of a crack is calculated from force equilibrium as follows:

$$f_{scr} = f_{s,avg} + f_{ct,avg} / \rho_s \quad (4.4.8.6)$$

4.5 Tension Softening

Tension softening refers to the presence of post-cracking tensile stresses in plain concrete. Under increased tensile straining, the tensile stresses diminish to zero. This phenomenon is attributable to the fact that concrete is not perfectly brittle. Rather, as described by fracture mechanics approaches, the formation of a localized crack requires energy. As the fracture process progresses and the crack widens, concrete in the vicinity of the crack is gradually relieved of stress, and the dissipated energy propagates the crack tip.

Tension softening is significant in several ways to the analysis of reinforced concrete structures, particularly those having lightly reinforced regions. The tension softening response may be important to modeling the stress redistribution and localized damage of lightly reinforced structures exhibiting brittle failure modes. By including a descending post-cracking stress-strain branch for plane concrete, it is possible to more accurately determine the load-deformation response and ductility of the member. Further, tension softening may mitigate inaccuracies associated with the coarseness of the finite element mesh. Due to their finite size, the elements invariably include both cracked and uncracked concrete. Accounting for the post-cracking tensile stress in cracked elements represents to some extent the stiffness contribution of uncracked concrete, and prevents undue stress concentration in adjacent uncracked elements.

In VecTor2, tension softening is effected by descending post-cracking average tensile stress-strain curves for concrete described in the subsequent discussion. The average concrete tensile stress due to tension softening is denoted by f_{c1}^b , to distinguish it from the average concrete tensile stress due to tension stiffening effects, denoted by f_{c1}^a . The larger of the two tensile stresses is assumed to be the average post-cracking concrete tensile stress:

$$f_{c1} = \max(f_{c1}^a, f_{c1}^b) \quad (4.5.1)$$

It is convenient to define common parameters in the tension-stiffening models. The fracture energy, G_f , is the energy required to form a complete crack of unit area. It describes the resistance of the concrete to cracking and is equivalent to the area beneath a plot of tensile stress versus crack width. The

fracture energy is independent of element size, and is assigned a value of 75N/m in VecTor2. The representative length, L_r , is the distance over which the crack is assumed to be uniformly distributed, and is assigned a value of half the crack spacing. The characteristic strain, ε_{ch} , of the tension softening curve is determined as follows:

$$\varepsilon_{ch} = \frac{2G_f}{L_r \cdot f_{cr}}, \quad 1.1\varepsilon_{cr} < \varepsilon_{ch} < 10\varepsilon_{cr} \quad (4.5.2)$$

The corresponding tensile stress, f_{ch} , is the characteristic stress of the tension softening curve. The terminal strain, ε_{te} , is the strain at which the tension softening stress diminishes to zero, determined as:

$$\varepsilon_{te} = 5 \varepsilon_{ch} \quad (4.5.3)$$

In models, without residual tension, the tensile stress due to tension softening is equal to the tensile stress, $f_{ts,base}$, computed from the tension softening base curve.

$$f_{c1}^b = f_{ts,base} \quad (4.5.4)$$

In models with a sustained residual tension, f_{res} , the residual stress is calculated as follows:

$$f_{res} = \begin{cases} 0.1f_{cr} & \text{for } 0 < w < 5mm \\ 0.1f_{cr}(3 - w/2.5) \geq 0 & \text{for } 5mm < w \end{cases} \quad (4.5.5)$$

For these models, the tensile stress due to tension softening is taken as the maximum of the tensile stress, and the residual stress, f_{res} as follows:

$$f_{c1}^b = \max(f_{ts,base}, f_{res}) \quad (4.5.6)$$

Residual tension should not be utilized in structures predominantly subject to tension stresses.

4.5.1 Not Considered

Post-cracking tensile stresses due to tension stiffening are not considered:

$$f_{c1}^b = 0 \quad (4.5.1.1)$$

4.5.2 Linear

The tension softening base curve descends linearly from the cracking stress and strain to zero stress at the characteristic strain (i.e. the terminal strain is taken as the characteristic strain). The curve, as shown in Figure 37 with and without the residual branch, is given as follows:

$$f_{ts,base} = f_{cr} \left[1 - \frac{(\epsilon_{c1} - \epsilon_{cr})}{(\epsilon_{ch} - \epsilon_{cr})} \right] \geq 0, \quad \text{for } \epsilon_{cr} < \epsilon_{c1} \quad (4.5.2.1)$$

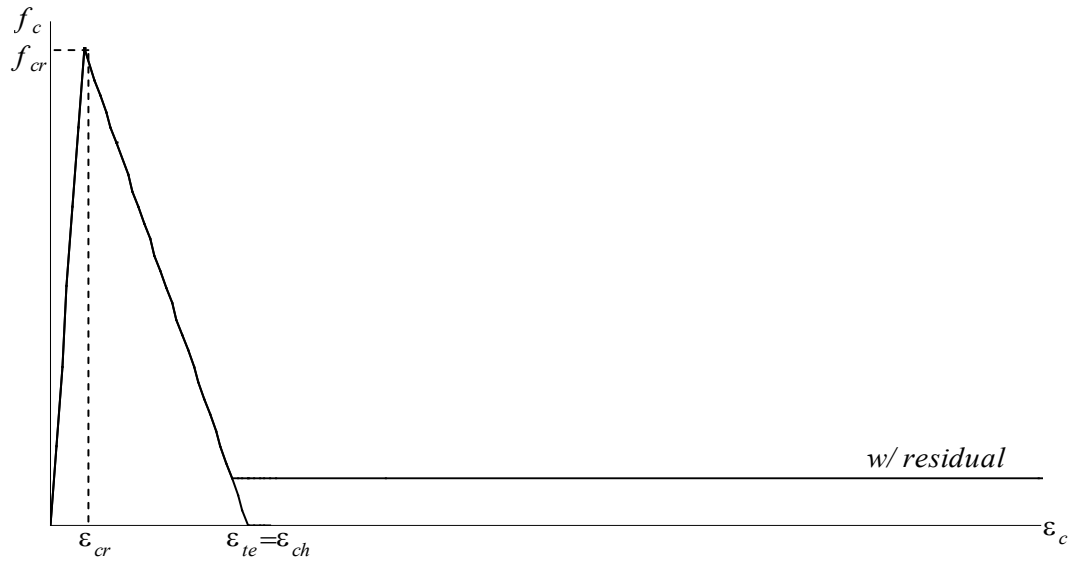


Figure 37: Linear tension softening response with and without residual

4.5.3 Bilinear

There are numerous bilinear tension softening models that have been proposed by different researchers. The CEB-FIP model is discussed in this manual.

The 1990 CEB-FIP model code provides a bilinear model for the stress-strain relationship of concrete. For a cracked concrete section, Figure 38 summarizes the stress-strain relationship:

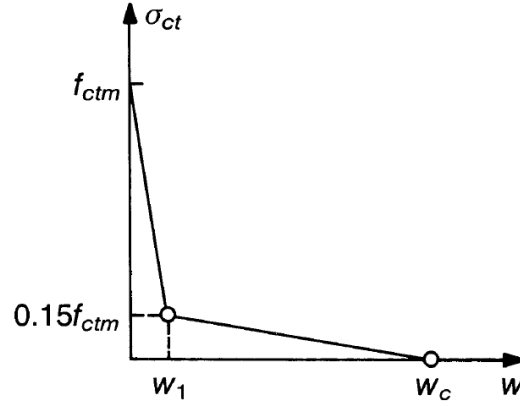


Figure 38: CEB-FIP tension softening curve (CEB-FIP, 1990)

The equations that summarize the CEB-FIP stress-strain relationship are (CEB-FIP, 1990):

$$\sigma_{ct} = \begin{cases} f_{ctm} \left(1 - 0.85 \frac{w}{w_1}\right) & \text{for } 0.15f_{ctm} \leq \sigma_{ct} \leq f_{ctm} \\ \frac{0.15f_{ctm}}{w_c - w_1} (w_c - w) & \text{for } 0 \leq \sigma_{ct} < 0.15f_{ctm} \end{cases} \quad (4.5.3.1)$$

$$w_1 = 2 \frac{G_f}{f_{ctm}} - 0.15w_c \quad (4.5.3.2)$$

$$w_c = \alpha_F \frac{G_f}{f_{ctm}} \quad (4.5.3.3)$$

where w is the crack opening width (mm), w_1 is the crack opening (mm) for $\sigma_{ck} = 0.15f_{ctm}$, w_c is the crack opening for $\sigma = 0$, f_{ctm} is the tensile strength (MPa), and α_F is a coefficient related to maximum aggregate size.

Equations for fracture energy, G_f , and tensile strength, f_{ctm} , are also found in the CEB-FIP design guide.

The bilinear tension softening model implemented in VecTor2, adapted from the above formulations, is shown below in Figure 39:

$$f_{c1} = \begin{cases} f_{cr} \left(1 - 0.80 \left(\frac{\varepsilon_{c1} - \varepsilon_{cr}}{\varepsilon_{ch3} - \varepsilon_{cr}}\right)\right) & \text{for } \varepsilon_{c1} < \varepsilon_{ch3} \\ 0.2f_{cr} \left(1 - \left(\frac{\varepsilon_{c1} - \varepsilon_{ch3}}{\varepsilon_{ch4} - \varepsilon_{ch3}}\right)\right) & \text{for } \varepsilon_{ch3} \leq \varepsilon_{c1} < \varepsilon_{ch4} \\ 0 & \text{otherwise} \end{cases} \quad (4.5.3.4)$$

where

$$\varepsilon_{ch3} = 0.64\varepsilon_{ch} + \varepsilon_{cr} \quad (4.5.3.5)$$

$$\varepsilon_{ch4} = 6.8\varepsilon_{ch} + \varepsilon_{cr} \quad (4.5.3.6)$$

$$\varepsilon_{ch} = \frac{G_f}{L_{ref} f_{cr}} ; \text{characteristic strain using } G_f \text{ from (Bazant, 2002)} \quad (4.5.3.10)$$

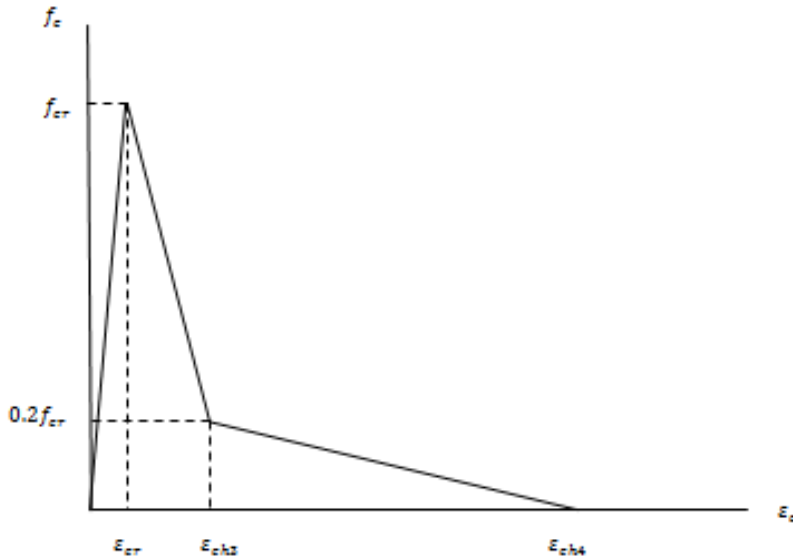


Figure 39: Bilinear Tension softening model implemented in VecTor2

4.5.4 Nonlinear (Yamamoto 1999 – No residual)

As proposed by Yamamoto (1999), the tension softening base curve descends non-linearly from the cracking stress to the characteristic stress and strain, then linearly to zero stress at the terminal strain.

The curve, shown in Figure 40 with and without the residual branch, is given as follows:

$$f_{ts,base} = \begin{cases} \frac{f_{cr}}{1 + \sqrt{c(\varepsilon_{c1} - \varepsilon_{cr})}} & \text{for } \varepsilon_{cr} < \varepsilon_{c1} < \varepsilon_{ch} \\ f_{ch} \frac{(\varepsilon_{te} - \varepsilon_{c1})}{(\varepsilon_{te} - \varepsilon_{ch})} \geq 0 & \text{for } \varepsilon_{ch} < \varepsilon_{c1} \end{cases} \quad (4.5.3.1)$$

The tension softening coefficient, c , is determined such that area beneath the tension softening curve is equal to the ratio of the fracture energy to the characteristic length as follows:

$$\frac{G_f}{L_r} = \int_0^{\infty} f_{ts,base} d\varepsilon_{c1} \quad (4.5.3.2)$$

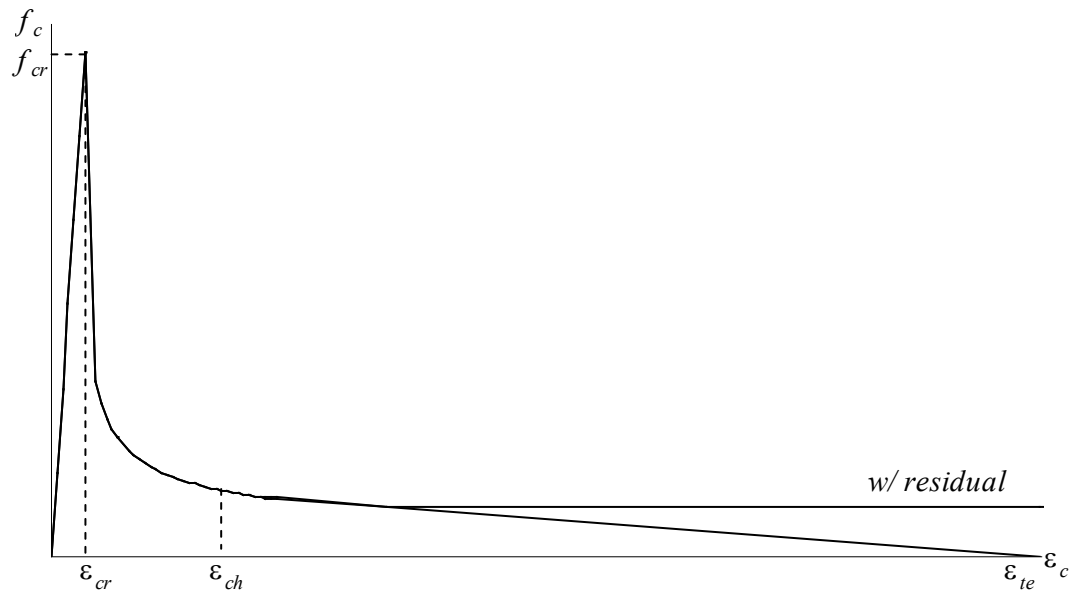


Figure 40: Yamamoto tension softening response with and without residual

4.5.5 Nonlinear (Hordijk)

Hordijk et al. carried out experiments on the crack softening behaviour of normal-weight and light-weight concrete, resulting in nonlinear curves for the post-peak tensile stress-strain behaviour for both concrete types. Both deformation controlled tensile tests and cyclic tests were performed. From their experiments, Hordijk obtained stress-deformation envelope curves.

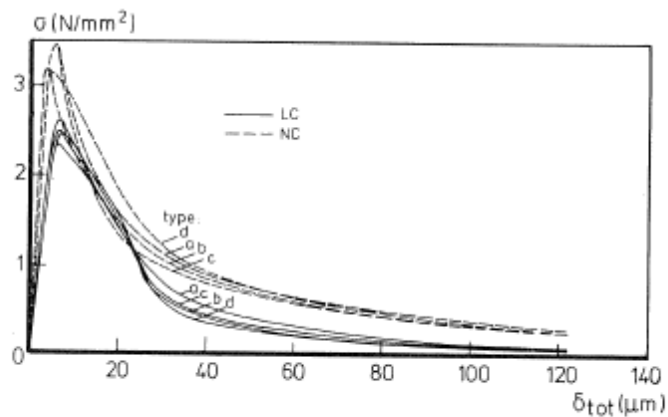


Figure 41: Envelope curves for normal and light-weight concrete (Cornelissen et al, 1986)

Stress-crack opening relationships were developed from the envelope curves shown in Figure 41 above, and a mathematical model was derived.

This mathematical model for both concrete types is shown below (Cornelissen et al, 1986):

$$\sigma/f_t = f(\delta) - (\delta/\delta_0)f(\delta = \delta_0) \quad (4.5.5.1)$$

$$f(\delta) = (1 + (C_1\delta/\delta_0)^3) \exp(-C_2\delta/\delta_0) \quad (4.5.5.2)$$

Where δ_0 is the crack opening at which stress cannot be transferred. The values for δ_0 and the two constants are shown in Figure 42.

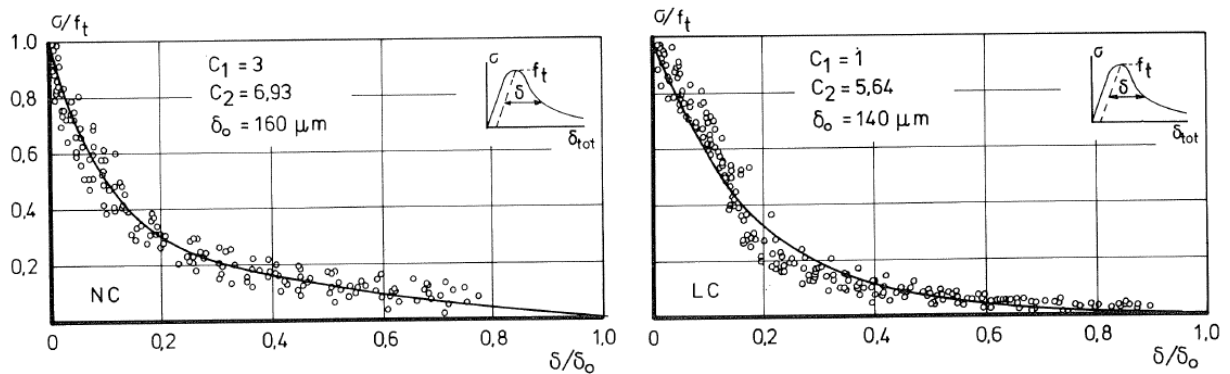


Figure 42: Stress-crack opening relationships (Cornelissen et al., 1986)

The above model has been adapted for VecTor2 and is implemented using the following formulation:

$$f_{c1} = f_{cr} \left[\left(1 + \left(C_1 \frac{w_{crx}}{w_{ult}} \right)^3 \right) \exp \left(-C_2 \frac{w_{crx}}{w_{ult}} \right) - \frac{w_{crx}}{w_{ult}} (1 + C_1^3) \exp(-C_2) \right] \quad (4.5.5.3)$$

where

$$C_1 = 3 \quad (4.5.5.4)$$

$$C_2 = 6.93 \quad (4.5.5.5)$$

$$w_{ult} = \frac{5.136G_F}{f_{cr}} \quad (4.5.5.6)$$

4.5.6 Exponential

This tension softening formulation is recommended for FRC members, and is implemented in VecTor2 as follows:

$$f_{c,t} = f_{cr} \exp\left(-\frac{f_{cr} w_{cr}}{G_f}\right) \quad (4.5.6.1)$$

where G_f is the concrete fracture energy.

4.5.7 Custom Input-Strain Based

A custom tension softening curve can be input by entering four stress-strain values in the Auxiliary Tab of the Model Page. This strain-based custom tension softening model is based on tension prism or dog-bone responses (direct tension test results) and requires the manual input of $f_{c1} - \epsilon_{c1}$ data. Based on the input stress-strain values, VecTor2 constructs a tension softening response; for strain values between the specified data points, the program calculates the stress through linear interpolation.

Figure 43 illustrates the custom input-strain based curve.

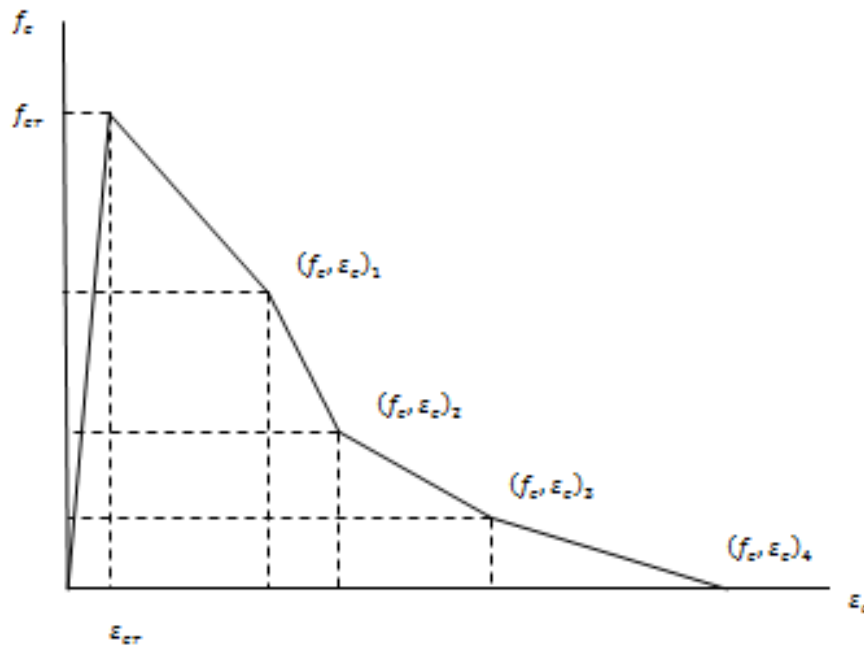


Figure 43: Custom input-strain based tension softening in VecTor2

4.5.8 Custom Input-Crack Based

This type of custom tension softening is also based on dog-bone responses and requires the manual input of $f_{c1} - w$ data.

For the crack based tension softening response, the user still inputs the tension softening data as $f_{c1} - \varepsilon_{c1}$ data points, and VecTor2 converts them to $f_{c1} - w$ data as follows:

$$w = 1000 \cdot \frac{\varepsilon_{c1}}{s_{cr1}} \quad (4.5.8.1)$$

Similar to the strain-based input, stress is calculated through linear interpolation between the input data points.

4.5.9 FRC (fib Model Code 2010)

The fib Model Code formulation for FRC in tension is based on the bending test results of a rectangular beam with a notch. The load-displacement response of the flexural member is used for an evaluation of the tensile stress-crack mouth opening displacement (CMOD), which is then employed to derive a simple linear post-crack constitutive law for the tensile stress-crack width response of FRC in tension.

From the two residual flexural strengths, f_{R1} and f_{R3} , at the CMODs of 0.5 and 2.5 mm, respectively, the tensile stresses at a crack width, w_{cr} , can be evaluated as follows:

$$f_{Fts} = 0.45 f_{R1} \quad (4.5.9.1)$$

$$f_{Ftu} = f_{Fts} - \frac{w_{cr}}{CMOD_3} (f_{Fts} - 0.5f_{R3} + 0.2f_{R1}) \geq 0 \quad (4.5.9.2)$$

where, f_{Fts} is the residual tensile stress at an initial crack opening. The figures below illustrate the relationship between the stress-CMOD response measured from the bending test and the stress-crack width response of FRC in tension.

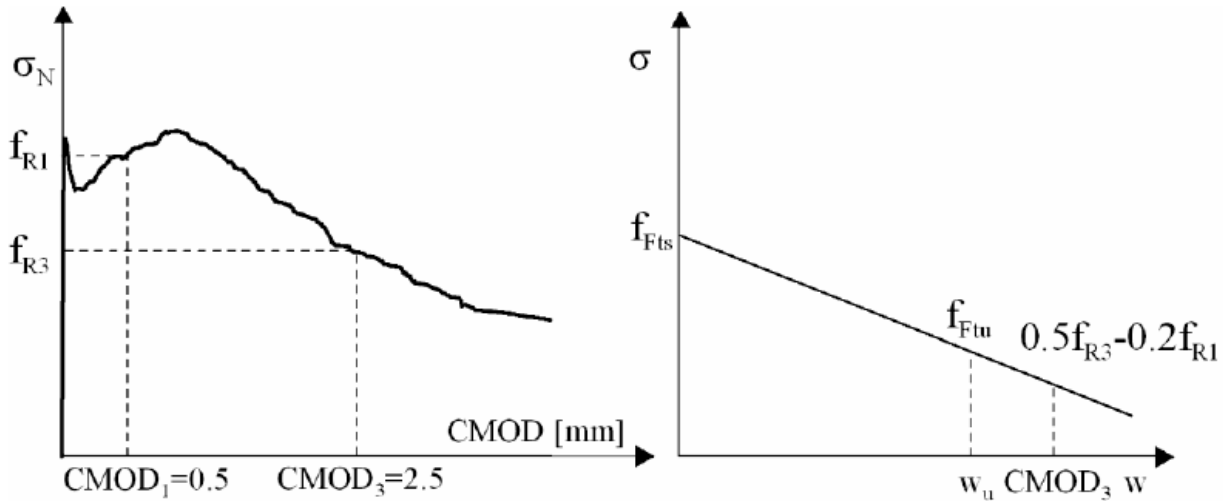


Figure 44 tension-crack opening relationship in fib model code 2010 (fib, 2010)

4.6 FRC Tension

A number of models are available in VecTor2 specifically for the consideration of the contribution of steel fibre reinforcement to concrete tensile strength. This section describes the available formulations.

4.6.1 Not Considered

This option should be used for regular reinforced concrete, where no steel fibres are added.

4.6.2 SDEM-Monotonic (Lee et al 2012)

The Simplified Diverse Embedment Model (SDEM) for monotonic loading conditions expresses the tensile stress in the fibres through the frictional bond behavior in straight fibres and the additional mechanical anchorage in hooked-end fibres.

For both hooked and straight fibres the tensile stress attained by the frictional bond behavior of fibres is:

$$f_{st} = \alpha_f V_f K_{st} \tau_{f,max} \frac{l_f}{d_f} \left(1 - \frac{2w_{cr}}{l_f}\right)^2 \quad (4.6.2.1)$$

where

$$K_{st} = \begin{cases} \frac{\beta_f w_{cr}}{3 s_f} & \text{for } w_{cr} \leq s_f \\ 1 - \sqrt{\frac{s_f}{w_{cr}}} + \frac{\beta_f}{3} \sqrt{\frac{s_f}{w_{cr}}} & \text{for } w_{cr} > s_f \end{cases} \quad (4.6.2.2)$$

$$\tau_{f,max} = 0.396\sqrt{f'_c} \quad (4.6.2.3)$$

$$\beta_f = 0.6$$

and α_f is the fibre orientation factor (=0.5 for a 3D infinite element), V_f is the fibre volumetric ratio, K_{st} is the bond modulus, l_f is the fibre length.

The value of $\beta_f = 0.6$ is used in order to prevent the tensile stress due to fibres being overestimated, which correlates well with data from the Diverse Embedment Model.

For end-hooked fibres, additional tensile stress is attained from the mechanical anchorage of the hooked ends. The tensile stress attained through this anchorage is calculated in VecTor2 using the following formulation:

$$f_{eh} = \alpha_f V_f K_{eh} \tau_{eh,max} \frac{2(l_i - 2w_{cr})}{d_f} \quad (4.6.2.4)$$

where

$$K_{eh} = \begin{cases} \beta_{eh} \left[\frac{2 w_{cr}}{3 s_{eh}} - \frac{1}{5} \left(\frac{w_{cr}}{s_{eh}} \right)^2 \right] & \text{for } w_{cr} \leq s_{eh} \\ 1 + \left(\frac{7\beta_{eh}}{15} - 1 \right) \sqrt{\frac{s_{eh}}{w_{cr}}} - \frac{2(\sqrt{w_{cr}} - \sqrt{s_{eh}})^2}{l_f - l_i} & \text{for } s_{eh} < w_{cr} \leq \frac{l_f - l_i}{2} \end{cases} \quad (4.6.2.5)$$

$$\tau_{eh,max} = \frac{4P_{eh,max}}{\pi d_f^2} = 0.429\sqrt{f'_c} \quad (4.6.2.6)$$

$$\beta_{eh} = 0.8 \quad (4.6.2.7)$$

The value of $\beta_{eh} = 0.8$ is used in order to prevent the tensile stress due to fibres being overestimated, which correlates well with data from the Diverse Embedment Model.

Thus the tensile stress attained by steel fibres according to SDEM-Monotonic is:

$$f_f = f_{st} \quad \text{for straight fibres} \quad (4.6.2.8)$$

$$f_f = f_{st} + f_{eh} \quad \text{for hooked end fibres} \quad (4.6.2.9)$$

4.6.3 SDEM-Cyclic

For the cyclic behavior of fibre-reinforced concrete, the SDEM-Cyclic model calculates the unloading and reloading stiffness for the tensile stress attained by the fibres. For the envelope tensile stress-crack width response of fibre-reinforced concrete, the formulations for the stress attained by the fibres are the same as SDEM-Monotonic. The formulations for the stiffness of the unloading and reloading paths are the following:

$$E_{un} = E_{st} + E_{eh} \quad (4.6.3.1)$$

$$E_{st} = \alpha_f V_f \tau_{f,max} \frac{l_f}{d_f} \frac{\beta_f}{3s_f} \left(1 - \frac{2w_{cr,exp}}{l_f} \right) \quad (4.6.3.2)$$

$$E_{eh} = \alpha_f V_f \tau_{eh,max} \frac{l_i}{d_f} \frac{4\beta_{eh}}{3s_{eh}} \frac{l_i - 2w_{cr,exp}}{l_f} \quad (4.6.3.3)$$

In the above formulations, E_{st} is the stiffness due to the frictional bond behavior of the steel fibres, E_{eh} is the stiffness due to mechanical anchorage, and $w_{cr,exp}$ is the maximum experienced crack width.

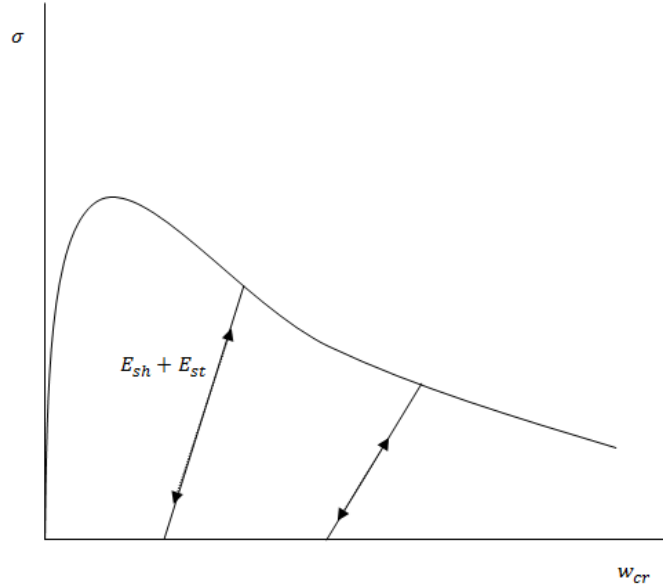


Figure 45: Stiffness for the re- and unloading response of FRC in cyclic tension

4.6.4 Diverse Embedment Model (DEM, Lee et al 2011)

The Diverse Embedment Model (DEM) considers various mechanisms involved in the tensile behaviour of SFRC. The DEM considers the pullout behaviour of individual fibres, the random distribution of fibres, and the effects of finite member dimensions. The fibre tensile stress at a crack can be calculated from the analysis for the pullout behaviour of a fibre embedded on both sides; both the frictional bond behaviour of a straight fibre and the mechanical anchorage effect of an end-hooked fibre are accounted for.

The fibre tensile stress at a crack is affected by the fibre inclination angle and fibre embedment length, thus the average fibre tensile stress at a crack, for a three-dimensional infinite element, can be expressed by the following equation:

$$\sigma_{f,cr,avg} = \frac{2}{l_f} \int_0^{l_f/2} \int_0^{\pi/2} \sigma_{f,cr}(l_a, \theta) \sin \theta \, d\theta \, dl_a \quad (4.6.4.1)$$

where l_f is the fibre length, l_a is the fibre embedment length for the shorter embedded part across a crack, $\sigma_{f,cr}$ is the fibre stress at a crack with a given fibre inclination angle and embedment length, and θ is the fibre inclination angle from the axis perpendicular to the crack surface. In this formulation $\sin \theta$ is the probability function for the fibre inclination angle. From the average fibre stress at a crack, the tensile stress attained by the fibres can be calculated by accounting for the fibre orientation factor and volumetric ratio:

$$f_f = \alpha_f V_f \sigma_{f,cr,avg} \quad (4.6.4.2)$$

where α_f is the fibre orientation factor and V_f is the volumetric ratio. The fibre orientation factor varies in regions where the distance to a boundary surface is less than the fibre length; moving inward away from all boundaries, the factor converges to 0.5. In VecTor2, the fibre orientation factor is calculated using the following expression, where h is the member thickness:

$$\alpha_f = \begin{cases} -0.05 \left(\frac{h}{l_f}\right)^{2.8} + 0.64 & \text{for } \frac{h}{l_f} \leq 1 \\ 0.087 \left(\frac{l_f}{h}\right)^{1.12} + 0.5 & \text{for } \frac{h}{l_f} > 1 \end{cases} \quad (4.6.4.3)$$

4.6.5 Variable Engagement Model (VEM: Voo & Foster 2003)

The Variable Engagement Model (VEM) expresses the force in a single steel fibre based on the calculation of the crack opening displacement at which the fibres become actively engaged; for mechanically anchored fibres, once the adhesive between the concrete and fibre is broken, slip must occur before anchorage is engaged.

In VEM, the tensile stress attained by fibres can be evaluated as:

$$\sigma = K_f K_d \frac{d_f}{l_f} V_f \tau_b \quad (4.6.5.1)$$

Where τ_b is the bond strength of a fibre, K_d is the damage factor or fibre efficiency factor, which accounts for the effect that the pullout of adjacent fibres has on the bond efficiency in a particular fibre; the damage factor decreases as the volume of fibres increases, but generally taken as one. K_f is the factor to account for fibre orientation and engagement. Where fibre fracture is not possible, K_f is calculated using the following equation:

$$K_f = \frac{\tan^{-1}(w/\alpha)}{\pi} \left(1 - \frac{2w}{l_f}\right)^2 \quad (4.6.5.2)$$

Where fibre fracture is possible, numerical integration is used to calculate K_f :

$$K_f = \left[\frac{2}{\pi} \cdot \frac{1}{l_f/2 - w} \int_0^{\theta_{crit}} \int_w^{l_{a,crit}} k(l_a, \theta) dl_a d\theta \right] \cdot \left(1 - \frac{2w}{l_f}\right); \quad (4.6.5.3)$$

$$l_{a,crit} = \min\left(\frac{d_f \sigma_{fu}}{4 \tau_b} + w_e, l_f/2\right) \quad (4.6.5.4)$$

$$\theta_{crit} = \tan^{-1}(w/\alpha) \quad (4.6.5.5)$$

where θ is a fibre inclination angle from the normal direction to crack surface, and $l_{a,crit}$ is the critical fibre embedment length for fibre fracture. When fibre fracture is not possible, the critical embedment length for fracture is equal to $l_f/2$ and equation (4.6.5.3) reduces to equation (4.6.5.2). In equation (4.6.5.2) and equation (4.6.5.5), α is an engagement factor which is usually chosen as $d_f/3.5$.

4.6.6 fib Model Code 2010

FRC in tension, according to fib Model Code 2010, has been described in Section 4.5.9 of this manual.

4.7 Lateral Expansion

Lateral expansion effects are modeled in VecTor2 according to the formulation discussed in Section 2.5.1. Due to internal microcracking, the rate of concrete lateral expansion increases as the compressive stress increases. Near the peak compressive stress, the volume of concrete expands as cracking becomes extensive. When confined by reinforcement, the lateral expansion gives rise to passive confining pressures, which may significantly enhance the strength and ductility of concrete in compression.

For concrete in tension, the Poisson's ratios are computed in the following manner regardless of the selected lateral expansion model. If the concrete is uncracked, then ν_{12} and ν_{21} are equal to the initial Poisson's ratio, ν_o . If the concrete is cracked, then the Poisson's ratio decreases linearly from ν_o at the cracking strain, ε_{cr} , to zero at two times the cracking strain.

$$\nu_{12} = \nu_{21} = \begin{cases} \nu_o & \text{for } 0 < \varepsilon_{c1} < \varepsilon_{cr} \\ \nu_o \left(1 - \frac{\varepsilon_{c1}}{2\varepsilon_{cr}} \right) \geq 0 & \text{for } \varepsilon_{cr} < \varepsilon_{c1} \end{cases} \quad (4.7.1)$$

The following lateral expansion models pertain to the determination of the Poisson's ratio, ν_{ij} , relating the expansion of concrete in the principal i -direction due to compressive straining, ε_{cj} , in the principal j -direction.

4.7.1 Constant Poisson's ratio

The Poisson's ratios ν_{ij} are always equal to the initial value, ν_o .

$$\nu_{ij} = \nu_o \quad \text{for } \varepsilon_{cj} < 0 \quad (4.7.1.1)$$

4.7.2 Variable Poisson's Ratio – Kupfer

Based on strain data of Kupfer et al. (1969), the Poisson's ratio ν_{ij} increases nonlinearly as compressive strain increases. The Poisson's ratio, shown in Figure 46, is computed as follows:

$$\nu_{ij} = \begin{cases} \nu_o & \text{for } -0.5\varepsilon_p < \varepsilon_{cj} < 0 \\ \nu_o \left[1 + 1.5 \left(\frac{-2\varepsilon_{cj}}{\varepsilon_p} - 1 \right)^2 \right] \leq 0.5 & \text{for } \varepsilon_{cj} < -0.5\varepsilon_p \end{cases} \quad (4.7.2.1)$$

where ε_p is the strain corresponding to the peak compressive stress.

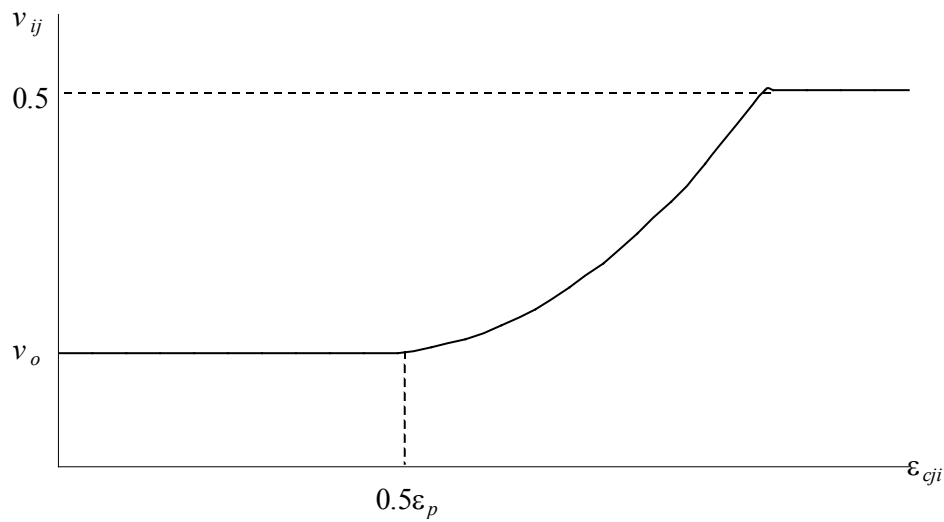


Figure 46: Kupfer variable Poisson's ratio model

4.7.3 Variable Poisson's Ratio – Montoya

This concrete dilation model from Montoya was proposed in conjunction with the concrete compression post-peak stress-strain curve described in section 4.2.6. As mentioned previously, the model was verified with and accounts for a wide range of confinement levels, with lateral pressures of up to 100% of the unconfined concrete strength. The formulation models concrete dilation as a function of the lateral pressure ratio and the concrete compressive strength. The model proposed by Montoya was based on cylinder tests carried out by Imran and Pantazopoulou, where the cylinders were subjected to different confinement levels and loading paths. The resulting proposed model is (Montoya et al, 2006):

$$\varepsilon_{cl} = \left(1.9 + 24.2 \frac{f_{cl}}{f'_c} \right) \left(\frac{\varepsilon_c}{\varepsilon_{cc}} \right)^2 \quad (4.7.3.1)$$

$$\nu = \left(1.9 + 24.2 \frac{f_{cl}}{f'_c}\right) \frac{\varepsilon_c}{\varepsilon_{cc}^2} \cdot 10^{-3} + \nu_o \quad (4.7.3.2)$$

$$\nu_o \leq \nu \leq 1.1 \quad (4.7.3.3)$$

$$f_{cli} = -\frac{(f_{cj} + f_{ck})}{2}; \quad f_{cli} > 0, \quad f_{cj}, f_{ck} < 0 \quad (4.7.3.4)$$

where f_{c1} is the lateral pressure, f'_c is the unconfined concrete strength, ε_{cc} is the strain at peak stress, ν is the secant poisson ratio, and j, k , are the principle directions normal to i .

These relationships are based on cylinder tests with constant lateral pressure throughout loading. However, they can also be used in incremental calculations with varying lateral pressure and strain at peak stress. For constant lateral pressure and peak strain, the relationship becomes a straight line, where the lateral strain increases proportional to axial strain. Comparisons to experimental results are shown in Figure 47.

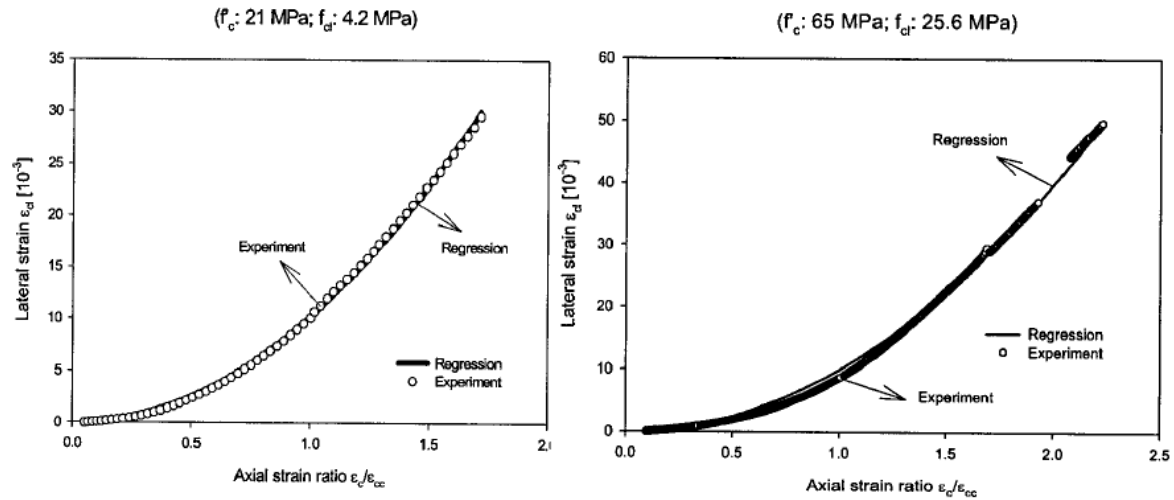


Figure 47: Lateral strain-axial strain curves for Imran-Pantazopoulou tests (Montoya, 2003)

There is no maximum value for the secant Poisson's ratio. However, in finite element programs, the deformation capacity of the elements used will provide a limit (Montoya, 2003).

4.7.4 Variable Montoya With Limit

In this model, the lateral pressure and poisson's ratio is calculated in the same way as the Montoya 2003 model. The only modification in this model is that a limit of $\nu = 0.50$ is imposed on the calculated Poisson's ratio.

4.8 Confinement Strength

Confined concrete exhibits enhanced strength and ductility in compression. In VecTor2, strength enhancement due to confinement is effected by a strength enhancement factor, β_l , which is calculated by the confinement strength models. The value of β_l serves to modify the concrete compression response curves by increasing both the uniaxial compressive strength, f'_c , and corresponding strain, ϵ_o , to determine the peak compressive strength, f_p , and corresponding strain, ϵ_p , as follows:

$$f_p = \beta_d \beta_l f'_c \quad (4.8.1)$$

$$\epsilon_p = \beta_d \beta_l \epsilon_o \quad (4.8.2)$$

(The parameter, β_d , accounts for compression softening. Also, note that the calculation of ϵ_p is subject to modification if certain compression softening models are selected.)

4.8.1 Strength Enhancement Neglected

The uniaxial compressive strength and corresponding strain are not enhanced for confinement.

$$\beta_l = 1 \quad (4.8.1.1)$$

4.8.2 Kupfer / Richart Model

In the case of triaxial compression, in which $f_{c3} < f_{c2} < f_{c1} < 0$, the strength enhancement factor for the direction of the largest compressive stress, f_{c3} , is determine by the equation below. The first term is an adaptation of the relationship proposed by Kupfer et al. (1969) to determine the strength of concrete subject to biaxial compression. The second term is the stress enhancement in columns with spiral reinforcement as noted by Richart et al. (1928).

$$\beta_l = \left[1 + 0.92 \left(\frac{f_{cn}}{f'_c} \right) - 0.76 \left(\frac{f_{cn}}{f'_c} \right)^2 \right] + 4.1 \left(\frac{f_{cl}}{f'_c} \right), \quad f_{c2} < f_{c1} < 0 \quad (4.8.2.1)$$

where f'_c is the uniaxial concrete cylinder compressive strength, f_{cn} is the difference in normal lateral stresses acting on the concrete:

$$f_{cn} = -(f_{c2} - f_{c1}) > 0 \quad (4.8.2.2)$$

and f_{cl} is the lateral confining stress on the concrete:

$$f_{cl} = -f_{c1} > 0 \quad (4.8.2.3)$$

The strength enhancement factor for the other compressive stress directions are similarly determined by interchanging f_{c3} , f_{c2} , f_{c1} as necessary.

The above expressions can be extended to the case of biaxial compression, in which $f_{c3} < f_{c2} < 0$ and $f_{c1} = 0$, to determine the strength enhancement factor for the direction of the largest compressive stress, f_{c3} . Strength enhancement in the direction of f_{c2} , is similarly determined by interchanging f_{c3} for f_{c2} in the above equations. Note that in either case, the second term of equation 4.8.2.1 is zero.

4.8.3 Selby Model

In this model, the stress required to cause failure in the direction of the maximum compressive stress, f_{c3f} , in the presence of compressive stresses, f_{c1} and f_{c2} is determined by numerically solving the failure surface of Hsieh et al. (1979):

$$2.0108 \frac{J_2}{f'_c{}^2} + 0.9714 \frac{\sqrt{J_2}}{f'_c} + 9.1412 \frac{f_{c1}}{f'_c} + 0.2312 \frac{I_1}{f'_c} - 1 = 0 \quad (4.8.3.1)$$

where I_1 is the first stress invariant determined as:

$$I_1 = f_{c1} + f_{c2} + f_{c3f} \quad (4.8.3.2)$$

and J_2 is the second deviatoric stress invariant determined as:

$$J_2 = \frac{1}{6} \left[(f_{c1} - f_{c2})^2 + (f_{c2} - f_{c3f})^2 + (f_{c3f} - f_{c1})^2 \right] \quad (4.8.3.3)$$

The stress enhancement factor β_l is the ratio of the failure stress, f_{c3f} , to the uniaxial concrete cylinder strength, f'_c :

$$\beta_t = \frac{f_{c3f}}{f'_c} \quad (4.8.3.4)$$

4.8.4 Montoya / Ottosen

In this model, the stress required to cause failure in the direction of the maximum compressive stress, f_{c3f} , in the presence of compressive stresses, f_{c1} and f_{c2} is determined by numerically solving the four parameter failure surface of Ottosen (1979):

$$\frac{A \cdot J_2}{f'_c{}^2} + \frac{\lambda \sqrt{J_2}}{f'_c} + \frac{B \cdot I_1}{f'_c} - 1 = 0 \quad (4.8.4.1)$$

I_1 is the first stress invariant determined by Equation 4.8.3.2 and J_2 is the second deviatoric stress invariant determined by Equation 4.8.3.3.

The first dimensionless parameter A is computed as follows:

$$A = \begin{cases} 2.731 & \text{for } R < 0.2 \text{ and } f'_c \leq 40 \text{ MPa} \\ 12.039 & \text{for } R < 0.2 \text{ and } f'_c > 40 \text{ MPa} \\ 2.327 & \text{for } R > 0.2 \text{ and } f'_c \leq 40 \text{ MPa} \\ 14.128 & \text{for } R > 0.2 \text{ and } f'_c > 40 \text{ MPa} \end{cases} \quad (4.8.4.2)$$

R is the ratio of the lateral compressive stress, f_l to the uniaxial concrete strength, f'_c , computed as follows:

$$R = \frac{f_{cl}}{f'_c} \quad (4.8.4.3)$$

$$f_{cl} = -\frac{(f_{c1} + f_{c2})}{2} \quad (4.8.4.4)$$

The second dimensionless parameter B is determined from the concrete tensile strength, f_t , and the concrete biaxial compressive strength, f_{bc} , as follows:

$$B = \frac{A}{9} \cdot \frac{f_{bc} - f_t}{f'_c} + \frac{1}{3} \left(\frac{f'_c}{f_t} - \frac{f'_c}{f_{bc}} \right) \quad (4.8.4.5)$$

$$f_t = 0.65(f'_c)^{0.33} \quad (4.8.4.6)$$

$$f_{bc} = 1.16f'_c \quad (4.8.4.7)$$

The value of λ is computed using the third and fourth dimensionless parameters, K_1 and K_2 , as follows:

$$\lambda = K_1 + K_2 \cos 3\theta \quad (4.8.4.8)$$

$$K_1 = \frac{\sqrt{3}}{2} \left[\frac{f'_c}{f_t} - \left(\frac{A}{3} \right) \left(\frac{f_t}{f'_c} + 1 \right) + 1 \right] \quad (4.8.4.9)$$

$$K_2 = \frac{\sqrt{3}}{2} \left[\frac{f'_c}{f_t} - \left(\frac{A}{3} \right) \left(\frac{f_t}{f'_c} - 1 \right) - 2B - 1 \right] \quad (4.8.4.10)$$

The invariant $\cos 3\theta$ is computed as follows:

$$\cos 3\theta = \frac{5.196J_3}{2J_2^{1.5}} \quad (4.8.4.11)$$

where the third deviatoric stress invariant J_3 is given by:

$$J_3 = \left(f_{c1} - \frac{I_1}{3} \right) \left(f_{c2} - \frac{I_1}{3} \right) \left(f_{c3f} - \frac{I_1}{3} \right) \quad (4.8.4.12)$$

The stress enhancement factor β_l is the ratio of the failure stress, f_{c3f} , to the uniaxial concrete cylinder strength, f'_c :

$$\beta_l = \frac{f_{c3f}}{f'_c} \quad (4.8.4.13)$$

4.9 Cracking Criterion

The cracking strength of concrete, f_{cr} , is not an inherent material property. In addition to factors such as specimen size, and compressive strength, the cracking strength varies with the stress states. In particular, the cracking strength generally decreases as transversely acting compressive stresses increase. The cracking criterion accounts for this effect by computing f_{cr} , based on the coexisting compressive stresses or strains. Therefore, f_{cr} is generally different from the input value of concrete tensile strength, f'_t . Having determined f_{cr} , the cracking strain, ε_{cr} , is computed by assuming a linear-elastic relationship before cracking:

$$\varepsilon_{cr} = \frac{f_{cr}}{E_c} \quad (4.9.1)$$

where E_c is initial tangent stiffness of concrete. The values of f_{cr} and ε_{cr} are then used in the tension stress-strain response and tension stiffening models. The following discussion describes the available cracking criterion models.

4.9.1 Uniaxial cracking stress

The cracking strength is taken as the specified uniaxial cracking strength:

$$f_{cr} = f'_t \quad (4.9.1.1)$$

4.9.2 Mohr-Coulomb (Stress)

The Mohr-Coulomb criterion is often used to determine the failure shear stress and failure plane for a given set of coexisting normal stresses in a frictional material, concrete in this case. It is implicitly assumed that the concrete is sufficiently ductile to redistribute stresses along the failure plane. The failure envelope is tangent to the Mohr's circles defining combinations of shear stress, τ , and normal stresses, f_{c1} and f_{c3} , resulting in shear failure.

As shown in Figure 48, the shear strength is comprised of a stress-independent component and a stress-dependent component. The latter is the internal angle of friction, ϕ , which VecTor2 assumes is 37° . The former is the cohesion, c , which is determined by noting that at failure in uniaxial compression, the maximum compressive stress, f_{c3} , is equal to the concrete cylinder strength, f'_c , and f_{c1} is zero. Therefore:

$$c = f'_c \frac{1 - \sin \phi}{2 \cos \phi} \quad (4.9.2.1)$$

Further, when $f_{c3} = 0$, the failure tensile stress f_{c1} is equal to f_{cru} , which is computed from the envelope as:

$$f_{cru} = f'_c \frac{2c \cdot \cos \phi}{2 \cos \phi} \quad (4.9.2.2)$$

Given a set of principal concrete strains, $\varepsilon_{c3} < \varepsilon_{c2} < \varepsilon_{c1}$, the principal compressive stress, f_{c3} , is computed as follows:

$$f_{c3} = \begin{cases} -f'_c \left[2 \left(\frac{\varepsilon_{c3}}{\varepsilon_o} \right) - \left(\frac{\varepsilon_{c3}}{\varepsilon_o} \right)^2 \right] & \text{for } \varepsilon_{c3} < \varepsilon_o < 0 \\ -f'_c & \text{for } \varepsilon_o < \varepsilon_{c3} < 0 \\ 0 & \text{for } 0 < \varepsilon_{c3} \end{cases} \quad (4.9.2.3)$$

Having defined the principal compressive stress, the cracking strength is the principal tensile stress, f_{c1} , of the Mohr's circle tangent to the failure envelope. The value of f_{cr} is computed as follows:

$$f_{cr} = f_{cru} \left(1 + \frac{f_{c3}}{f'_c} \right), \quad 0.20f'_t \leq f_{cr} \leq f'_t \quad (4.9.2.4)$$

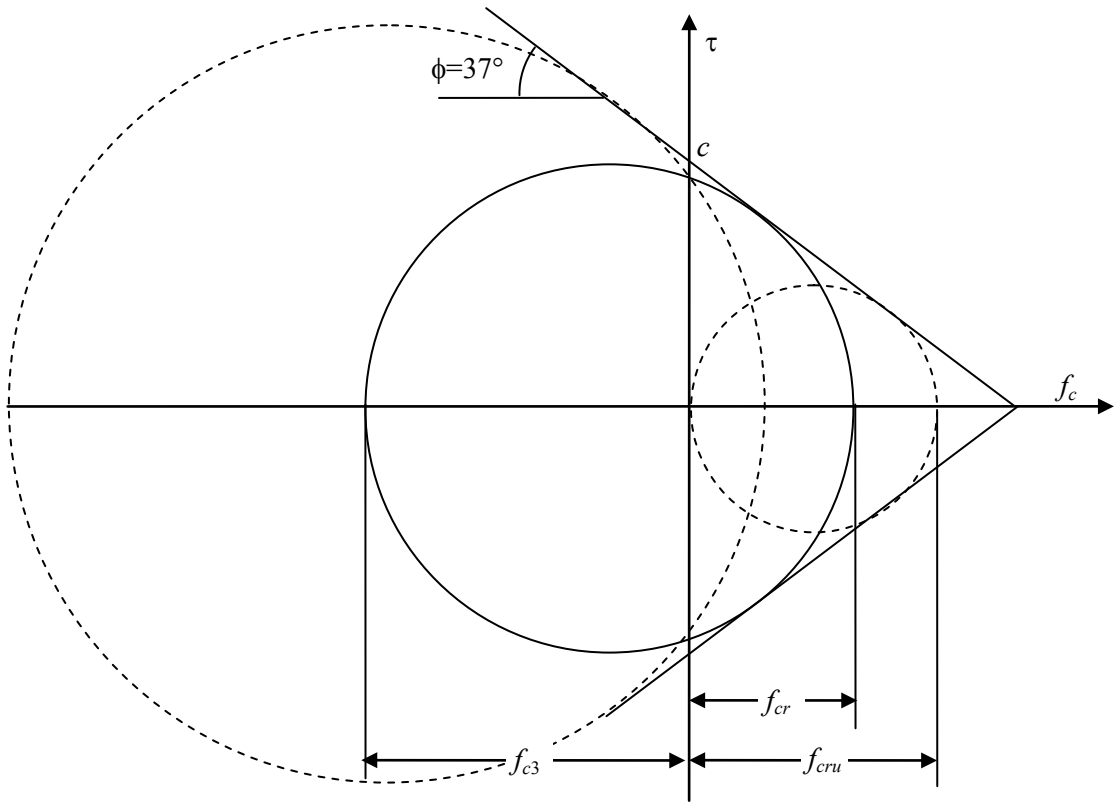


Figure 48: Mohr-Coulomb (Stress) cracking criterion

4.9.3 Mohr-Coulomb (Strain)

This model is similar to the Mohr-Coulomb (Stress) model. Given a set of principal concrete strains, $\varepsilon_{c3} < \varepsilon_{c2} < \varepsilon_{c1}$, and the strain ε_o corresponding to the uniaxial concrete cylinder compressive strength, the failure cracking strength is computed as follows:

$$f_{cr} = f_{cru} \left(1 - \frac{\varepsilon_{c3}}{\varepsilon_o} \right), \quad 0.20f'_t \leq f_{cr} \leq f'_t \quad (4.9.3.1)$$

4.9.4 CEB-FIP Model

The CEB-FIP model reduces the cracking strength for increasing biaxial compression, based on the linear relationship proposed by Kupfer et al. (1973):

$$f_{cr} = f_{cru} \left(1 + 0.8 \frac{f_{c3}}{f'_c} \right), \quad 0.20f'_t \leq f_{cr} \leq f'_t \quad (4.9.4.1)$$

The principal compressive stress, f_{c3} , is computed from equation 4.9.2.3. The unconfined cracking strength, f_{cru} , is computed from the compressive strength, f'_c , as follows:

$$f_{cru} = 0.6\sqrt{f'_c} \quad (4.9.4.2)$$

4.9.5 Gupta 1998 Model

In an investigation of reinforced concrete members subject to high levels of axial compression and shear, Gupta (1998) observes that the predicted shear capacity is sensitive to the assumed cracking strength, f_{cr} . In examining data from Kupfer et al. (1969), Gupta notes that the cracking strength of concrete reduces rapidly at high levels of compression due to internal microcracking. Gupta proposes a linear reduction in cracking strength, with increasing compressive strain as follows:

$$f_{cr} = f'_t \left(1 - \frac{\varepsilon_{c2}}{\varepsilon_o} \right), \quad 0.25f'_t \leq f_{cr} \leq f'_t \quad (4.9.5.1)$$

where ε_{c2} is the principal compressive strain, ε_o is the strain corresponding to the concrete cylinder compressive strength, f'_c .

4.10 Crack Stress Check

Calculation of the shear stress on a crack is included in VecTor2. The basic method for calculating this stress is the DSFM/MCFT. An advanced option for calculation stress along a crack is also available in VecTor2 and utilizes a different convergence criteria.

4.10.1 Crack Stress Calc Omitted

Calculation of shear stress on the crack is ignored.

4.10.2 Basic (DSFM/MCFT)

The basic option for crack stress calculation is based on the Modified Compression Field Theory (MCFT) and Disturbed Stress Field Model (DSFM). The MCFT stress calculations are based on Vecchio-Collins (1986). In the MCFT, stress is transferred across a crack through aggregate interlock.

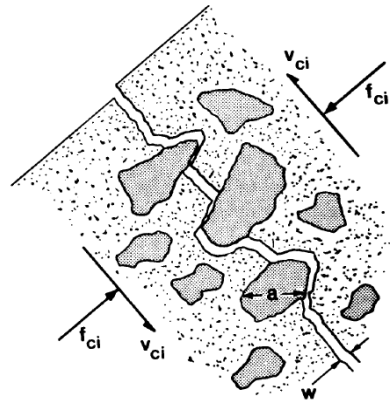


Figure 49: Shear across with crack through aggregate interlock

The tensile stresses at a crack are zero, but the local shear stresses on the crack, v_{ci} are calculated using the equation below, and are accompanied by small local compressive stresses across the crack, f_{ci} , based on work by Walraven (Vecchio-Collins, 1986).

$$v_{ci} = 0.18v_{ci,max} + 1.64f_{ci} - 0.82 \frac{f_{ci}^2}{v_{ci,max}} \quad (4.10.2.1)$$

where

$$v_{ci,max} = \frac{\sqrt{-f'_c}}{0.31+24w/(a+16)} \quad (4.10.2.2)$$

$$w = \epsilon_1 \cdot s_{cr} \quad (4.10.2.3)$$

The formulation for s_{cr} is described in detail in section 2.5.11.

Shear stress on the crack can also be calculated by the Disturbed Stress Field Model (DSFM), which builds on the MCFT. The calculation for the maximum shear stress on the crack is formulated in VecTor2 as follows:

$$v_{ci,max} = \frac{0.18 \sqrt{f'_c}}{0.31 + \frac{24w_{cr}}{a_g + 16}} \quad (4.10.2.4)$$

4.10.3 Advanced (Lee 2009)

The advanced crack stress calculation differs in terms of the convergence criteria used; this model employs a bi-section method of convergence. The crack stress formulation, however, is the same.

4.11 Crack Width Check

The crack width check serves to reduce average compressive stresses when crack widths exceed a specified limit. This check was implemented for the analysis shear-critical reinforced concrete beams having little or no shear reinforcement (Vecchio, 2000), in which element shear-slip distortions were not considered. Such beams exhibit a dominant shear crack of considerable width at failure. It is necessary to limit the compressive stress in elements with excessive crack widths for two reasons. First, concrete near the crack exhibits tensile strains, which may exceed the calibration range of compression softening models and warrant additional softening. Secondly, if shear-slip distortions are not considered, the reorientation of the principal stresses tends to be overestimated, thereby implying a transmission of local compressive stresses across the crack. Yet, such transmission is unlikely when cracks exceed the specified limit. It was found that rapidly reducing the average compressive stress when the crack limit is exceeded provides more accurate predictions of the load-deformation response. However, it may be preferable to include element slip distortions in the analysis instead of including the crack width check.

The crack width check is implemented by reducing the average compressive stress computed from the stress-strain response, f_{c2}^* , by a crack coefficient β_{cr} as follows:

$$f_{c2} = \beta_{cr} f_{c2}^* \quad (4.11.1)$$

If the crack width check is omitted, $\beta_{cr} = 1.0$. Otherwise β_{cr} is computed as follows:

$$\beta_{cr} = \begin{cases} 1 & \text{for } w < w_l \\ 1 - (w - w_l)/3 \geq 0 & \text{for } w_l < w \end{cases} \quad (4.11.2)$$

where w is the crack width in the element, and w_l is the limiting crack width. The limiting crack width may be selected as a quarter or half the aggregate size, or widths of 1mm, 2mm, or 5mm.

When FRC is used, a maximum crack width check is automatically performed in VecTor2, limiting the tensile stress attained by the fibres. The maximum crack width for an infinite element is calculated from the average crack width, as follows (Deluce et al 2012):

$$w_{cr,max} = \left(1.7 + 3.4 \frac{V_f l_f}{d_f} \right) w_{cr,avg} \quad (4.11.1.1)$$

In order to consider the effect of element size on the difference between the maximum and average crack widths, a linear interpolation between the average crack spacing and 1000 mm is employed, as illustrated in Figure 50.

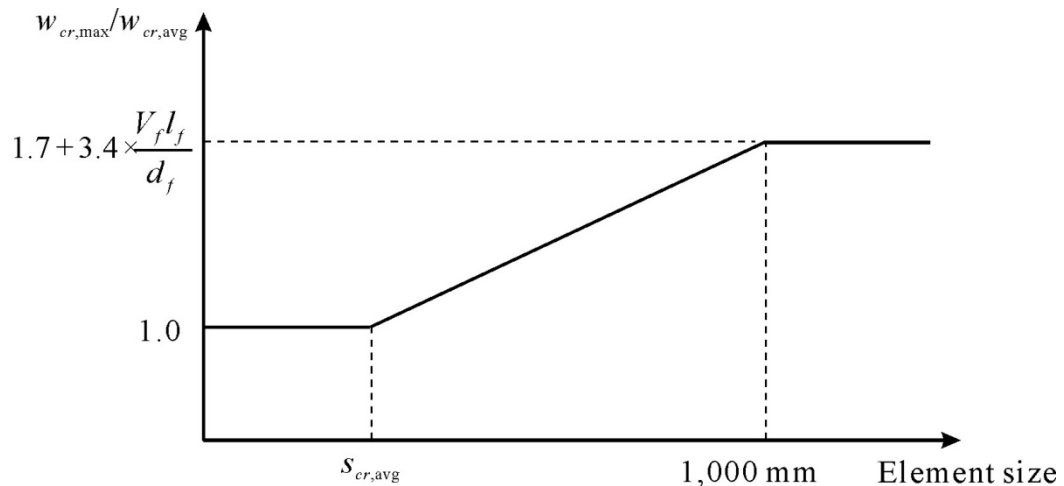


Figure 50: Maximum crack width check including effect of element size

As a result of this crack width check, the tensile stress attained by the fibres at an average crack width is limited by the stress that can be attained by the fibres at the maximum crack width:

$$f_{f,w_{cr,avg}} \leq f_{f,w_{cr,max}} \quad (4.11.1.2)$$

4.12 Crack Slip Calculation

The element slip distortion models allow the VecTor2 analysis to explicitly account for strains due to shear slip along the crack, in the manner of the Disturbed Stress Field Model. As described in Section 2.3.4, three methods are available for determining the shear slip, δ_s , along the crack: stress-based models, constant rotation lag models, and hybrid models.

Stress-based models relate the shear slip, δ_s , along the crack to the local shear stress, v_{ci} , along the crack. The shear slip strain, γ_s , is computed as the shear slip divided by the crack spacing, s :

$$\gamma_s^a = \frac{\delta_s}{s} \quad (4.12.1)$$

Note that the implemented versions of these models do not account for shear slip before the crack surfaces develop traction. As well, these models compute zero shear slip in unreinforced elements, as the local shear stress for such elements is always computed as zero.

Constant rotation lag models relate the post-cracking rotation of the principal stress field, $\Delta\theta_\sigma$, to the post-cracking rotation of the principal strain field, $\Delta\theta_\varepsilon$, by a specified rotation lag, θ^l , as follows:

$$\Delta\theta_\sigma = \begin{cases} \Delta\theta_\varepsilon & \text{for } |\Delta\theta_\varepsilon| \leq \theta^l \\ (\Delta\theta_\varepsilon - \theta^l) & \text{for } |\Delta\theta_\varepsilon| > \theta^l \end{cases} \quad (4.12.2)$$

The inclination of the principal stress field is determined by adding $\Delta\theta_\sigma$ to the inclination at cracking, θ_{ic} :

$$\theta_\sigma = \theta_{ic} + \Delta\theta_\sigma \quad (4.12.3)$$

Shear strains can then be determined from Mohr's circle transformation of the total strains as follows:

$$\gamma_s^b = \gamma_{xy} \cdot \cos 2\theta_\sigma + (\varepsilon_y - \varepsilon_x) \cdot \sin 2\theta_\sigma \quad (4.12.4)$$

Note that constant rotation lag models may be unsuitable at higher load intensities when the amount of lag increases and shear slip depends increasingly on the shear stress on the crack.

Hybrid models compute the shear slip strains according to both a stress-based model and a constant rotation lag model, and utilize the greater of the two values.

$$\gamma_s = \max(\gamma_s^a, \gamma_s^b) \quad (4.12.5)$$

At low load intensities, the shear slip is generally governed by the constant rotation lag model, which captures the initial slip as the crack surfaces develop traction. At higher load intensities, the shear slip is generally governed by the stress-based model, which captures the increasing slip.

Lai (2001) made the following conclusions regarding the merits of the approaches. In monotonic loading, the three stress based models (Walraven, Maekawa, and Lai/Vecchio) provided comparable levels of accuracy. In cyclic loading the Walraven model appears to be more accurate and stable. In constant rotation lag models, the lag should be taken as 10° for unreinforced elements, 7.5° for uniaxially reinforced elements and 5° for biaxially reinforced elements.

4.12.1 Not considered

As in the Modified Compression Field Theory, the analysis does not account for shear slip along the crack:

$$\gamma_s = 0 \quad (4.12.1.1)$$

4.12.2 Vecchio-Lai (Cyclic)

This model, proposed by Vecchio and Lai (2002), is a combination of the Walraven and Maekawa models and is found to provide levels of accuracy comparable to these models. The slip along the crack, δ_s , is computed as follows:

$$\delta_s = \delta_s^* \sqrt{\frac{\Psi}{1 - \Psi}} \leq 2w \quad (4.12.2.1)$$

where

$$\delta_s^* = \frac{0.5v_{ci \max} + v_{co}}{1.8w^{-0.8} + (0.234w^{-0.707} - 0.20) \cdot f_{cc}} \quad (4.12.2.2)$$

$$\Psi = \frac{v_{ci}}{v_{ci \max}} \quad (4.12.2.3)$$

$$v_{ci \max} = \frac{\sqrt{f'_c}}{0.31 + 24w/(a + 16)} \quad (4.12.2.4)$$

$$v_{co} = \frac{f_{cc}}{30} \quad (\text{in MPa}) \quad (4.12.2.5)$$

Additionally, v_{ci} is the local shear stress on the crack, f'_c is the concrete cylinder compressive strength, w is the average crack width, a is the maximum aggregate size, and f'_{cc} is the concrete cube strength, taken as $1.2f'_c$. The term v_{co} , implements an initial offset in the crack shear-slip relationship.

4.12.3 Maekawa (Monotonic)

This model is proposed by Okamura and Maekawa (1991) and utilized in their fixed non-orthogonal crack model. The slip along the crack, δ_s , is computed as follows:

$$\delta_s = w \sqrt{\frac{\Psi}{1 - \Psi}} \leq 2w \quad (4.12.3.1)$$

where,

$$\Psi = \frac{v_{ci}}{v_{ci \max}} \quad (4.12.3.2)$$

$$v_{ci \max} = \frac{\sqrt{f'_c}}{0.31 + 24w/(a + 16)} \quad (4.12.3.3)$$

Additionally, v_{ci} , f'_c , w and a are as previously defined.

4.12.4 Stress Model (Walraven)

This model is an adaptation of the formulations of proposed by Walraven and Reinhardt (1981), based on an analysis of crack structure and contact area of crack faces. The slip along the crack, δ_s , is computed as follows:

$$\delta_s = \frac{v_{ci} + v_{co}}{1.8w^{-0.8} + (0.234w^{-0.707} - 0.20) \cdot f'_{cc}} \leq 2w \quad (4.12.4.1)$$

where v_{ci} , v_{co} , w and f'_{cc} are as previously defined.

4.12.5 Hybrid-I, II, and III Models

The Hybrid-I Model combines the Walraven model with the constant rotation lag model.

The Hybrid-II Model combines the Vecchio-Lai model with the constant rotation lag model.

The Hybrid-III model combines the Maekawa model with the constant rotation lag model.

In these hybrid models, the constant rotation lag, θ^l , is taken as 10° for unreinforced elements, 7.5° for elements with one smeared reinforcement component and 5° for elements with two or more smeared reinforcement components.

4.13 Creep and Relaxation

Currently, this option is not available in VecTor2.

4.14 Hysteretic Response

As a consequence of internal damage, the stress-strain response curves of concrete under loading, unloading and reloading are non-coincident. The resulting plastic offset strains along with the area delineated by the hysteretic loops, are indicative of the internal damage and energy dissipation under cyclic loading. As such, the hysteretic response is a critical influence on the strength and ductility of reinforced concrete structures subjected to cyclic and reverse cyclic loading.

The following hysteretic response models describe how concrete reloads to and unloads from the monotonic concrete stress-strain curve. As such, the monotonic stress-strain curve is likened to a backbone, to which unloading and reloading curves attach. The hysteretic response also incorporates the plastic strain offsets that define the unloading path.

4.14.1 No Plastic Offsets

The concrete reloads linearly from and unloads linearly to the point of zero strain and zero stress of the monotonic stress-strain curve.

When reloading in the compression domain to a compressive strain of ε_c , the concrete compressive stress, f_c , is computed as follows:

$$f_c = \begin{cases} 0 & \text{for } 0 < \varepsilon_c \\ \frac{\varepsilon_c}{\varepsilon_{cm}} \cdot f_{cm} & \text{for } \varepsilon_{cm} < \varepsilon_c < 0 \\ f_{bc}(\varepsilon_c) & \text{for } \varepsilon_c < \varepsilon_{cm} < 0 \end{cases} \quad (4.14.1.1)$$

where ε_{cm} is the maximum previously attained compressive strain, f_{cm} is the corresponding stress, and $f_{bc}(\varepsilon_c)$ is the function defining the monotonic compression stress-strain base curve. In the latter case, ε_{cm} and f_{cm} are updated as ε_c and f_c respectively.

Unloading in compression results in concrete stresses as follows:

$$f_c = E_{cm}^- \cdot \varepsilon_c \quad (4.14.1.2)$$

where, E_{cm}^- is the unloading modulus in compression, computed as:

$$E_{cm}^- = \frac{f_{cm}}{\varepsilon_{cm}} \quad (4.14.1.3)$$

When reloading in the tensile domain to a tensile strain of ε_c , the concrete tensile stress, f_c , is computed as follows:

$$f_c = \begin{cases} \frac{\varepsilon_c}{\varepsilon_{tm}} \cdot f_{tm} & \text{for } 0 < \varepsilon_c < \varepsilon_{tm} \\ f_{bt}(\varepsilon_c) & \text{for } \varepsilon_{cm} < \varepsilon_c \end{cases} \quad (4.14.1.4)$$

where ε_{tm} is the maximum previously attained tensile strain, f_{tm} is the corresponding stress, and $f_{bt}(\varepsilon_c)$ is the function defining the monotonic tensile stress-strain base curve. In the latter case, ε_{tm} and f_{tm} are updated as ε_c and f_c respectively.

Unloading in tension results in concrete stresses as follows:

$$f_c = E_{tm}^- \cdot \varepsilon_c \quad (4.14.1.5)$$

where, E_{tm}^- is the unloading modulus in tension, computed as:

$$E_{tm}^- = \frac{f_{tm}}{\varepsilon_{tm}} \quad (4.14.1.6)$$

4.14.2 Plastic offsets; linear loading/unloading

This model is similar to the preceding model, except that it includes plastic offset strains as proposed by Vecchio (1999).

When reloading in the compression domain to a compressive strain of ε_c , the concrete compressive stress, f_c , is computed as follows:

$$f_c = \begin{cases} 0 & \text{for } \varepsilon_c^p < \varepsilon_c < 0 \text{ or } 0 < \varepsilon_c \\ \frac{\varepsilon_c - \varepsilon_c^p}{\varepsilon_{cm} - \varepsilon_c^p} \cdot f_{cm} & \text{for } \varepsilon_{cm} < \varepsilon_c < \varepsilon_c^p < 0 \\ f_{bc}(\varepsilon_c) & \text{for } \varepsilon_c < \varepsilon_{cm} < 0 \end{cases} \quad (4.14.2.1)$$

where ε_c^p is the current plastic offset strain, ε_{cm} is the maximum previously attained compressive strain, f_{cm} is the corresponding stress, and $f_{bc}(\varepsilon_c)$ is the function defining the monotonic compression stress-strain base curve. In the latter case, ε_{cm} and f_{cm} are updated as ε_c and f_c respectively.

At a given compressive strain, ε_c , the instantaneous plastic strain, $\varepsilon_c^{p'}$, is computed as follows:

$$\varepsilon_c^{p'} = \begin{cases} \varepsilon_c - \varepsilon_p \left[0.87 \left(\frac{\varepsilon_c}{\varepsilon_p} \right) - 0.29 \left(\frac{\varepsilon_c}{\varepsilon_p} \right)^2 \right] & \text{for } 1.5\varepsilon_p < \varepsilon_c \\ \varepsilon_c - 0.001305 \left(\frac{\varepsilon_p}{0.002} \right) & \text{for } \varepsilon_c < 1.5\varepsilon_p \end{cases} \quad (4.14.2.2)$$

where ε_p is the strain corresponding to the peak stress on the compression base curve. If $\varepsilon_c^{p'}$ is more compressive than ε_c^p , then ε_c^p is updated as $\varepsilon_c^{p'}$.

Unloading in compression results in concrete stress, f_c , is as follows:

$$f_c = E_{cm}^- (\varepsilon_c - \varepsilon_c^p) \quad (4.14.2.3)$$

where E_{cm}^- is the unloading modulus in compression, computed as:

$$E_{cm}^- = \frac{f_{cm}}{(\varepsilon_{cm} - \varepsilon_c^p)} \quad (4.14.2.4)$$

When reloading in the tensile domain to a tensile strain of ε_c , the concrete tensile stress, f_c , is computed as follows:

$$f_c = \begin{cases} \frac{\varepsilon_c - \varepsilon_c^p}{\varepsilon_{tm} - \varepsilon_c^p} \cdot f_{tm} & \text{for } \varepsilon_c^p < \varepsilon_c < \varepsilon_{tm} \\ f_{bt}(\varepsilon_c) & \text{for } \varepsilon_{cm} < \varepsilon_c \end{cases} \quad (4.14.2.5)$$

where ε_c^p is the current plastic offset strain, ε_{tm} is the maximum previously attained tensile strain, f_{tm} is the corresponding stress, and $f_{bt}(\varepsilon_c)$ is the function defining the monotonic tensile stress-strain base curve. In the latter case, ε_{tm} and f_{tm} are updated as ε_c and f_c respectively.

For a given strain, ε_c , in the tension domain, the instantaneous plastic strain, $\varepsilon_c^{p'}$, is initially the strain at which the response first traverses from the compression to tension domain. Thereafter, the monotonic stress-strain response is calculated with respect to that strain. Subsequently $\varepsilon_c^{p'}$ is updated until non-negative and held at zero afterwards such that no plastic offset strains are considered in the tension domain.

Unloading in tension results in concrete stress, f_c , as follows:

$$f_c = E_{tm}^- (\varepsilon_c - \varepsilon_c^p) \quad (4.13.2.6)$$

where E_{tm}^- is the unloading modulus in tension, computed as:

$$E_{tm}^- = \frac{f_{tm}}{(\varepsilon_{tm} - \varepsilon_c^p)} \quad (4.14.2.7)$$

4.14.3 Plastic offsets; nonlinear loading/unloading

This model proposed by Vecchio is similar to the preceding model except that unloading in the compression and tension domains follows nonlinear Ramsberg-Osgood formulations.

Unloading in compression to a strain of ε_c results in concrete stress, f_c , is as follows:

$$f_c = f_{cm} + E_c (\varepsilon_c - \varepsilon_{cm}) + \frac{E_c (\varepsilon_c - \varepsilon_{cm})^{N_c}}{N_c (\varepsilon_c^p - \varepsilon_{cm})^{N_c - 1}} \quad \text{for } 1 \leq N_c \leq 20 \quad (4.14.3.1)$$

where ε_c^p is the current plastic offset strain, ε_{cm} is the maximum previously attained compressive strain, f_{cm} is the corresponding stress. N_c is the Ramsberg-Osgood power term representing the deviation from linear elasticity. It is computed such that the initial unloading modulus is equal to the initial tangent stiffness of concrete, E_c , as follows:

$$N_c = \frac{E_c \cdot (\varepsilon_c^p - \varepsilon_{cm})}{f_{cm} + E_c (\varepsilon_c^p - \varepsilon_{cm})} \quad (4.14.3.2)$$

In the case that N_c is less than one or greater than twenty, f_c is computed by a linear unloading response between from ε_c to ε_c^p :

$$f_c = E_c (\varepsilon_c - \varepsilon_c^p) \quad \text{for } N_c \leq 1 \text{ or } 20 \leq N_c \quad (4.14.3.3)$$

Unloading in tension results in concrete stress, f_c , as follows:

$$f_c = f_{tm} - E_c (\varepsilon_{tm} - \varepsilon_c) + \frac{E_c (\varepsilon_{tm} - \varepsilon_c)^{N_t}}{N_t (\varepsilon_{tm} - \varepsilon_c^p)^{N_t - 1}} \quad \text{for } 1 \leq N_t \leq 20 \quad (4.14.3.4)$$

where ε_c^p is the current plastic offset strain, ε_{tm} is the maximum previously attained tensile strain, f_{tm} is the corresponding stress. N_t is computed as follows such that the initial unloading modulus is equal to the initial tangent stiffness of concrete, E_c :

$$N_t = \frac{E_c \cdot (\varepsilon_{tm} - \varepsilon_c^p)}{E_c (\varepsilon_{tm} - \varepsilon_c^p) - f_{tm}} \quad (4.14.3.5)$$

In the case that N_t is less than one or greater than twenty, f_c is computed by a linear unloading response between from ε_c to ε_c^p :

$$f_c = E_c (\varepsilon_c - \varepsilon_c^p) \quad \text{for } N_t \leq 1 \text{ or } 20 \leq N_t \quad (4.14.3.6)$$

4.14.4 Plastic offsets; nonlinear w/ cyclic decay (Palermo Model)

The model proposed by Palermo and Vecchio (2002) is similar to the preceding model. Modifications include modeling of damage in the reloading curves, consideration for partial unloading and reloading, the shape of the unloading of curves, and calculations of the instantaneous plastic offset strains, in both the compression and tension domains. The shape of the hysteretic responses in compression and tension are shown in Figure 51 and Figure 52, respectively.

When reloading in the compression domain to a compressive strain of ε_c , the concrete compressive stress, f_c , is computed as follows:

$$f_c = f_{ro} + E_{cm}^+ (\varepsilon_c - \varepsilon_{ro}) \quad (4.14.4.1)$$

where ε_{ro} is the strain at load reversal in the current hysteretic loop, f_{ro} is the corresponding stress, ε_{cm} is the unloading strain in the current hysteretic loop are ε_{cm} and f_{cm} is the corresponding stress.

The reloading modulus in compression, E_{cm}^+ , is computed as follows

$$E_{cm}^+ = \frac{\beta_d \cdot f_{cm} - f_{ro}}{\varepsilon_{cm} - \varepsilon_{ro}} \quad (4.14.4.2)$$

The damage indicator, β_d , serves to degrade E_{cm}^+ , such that additional straining is required to intersect the base-curve. The damage is a function of the strain recovered in unloading of the current hysteretic loop, ε_{rec} , and is computed as follows:

$$\beta_d = \begin{cases} \frac{1}{1 + 0.10(\varepsilon_{rec}/\varepsilon_p)^{0.5}} & \text{for } |\varepsilon_c| < |\varepsilon_p| \\ \frac{1}{1 + 0.175(\varepsilon_{rec}/\varepsilon_p)^{0.6}} & \text{for } |\varepsilon_c| > |\varepsilon_p| \end{cases} \quad (4.14.4.3)$$

$$\varepsilon_{rec} = \varepsilon_{cm} - \varepsilon_{ro} \quad (4.14.4.4)$$

where ε_p is the strain corresponding to the peak stress in the base-curve.

The instantaneous plastic strain, $\varepsilon_c^{p'}$, for the compression domain is computed as follows:

$$\varepsilon_c^{p'} = \varepsilon_p \left[0.166 \left(\frac{\varepsilon_{cm}}{\varepsilon_p} \right)^2 + 0.132 \left(\frac{\varepsilon_{cm}}{\varepsilon_p} \right) \right] \quad (4.14.4.5)$$

If $\varepsilon_c^{p'}$ is more compressive than ε_c^p , then ε_c^p is updated as $\varepsilon_c^{p'}$.

Unloading in compression to a strain of ε_c results in concrete stress, f_c , is as follows:

$$f_c = f_{cm} + E_c (\varepsilon_c - \varepsilon_{cm}) + \frac{E_c (0.071 - 1) (\varepsilon_c - \varepsilon_{cm})^{N_c}}{N_c (\varepsilon_c^p - \varepsilon_{cm})^{N_c - 1}} \quad (4.14.4.6)$$

where ε_c^p is the current plastic offset strain, ε_{cm} is the maximum previously attained compressive strain, f_{cm} is the corresponding stress. N_c is the Ramsberg-Osgood power term representing the deviation from linear elasticity. It is computed such that the unloading modulus is equal to the initial tangent stiffness of concrete, E_c , at the beginning of the unloading branch and equal to $0.071 E_c$ at the end of the unloading branch, as follows:

$$N_c = \frac{E_c (1 - 0.071) (\varepsilon_c^p - \varepsilon_{cm})}{f_{cm} + E_c (\varepsilon_c^p - \varepsilon_{cm})} \quad (4.14.4.7)$$

When reloading in the tensile domain to a tensile strain of ε_c , the concrete tensile stress, f_c , is computed as follows:

$$f_c = \beta_t \cdot f_{tm} - E_{tm}^+ (\varepsilon_{tm} - \varepsilon_c) \quad (4.14.4.8)$$

where ε_{tm} is the unloading strain in the current hysteretic loop, f_{cm} is the corresponding stress, and E_{cm}^+ is the reloading modulus in tension, computed as follows

$$E_{tm}^+ = \frac{\beta_t \cdot f_{tm} - f_{ro}}{\varepsilon_{tm} - \varepsilon_{ro}} \quad (4.14.4.9)$$

The damage indicator, β_t , serves to degrade E_{tm}^+ , such that additional straining is required to intersect the base-curve. The damage is a function of the strain recovered in unloading of the current hysteretic loop, ε_{rec} , and is computed as follows:

$$\beta_d = \frac{1}{1 + 1.15(\varepsilon_{rec})^{0.25}} \quad (4.14.4.10)$$

$$\varepsilon_{rec} = \varepsilon_{tm} - \varepsilon_{ro} \quad (4.14.4.11)$$

The instantaneous plastic strain, $\varepsilon_c^{p'}$, for the tension domain is computed as follows:

$$\varepsilon_c^{p'} = 146\varepsilon_{tm}^2 + 0.523\varepsilon_{tm} \quad (4.14.4.12)$$

If $\varepsilon_c^{p'}$ is more tensile than ε_c^p , then ε_c^p is updated as $\varepsilon_c^{p'}$.

Unloading in tension results in concrete stress, f_c , as follows:

$$f_c = f_{tm} - E_c (\varepsilon_{tm} - \varepsilon_c) + \frac{(E_c - E_c^f)(\varepsilon_{tm} - \varepsilon_c)^{N_t}}{N_t (\varepsilon_{tm} - \varepsilon_c^p)^{N_t - 1}} \quad (4.14.4.13)$$

where ε_c^p is the current plastic offset strain, ε_{tm} is the maximum previously attained tensile strain, f_{tm} is the corresponding stress. N_t is computed as follows such that the unloading modulus is equal to the initial tangent stiffness of concrete, E_c at the beginning of the unloading branch, and equal to E_c^f at the end of the unloading branch, and is computed as follows:

$$N_t = \frac{(E_c - E_c^f) \cdot (\varepsilon_{tm} - \varepsilon_c^p)}{E_c (\varepsilon_{tm} - \varepsilon_c^p) - f_{tm}} \quad (4.14.4.14)$$

$$E_c^f = \begin{cases} 0.071 \cdot E_c(0.001/\varepsilon_{tm}) & \text{for } \varepsilon_{tm} < 0.001 \\ 0.053 \cdot E_c(0.001/\varepsilon_{tm}) & \text{for } \varepsilon_{tm} < 0.001 \end{cases} \quad (4.14.4.15)$$

Partial unloading and reloading is effected by similar equations with modifications to the reversal and maximum strains under consideration.

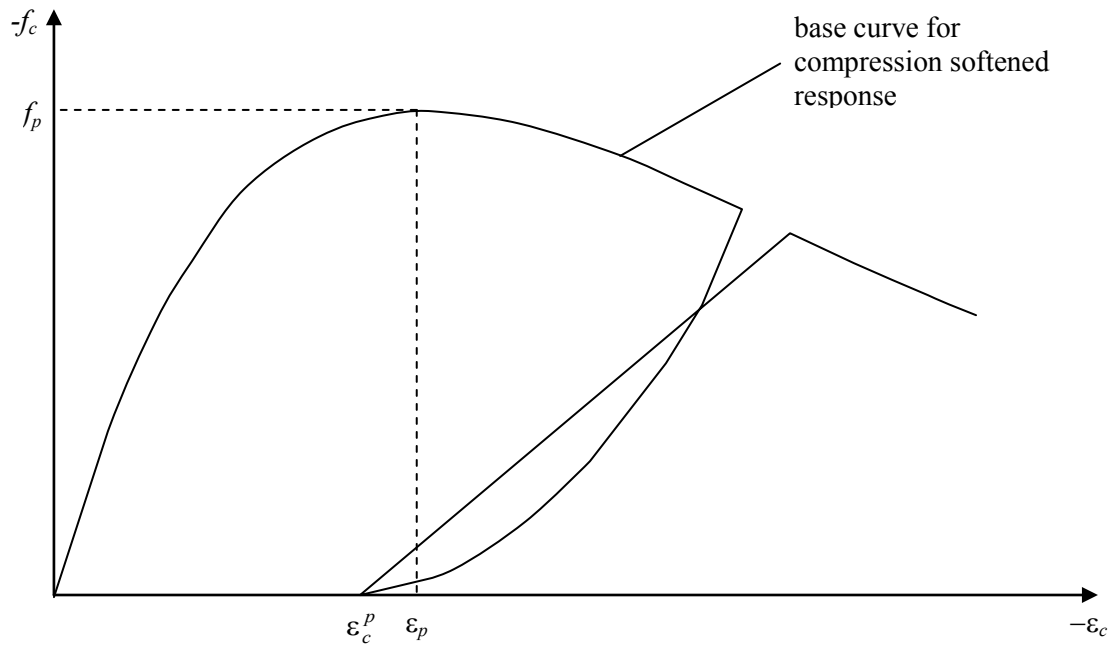


Figure 51: Palermo model of concrete hysteretic response in compression

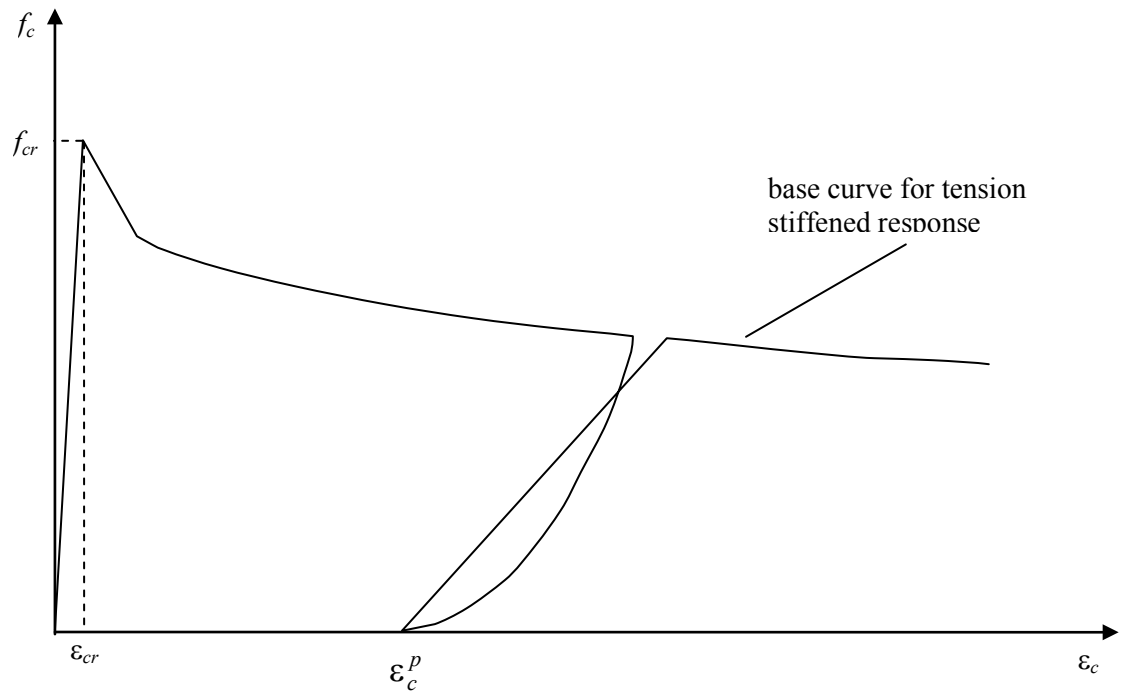


Figure 52: Palermo model of concrete hysteretic response in tension

5 Models for other material types

The original material type modeled in VecTor2 is reinforced concrete; the majority of this manual is dedicated to the discussion of material and behaviour models for concrete. The following materials can also be modeled as the main material type in VecTor2: structural steel, masonry, and orthotropic wood. In addition, using the main material types and smeared reinforcement types the following laminates can be modeled in VecTor2: concrete-steel laminate, concrete-SFRC laminate, masonry-SFRC laminate, concrete-wood laminate. This section contains a discussion of the above materials and how they are analyzed in VecTor2. A discussion of how to model them in FormWorks is included in the Reinforced Concrete Material Types part of the FormWorks section of this user manual.

5.1 Structural Steel

Structural steel is modeled in VecTor2 as a linear-elastic material up to the point of yielding, after which plastic deformation and strain hardening occur. Strain hardening is modeled in VecTor2 using a trilinear relationship, illustrated in Figure 53.

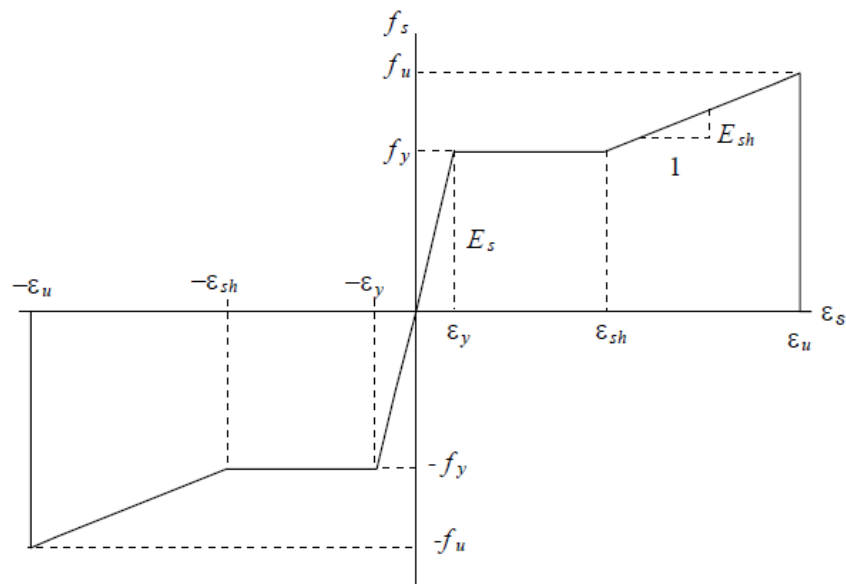


Figure 53: Stress-strain behavior of structural steel in VecTor2

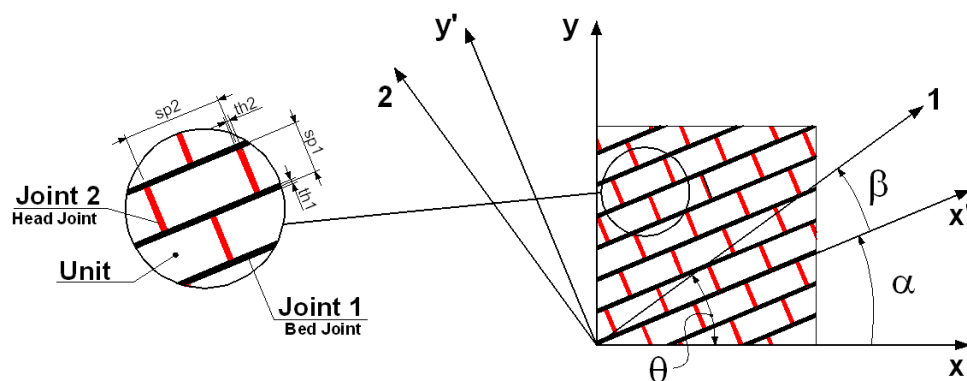
Steel hysteresis is also considered, and is described in section 6.2. In VecTor2, the hysteresis model for structural steel is the same as for reinforcing steel.

The main different between the modeling of structural steel and reinforcing steel in VecTor2 is the consideration of biaxial loading. For structural steel, particularly steel plates, biaxial effects are important; the Von Mises failure criterion is used for structural steel and is discussed further in the concrete-steel laminate section of the manual, section 5.4. For reinforcing steel, biaxial effects are not considered.

5.2 Masonry

5.2.1 Introduction

Masonry is an orthotropic material consisting of masonry units and mortar joints, shown in Figure 54. As with the smeared crack approach to the analysis of cracked concrete, for sufficiently large masonry structures, the masonry can be modeled as a continuum with average properties where joint failures are smeared across the single finite element.



- $x-y$ = global axes
- $x'-y'$ = orthotropy axes
- 1-2 = principal stress axes
- β = angle between the axes x' and 1
- θ = angle between the axes x and 1
- α = direction of the bed joints with respect to x

Figure 54: Masonry joints

In Figure 54, sp_2 is the spacing between head joints and sp_1 is the spacing between bed joints. These are entered in the Define Reinforced Concrete Materials tab of FormWorks as S_x and S_y , respectively.

5.2.2 Compressive Behavior

The uniaxial compressive pre-peak stress-strain behaviour of unreinforced masonry (URM) can be modeled with a relationship similar to the one used to model the compressive response of reinforced concrete. When modeling URM in VecTor2, because the initial tangent modulus is not necessarily directly related to the peak stress-strain ratio, the Hoshikuma et al. model is recommended, as it allows for the independent definition of peak stress, peak strain, and initial tangent modulus.

The material strength and elastic modulus of URM change with the direction of the axes of orthotropy. Ganz' failure criteria for URM is implemented in VecTor2, expressed in terms of the principal stresses.

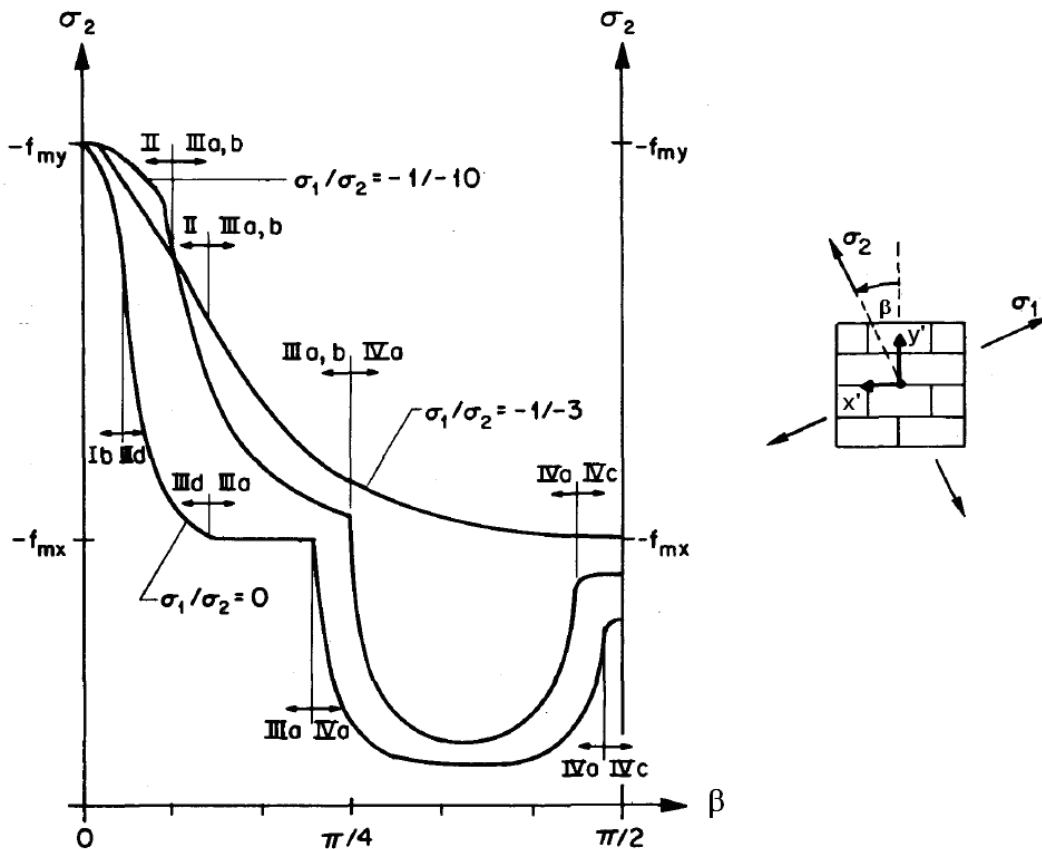


Figure 55: Ganz failure criterion implemented in VecTor2 (Ganz, 1985)

The following equations define the failure criteria above:

Equation Ib:

$$\begin{aligned} & ((1 - \omega_m R)(\omega_m - R))\sigma_2^2 + t^2 \left((R - 1)(f_{my} - f_{mx})(\omega_m + 1)^2 - f_{my}R(1 + \omega_m^2) + \right. \\ & \left. f_{mx}(R - \omega_m^2) + 2\omega_m^2 f_{my} + f_{mx}\omega_m(R - 1) \right) \sigma_2 + (f_{my} - f_{mx})f_{my}\omega_m - f_{mx}f_{my}\omega_m^2 \leq 0 \end{aligned} \quad (5.2.2.1)$$

Equation II:

$$-R\sigma_2^2 - (t^2(f_{my} - f_{mx})(1 - R) + f_{mx} + Rf_{my})\sigma_2 - f_{mx}f_{my} \leq 0 \quad (5.2.2.2)$$

Equation III d:

$$\begin{aligned} & \left(-(1 + \omega_m)^2(R - 1)^2t^4 + 2(R - 1)(-2\omega_m + R(1 + \omega_m^2)) - (R(\omega_m - 1))^2 \right) \sigma_2^2 + \\ & \left(2\omega_m f_{mx}(1 - \omega_m)(t^2 + R(1 - t^2)) \right) \sigma_2 - (\omega_m f_{mx})^2 \leq 0 \end{aligned} \quad (5.2.2.3)$$

Equation III a,b:

$$(t^2 + R^2 - R^2t^2)\sigma_2 + f_{mx}(t^2 + R(1 - t^2)) \leq 0 \quad (5.2.2.4)$$

Equation IV a:

$$\left((R - 1)^2t^2(1 - t^2) - (\tan \varphi (1 + t^2(R - 1)))^2 \right) \sigma_2^2 + 2c \tan \varphi (1 + t^2(R - 1))\sigma_2 - c^2 \leq 0 \quad (5.2.2.5)$$

Equation IV c:

$$\begin{aligned} & \left(R^2(et^4 + t^2(1 - 4m^2 - 2\lambda m(1 + 2m)) + (1 + 2\lambda)m^2) + R(-2et^4 + t^2(4m(1 + \lambda) + \right. \\ & \left. 2m^2(1 + 2\lambda) - 2m(1 + \lambda)) + et^4 - t^2(1 + 2m(1 + \lambda)) + 1) \right) \sigma_2^2 + \left(2m(R + t^2(1 - R))(f'_{xy}(1 + \right. \\ & \left. 2\lambda) - \xi) + 2(1 + t^2(R - 1))(\xi - f'_{xy}(1 + \lambda)) \right) \sigma_2 + f'_{xy}(f'_{xy} - 2(\xi - \lambda f'_{xy})) \leq 0 \end{aligned} \quad (5.2.2.6)$$

where

$$t = \sin \beta$$

$$R = \sigma_1/\sigma_2$$

$$\lambda = \sin \varphi / (1 - \sin \varphi)$$

$$\xi = c \cdot \tan\left(\frac{\pi}{4} + \frac{\varphi}{2}\right)$$

$$e = m(m + 2(1 + \lambda + \lambda m)) \text{ where } m = \frac{f'_{ty}}{\mu f_{mx}}$$

And β is the angle between the principal axes and axes of orthotropy, R is the ratio of principal stresses, φ is the friction angle of the mortar bed joint interface, f_{mx} is the compressive strength in the x-direction with bed joint aligned horizontally (at $\alpha = 0$), f_{my} is the compressive strength in the y-direction with bed joint aligned horizontally, c is the cohesion of the mortar bed joint interface, f'_{ty} is the tensile strength of the mortar bed joint interface in the x-direction (perpendicular to the bed joints), ω_m is the ratio between the tensile strength in the x-direction (for $\alpha = 0$) and compressive strength f_{my} , and μ is the reduction coefficient for the strength f_{mx} .

Within the implementation of the Ganz failure criteria in VecTor2, in order to properly account for the orthotropic behaviour of masonry, the maximum compressive strength of the masonry is limited by defining a factor β_m , the ratio of the maximum principal compressive strength and the compressive strength f_{my} .

$$f_p = \beta_d \beta_1 \beta_m f'_c \quad (5.2.2.7)$$

where β_d is the compression softening parameter (coincident with the Vecchio 1992-A model for RC), β_1 is the parameter accounting for confinement effect, $\beta_m (= \sigma_{2,max}/f_{my})$ is a parameter accounting for orthotropic effect on compressive strength, $\sigma_{2,max}$ is the principal compressive strength defined according to the Ganz failure criteria, $f'_c = f_{my}$ is the maximum compressive strength of masonry, and f_p is the actual compressive strength of masonry.

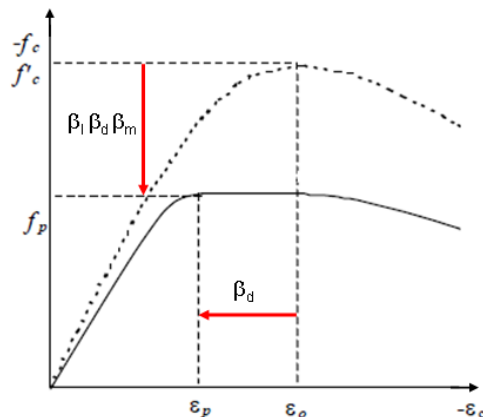


Figure 56: Masonry compressive stress-strain behavior

In VecTor2, when modeling masonry structures, the maximum compressive masonry strength, f_{my} , is entered as the cylinder compressive strength, f'_c , in the *Define Reinforced Concrete Properties* tab of FormWorks.

Given that masonry is considered orthotropic in VecTor2, the elastic moduli are different in each direction of orthotropy. A smooth transition from the maximum modulus, E_{my} , to the minimum modulus, E_{mx} , is generated by evaluating the stresses and strains at various angles of β , and taking the ratio of the two to determine the modulus at each angle. Once the $E - \beta$ relationship is determined by VecTor2, as shown in Figure 57, the initial tangent modulus can be evaluated directly as a function of the direction of the principal axes with respect to the direction of the horizontal joints.

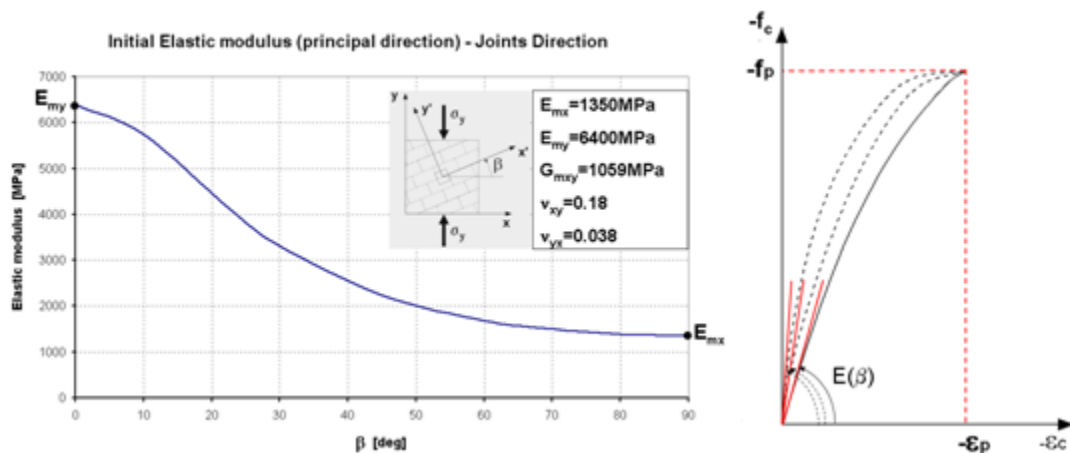


Figure 57: Variation in masonry elastic modulus

In the *Define Reinforced Concrete Materials* tab of FormWorks, the initial maximum elastic modulus, E_{my} , is entered in the Initial Tangent Elastic Modulus, E_c , space. The ratio between the two elastic moduli is entered in a different tab in FormWorks, as will be outlined in a subsequent section.

5.2.3 Tensile Behavior

The tensile behaviour of masonry in VecTor2 is modeled as isotropic linear elastic. The stress-strain relationship is linear until the tensile strength, f_{ty} , is reached, after which tension softening occurs. The suggested VecTor2 tension softening model is the Hordijk model. The tensile strength of masonry is

equal to the minimum tensile brick-mortar strength, perpendicular to the bed joints, and is entered as tensile strength, f'_t , in the *Define Reinforced Concrete Materials* tab of FormWorks .

5.2.4 Slip Along the Joints

Within the DSFM adaptation for masonry materials, masonry is modeled as a continuum that may slip along the head and bed joints, even when the material is uncracked.

From the total stress vector, the shear stress and shear strain parallel to the joints can be determined. Based on the calculated shear strain along the joints, the shear slip, δ_s , can be determined:

$$\delta_s = \gamma \cdot th_i \quad (5.2.4.1)$$

where th_i is the thickness of the joint.

The average shear slip strain can also be calculated as follows:

$$\gamma_s = \frac{\delta_s}{sp_i} \quad (5.2.4.2)$$

where δ_s is the slip along the joints and sp_i is the joint spacing.

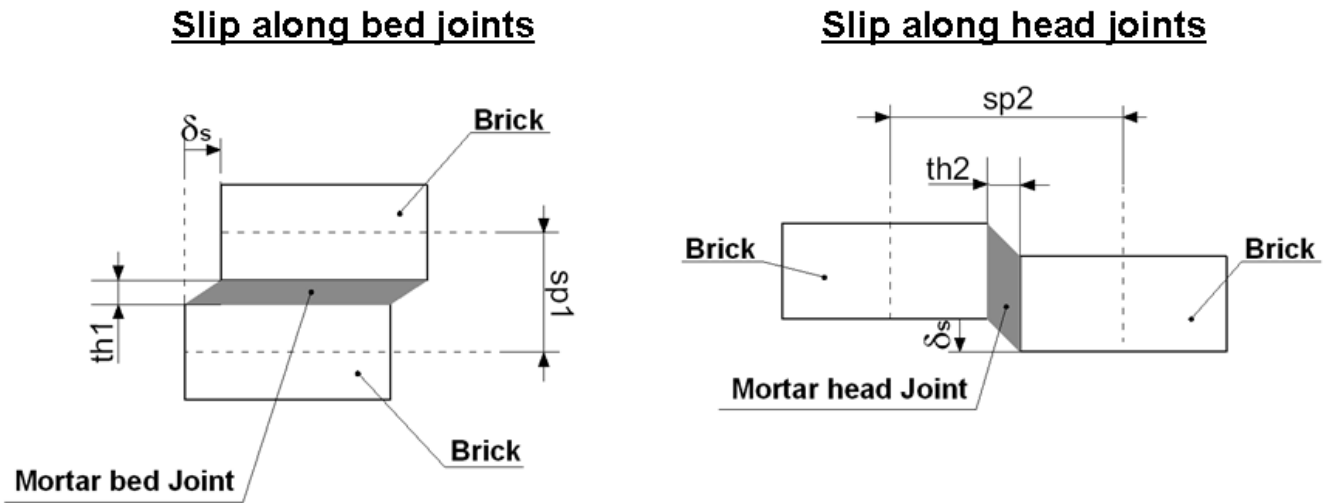


Figure 58: Masonry Joint Slip

In VecTor2, by default, the crack slip check is not considered.

5.3 Wood (Fixed Orthotropic)

In VecTor2, wood is modeled as a fixed orthotropic material. The two directions of orthotropy are parallel to the grain and perpendicular to the grain. The longitudinal direction is defined as parallel to the grain; the transverse direction is perpendicular to the grain. When modeling wood in FormWorks, one must define the compressive and tensile strength, as well as the elastic moduli and Poisson's ratios, in both the longitudinal and transverse directions. No default values will be applied by VecTor2 if an input is left blank. This is discussed more in the FormWorks-Reinforced Concrete Material Types section of the manual.

The stress-strain curve for wood is currently linear-elastic.

The following relations are used to model the stress-strain behaviour of wood in VecTor2.

$$e_{xx} = \frac{1}{E_{xx}} \sigma_{xx} - \frac{\nu_{yx}}{E_{yy}} \sigma_{yy} \quad (5.3.1)$$

$$e_{yy} = -\frac{\nu_{xy}}{E_{xx}} \sigma_{xx} + \frac{1}{E_{yy}} \sigma_{yy} \quad (5.3.2)$$

$$\gamma_{xy} = \frac{1}{G_{xy}} \sigma_{xy} \quad (5.3.3)$$

In these equations, we can consider the x-axis to be the longitudinal direction. Thus, the stress-strain behaviour of wood can be characterized by the following equations:

$$e_{ll} = \frac{1}{E_l} \sigma_{ll} - \frac{\nu_{tl}}{E_t} \sigma_{tt} \quad (5.3.4)$$

$$e_{tt} = -\frac{\nu_{lt}}{E_l} \sigma_{ll} + \frac{1}{E_t} \sigma_{tt} \quad (5.3.5)$$

$$\gamma_{lt} = \frac{1}{G_{lt}} \sigma_{lt} \quad (5.3.6)$$

where e_{ll} is the longitudinal strain, e_{tt} is the transverse strain, E_l is the elastic modulus in the longitudinal direction, E_t is the elastic modulus in the transverse direction, ν_{lt} is the Poisson's ratio (longitudinal stress-transverse strain), ν_{tl} is the Poisson's ratio (transverse stress-longitudinal strain), σ_{ll} is the longitudinal stress, σ_{tt} is the transverse stress.

5.4 Concrete-Steel Laminate

Steel-concrete composite wall elements typically consist of a thick concrete core integrated with two thin steel faceplates, where forces are generally transferred between the concrete and the steel through shear studs. In VecTor2, the DSFM is the basis for the analysis of concrete-steel laminates. As VecTor2 is a 2D finite element program, the different materials must be modeled as a smeared/combined element with properties representative of the two materials, as outlined below and described fully in Vecchio and McQuade (2011). A typical concrete-steel laminate is illustrated in Figure 59.

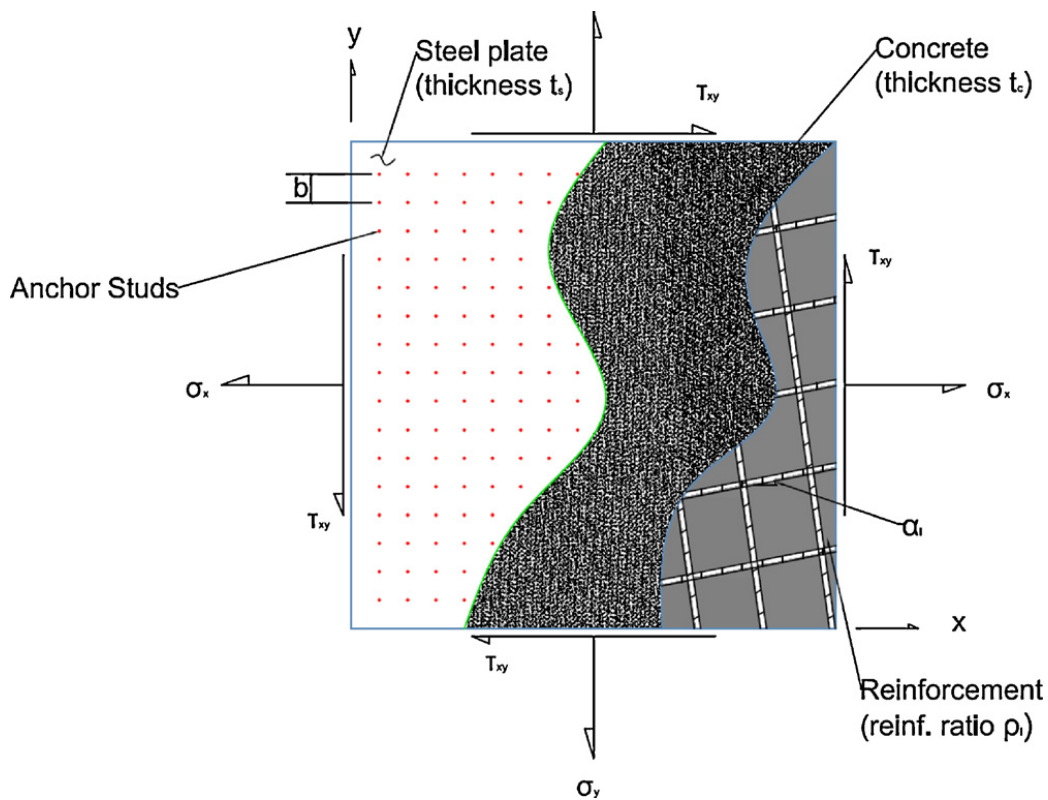


Figure 59: Concrete-steel laminate element (Vecchio and McQuade, 2011)

The element is analyzed using the same principals of solid mechanics as a typical concrete element, where:

$$[\sigma] = [D][\varepsilon] - [\sigma^0] \quad (5.4.1)$$

The composite material stiffness matrix, $[D]$, and the prestress vector, $[\sigma^0]$, are formulated as

$$[D] = \frac{t_c}{(t_c + 2t_s)} [D_c] + \sum_{i=1}^n \frac{t_c}{(t_c + 2t_s)} [D_r]_i + \frac{2t_s}{(t_c + 2t_s)} [D_s] \quad (5.4.2)$$

$$[\sigma^0] = [D_c]([\varepsilon_c^e] + [\varepsilon_c^p] + [\varepsilon_c^s]) + \sum_{i=1}^n [D_r]_i([\varepsilon_r^e]_i + [\varepsilon_r^p]_i) + [D_s]([\varepsilon_s^e] + [\varepsilon_s^p]) \quad (5.4.3)$$

The formulation of $[D_c]$ and $[D_r]$ is described fully in (Vecchio, 2000b). The material stiffness matrix for the steel faceplates is a diagonal matrix with respect to the principal stress directions.

For the yield criteria for the steel plates, the von Mises criterion is used, where:

$$(f_{s1} - f_{s2})^2 + (f_{s2} - f_{s3})^2 + (f_{s3} - f_{s1})^2 = 2(f_y)^2 \quad (5.4.4)$$

In terms of the contribution of the steel plates to the tension stiffening response of concrete, no experimental data is currently available. However, due to the fact that the steel plate is typically quite thin compared to the concrete core and the bond between plates and the concrete is weaker than that of fully embedded deformed rebar, it is assumed that the steel faceplates do not contribute to concrete tension –stiffening (Vecchio and McQuade, 2011). In addition, in accordance with the Canadian Design Code A23.3, for steel-concrete elements with no in-plane reinforcement, the maximum crack spacing is considered equal to the element thickness.

A detailed explanation of the modeling of steel-concrete composite structures, specifically wall elements, can be found in Vecchio and McQuade (2011).

5.5 Concrete-SFRC Laminate and Masonry-SFRC Laminate

Similar to the concrete-steel laminate, a concrete-SFRC laminate combines a concrete core with steel-fibre reinforced concrete faceplates. Using an SFRC laminate will result in a higher capacity and a more ductile response; a common application of the SFRC laminate is in strengthening of RC slabs, whereby a thin layer of SFRC is attached to an existing RC slab. Adding the SFRC laminate to the compression zone (ie. the top of the slab) can significantly increase the flexural capacity of an existing RC slab. There are also benefits in shear capacity. An overlayer of SFRC also allows for increased post-cracking residual stress as the steel fibres are efficient at controlling large cracks in most circumstances.

For more details on the concrete or SFRC behaviour, see sections 4 or 6.5, respectively. For details on how to model this material in FormWorks, see section 10.4.1.6.

The masonry-SFRC laminate is similar to the concrete-SFRC laminate, and is defined in FormWorks in much the same way. For a detailed description of the behaviour of masonry, see section 5.2. Section 6.5 describes the stress-strain response of SFRC. For information on how to model masonry-SFRC laminate in FormWorks, see section 10.4.1.7 of this manual.

5.6 Concrete-Ortho Laminate

Concrete-wood laminates are commonly used in both floor and beam construction. In new floor construction, solid concrete is typically placed on timber floor beams or a solid layer of wood. The wood layer functions to replace the cracked concrete-steel reinforcement section of a solid concrete slab, and also reduces the need for formwork. Similarly, deep beams benefit from concrete-wood composite construction, as wood can eliminate the high tensile stresses in the concrete. Hence, bridges can also utilize composite concrete-timber beams. As with other laminates, forces must be transferred between the concrete and the wood, most likely through shear studs.

Section 4 describes in detail the behaviour models for concrete. For the stress-strain behaviour of orthotropic wood, see section 5.3. Details on how to model concrete-ortho laminates are provided in section 10.4.1.8 of this manual.

6 Models for Reinforcement Materials

The following discussion describes the constitutive and behavioral models pertaining to the response of reinforcement materials. The monotonic stress-strain response of reinforcement is discussed, followed by the hysteretic response models. Subsequently, dowel action and reinforcement buckling models are discussed.

After the discussion of conventional steel reinforcement, the modeling of Steel Fibre Reinforced Concrete in VecTor2 is discussed. Subsequently, a brief discussion of laminates and shape memory alloys in VecTor2 is included.

6.1 Stress-Strain Response

The following models describe the monotonic stress-strain response of reinforcement materials. These models are categorized by reference types of reinforcement: ductile steel reinforcement, prestressing steel, tension only reinforcement, compression only reinforcement, and externally bonded FRP reinforcement.

6.1.1 Ductile Steel Reinforcement

The reinforcement stress-strain response is composed mainly of three parts, as shown in Figure 60, including an initial linear-elastic response, a yield plateau, and either a linear or nonlinear strain-hardening phase until rupture. Moreover, this monotonic stress-strain curve describes the back-bone curve of the Seckin or Menegotto-Pinto models, as discussed below for the hysteretic response. The reinforcement stress, f_s , in tension and compression is determined as follows:

$$f_s = \begin{cases} E_s \varepsilon_s & \text{for } \varepsilon_s \leq \varepsilon_y \\ f_y & \text{for } \varepsilon_y < \varepsilon_s \leq \varepsilon_{sh} \\ f_u + (f_y - f_u) \left(\frac{\varepsilon_u - \varepsilon_s}{\varepsilon_u - \varepsilon_{sh}} \right)^P & \text{for } \varepsilon_{sh} < \varepsilon_s \leq \varepsilon_u \\ 0 & \text{for } \varepsilon_u < \varepsilon_s \end{cases} \quad (6.1.1.1)$$

where ε_s is the reinforcement strain ($\varepsilon_s = |\varepsilon_s|$), ε_y is the yield strain, ε_{sh} is the strain at the onset of the strain hardening, ε_u is the ultimate strain, E_s is the elastic modulus, f_y is the yield strength, f_u is the ultimate strength, and P is the strain-hardening parameter.

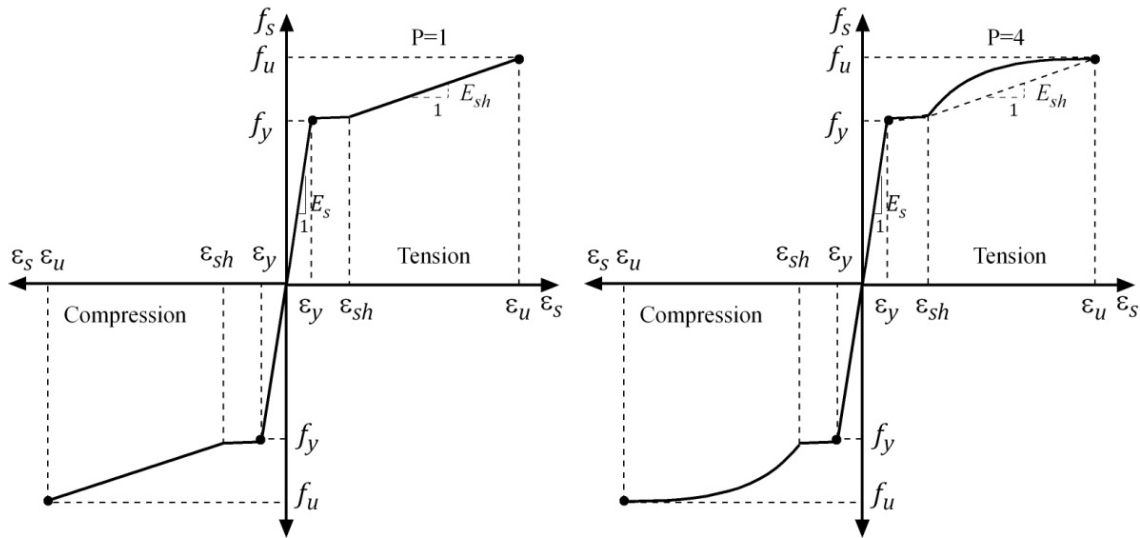


Figure 60: Ductile steel reinforcement stress-strain response
[left(a): Linear strain-hardening (Trilinear); right (b): Nonlinear strain-hardening (HP4)]

There are two options for the strain-hardening phases after the yield plateau; these are linear strain-hardening (trilinear, $P=1$) and nonlinear strain-hardening (HP4, $P=4$), as shown in Figure 60. Elastic-plastic or bilinear stress-strain curves are generated by the trilinear option given in Figure 60a. The default option is HP4. (The default option can be changed from the hysteretic response section of reinforcement models.) The strain hardening modulus, E_{sh} is defined as follow:

$$E_{sh} = \frac{(f_u - f_y)}{(\varepsilon_u - \varepsilon_{sh})} \quad (6.1.1.2)$$

6.1.2 Prestressing Steel

This model is appropriate for cold-worked steel reinforcement that does not exhibit a distinct yield plateau, but rather an initial linear-elastic branch, followed by a transition curve to a second hardening linear branch, as shown in Figure 61. The reinforcement stress, f_s , in tension and compression is determined by a Ramsberg-Osgood formulation as follows:

$$f_s = E_s \varepsilon_s \left\{ A + \frac{1 - A}{[1 + (B \varepsilon_s)^C]^{1/C}} \right\} \leq f_u \quad (6.1.2.1)$$

$$A = \frac{E_{sh}}{E_s} \quad (6.1.2.2)$$

$$B = \frac{E_s (1 - A)}{f_s^*} \quad (6.1.2.2)$$

$$C = \text{transition coefficient} \quad (6.1.2.3)$$

where ε_s is the reinforcement strain, E_s is the initial elastic modulus, f_u is the ultimate strength and f_s^* is the value at which the second linear branch intercepts the stress axis at zero strain. A representative value of the transition coefficient, C , for prestressing strands with an ultimate strength of 1860 MPa is 10 for low-relaxation steel, or 6 for stress-relieved steel.

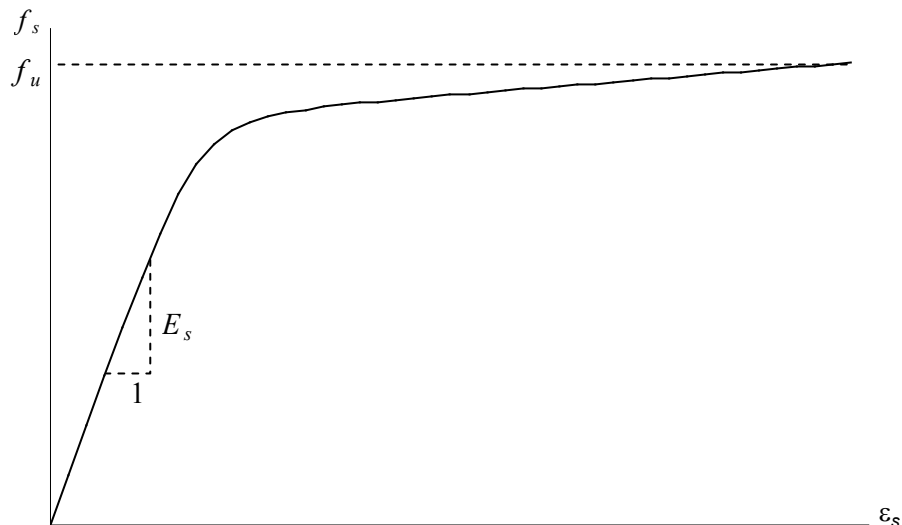


Figure 61: Prestressing steel reinforcement stress-strain response

6.1.3 Tension Only Reinforcement

In tension, the stress-strain response is the same as the trilinear relationship of the ductile steel reinforcement model. In compression, the reinforcement stress is always zero. This model may be utilized to represent fabric-type FRP reinforcement that offers no resistance in compression.

6.1.4 Compression Only Reinforcement

In compression, the stress-strain response is the same as the trilinear relationship of the ductile steel reinforcement model. In tension, the reinforcement stress is always zero. This response may be utilized to model contact phenomenon between two disjoint structures, by specifying an initial prestrain representing the relative movement prior to contact.

6.1.5 Externally Bonded FRP Reinforcement

This model is similar to the tension only reinforcement model, in that the reinforcement does not exhibit compressive stress. Additional modifications allow the local crack stresses in externally bonded FRP reinforcement to be more accurately calculated.

6.2 Hysteretic Response

The following hysteretic response models describe how the reinforcement reloads to and unloads from the monotonic stress-strain curve. As such, the monotonic stress-strain curve is likened to a backbone, to which unloading and reloading curve attach.

6.2.1 Linear

The reinforcement reloads linearly from and unloads linearly to the point of zero strain and zero stress of the monotonic stress-strain curve. No plastic offset strains result.

6.2.2 Seckin Model w/ Bauschinger Effect

The following model was proposed by Seckin (1981), as shown in Figure 62. This model includes the Bauschinger effect, in which the reinforcement exhibits premature yielding upon load reversal after plastic prestraining due to stress changes at the microscopic level. There are two options when using this model; these are Seckin w/ Bauschinger-Trilinear and Seckin w/ Bauschinger-HP4 as shown in Figure 62.

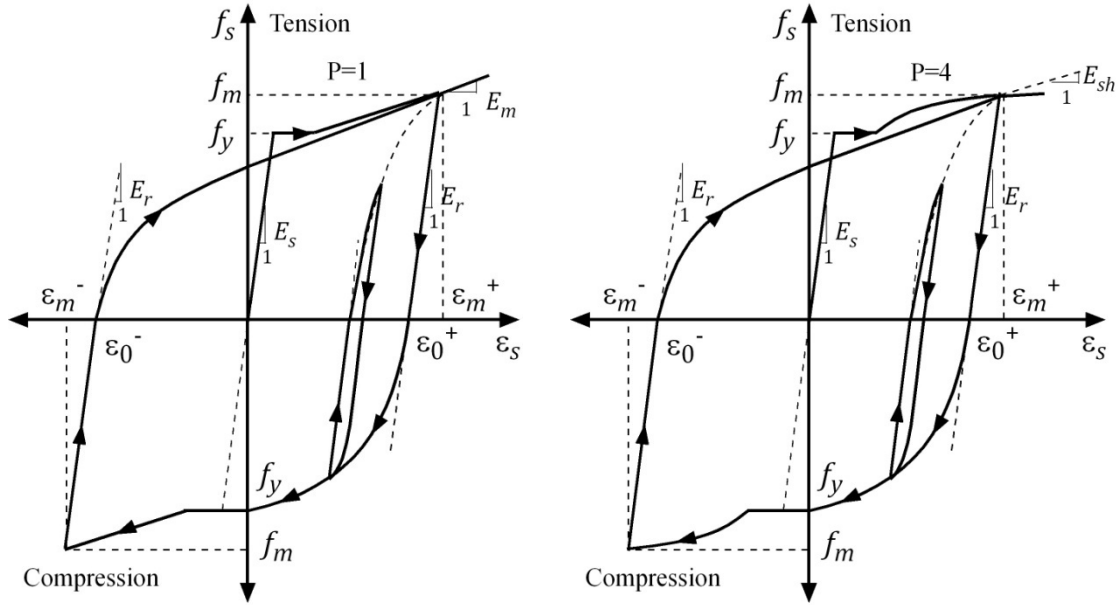


Figure 62: Seckin model of ductile steel reinforcement for hysteretic response
[left (a): Seckin w/ Bauschinger-Trilinear; right (b): Seckin w/ Bauschinger-HP4]

When reloading in a positive cycle to a strain of ε_j , the reinforcement stress is f_s , reflects the Bauschinger effect with a Ramberg-Osgood formulation as follows:

$$f_s = E_r (\varepsilon_j - \varepsilon_0) + \frac{E_m - E_r}{N (\varepsilon_m - \varepsilon_0)^{N-1}} (\varepsilon_j - \varepsilon_0)^N \quad (6.2.2.1)$$

$$N = \frac{(E_m - E_r)(\varepsilon_m - \varepsilon_0)}{f_m - E_r (\varepsilon_m - \varepsilon_0)} \quad (6.2.2.2)$$

$$E_r = \begin{cases} E_s & \text{for } (\varepsilon_m - \varepsilon_0) \leq \varepsilon_y \\ E_s \left(1.05 - 0.05 \frac{(\varepsilon_m - \varepsilon_0)}{\varepsilon_y} \right) & \text{for } \varepsilon_y < (\varepsilon_m - \varepsilon_0) < 4\varepsilon_y \\ E_s & \text{for } 4\varepsilon_y \leq (\varepsilon_m - \varepsilon_0) \end{cases} \quad (6.2.2.3)$$

where, ε_0 is the plastic offset strain in the current cycle, ε_y is the yield strain, ε_m is the maximum positive strain attained in previous cycles, E_m is the tangent stiffness at ε_m , E_r is the unloading modulus, E_s is the elastic modulus of the monotonic stress-strain response, and f_m is the stress corresponding to ε_m .

Unloading is linear and results in reinforcement stresses as follow:

$$f_s = f_{sj-1} + E_r (\varepsilon_j - \varepsilon_{j-1}) \quad (6.2.2.4)$$

6.2.3 Menegotto-Pinto Model w/ Bauschinger Effect

The following model was proposed by Menegotto and Pinto (1973), as shown in Figure 63. Similar to the Seckin model, this model includes the Bauschinger effect. There are two options when using this model; these are Menegotto-Pinto w/ Bauschinger-Trilinear and Menegotto-Pinto w/ Bauschinger-HP4 as shown in Figure 63. The Menegotto-Pinto model defines an asymptotic curve tangential to two asymptotic lines at the initial (origin) and end (target) points. The reloading part of the stress-strain curve is defined in a normalized form as follows:

$$f_{eq} = b\varepsilon_{eq} + \frac{(1-b)\varepsilon_{eq}}{(1 + \varepsilon_{eq}^R)^{1/R}} \quad (6.2.3.1)$$

$$f_{eq} = \frac{f_s - f_r}{f_p - f_r}, \quad \varepsilon_{eq} = \frac{\varepsilon_s - \varepsilon_r}{\varepsilon_p - \varepsilon_r}, \quad (\varepsilon_r = \varepsilon_0 \text{ and } f_r = 0) \quad (6.2.3.2)$$

$$b = \frac{E_m}{E_r}, \quad R = R_0 - \frac{a_1 \xi}{a_2 + \xi}, \quad \xi \varepsilon_y = (\varepsilon_m - \varepsilon_p) \quad (6.2.3.3)$$

$$E_r = E_s \left(0.8 + \frac{1}{5 + 1000 \varepsilon_m} \right) \quad (6.2.3.4)$$

where f_{eq} and ε_{eq} are normalized stress and strain, and f_p and ε_p are stress and strain at the intersection point between the initial tangent at the origin and the asymptote at the target, respectively. b is the strain-hardening ratio of the intended slope (E_m) at the target point to the unloading or initial reloading stiffness (E_r) at the origin. R is the independent parameter which defines the curvature according to experimental parameters, R_0 , a_1 , and a_2 . In the VecTor2 implementation, R_0 , a_1 , and a_2 are taken 15, 18.5 and 0.15, respectively and the values of R are limited between 1 and 15. $\xi\varepsilon_y$ is the strain difference between the strain at the intersection point, ε_p and the maximum (target) strain attained at the previous cycle, ε_m . In addition, f_m is the stress corresponding to ε_m , E_m is the tangent stiffness at ε_m , E_r is the unloading or initial reloading modulus, proposed by Dodd and Restrepo-Posoda (1995), ε_o is the plastic offset strain in the current cycle, f_y is yield strength corresponding to the yield strain, ε_y , and E_s is the elastic modulus of the monotonic stress-strain response.

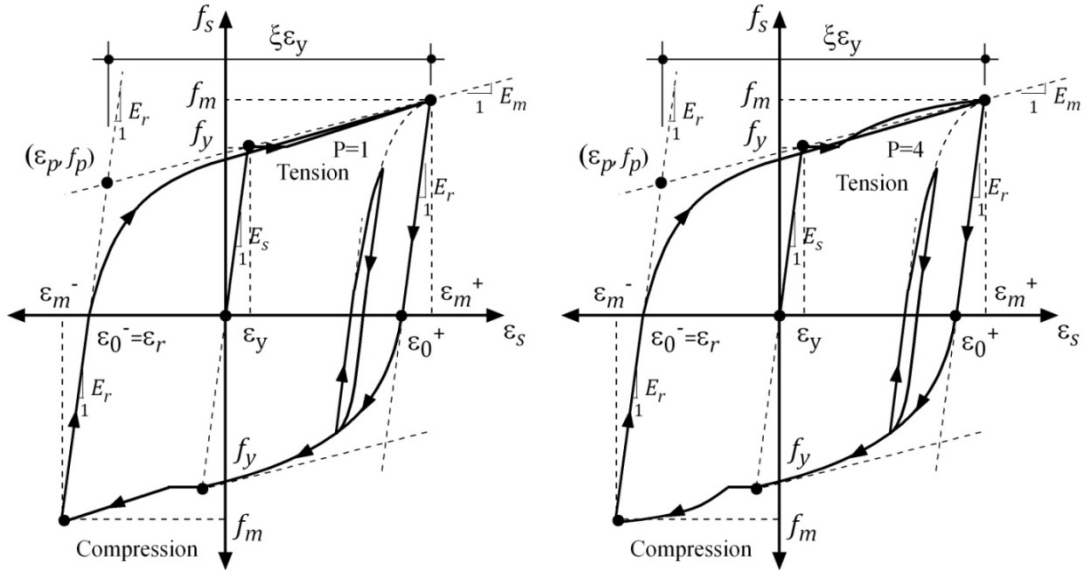


Figure 63: Menegotto-Pinto model of ductile steel reinforcement for hysteretic response [left (a): Menegotto-Pinto w/ Baushinger-Trilinear ; right (b): Menegotto-Pinto w/ Baushinger-HP4

Unloading is linear and results in reinforcement stresses as follow:

$$f_s = f_{sj-1} + E_r (\varepsilon_j - \varepsilon_{j-1}) \tag{5.2.3.5}$$

6.2.4 Elastic Hardening (Curvilinear)

Figure 64 illustrates the curvilinear stress-strain model.

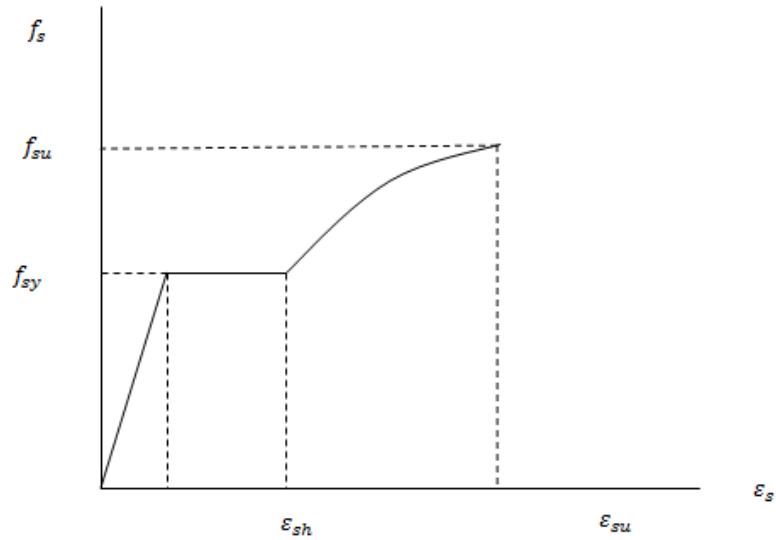


Figure 64: curvilinear strain hardening

The equation for the curvilinear portion of the response is:

$$f_s = f_{su} - (f_{su} - f_{sy}) \left(\frac{\epsilon_{su} - \epsilon_s}{\epsilon_{su} - \epsilon_{sh}} \right)^4 \tag{6.2.4.1}$$

6.2.5 Elastic-Hardening (Trilinear)

The monotonic stress-strain curve is trilinear, as described for the ductile steel reinforcement. The reinforcement unloads and reloads linearly with a modulus equal to elastic modulus of the reinforcement, E_s . As such, plastic strain offsets result.

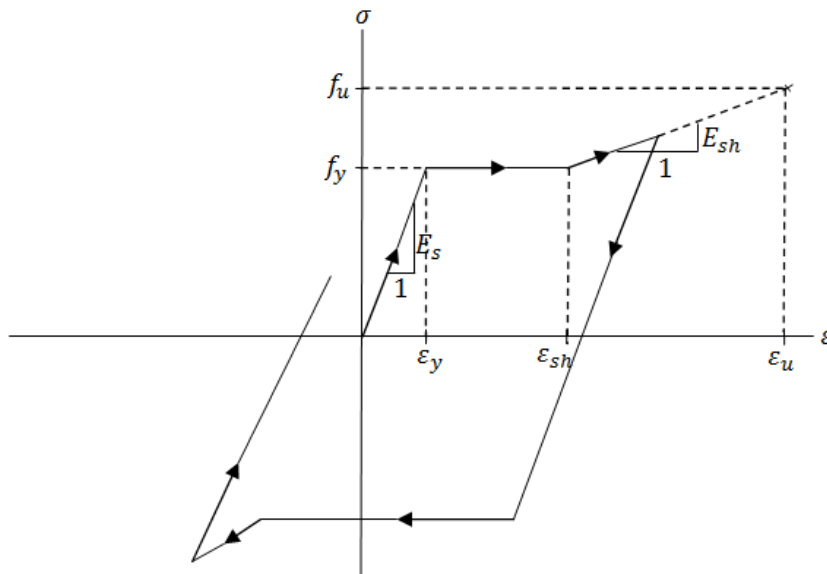


Figure 65: Trilinear stress-strain response

6.2.6 Elastic Plastic (Bilinear)

The monotonic stress-strain curve is bilinear, comprised of an initial linear-elastic branch, followed by a yield plateau. The reinforcement unloads and reloads linearly with a modulus equal to elastic modulus of the reinforcement, E_s . Figure 66 illustrates this stress-strain model.

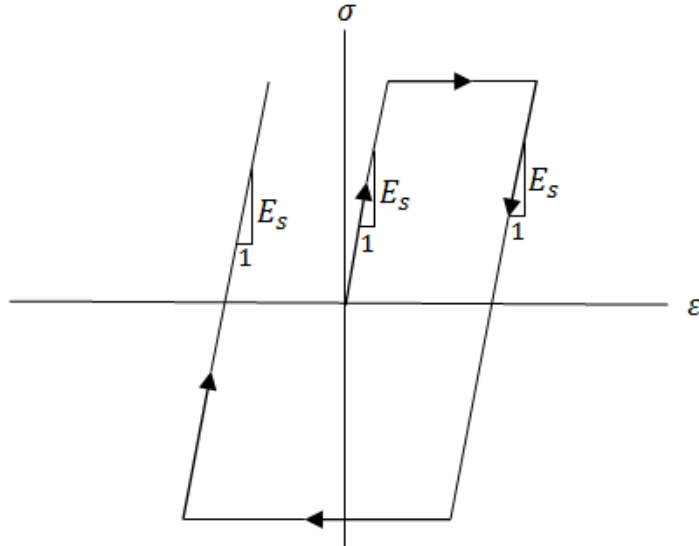


Figure 66: Elastic-plastic stress-strain response

6.3 Dowel Action

Dowel action refers to shear resistance offered by reinforcing bars crossing a crack as the crack slips transversely to the axis of the reinforcement. In some circumstances, such as beams with small amounts of transverse reinforcement, dowel action may contribute significantly to the shear strength and post-peak ductility of reinforced concrete members.

The model is used in conjunction with the Vecchio/Lai and Walraven stress-based element slip distortion models and their hybrid formulations. The shear resistance due to dowel action, v_{dt} , is computed as a function of the shear slip, δ_s , at the crack. This shear resistance is subsequently subtracted from the local shear stress on the crack, v_{ci} , thereby reducing the amount of computed shear slip.

6.3.1 Not considered

The shear resistance at a crack due to dowel action is not considered.

6.3.2 Tassios Model

The dowel force-displacement relationship is modeled as elastic-plastic. For simplicity, consider a reinforcing bar perpendicularly crossing a crack as shown in Figure 67. (Reinforcing bars crossing cracks at oblique angles are also accommodated.) As described by He and Kwan (2001), the dowel action of the reinforcement may modeled as a beam on an elastic concrete foundation. The dowel force, V_d , due to the relative displacement, δ_s , of the cracks is computed as follows:

$$V_d = E_s I_z \lambda^3 \delta_s \leq V_{du} \quad (6.3.2.1)$$

$$I_z = \frac{\pi d_b^4}{64} \quad (6.3.2.2)$$

$$\lambda = \sqrt[4]{\frac{k_c d_b}{4 E_s I_z}} \quad (6.3.2.3)$$

$$k_c = \frac{127 \cdot c \sqrt{f'_c}}{d_b^{2/3}} \quad (6.3.2.4)$$

$$c = 0.8 \quad (6.3.2.5)$$

$$V_{du} = 1.27 d_b^2 \sqrt{f'_c f_y} \quad (6.3.2.6)$$

where δ_s is the shear slip along the crack, d_b is the diameter of the reinforcement, E_s is the elastic modulus of the reinforcement, f_y is the yield strength of the reinforcement, f'_c is the compressive strength of the concrete. The parameter I_z is the area moment of inertia of the reinforcement. The parameter λ compares the stiffness of the concrete to that to the reinforcing bar. The parameter k_c is the stiffness of notional concrete foundation, where c is an experimentally based coefficient to reflect the bar spacing. The ultimate dowel force, V_{du} , corresponds to plastic hinging of the reinforcement and crushing of the surrounding concrete in multiaxial compression.

The shear resistance due to dowel action is computed as a smeared contribution as follows:

$$v_d = \frac{\rho_s V_d}{A_s} \quad (6.3.2.7)$$

where ρ_s is the reinforcement ratio and A_s is the area of the reinforcement.

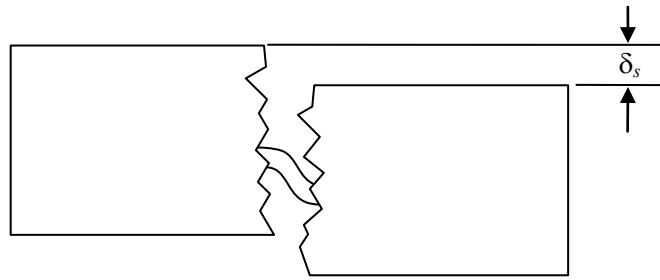


Figure 67: Dowel resistance mechanism

The Tassios (Crack Slip) and Tassios (Crack Strength) options are available in VecTor2 for calculating rebar dowel action. In the crack slip option, the dowel force V_d is subtracted from the stress of the concrete at a crack. For crack strength, the dowel force acts as a resisting force.

The default option is Tassios Crack Slip Model. In general, this option is used unless stability issues related to reinforcement shearing occur during the analysis, in which case the Tassios Strength Model is used.

6.4 Reinforcement Buckling

Three models are available for the consideration of reinforcing bar buckling. These are the Dhakal-Maekawa 2002 model (DM), the Refined Dhakal-Maekawa model (RDM), and the Asatsu model. Both the DM and RDM models are mainly based on the model of Dhakal and Maekawa (2002a, and b). By using the formulations of Dhakal and Maekawa (2002b), the Seckin and Menegotto-Pinto hysteretic models were modified by Akkaya et al. (2013) for ductile reinforcement including buckling effects. The DM and the RDM models can be used only if the ductile steel reinforcement and one of the Seckin or the Menegotto-Pinto models are selected. Both models assume that the reinforcement buckling begins to occur when the unsupported length to diameter ratio ($b/t=L/D$) for the reinforcing bars exceeds 5.0 and the compressive reinforcement strain exceeds its yield strain ε_y . Consequently, to take into account the rebar buckling effect, both models require the input of L/D prior to an analysis for $L/D \geq 5.0$. For the

default value of L/D and $L/D < 5$, there is no rebar buckling effects considered for the reinforcing bars.

When using the Asatsu model, there is no requirement for the input of L/D .

6.4.1 Dhakal-Maekawa Model 2002 (DM) Model

The following model was proposed by Dhakal and Maekawa (2002a,b) as shown in Figure 68.

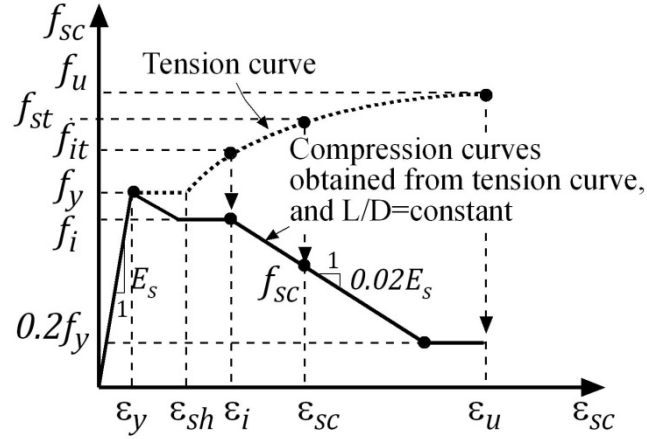


Figure 68: Compressive stress-strain relationships (Dhakal and Maekawa, 2002a, b)

The DM model defines an intermediate point (ε_i, f_i) to obtain the average compressive stress-strain curves.

After this intermediate point, a constant negative stiffness of $0.02E_s$ is assumed until the average compressive stress becomes equal to $0.2f_y$. In this formulation,

$$r_b = \sqrt{\frac{f_y}{100}} \frac{L}{D} \quad (6.4.1.1)$$

$$\varepsilon_i = \varepsilon_y [55 - 2.3r_b] \quad \text{for } \varepsilon_i \geq 7\varepsilon_y, \text{ otherwise } \varepsilon_i = 7\varepsilon_y \quad (6.4.1.2)$$

$$f_{it} = f_y \quad \text{for } \varepsilon_i \leq \varepsilon_{sh} ; \quad f_{it} = f_u + (f_y - f_u) \left(\frac{\varepsilon_u - \varepsilon_i}{\varepsilon_u - \varepsilon_{sh}} \right)^2 \quad \text{for } (\varepsilon_{sh} < \varepsilon_i \leq \varepsilon_u) \quad (6.4.1.3)$$

$$f_{st} = f_y \quad \text{for } \varepsilon_{sc} \leq \varepsilon_{sh} ; \quad f_{st} = f_u + (f_y - f_u) \left(\frac{\varepsilon_u - \varepsilon_{sc}}{\varepsilon_u - \varepsilon_{sh}} \right)^2 \quad \text{for } (\varepsilon_{sh} < \varepsilon_{sc} \leq \varepsilon_u) \quad (6.4.1.4)$$

where, r_b is slenderness ratio, f_y is the yield stress in MPa, f_{it} and f_{st} are the stress in the tension curve corresponding to the intermediate strain ε_i and the current strain ε_{sc} , respectively. At the intermediate point, the stress f_i on the compression curve is determined as follows:

$$f_i = f_{it} \alpha [1.1 - 0.016 r_b] \quad \text{for } f_i \geq 0.2 f_y, \text{ otherwise } f_i = 0.2 f_y \quad (6.4.1.5)$$

The following equations are used for the determination of α :

$$\alpha = 0.75 + \frac{\varepsilon_u - \varepsilon_{sh}}{300 \varepsilon_y} \quad \text{for } \alpha \leq \frac{f_u}{1.5 f_y} \text{ and } 0.75 \leq \alpha \leq 1.0 \quad (6.4.1.6)$$

The compressive stress-strain (f_{sc}, ε_{sc}) relationship are then determined as follows:

$$f_{sc} = E_s \varepsilon_{sc} \quad \text{for } \varepsilon_{sc} \leq \varepsilon_y \quad (6.4.1.7)$$

$$f_{sc} = f_{st} \left[1 - \left(1 - \frac{f_i}{f_{it}} \right) \left(\frac{\varepsilon_{sc} - \varepsilon_y}{\varepsilon_i - \varepsilon_y} \right) \right] \quad \text{for } \varepsilon_y < \varepsilon_{sc} \leq \varepsilon_i \quad (6.4.1.8)$$

$$f_{sc} = \max \left[\left(f_i - 0.02 E_s (\varepsilon_{sc} - \varepsilon_i) \right); 0.2 f_y \right] \quad \text{for } \varepsilon_i < \varepsilon_{sc} \leq \varepsilon_u \quad (5.4.1.9)$$

6.4.2 Refined Dhakal-Maekawa (RDM) Model

Although the DM model provides good approximation in general sense to the buckling behaviors of reinforcing bars, to improve the performance of the DM model for reinforcing bars with any geometric and material properties, and to eliminate some criticized points on the DM model, a refined model (RDM) was proposed by Akkaya et al. (2013). As the RDM model covers the DM model, the performance of the RDM model is similar to or better than the performance of the DM model. By comparison with the DM model, the intermediate stress, f_i is determined more effectively as per the location of the intermediate strain, ε_i on the tension curve in the RDM model. In particular, RDM model gives better results than the

DM model when the intermediate strain, ε_i , is on the strain-hardening region of the tension curve for reinforcing bars with a high strain-hardening parameter ($P=4$) and small slenderness ratios ($r_b < 21$), and for reinforcing bars with tension stress-strain response where $\varepsilon_i < \varepsilon_u$ and $\varepsilon_{imax} > \varepsilon_u$. A typical average compressive response obtained from this model is presented in Figure 69.

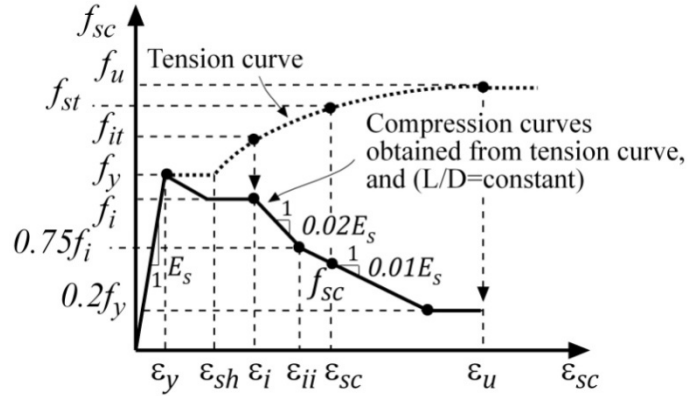


Figure 69: Compressive stress-strain relationships (Akkaya et al., 2013)

The compression curves are developed through the definition of an intermediate point (ε_i, f_i) on the average compression stress-strain curves. The intermediate strain ε_i and the maximum intermediate strain ε_{imax} are determined as follows:

$$r_b = \sqrt{\frac{f_y}{100}} \frac{L}{D} \quad (6.4.2.1)$$

$$\varepsilon_{imax} = \varepsilon_y \left[55 - 2.3 \sqrt{\frac{f_y}{100}} \times 5 \right] \quad (6.4.2.2)$$

$$\varepsilon_i = \beta \varepsilon_y [55 - 2.3 r_b] \text{ for } \varepsilon_i \geq 7 \varepsilon_y, \text{ otherwise } \varepsilon_i = 7 \varepsilon_y \quad (6.4.2.3)$$

where r_b is slenderness ratio and f_y is the yield stress in MPa. Maximum intermediate strain ε_{imax} is used to define different tension curves using β and P constants as follow:

$$\beta = \varepsilon_u / \varepsilon_{imax} \text{ for } (\varepsilon_i^{\beta=1} < \varepsilon_u \text{ and } \varepsilon_{imax} > \varepsilon_u); \text{ otherwise } \beta = 1 \quad (6.4.2.4)$$

$$P = 1 \text{ for } (\varepsilon_{i\max} \geq \varepsilon_u \text{ and } \varepsilon_i = 7\varepsilon_y); \text{ otherwise } P = 4 \quad (6.4.2.5)$$

$$f_{it} = f_y \text{ for } \varepsilon_i \leq \varepsilon_{sh}; f_{it} = f_u + (f_y - f_u) \left(\frac{(\varepsilon_u - \varepsilon_i)}{(\varepsilon_u - \varepsilon_{sh})} \right)^P \text{ for } \varepsilon_i > \varepsilon_{sh} \quad (6.4.2.6)$$

$$f_{st} = f_y \text{ for } \varepsilon_{sc} \leq \varepsilon_{sh}; f_{st} = f_u + (f_y - f_u) \left(\frac{(\varepsilon_u - \varepsilon_{sc})}{(\varepsilon_u - \varepsilon_{sh})} \right)^P \text{ for } (\varepsilon_{sh} < \varepsilon_{sc} \leq \varepsilon_i) \quad (6.4.2.7)$$

where, f_{it} and f_{st} are the stress in the tension curve corresponding to the intermediate strain ε_i and current strain ε_{sc} , respectively. At the intermediate point, the stress f_i on the compression curves is determined as follow:

$$f_i = \alpha f_y; f_i \leq f_{it} \quad (6.4.2.8)$$

The following equations are used for the determination of α based on the location of ε_i on the tension curve:

$$\alpha = [1.1 - 0.016r_b] \left[0.8 + 1.8 \frac{f_u D}{f_y L} \right] \text{ for } \varepsilon_i > \varepsilon_{sh} \quad (6.4.2.9)$$

$$\alpha = 0.75 [1.1 - 0.016r_b] \left[0.8 + 1.8 \frac{f_u D}{f_y L} \right] \text{ for } \varepsilon_i \leq \varepsilon_{sh} \quad (6.4.2.10)$$

$$\alpha = 0.75 \frac{f_{it}}{f_y} [1.1 - 0.016r_b] \text{ for } (\varepsilon_{i\max} \geq \varepsilon_u \text{ and } \varepsilon_i = 7\varepsilon_y) \quad (6.4.2.11)$$

The compressive stress-strain (f_{sc}, ε_{sc}) response including rebar buckling is then determined as follows:

$$f_{sc} = E_s \varepsilon_{sc} \text{ for } \varepsilon_{sc} \leq \varepsilon_y \quad (6.4.2.12)$$

$$f_{sc} = f_{st} \left[1 - \left(1 - \frac{f_i}{f_{it}} \right) \left(\frac{\epsilon_{sc} - \epsilon_y}{\epsilon_i - \epsilon_y} \right) \right] \text{ for } \epsilon_y < \epsilon_{sc} \leq \epsilon_i \tag{6.4.2.13}$$

$$f_{sc} = \max \left[\left(f_i - 0.02 E_s (\epsilon_{sc} - \epsilon_i) \right); 0.2 f_y \right] \text{ for } (\epsilon_i \leq \epsilon_{sc} < \epsilon_{ii}) \tag{6.4.2.14}$$

$$f_{sc} = \max \left[\left(0.75 f_i - 0.01 E_s (\epsilon_{sc} - \epsilon_{ii}) \right); 0.2 f_y \right] \text{ for } (\epsilon_{ii} \leq \epsilon_{sc} < \epsilon_u) \tag{6.4.2.15}$$

6.4.3 RDM and DM buckling models for hysteretic response

When the unsupported length ratio is equal to or larger than 5, the backbone compressive stress-strain curve are defined by the selected RDM or DM models as shown in Figure 70. The stiffness (E_m) at the target point and the unloading-reloading stiffness (E_{rb}) on the compressive strain region are also changed due to buckling.

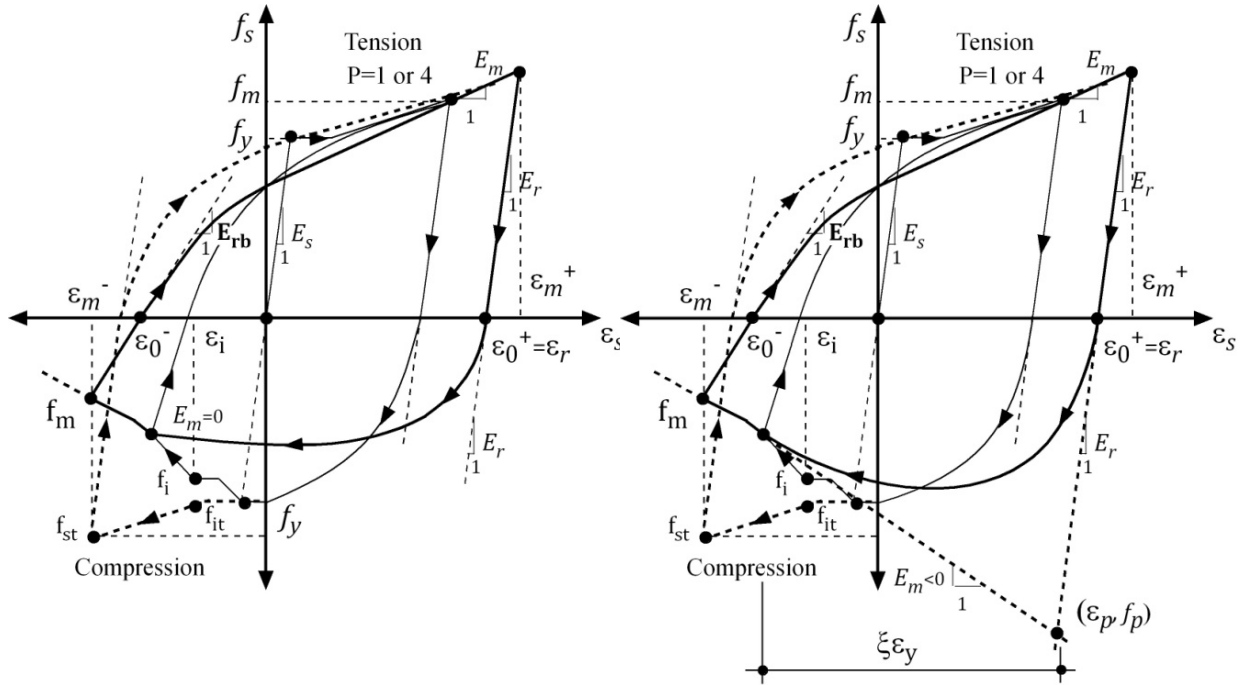


Figure 70: Hysteretic models for ductile reinforcement including buckling
 [left (a): Seckin; right (b): Menegotto-Pinto]

In the Seckin model, Figure 70a, the stiffness (E_m) at the target point on the compressive strain zone is assumed to be zero when the compressive stress (f_m) is smaller than yield stress (f_y). In Menegotto-Pinto

model, Figure 70b, the same stiffness (E_m) at the target stress-strain point (f_m, ε_m) on the compressive strain zone are limited with a negative value as follows:

$$E_m = \frac{(f_m - f_y)}{(\varepsilon_m - \varepsilon_y)} \geq -0.02E_s \quad (6.4.3.1)$$

For both hysteretic models, in Figure 70, the unloading-reloading stiffness (E_{rb}) on the compressive strain zone are reduced as follow:

$$E_{rb} = E_s \left(\frac{f_m}{f_{st}} \right)^2 \quad \text{for } |\varepsilon_m^-| \leq \varepsilon_i \quad (6.4.3.2)$$

$$E_r = E_s \left(\frac{f_m}{f_{st}} \right) \left(\frac{f_i}{f_y} \right) \quad \text{for } |\varepsilon_m^-| > \varepsilon_i \quad (6.4.3.3)$$

6.4.4 Determination of the Unsupported Length Ratio ($b/t=L/D$)

The accuracy of reinforcement buckling models depends on defining the unsupported length ratio (b/t) correctly. Because RC members have the numerous reinforcement configurations, there are difficulties in determining b/t automatically. Consequently, b/t should be input manually. One method is proposed by Dhakal and Maekawa (2002c) for this purpose as follows:

This method requires determining the reduced flexural rigidity ($E_r I$) of a rebar as follows:

$$I = \pi D^4 / 64, \quad E_r I = 0.5 E_s I / \sqrt{(f_y / 400)} \quad (6.4.4.1)$$

where, I , D , E_s , and f_y are the moment of inertia, diameter, modulus of elasticity, and yield strength (MPa) of the reinforcing bar including buckling, respectively. Normalized stiffness k of the rebar, tie stiffness k_t , and equivalent stiffness ratio k_{eq} are calculated as follows:

$$k = \frac{\pi^4 E_r I}{s^3}, \quad k_t = \frac{E_t A_t n_l}{l_e n_b}, \quad k_{eq} = \frac{k_t}{k} \quad (6.4.4.2)$$

where s is the tie spacing, A_t is the sectional area of the one tie leg, l_e is the length of the tie leg, E_t is the modulus of elasticity of the tie, n_b is the number of longitudinal bars supported by these tie legs, and n_l is the number of tie legs parallel to the lateral load. Dhakal and Maekawa (2002c) propose the values for n_b and n_l for common arrangements of longitudinal and lateral reinforcement as shown in Figure 71.

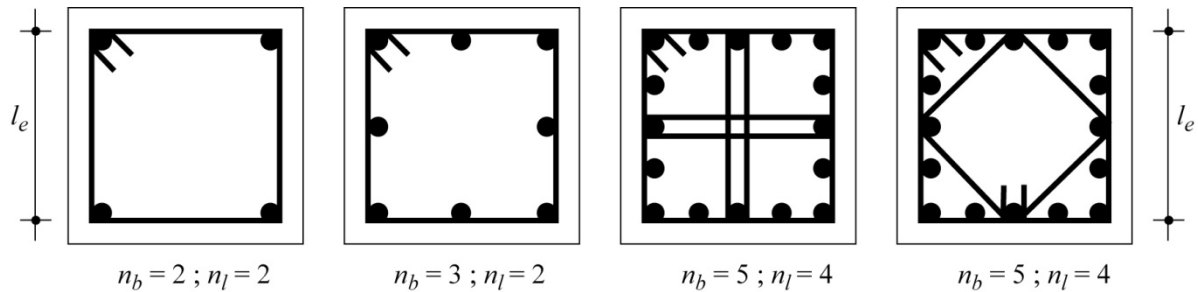


Figure 71: Values of n_b and n_l for common reinforcement

The buckling length is then determined as follow:

$$L = n \cdot s \quad (6.4.4.3)$$

where, n is the number of spaces between ties over the buckling length which may be chosen from Table 1.

Table 1: Determination of n (Dhakal and Maekawa 2002c)

| L=n s | |
|-----------------|--------|
| k_{eq} | n |
| $k_{eq} > 0.75$ | 1 |
| 0.7500-0.5000 | 1 or 2 |
| 0.5000-0.1649 | 2 |
| 0.1649-0.0976 | 3 |
| 0.0976-0.0448 | 4 |
| 0.0448-0.0084 | 5 |
| 0.0084-0.0063 | 6 |
| 0.0063-0.0037 | 7 |
| 0.0037-0.0031 | 8 |

In Table 2, the slenderness ratio, r_b indicates approximately the reduction of normalized stress (f_i/f_y) on the modified compressive stress-strain curve due to buckling. The calculated unsupported length ratio can be used together with Table 2 when determining the unsupported length ratio. If the calculated value of r_b is smaller than 8, there is no rebar buckling effect. For other values, Akkaya et al. (2013) recommend the followings:

- 1) If the calculated value of r_b is between 8 and 16, assume r_b is 16.
- 2) If the calculated value of r_b is between 16 and 21, assume r_b is 21.
- 3) If the calculated value of r_b is larger than 21, use the calculated value of r_b .

Table 2: Relationships between the buckling length and normalized intermediate stress ratio

| $r_b = \frac{L}{D} \sqrt{\frac{f_y}{100}}$ | f_i/f_y | Buckling affect level |
|--------------------------------------------|-----------|-----------------------|
| <8 | - | No effect |
| (8-16) | (1.0-0.8) | Small |
| (16-34) | (0.8-0.4) | High |
| (34-50) | (0.4-0.2) | Very high |

6.4.5 Asatsu Model

In order to use this model, the reinforcement bars subject to buckling must be modeled discretely by truss bar elements and connected to the concrete elements with bond (link or contact) elements. A full description of the determination of the buckling length and buckling criteria are beyond the scope of this discussion. In brief, the criteria for reinforcement buckling are that reinforcement is plasticized, is subject to compressive stresses exceeding eighty percent of the yield strength and that the bond deterioration is severe, such that the cumulative energy consumption exceeds the fracture energy G_f .

6.5 Steel Fibre Reinforced Concrete

The following sections describe the response of Steel Fibre Reinforced Concrete (SFRC). The two types of fibres that can be used to model SFRC in VecTor2 are straight fibres and hooked fibres. The main difference between the two types of fibres is in the quality of bond between the fibres and the concrete matrix. The deformed ends of the hooked fibres enable a stronger bond between the steel fibres and the concrete compared to the straight fibres.

6.5.1 Introduction

The effect of fibres on the behaviour of concrete is dependent on fibre volume content, fibre length, fibre aspect ratio, fibre tensile strength, concrete strength, and fibre orientation. The majority of these are required inputs in FormWorks. The following properties are considered when SFRC is analyzed using VecTor2:

- Fibre Volume Fraction, V_f
- Fibre Length, L_f
- Fibre Diameter, D_f
- Fibre Tensile Strength, F_u
- Fibre Bond Strength, T_u

Note that the fibre aspect ratio mentioned above is the ratio of fibre length to fibre diameter, and is a measure of the stiffness of the fibre. A brief description of the effect of the factors listed above on the behaviour of SFRC can be found in (Susetyo, 2009).

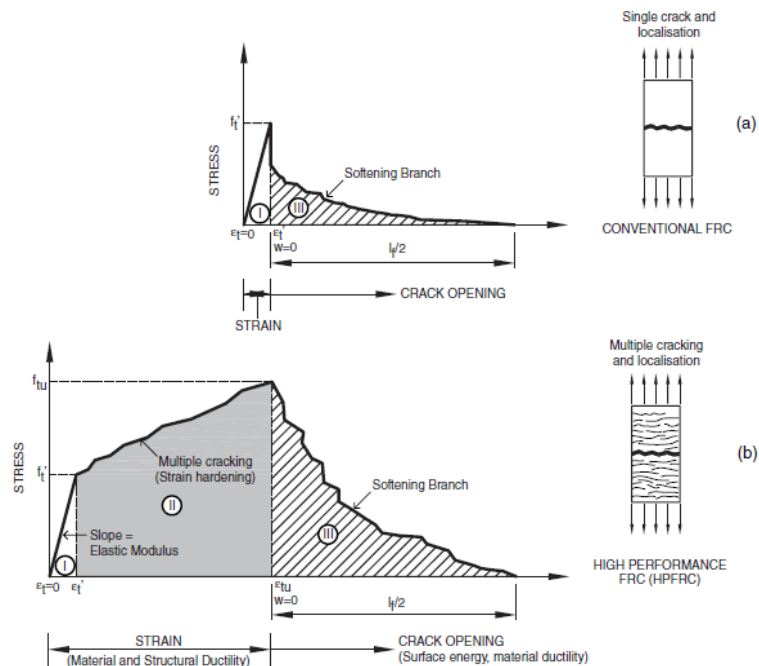
6.5.2 Stress-Strain Behavior of SFRC

This section outlines the tensile and compressive stress-strain behaviour of SFRC.

An important function of steel fibres in SFRC is to provide post-cracking tensile capacity. In SFRC, while the concrete stress reduces after cracking, the strain may still increase substantially prior to a reduction in tensile strength. At higher fibre volumes, strain hardening may also occur (Susetyo, 2009). Figure 72 illustrates the stress-strain response of both high and low fibre volume content concrete.

There are a variety of options available with SFRC. Steel fibre reinforcement can be used in normal SFRC or as part of a composite material. The two SFRC composite materials available in VecTor2 are Concrete-SFRC Laminate and Wood-SFRC Laminate. For both regular SFRC and the SFRC used in composite material models, either straight or hooked fibres can be used. The required input properties for steel fibres are the same for types of fibres.

There are also a number of models available in VecTor2 for SFRC. For the compression stress-strain response of SFRC, the Lee et al 2011 (FRC) model is available and is described in Section 4.2.7. Two tension softening models for FRC are also available in VecTor2. An exponential tension softening model and the fib FRC tension softening models are discussed in sections 4.5.6 and 4.5.9, respectively.



Numerous FRC tension models are also available and are described in section 4.6.

Figure 72: Tensile stress-strain response of FRC for low and high fibre volume contents (Susetyo, 2009)

The addition of fibre to concrete makes the post-peak compressive response more gradual, less steep compared to plain concrete. The higher the aspect ratio or volume content of the fibres, the more gradual the post-peak compressive response. The compressive response of SFRC is illustrated in Figure 73.

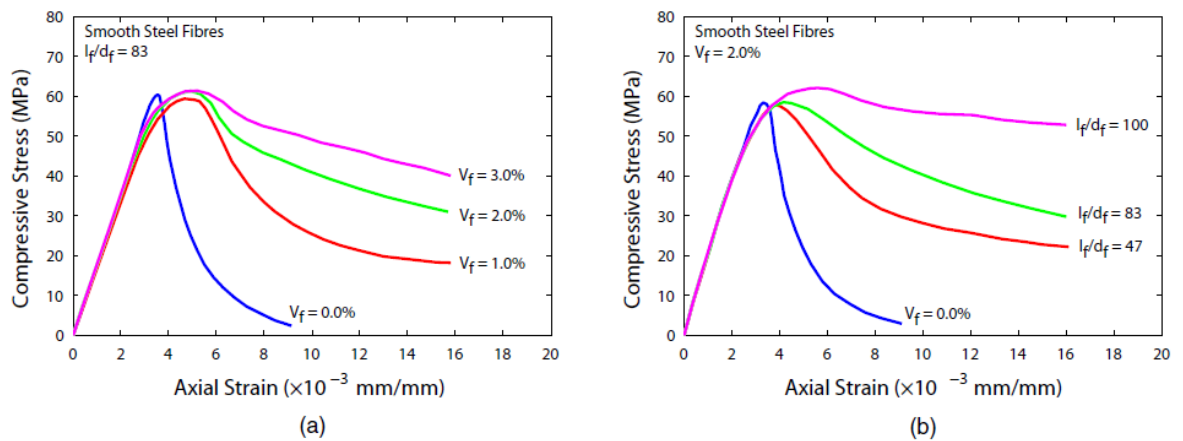


Figure 73: Compressive stress-strain curve of SFRC, illustrating a) fibre content and b) fibre aspect ratio (Susetyo, 2009)

6.6 Laminates

Four different types of laminate can be modeled in VecTor2. The most common is the concrete-steel laminate, where a concrete core is located between two steel face plates.

The **Steel Skin Plate** option is used as the reference reinforcement type in the *Define Reinforced Concrete Properties* tab when modeling concrete-steel composite elements. The steel plate is analyzed in accordance with the DSFM, where steel stresses are determined from uniaxial stress-strain relationships. For the monotonic response of steel skin plates, VecTor2 employs a tri-linear elastic-plastic strain hardening model. Yielding, strain hardening, and Bauschinger's effect for reverse cyclic loading are all considered in VecTor2, and yielding of the plates under biaxial stress is determined using the Von Mises criterion:

$$(f_{s1} - f_{s2})^2 + (f_{s2} - f_{s3})^2 + (f_{s3} - f_{s1})^2 = 2(f_y)^2 \quad (6.6.1)$$

where f_{s1} , f_{s2} , and f_{s3} are the principal stresses in the plate, one of which is always zero.

The hysteretic response of the steel plate, which includes the Bauschinger effect as mentioned above, is modeled using a modified Seckin formulation. After the steel plate buckles in compression, it can sustain additional loading in tension but cannot sustain further compressive stress upon load reversal.

It is assumed in VecTor2 that the anchor studs prevent slip between the concrete and steel skin plates. A more detailed response of the FEM formulation of steel-concrete elements is found in Vecchio and McQuade (2011).

SFRC can also be used as a laminate; both SFRC—straight fibres and SFRC—hooked fibres are possible laminate options. The stress-strain behaviour of SFRC was discussed in the preceding section. Orthotropic laminate can also be used as smeared reinforcement. The stress-strain behaviour of orthotropic wood was discussed in section 5.3.

6.7 Shape Memory Alloy Type 1 and Type 2

Shape Memory Alloy materials are used to replace conventional reinforcing steel under seismic loading conditions, and are useful due to the material's ability to dissipate large amounts of energy without excessive permanent deformation. The hysteresis for conventional reinforcing steel includes large strain offsets; after an earthquake, the structure may have large permanent displacements. Shape memory alloys minimize or eliminate these large strain offsets such that after a seismic event, the structure will retain its original shape or the deformations will be much smaller than if conventional reinforcing steel was used.

6.7.1 Shape Memory Alloy 1 (SMA 1)

The idealized behaviour of the SMA 1, with no strain offsets is modeled with SMA 1. It has a flag-shaped hysteresis, as shown in Figure 74.

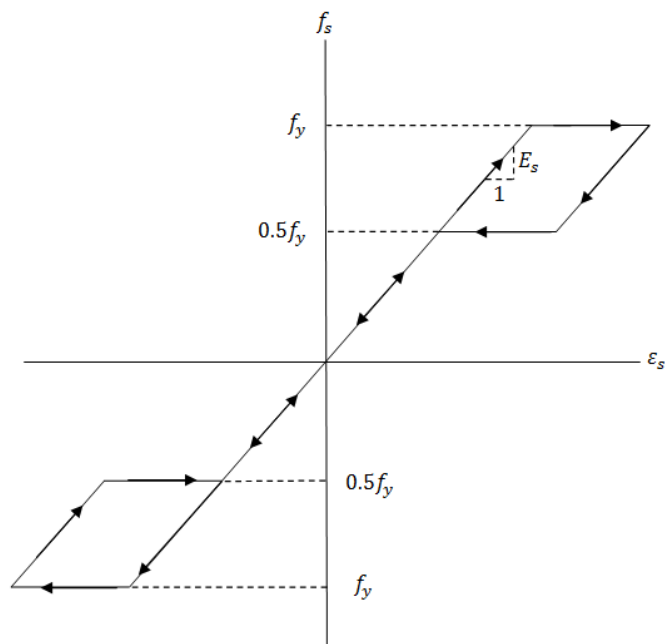


Figure 74: Stress-strain response for SMA 1

6.7.2 Shape Memory Alloy 2 (SMA 2)

Developed at the University of Ottawa, the hysteresis for SMA 2 differs from SMA 1 in that it incorporates strain hardening as well as small strain offsets. Figure 75 illustrates the stress-strain curve and hysteresis for SMA 2.

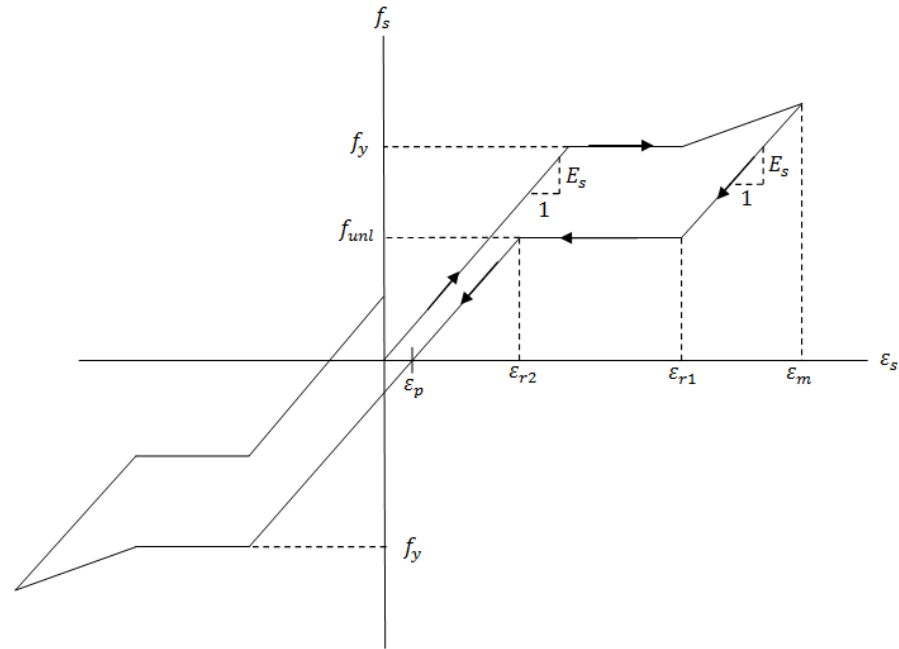


Figure 75: Stress-strain response for SMA2

In the figure above, f_y is the yield stress, f_{unl} is the unloading stress, ε_p is the strain offset, ε_{r1} and ε_{r2} are reference strains, and ε_m is the maximum strain.

Both the unloading stress and strain offset are functions of the maximum strain.

$$f_{unl} = f_y \cdot (0.70188 - 0.003127\varepsilon_m - 0.00003214\varepsilon_m^2) \quad 0.25f_y \leq f_{unl} \leq 0.75f_y \quad (6.7.2.1)$$

$$\varepsilon_p = 0.001\varepsilon_m^2 - 0.005\varepsilon_m + 0.4323 \quad (6.7.2.2)$$

7 Models for Bond

The following discussion describes the monotonic bond stress-slip models for bond elements. In VecTor2, the bond materials are divided into two categories: models for embedded bars (smooth and embedded) and models for externally bonded plates or sheets. For the former, the bond stress-slip relationship is internally calculated by VecTor2 according to the selected model, while for the latter, the bond stress-slip relationship is specified by the user by a series of reference bond stress and slips. Hysteretic response is included in the models, but not discussed here.

7.1 Bond Stress-Slip Models for Embedded Bars

For embedded bars, the bond model first determines the stress-slip relationship for two distinct cases: confined bars and unconfined bars. The stronger relationship for confined bars corresponds to pull-out type bond failure, whereas the relationship for unconfined bars corresponds to splitting failure. Both the confined and unconfined bond stress-slip relationships are defined by a series of reference bond stresses, τ , and bond slips, Δ . Those pertaining to pullout failure are subscripted as τ_p, Δ_p while those pertaining to splitting failure are subscripted, τ_s, Δ_s .

The actual bond stress-slip model is defined by a series of reference bond stresses and slips, τ_{sp}, Δ_{sp} . These are determined by linearly interpolating between the unconfined and confined reference bond stresses and slips using the confinement pressure factor, β . A confinement pressure of zero corresponds to the unconfined case of splitting failure, while a confinement pressure of 7.5 MPa corresponds to the confined case of pullout failure. Based on the anticipated confining pressure, σ , the confinement pressure factor may be computed as follows:

$$\beta = \frac{\sigma}{7.5}, \quad (\text{in MPa}) \quad 0 \leq \beta \leq 1, \quad (7.1.1)$$

The following models utilize several properties pertaining to the reinforcing bars and their placement to compute the bond stress-slip relationship. The minimum of the concrete cover and half of

the bar spacing is denoted, c . For deformed reinforcement bars, VecTor2 computes the lug spacing, S , and lug height, H , depending on the reinforcement bar diameter, d_b , as follows:

$$S, H = \begin{cases} 39.4 \text{ mm}, 2.55 \text{ mm} & \text{for } 55 \text{ mm} \leq d_b \\ 30.6 \text{ mm}, 2.20 \text{ mm} & \text{for } 43 \text{ mm} \leq d_b < 55 \text{ mm} \\ 25.0 \text{ mm}, 1.79 \text{ mm} & \text{for } 35 \text{ mm} \leq d_b < 43 \text{ mm} \\ 20.9 \text{ mm}, 1.48 \text{ mm} & \text{for } 29 \text{ mm} \leq d_b < 35 \text{ mm} \\ 17.6 \text{ mm}, 1.26 \text{ mm} & \text{for } 25 \text{ mm} \leq d_b < 29 \text{ mm} \\ 13.6 \text{ mm}, 0.98 \text{ mm} & \text{for } 19 \text{ mm} \leq d_b < 25 \text{ mm} \\ 11.2 \text{ mm}, 0.72 \text{ mm} & \text{for } 15 \text{ mm} \leq d_b < 19 \text{ mm} \\ 7.9 \text{ mm}, 0.45 \text{ mm} & \text{for } 11 \text{ mm} \leq d_b < 15 \text{ mm} \\ 0.70d_b, 0.04d_b & \text{for } 0 \text{ mm} \leq d_b < 11 \text{ mm} \end{cases} \quad (7.1.2)$$

For smooth bars, VecTor2 computes the lug spacing according to Equation 7.1.2, but computes the lug height as follows:

$$H = \frac{S}{75} \quad (7.1.3)$$

The model for hooked bars is different is described subsequently.

7.1.1 Perfect bond

The bond material is assigned a numerically large stiffness and strength to prevent deformation of the bond element.

7.1.2 Eligehausen Model

As proposed by Eligehausen et al. (1983), the confined and unconfined bond stress-slip relationships are described by an ascending non-linear branch, a constant bond stress plateau, a linearly declining branch, and a sustaining residual stress branch, as shown in Figure 76.

The confined stress-slip relationship is summarized as follows:

$$\tau = \begin{cases} \tau_{p1} \left(\frac{\Delta}{\Delta_{p1}} \right)^\alpha & \text{for } \Delta \leq \Delta_{p1} \\ \tau_{p2} & \text{for } \Delta_{p1} < \Delta \leq \Delta_{p2} \\ \tau_{p2} - \left[\frac{(\Delta - \Delta_{p2})}{(\Delta_{p3} - \Delta_{p2})} (\tau_{p2} - \tau_{pf}) \right] & \text{for } \Delta_{p2} < \Delta \leq \Delta_{p3} \\ \tau_{pf} & \text{for } \Delta_{p3} < \Delta \end{cases} \quad (7.1.2.1)$$

where

$$\tau_{p1} = \left(20 - \frac{d_b}{4}\right) \sqrt{\frac{f'_c}{30}} \quad (7.1.2.2)$$

$$\tau_{p2} = \tau_{p1} \quad (7.1.2.3)$$

$$\tau_{pf} = \left(5.5 - 0.07 \frac{S}{H}\right) \sqrt{\frac{f'_c}{27.6}} \quad (7.1.2.4)$$

$$\Delta_{p1} = \sqrt{\frac{f'_c}{30}} \quad (7.1.2.5)$$

$$\Delta_{p2} = 3.0 \text{ mm} \quad (7.1.2.6)$$

$$\Delta_{p3} = S \quad (7.1.2.7)$$

$$\alpha = 0.4 \quad (7.1.2.8)$$

The unconfined stress-slip relationship is summarized as follows:

$$\tau = \begin{cases} \tau_{s1} (\Delta / \Delta_{s1})^\alpha & \text{for } \Delta \leq \Delta_{s1} \\ \tau_{s2} & \text{for } \Delta_{s1} < \Delta \leq \Delta_{s2} \\ \tau_{s2} - \left[\frac{(\Delta - \Delta_{s2})}{(\Delta_{s3} - \Delta_{s2})} (\tau_{s2} - \tau_{sf}) \right] & \text{for } \Delta_{s2} < \Delta \leq \Delta_{s3} \\ \tau_{sf} & \text{for } \Delta_{s3} < \Delta \end{cases} \quad (7.1.2.9)$$

where

$$\tau_{s1} = 0.748 \sqrt{\frac{f'_c \cdot c}{d_b}} \leq \tau_{p1} \quad (7.1.2.10)$$

$$\tau_{s2} = \tau_{s1} \quad (7.1.2.11)$$

$$\tau_{sf} = 0.234 \sqrt{\frac{f'_c \cdot c}{d_b}} \leq \tau_{pf} \quad (7.1.2.12)$$

$$\Delta_{s1} = \Delta_{p1} \exp \left[\frac{1}{\alpha} \ln \left(\frac{\tau_{s1}}{\tau_{p1}} \right) \right] \quad (7.1.2.13)$$

$$\Delta_{s2} = \Delta_{p2} \quad (7.1.2.14)$$

$$\Delta_{s3} = \Delta_{p3} \quad (7.1.2.15)$$

Given a confinement pressure factor, β , the bond stress-slip relationship is defined as follows:

$$\tau = \begin{cases} \tau_{sp1} \left(\frac{\Delta}{\Delta_{sp1}} \right)^\alpha & \text{for } \Delta \leq \Delta_{sp1} \\ \tau_{sp1} - \left[\frac{(\Delta - \Delta_{sp12})}{(\Delta_{sp3} - \Delta_{sp2})} (\tau_{sp2} - \tau_{spf}) \right] & \text{for } \Delta_{sp1} < \Delta \leq \Delta_{sp2} \\ \tau_{sp2} - \left[\frac{(\Delta - \Delta_{sp2})}{(\Delta_{sp3} - \Delta_{sp2})} (\tau_{sp2} - \tau_{spf}) \right] & \text{for } \Delta_{sp2} < \Delta \leq \Delta_{sp3} \\ \tau_{spf} & \text{for } \Delta_{sp3} < \Delta \end{cases} \quad (7.1.2.16)$$

$$\tau_{sp1} = \tau_{s1} + \beta(\tau_{p1} - \tau_{s1}) \quad (7.1.2.17)$$

$$\tau_{sp2} = \tau_{sp1} \quad (7.1.2.18)$$

$$\tau_{spf} = \tau_{s1} + \beta(\tau_{pf} - \tau_{sf}) \quad (7.1.2.19)$$

$$\Delta_{sp1} = \Delta_{s1} + \beta(\Delta_{p1} - \Delta_{s1}) \geq \Delta_{s1} \quad (7.1.2.20)$$

$$\Delta_{sp2} = \Delta_{p2} \quad (7.1.2.21)$$

$$\Delta_{sp3} = \Delta_{p3} \quad (7.1.2.22)$$

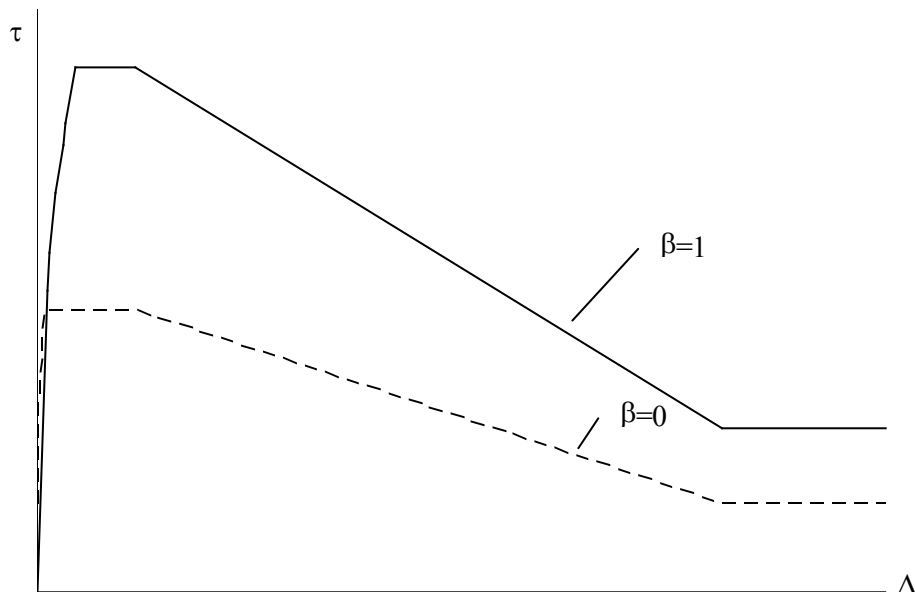


Figure 76: Eligehausen bond stress-slip response

7.1.3 Gan Model

The Gan confined bond stress-slip relationship, as shown in Figure 77, is the same as the Eligehausen model for the confined stress-slip relationship as summarized by equations 7.1.2.1 to 7.1.2.8.

The unconfined bond stress-slip relationship is described by an ascending non-linear branch, a descending linear branch, and a sustaining residual stress branch, summarized as follows:

$$\tau = \begin{cases} \tau_{s1} (\Delta/\Delta_{s1})^\alpha & \text{for } \Delta \leq \Delta_{s1} \\ \tau_{s1} - \left[\frac{(\Delta - \Delta_{s1})}{(\Delta_{s2} - \Delta_{s1})} (\tau_{s1} - \tau_{sf}) \right] & \text{for } \Delta_{s1} < \Delta \leq \Delta_{s2} \\ \tau_{sf} & \text{for } \Delta_{s2} < \Delta \end{cases} \quad (7.1.3.1)$$

where

$$\tau_{s1} = 0.748 \sqrt{\frac{f'_c \cdot c}{d_b}} \leq \tau_{p1} \quad (7.1.3.2)$$

$$\tau_{s2} = 0.15 \tau_{s1} \quad (7.1.3.3)$$

$$\tau_{sf} = \tau_{s2} \quad (7.1.3.4)$$

$$\Delta_{s1} = \Delta_{p1} \exp \left[\frac{1}{\alpha} \ln \left(\frac{\tau_{s1}}{\tau_{p1}} \right) \right] \quad (7.1.4.5)$$

$$\Delta_{s2} = 2.0 \text{ mm} \quad (7.1.3.6)$$

$$\Delta_{s3} = \Delta_{p3} \quad (7.1.3.7)$$

Given a confinement pressure factor, β , the bond stress-slip relationship is defined by equation

7.1.2.16, where:

$$\tau_{sp1} = \tau_{s1} + \beta(\tau_{p1} - \tau_{s1}) \quad (7.1.3.8)$$

$$\tau_{sp2} = \tau_{s2} + \beta(\tau_{p2} - \tau_{s2}) \quad (7.1.3.9)$$

$$\tau_{spf} = \tau_{sf} + \beta(\tau_{pf} - \tau_{sf}) < \tau_{sf} \quad (7.1.3.10)$$

$$\Delta_{sp1} = \Delta_{s1} + \beta(\Delta_{p1} - \Delta_{s1}) \geq \Delta_{s1} \quad (7.1.3.11)$$

$$\Delta_{sp2} = \begin{cases} 2.0 \text{ mm} & \text{if } \beta = 0 \\ \Delta_{p2} & \text{if } 0 < \beta \end{cases} \quad (7.1.3.12)$$

$$\Delta_{sp3} = \begin{cases} 2.0 \text{ mm} & \text{if } \beta = 0 \\ \Delta_{p3} & \text{if } 0 < \beta \end{cases} \quad (7.1.3.13)$$

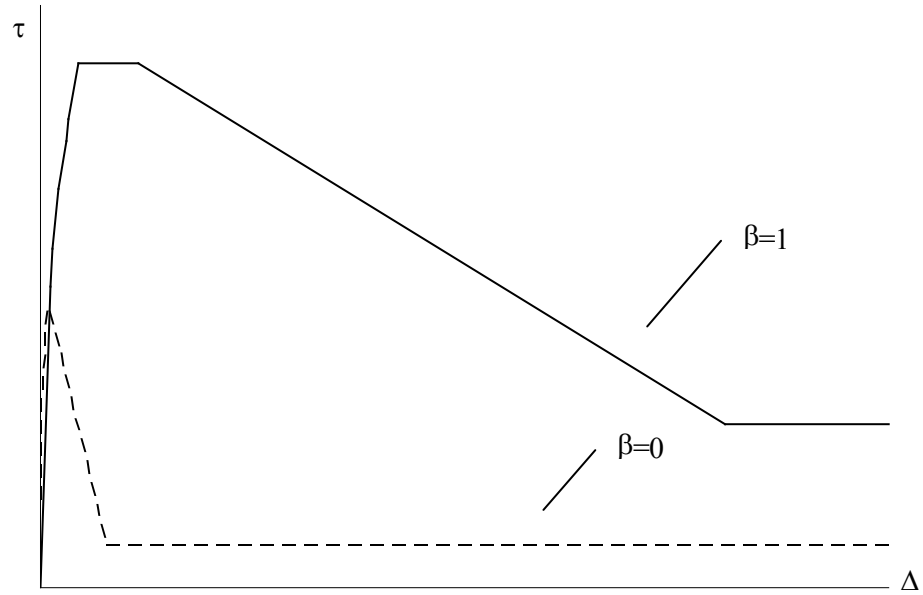


Figure 77: Gan bond stress-slip response

7.1.4 Harajli Model

Both the confined and unconfined bond stress-slip relationships are described by an ascending non-linear branch, a constant bond stress plateau, and linearly declining branch, and a sustaining residual stress branch, as shown in Figure 78.

The confined stress-slip relationship is summarized as follows:

$$\tau = \begin{cases} \tau_{p1} \left(\frac{\Delta}{\Delta_{p1}} \right)^\alpha & \text{for } \Delta \leq \Delta_{p1} \\ \tau_{p2} & \text{for } \Delta_{p1} < \Delta \leq \Delta_{p2} \\ \tau_{p2} - \left[\frac{(\Delta - \Delta_{p2})}{(\Delta_{p3} - \Delta_{p2})} (\tau_{p2} - \tau_{pf}) \right] & \text{for } \Delta_{p2} < \Delta \leq \Delta_{p3} \\ \tau_{pf} & \text{for } \Delta_{p3} < \Delta \end{cases} \quad (7.1.4.1)$$

where

$$\tau_{p1} = 2.575 \sqrt{f'_c} \quad (7.1.4.2)$$

$$\tau_{p2} = \tau_{p1} \quad (7.1.4.3)$$

$$\tau_{pf} = 0.35\tau_{p1} \quad (7.1.4.4)$$

$$\Delta_{p1} = 0.75(0.189S + 0.18) \quad (7.1.4.5)$$

$$\Delta_{p2} = 1.75(0.189S + 0.18) \quad (7.1.4.6)$$

$$\Delta_{p3} = S \quad (7.1.4.7)$$

$$\alpha = 0.3 \quad (7.1.4.8)$$

The unconfined stress-slip relationship is summarized as follows:

$$\tau = \begin{cases} \tau_{s1}(\Delta/\Delta_{s1})^\alpha & \text{for } \Delta \leq \Delta_{s1} \\ 0 & \text{for } \Delta_{s1} < \Delta \end{cases} \quad (7.1.4.9)$$

where

$$\tau_{s1} = \left(0.249 + 0.291 \frac{c}{d} \right) \sqrt{f'_c} \leq \tau_{p1} \quad (7.1.4.10)$$

$$\tau_{s2} = 0 \quad (7.1.4.11)$$

$$\tau_{sf} = 0 \quad (7.1.4.12)$$

$$\Delta_{s1} = \Delta_{p1} \exp \left[\frac{1}{\alpha} \ln \left(\frac{\tau_{s1}}{\tau_{p1}} \right) \right] \quad (7.1.4.13)$$

$$\Delta_{s2} = \Delta_{p2} \quad (7.1.4.14)$$

$$\Delta_{s3} = \Delta_{p3} \quad (7.1.4.15)$$

Given a confinement pressure factor, β , the bond stress-slip relationship is defined by equation

7.1.2.16 where:

$$\tau_{sp1} = \tau_{s1} + \beta(\tau_{p1} - \tau_{s1}) \quad (7.1.4.16)$$

$$\tau_{sp2} = \beta\tau_{p2} \quad (7.1.4.17)$$

$$\tau_{spf} = \beta\tau_{pf} \quad (7.1.4.18)$$

$$\Delta_{sp1} = \Delta_{s1} + \beta(\Delta_{p1} - \Delta_{s1}) \geq \Delta_{s1} \quad (7.1.4.19)$$

$$\Delta_{sp2} = \begin{cases} 3.0 \text{ mm} & \text{if } \beta = 0 \\ \Delta_{p2} & \text{if } 0 < \beta \end{cases} \quad (7.1.4.20)$$

$$\Delta_{sp3} = \begin{cases} 3.0 \text{ mm} & \text{if } \beta = 0 \\ \Delta_{p3} & \text{if } 0 < \beta \end{cases} \quad (7.1.4.21)$$

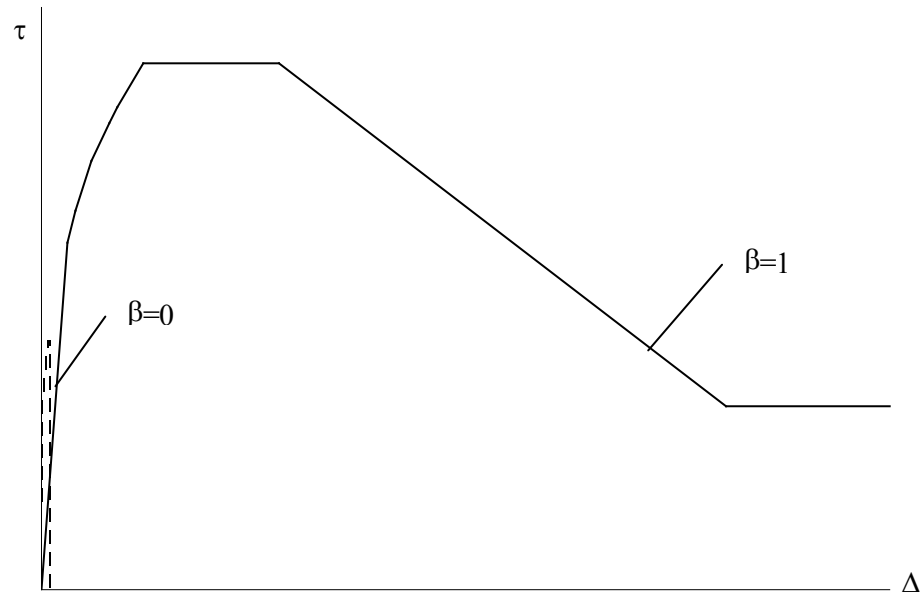


Figure 78: Harajli bond stress-slip response

7.1.5 Fujii Model

The Fujii model provides the lowest bond strength and ductility among the available models. Note that this is recommended for analyses where cover splitting is anticipated, but does not consider the effect of hooked bars. The model determines whether one of two cover splitting modes governs: side splitting, in which the entire volume of concrete cover spalls, and corner splitting, in which a fraction of the concrete cover spalls. Side splitting occurs when the side splitting length ratio, B_{is} , is less than the corner splitting length ratio, B_{ic} , and *vice versa*. The value B_{is} compares the thickness of the concrete to the cumulative diameter of reinforcing bars, while B_{ic} compares the cover to the diameter of a single bar. The exact computation is beyond the scope of this discussion.

The bond stress-slip relationships is described by an ascending linear branch, a constant stress plateau, a descending linear branch, and a sustaining residual stress branch, summarized as follows:

$$\tau = \begin{cases} \tau_1(\Delta/\Delta_{s1}) & \text{for } \Delta \leq \Delta_1 \\ \tau_2 & \text{for } \Delta_1 < \Delta \leq \Delta_2 \\ \tau_2 - \frac{(\Delta - \Delta_2)}{(\Delta_3 - \Delta_2)}(\tau_2 - \tau_f) & \text{for } \Delta_2 < \Delta \leq \Delta_3 \\ \tau_f & \text{for } \Delta_3 < \Delta \end{cases} \quad (7.1.6.1)$$

In the case of $\beta = 0$, the reference bond stress and slips are determined as follows:

$$\tau_1 = (Bi + 1.5)\sqrt{f'_c}/8 \quad (7.1.6.2)$$

$$\tau_2 = \tau_1 \quad (7.1.6.3)$$

$$\tau_f = 0.1 \text{ MPa} \quad (7.1.6.4)$$

$$\Delta_1 = \frac{\tau_1}{100} \quad (7.1.6.5)$$

$$\Delta_2 = 0.04Bi - \Delta_1 \quad (7.1.6.6)$$

$$\Delta_3 = \Delta_1/20 + \Delta_2 \quad (7.1.6.7)$$

$$Bi = \min(Bis, Bic) \quad (7.1.6.8)$$

In the case of $\beta \neq 0$, the reference bond stress and slips are determined as follows:

$$\tau_1 = \begin{cases} 0.313(0.307Bi + 0.427 + 24.9Q)\sqrt{f'_c} & \text{for } Q < 0.0035 \\ 0.313(0.307Bi + 1.3)\sqrt{f'_c} & \text{for } Q > 0.0035 \end{cases} \quad (7.1.6.9)$$

$$\tau_2 = \tau_1 \quad (7.1.6.10)$$

$$\tau_f = \begin{cases} 0.313(23.3Q + 0.3)\sqrt{f'_c} & \text{for } Q < 0.0035 \\ 0.35\sqrt{f'_c} & \text{for } Q > 0.0035 \end{cases} \quad (7.1.6.11)$$

$$\Delta_1 = \frac{\tau_1}{100} \quad (7.1.6.12)$$

$$\Delta_2 = \begin{cases} 20.7Q + 0.53 - \Delta_1/2 & \text{for } Q < 0.0035 \\ 1.25 - \Delta_1/2 & \text{for } Q > 0.0035 \end{cases} \quad (7.1.6.13)$$

$$\Delta_3 = \Delta_1/2 + \Delta_2 \quad (7.1.6.14)$$

$$Q = Q^*\beta(Bis + 1)/88 \quad (7.1.6.15)$$

$$Q^* = \begin{cases} 1 & \text{for } Bis < Bic \\ \sqrt{2} & \text{for } Bic < Bis \end{cases} \quad (7.1.6.16)$$

7.1.6 Eligehausen and Gan Models with No Cyclic Damage

Figure 79 shows the analytical model developed by Eligehausen et al from cyclic loading tests.

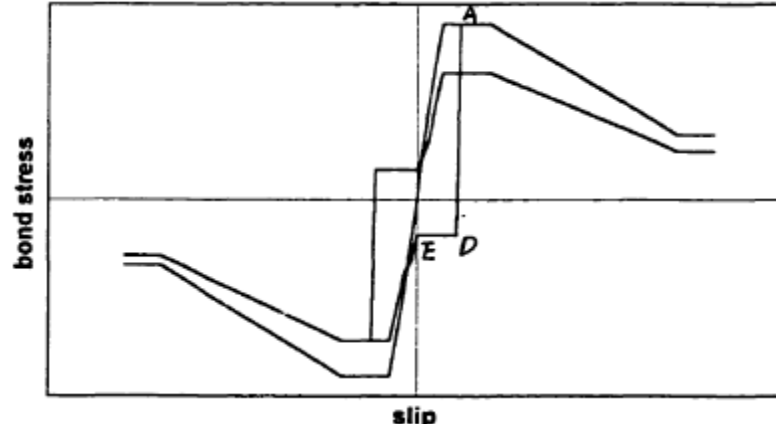


Figure 79: Eligehausen cyclic bond stress-slip relationship

The initial loading curve is monotonic, where the bond element stiffness is calculated as follows

(Gan, 2000):

$$G_n = A_k G_0 \quad \text{for linkage elements} \quad (7.1.6.1)$$

$$G_n = G_0 \quad \text{for contact elements} \quad (7.1.6.2)$$

Where,

$$G_0 = d\tau/d\Delta = \tau_1 \alpha \cdot 100^{1-\alpha} \quad \text{at } \Delta/\Delta_1 = 1/100 \quad (7.1.6.3)$$

For all other loading increments, the stiffness is calculated as:

$$G_n = A_k \tau/\Delta \quad \text{for linkage elements} \quad (7.1.6.4)$$

$$G_n = \tau/\Delta \quad \text{for contact elements} \quad (7.1.6.5)$$

Unloading occurs with constant bond stiffness, which is the same bond stiffness used during reloading. Unloading is shown by the curve ADE. The stress after unloading is related to the maximum bond stress reached at the end of the previous loading, τ_{pm} , as follows:

$$\tau_{un} = -0.25\tau_{pm} \quad (7.1.6.6)$$

The damage index, D , is used to calculate the reduction in bond resistance as both the slip and number of cycles increases. The damage index is equal to zero for no cyclic damage, and equal to one when $\tau = 0$ and bond has broken down entirely. Otherwise, D is calculated as follows.

$$D_i = 1 - e^a \quad (7.1.6.7)$$

$$a = -1.2(E_i/E_0)^{1.1} \quad (7.1.6.8)$$

where E_i is the hysteretic energy dissipation at the current unloading stage and E_0 is the energy equal to the area under the stress slip curve from the monotonic stage to Δ_3 .

The application of the damage index, D , to different types of failure including pull-out, splitting without confinement, and splitting with partial confinement is not outlined in this manual, but is discussed fully in (Gan, 2000). The equations used to calculate the energy E_i and E_0 are also discussed there.

7.2 Bond Stress-Slip Models for Externally Bonded Plates or Sheets

7.2.1 Perfect bond

Bond materials are assigned a large stiffness and strength to prevent deformation bond elements.

7.2.2 Other models

Regardless of which imperfect bond model is selected, the bond stress-slip relationship for externally bonded plates or sheets is described by a multilinear relationship as follows:

$$\tau = \begin{cases} \tau_1 (\Delta/\Delta_{s1}) & \text{for } \Delta \leq \Delta_1 \\ \tau_1 + \frac{(\Delta - \Delta_1)}{(\Delta_2 - \Delta_1)} (\tau_2 - \tau_1) & \text{for } \Delta_1 < \Delta \leq \Delta_2 \\ \tau_2 + \frac{(\Delta - \Delta_2)}{(\Delta_3 - \Delta_2)} (\tau_3 - \tau_2) & \text{for } \Delta_2 < \Delta \leq \Delta_3 \\ \tau_3 & \text{for } \Delta_3 < \Delta \end{cases} \quad (7.2.2.1)$$

The shape of the bond stress-slip relationship, as shown in Figure 80, may be modified by specifying the values of the reference bond stresses, τ_1 , τ_2 , and τ_3 and corresponding slips, $\Delta_1 < \Delta_2 < \Delta_3$.

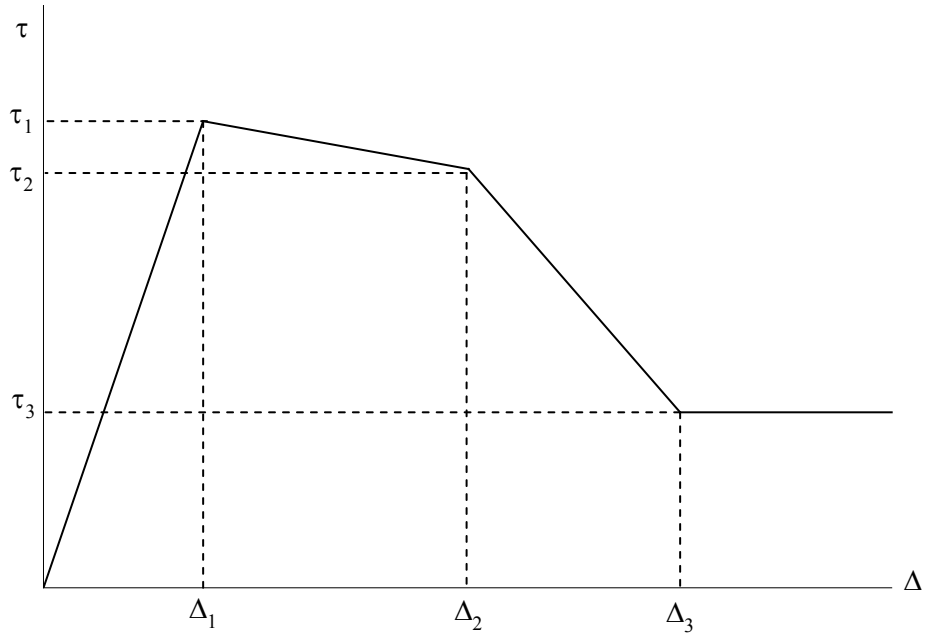


Figure 80: Bond stress-slip response for externally bonded plates or sheets

8 Part II: FormWorks

8.1 Introduction

FormWorks is a preprocessor software that generates input files for VecTor2, the nonlinear finite element analysis program for membrane structures. The role of FormWorks is to provide a user interface for generating, visualizing and checking the finite element model. This chapter provides assistance for using FormWorks and constructing the finite element model.

8.2 Installing FormWorks

The FormWorks program is written in the object-oriented C++ programming language and Microsoft Foundation Classes, and compiled with Microsoft Visual C++ Version 6.0. Formworks is designed to run in the Microsoft Windows operating system. The recommended minimum system requirements are:

- PC with 233 MHz or higher processor and 16 MB of RAM
- 5MB of free hard-disk space
- Microsoft Windows 95 or later operating system
- 16-bit color monitor
- mouse or equivalent pointing device.

At a minimum, the FormWorks package consists of the following files:

- FormWorks.exe: the executable FormWorks program.
- JobOpt.fwd: the FormWorks job options data file.
- StrOpt.fwd: the FormWorks structure options data file.
- LoadOpt.fwd: the FormWorks load options data file.
- FWK.ico: the FormWorks file icon.
- Vt2.exe: the executable VecTor2 program.
- DOS4GW.exe: an auxiliary executable program required by VecTor2.

To install and run FormWorks, complete the following procedure:

1. Create a new folder entitled **VecTor** in the C:\Program Files folder.
2. Copy all of the above files to the newly created folder.
3. Locate the **Control Panel** folder in the hard drive.
4. Open the **Folder Options** folder.
5. Select the **File Types** tab.
6. Click the **New** button.
7. In the Create New Extension dialog box, enter **FWK** in file extension field.
8. Click **OK**.
9. In the File Types tab, click the **Opens with: Change...** button.
10. Click the **Browse...** button.
11. Browse for and select the **FormWorks.exe** file in the newly created **VecTor** folder.
12. Click the **Open** button, then the **Ok** button.
13. In the File Types tab, click the **Advanced** button.
14. In the Edit File Type dialog box, click the **Change Icon...** button.
15. Browse for and select the **FWK.ico** file in the newly created **VecTor** folder.
16. Click the **Ok** button.
17. Double-click the **FormWorks.exe** icon in the newly created **VecTor** folder to run FormWorks.

8.3 An Overview of the FormWorks Modeling Process

The goal of the VecTor2 analysis is to approximate the response of an actual reinforced concrete structure to a given loading scenario and thereby solve a specific engineering question. The approach is to partition the structure into finite elements, generate solutions for each element, assemble the solutions and thereby determine the response of the entire structure. A requisite task for an accurate and relevant solution is a carefully considered finite element model. The subsequent discussion attempts to bring forth initial considerations in this process and describe the role of FormWorks in generating input files.

8.3.1 Before Using FormWorks

It is advisable to carefully define the structural analysis problem to be addressed by VecTor2 before embarking on the finite element modeling process. With some forethought and experience, it is possible to simplify input, create an efficient finite element model, and avoid the need for extraneous analyses. As VecTor2 provides copious amounts of analysis results, it is advisable whenever possible to construct the finite element model with the intent of determining a specific aspect of structural response. A numerical objective such as the maximum load factor, displacement or stress levels can suggest the necessary mesh features and appropriate material models. Assumptions should be considered regarding the stress-state, material properties, boundary conditions, structural and loading symmetry, and the nature of the loads. Further, it is useful to hypothesize which mechanisms are critical to the structural response so that they are adequately represented and suitable material models may be chosen.

8.3.2 VecTor2 Input and Output Files

To run a VecTor2 analysis, several input files are required. As the analysis proceeds, VecTor2 generates several output files. This process is summarized in Figure 81.

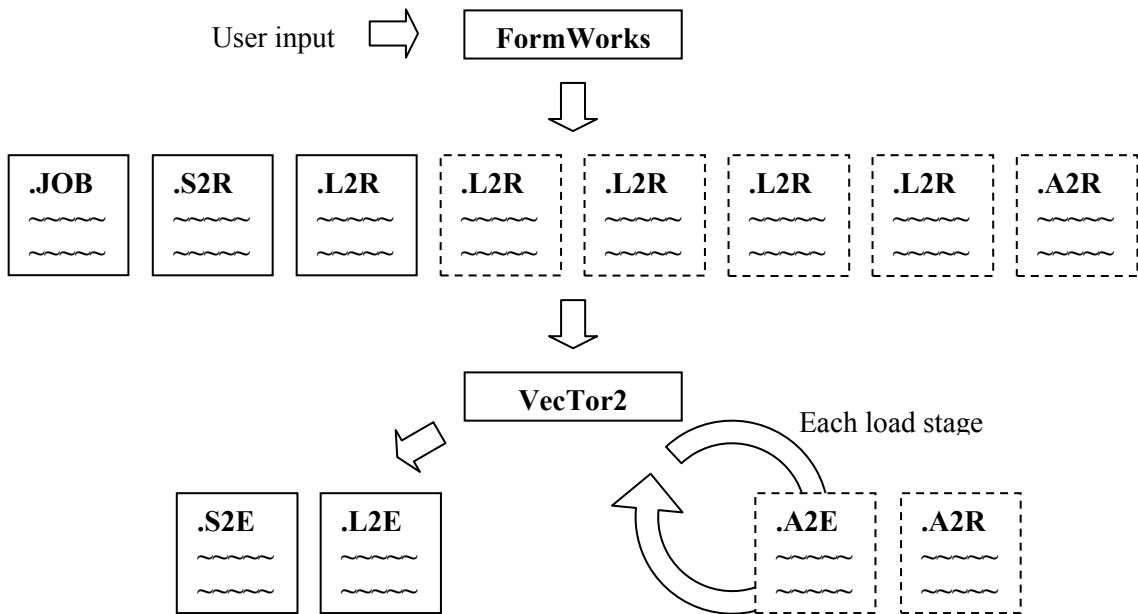


Figure 81: Input and output files for VecTor2 analysis

FormWorks receives user input and generates the following input files for VecTor2:

- **Job Data File (*JOB)**

VecTor2 reads one Job Data File. This file manages the execution of the VecTor2 analysis. It specifies the names of the Structure Data file and Load Case file, the load factors, the iteration parameters, and the selected material and analysis models.

- **Reduced Structure Data File (*S2R)**

VecTor2 reads one Reduced Structure Data File. This file describes the material properties, elements, material assignments, nodes and restraints in an abbreviated format.

- **Reduced Load Case Data File (*L2R)**

VecTor2 reads one to five Load Case Data Files. Each file describes nodal loads, support displacements, concrete prestrains, gravity loads, temperature loads, and ingress pressures for each load case in an abbreviated format. Individual load factors for each load case are specified in the Job Data file.

For some analyses, VecTor2 can also read an input **seed file**. Seed files are **Reduced Analysis Data** files with the extension ***A2R**, generated as output from a previous load stage. Seed files store the strain and stress history of the structure. These files may be used for analyzing repaired structures by running the analysis to an intermediate load stage, modifying the structure by disengaging or engaging elements, and resuming the analysis with the seed file.

During the analysis process, VecTor2 generates the following output files:

- **Expanded Structure Data File (*S2E)**

VecTor2 generates one expanded structure data file. This file prints out the structure data in greater detail than the reduced structure file by printing the attributes of every material type, node and element.

- **Expanded Load Case Data File (*L2E)**

VecTor2 generates one expanded load case data file for each reduced load case data file. This file prints the load case data in greater detail than the reduced load case data file.

- **Expanded Analysis Data File (*A2E)**

If desired, VecTor2 generates one expanded analysis file for each load stage, in ASCII format that may be read with a text editor. This file prints out convergence parameters, reactions, displacements, crack widths, stresses and strains for concrete and reinforcement, bond stresses and slips, and stiffness matrix coefficients.

- **Reduced Analysis Data File (*A2R)**

If desired, VecTor2 generates one reduced analysis file for each load stage, in binary format. These files are also used as seed files.

8.4 FormWorks Basics

8.4.1 The FormWorks Interface

Upon starting FormWorks, the FormWorks application window appears as shown in Figure 82. The exact configuration of the FormWorks screen elements may vary with the operating system and display hardware.

FormWorks is a multiple document interface. The FormWorks application window encloses one or more child Workspace windows. Each Workspace is a unique document that can be saved and opened as a FormWorks file and contains all the information required to generate the input files for one VecTor2 finite element mode. The application title bar indicates the name of the active workspace in brackets. In this case, the active workspace is **Workspace1**, which is created by default when the FormWorks application opens. The finite element model appears in the Workspace window as it is created.

A menu bar appears near the top of the FormWorks window. When a Workspace is open, the **File**, **Edit**, **View**, **Structure**, **Load**, **Analysis**, **Window** and **Help** menu items are visible. Some menu items appear greyed-out and become enabled as the finite element model proceeds.

Several toolbars are docked below the menu bar. These buttons provide easier access to the menu items having the same icon. Similarly, some buttons appear greyed-out and become enabled as the finite

element model proceeds. As the mouse lingers over the toolbar buttons, names of the buttons appear beneath the mouse pointer.

A status bar appears at the bottom of the FormWorks window. A prompt on the left side of the status bar describes the function of menu items and toolbar buttons as the mouse pointer lingers over them. In the right side, the Coordinate Pane displays the coordinates of the mouse crosshairs in the active Workspace window.

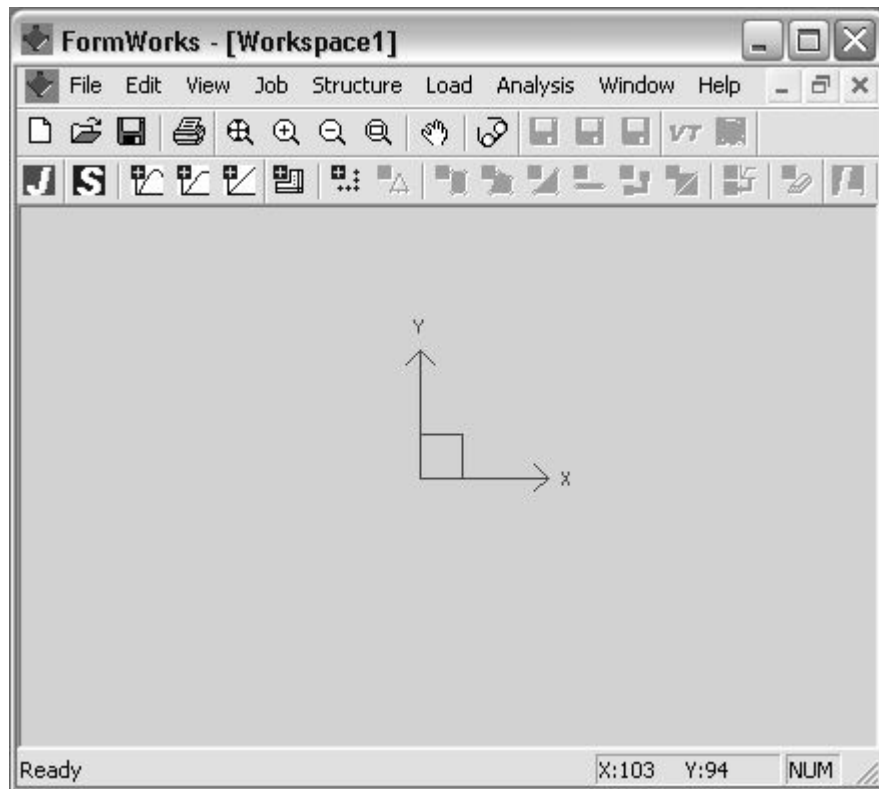


Figure 82: FormWorks application window

8.4.2 Creating a New Workspace

To start a new finite element model:

1. Select the **File/New** menu item. Or, click the **New** toolbar button.

By default, the new Workspace name reflects the order of their creation. For instance, two Workspace child windows, **Workspace1** and **Workspace2**, appear in Figure 83. The FormWorks window is titled **FormWorks-Workspace2**, indicating that the second Workspace is currently active.



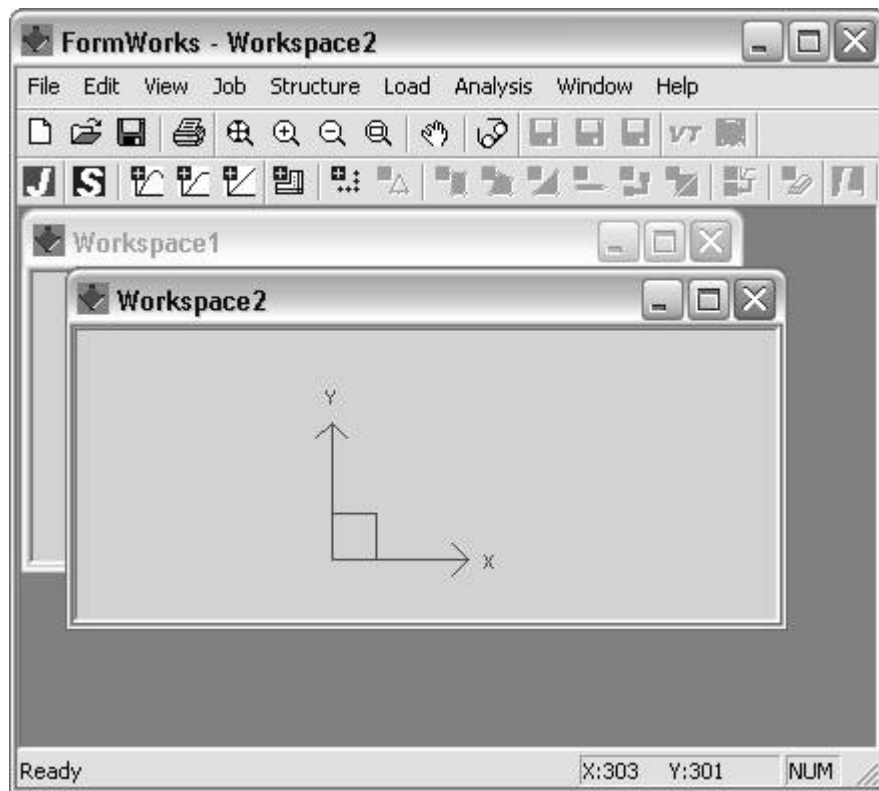


Figure 83: Creating new Workspace windows

8.4.3 Saving the Workspace

It is advisable to regularly save the Workspace for backup and later retrieval as the finite element model progresses. To save the active Workspace:

1. Select the **File/Save** menu item. Or, click the **Save** toolbar button. The **Save As** dialog box appears. 
2. Select a directory in which to save the Workspace. It is recommended that the .FWS file be saved in the directory containing the FormWorks application.
3. Enter a name for the Workspace in the File Name field.
4. Click **Save**.

A new Workspace file with the **.FWK** extension is created in the specified directory. Select the **File/Save** menu item or click the **Save** toolbar button to update an existing Workspace file. To save a version of the same Workspace in a different file, select the **File/Save As...** menu item and follow the preceding procedure.

8.4.4 Opening a Saved Workspace File

To open a saved Workspace file:

1. Select the **File/Open** menu item. Or, click the **Open** toolbar button. The **Open** dialog box appears.
2. Browse for and select the desired FormWorks file with the **.FWK** extension.
3. Click **Open**.



Alternatively, select the **File** menu and select from the four most recent Workspace files.

8.5 Viewing and Printing the Workspace

The active Workspace window displays a limited region of an infinite (x,y) plane, corresponding to the plane of stresses. As the modeling process proceeds, it is necessary to manipulate this view to display different parts of the finite element model. Furthermore, it may be desirable to control which model attributes are displayed. The following sections describe how to manipulate and print the Workspace.

8.5.1 Manipulating the View

8.5.1.1 Horizontal and Vertical Scaling

On the screen, the Workspace may be displayed with either equal or unequal scaling of the x and y distances. The former is generally desirable and is the default option. The latter option may be convenient for viewing structures in which the width is much greater than the height or *vice versa*.

Select the **View/Maintain Aspect Ratio** menu item to toggle between the two modes. When checked, the scaling is equal in the x and y directions. When unchecked, the scaling is unequal in the x and y directions, and depends on the current display limits.

8.5.1.2 Changing Display Limits

To specify the portion of x,y plane that is visible in the Workspace, complete the following steps.

1. Select the **View/Limits...** menu item. The Display Limits dialog appears as shown in Figure 84.
The current limits of the Workspace window are shown in the dialog box.
2. In the **Min X** entry field, enter the desired bottom coordinate of the Workspace window.
3. In the **Min Y** entry field, enter the desired left coordinate of the Workspace window.
4. In the **Max X** entry field, enter the desired right coordinate of the Workspace window.
5. In the **Max Y** entry field, enter the desired top coordinate of the Workspace window.
6. Click **Ok**.

The Workspace window is redrawn with (Min X, Min Y) as the bottom-left coordinates. If the Maintain Aspect Ratio item is checked the top-right coordinates of the Workspace window are adjusted to maintain equal horizontal and vertical scaling on the screen. If the Maintain Aspect Ratio item is not checked, the Workspace window is redrawn with (Max X, Max Y) as the top-right coordinates of the Workspace window.

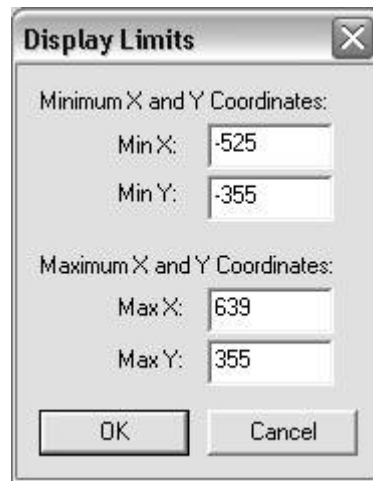


Figure 84: Display Limits dialog box

8.5.1.3 Zooming and Panning

Five options exist for zooming and panning the Workspace view. Select the desired option from the **View/Zoom** menu item or click the corresponding toolbar button.

- Select the **Zoom All** menu item or click the **Zoom All** toolbar button to display the entire finite element model in the Workspace View



- Select the **Zoom In** menu item or click the **Zoom In** toolbar button to increase the scale of the Workspace View by 10%. 
- Select the **Zoom Out** menu item or click the **Zoom Out** toolbar button to decrease the scale of the Workspace View by 10%. 
- Select the **Zoom Window** menu item or click the **Zoom Window** toolbar button. The mouse pointer appears as a magnifying glass. Left-click and drag the mouse pointer to specify the view window. 
- Select the **Pan** Menu item or click the **Pan** toolbar button. The mouse pointer appears as a hand. Left -click and drag the mouse pointer to translate the Workspace view window. 

8.5.1.4 Selecting Display Options

The display options hides or reveal attributes of the finite element model in the Workspace view.

Select the **View/Display Options** menu item or click the **Display Options** toolbar button to display the **Display Options** dialog box shown in Figure 85.



Node Options

- **Node Numbers**
Check to reveal the node number beside each node of the finite element model.
- **Restraints**
Check to reveal the support restraints on each node.
- **Nodal Loads**
Select to reveal applied nodal forces for the current load case.
- **Support Displacements**
Select to reveal imposed displacements for the current load case.
- **Impulse Forces**
Select to reveal time-varying forces for the current load case

- **Nodal Thermal Loads**

Select to reveal nodal thermal loads for the current load case

- **None**

Select to hide the above load types for the current load case.

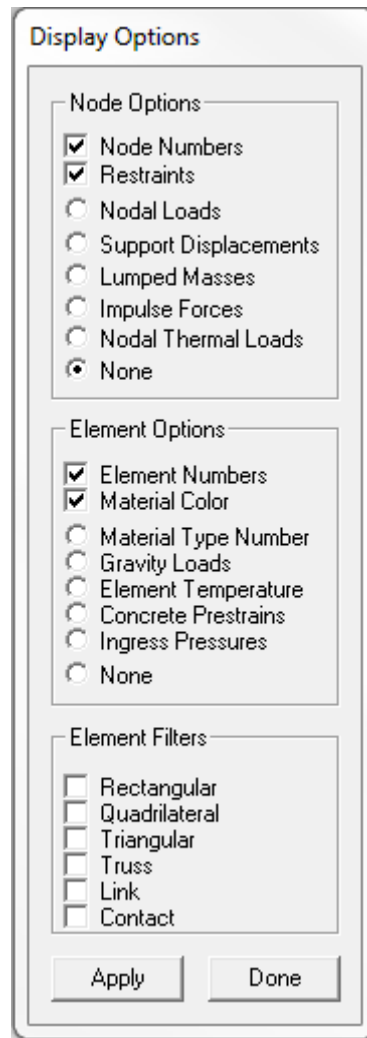


Figure 85: Display Options dialog box

Element Options

- **Element Numbers**

Check to reveal the element number in the center of each element of the finite element model.

- **Material Color**

Check to display elements with the color of the assigned material type or default color. Uncheck to view elements drawn in black and white.

- **Material Type Number**

Select to reveal the material types labels in the center of each element. Reinforced concrete materials are displayed as **Cn**, reinforcement materials are displayed as **Rn** and bond materials are displayed as **Bn**, where n is the ordinal of the material type.

- **Gravity Loads**

Select to reveal the density in kg/m^3 and G-forces applied to concrete elements in the load case.

- **Element Temperature**

Select to reveal the temperature gradient in degrees Celsius for concrete and reinforcement elements in the current load case.

- **Concrete Prestrains**

Select to reveal the elastic strain offset in millistrain applied to concrete elements in the load case.

- **Ingress Pressures**

Select to reveal ingress pressures in mega Pascal, applied to concrete elements in the load case.

- **None**

Select to hide all of the above load types for the current load case.

Element Filters

Elements are displayed in layers according to their element type. From bottom to top, the drawing order is as follows: rectangular elements, quadrilateral elements, triangular elements, truss elements, link elements, and contact elements. Occasionally, elements conceal elements or their attributes drawn beneath them. The Element Filters reveals or hides element types or makes them ineligible for mouse selection.

- **Rectangular, Quadrilateral and Triangular**

Check to hide the element attributes, (but not the element itself) and make the elements ineligible for mouse selection.

- **Truss, Link and Contact**

Check to hide the elements and their attributes, and make the elements ineligible for mouse selection.

8.5.2 Printing the Workspace

FormWorks allows the finite element model to be printed with a standard printer. The entire finite element model is scaled to fit the selected page format and printed with the same attributes that are shown in the Workspace view.

To print the finite element model, complete the following procedure:

1. Select the **File/Print Setup...** menu item. Select the desired paper properties and click **Ok**
2. Select the **File/Print Preview** menu item to preview the finite element model.
3. Select the **File/Print** menu item or click the **Print** toolbar button.
4. Click **Ok** to print the Workspace.



9 The Job Data

The first step in creating the VecTor2 input is to define the Job Data. At the time of analysis, FormWorks generates the *JOB file based on the defined Job Data.

9.1 The Job Control Page



1. Select the **Job/Define Job** menu item or click the **Define Job** toolbar button. The **Define Job** property sheet appears with the **Job Control** page displayed as shown in Figure 86.

Define Job

Job Control | Models | Auxiliary

Job Data

Job file name: VecTor

Job title: Enter Job Title

Date: Enter Date

Structure Data

Structure file name: Struct

Structure title: Enter Structure Title

Structure type: Plane Membrane (2-D)

Loading Data

Load series ID: ID Starting load stage no.: 1 No. of load stages: 1

Activate: Case 1 Case 2 Case 3 Case 4 Case 5

| | Case 1 | Case 2 | Case 3 | Case 4 | Case 5 |
|---------------------|-----------------------|-----------------------|-----------------------|-----------------------|-----------------------|
| Load file name: | NULL | NULL | NULL | NULL | NULL |
| Load case title: | Enter load case title |
| Initial factor: | 0 | 0 | 0 | 0 | 0 |
| Final factor: | 0 | 0 | 0 | 0 | 0 |
| Inc. factor: | 0 | 0 | 0 | 0 | 0 |
| Load type: | Monotonic | Monotonic | Monotonic | Monotonic | Monotonic |
| Repetitions: | 1 | 1 | 1 | 1 | 1 |
| Cyclic Inc. factor: | 0 | 0 | 0 | 0 | 0 |

Analysis Parameters

Seed file name: NULL

Max. no. of iterations: 60

Dynamic Averaging factor: 0.6

Convergence limit: 1.00001

Convergence criteria: Displacements - Weighted Average

Analysis Mode: Static Nonlinear - Load Step

Results files: ASCII Files Only

Output format: To Computer

OK Cancel Apply

Figure 86: Job Control property page

2. Input the job data as described in the subsequent sections.

3. When done, select the **Models** page.
4. When done selecting appropriate models, select the **Auxiliary** page.

9.1.1 Job Data Group

These entry fields manage the creation of the *JOB file.

- **Job File Name**

Enter an alpha-numeric file name up to 8 characters long without spaces. This defines the file name to which FormWorks appends the *JOB extension when saving the Job Data file.

- **Job Title**

Enter a descriptive identifier up to 30 characters long to differentiate this analysis from others.

- **Date**

Enter the date in a string up to 30 characters long.

9.1.2 Structure Data Group

These entry fields manage the creation of the *S2R file.

- **Structure File Name**

Enter an alpha-numeric file name up to 8 characters long without spaces. This defines the file name to which FormWorks appends the *S2R extension when saving the Structure Data file.

- **Structure Title**

Enter a descriptive identifier up to 30 characters long for the structure being analyzed.

- **Structure Type**

Select **Plane Membrane 2-D** for the VecTor2 analysis.

9.1.3 Load Data Group

9.1.3.1 Static Analysis

Each load case consists of a set of loads that are proportionally increased or decreased by a common load factor from one load stage to the next. While all load cases act simultaneously on the structure, different load cases can have different load factors. For instance, lateral loads defined in one

load case may be monotonically increased, while gravity loads defined in another load case remain constant.

Each load case is assigned one of three loading types, **Monotonic**, **Cyclic** and **Reversed Cyclic**. Examples of each are illustrated in Figure 87, Figure 88 and Figure 89, respectively.

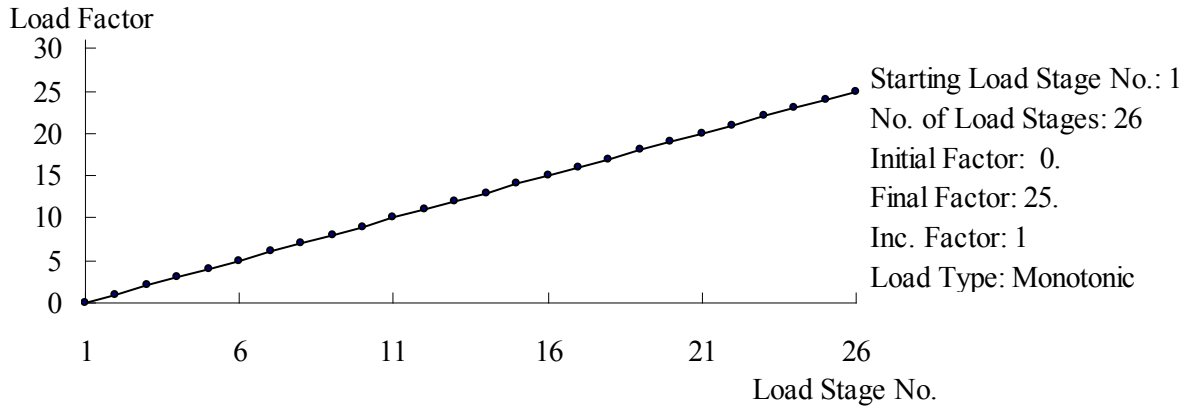


Figure 87: Monotonic type loading

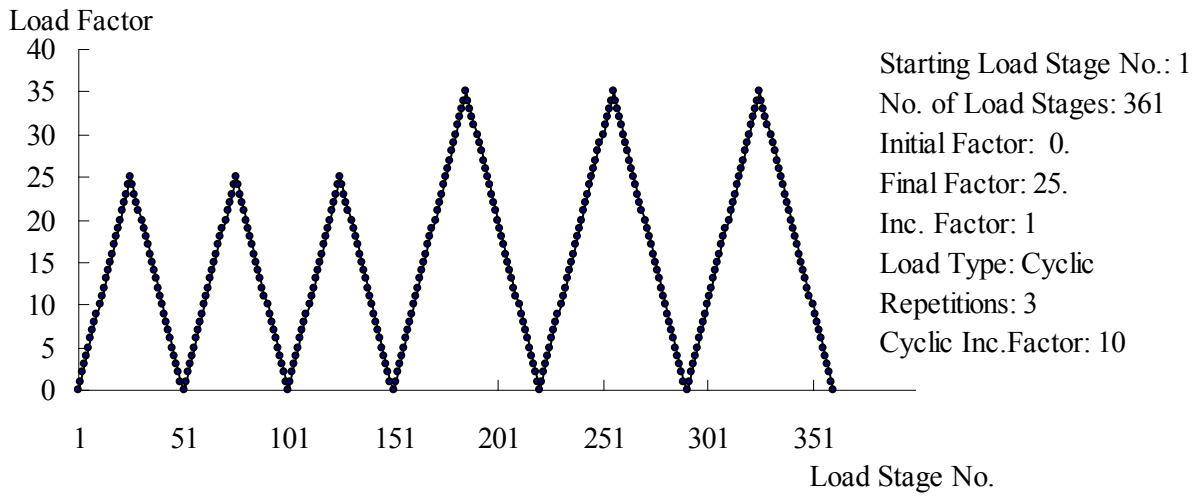


Figure 88: Cyclic type loading

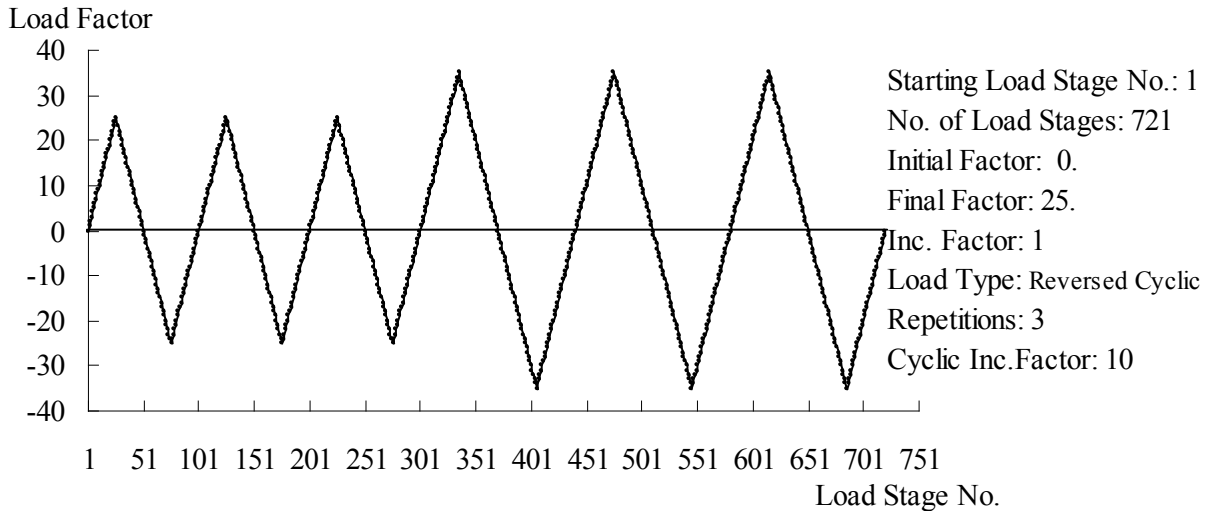


Figure 89: Reversed cyclic type loading

The size of the load steps, which is controlled by the size of the load factor increment, can appreciably impact the efficiency of the solution convergence. Many small load increments may be preferable to fewer large load increments, especially when the structure is at an advanced state of distress. Smaller load increments allow the solution to properly converge in a fewer number of iterations before the analysis proceeds to the next load step. Excessively large load increments may result in improper convergence. Given the overall softening response of concrete, improper convergence may overestimate the strength for an imposed displacement, and underestimate the displacement for an imposed load.

The following entry fields are common to all load cases. They define the name of the *A2E and *A2R output files generated by VecTor2 and the number of load stages to be analyzed. As the analysis proceeds, VecTor2 generates output files having the name **LoadCaseID_N.A2E** and/or **LoadCaseID_N.A2R**, where N is the current load stage number.

- **Load Case ID**

Enter an alpha-numeric file name up to 5 characters long without spaces. This defines the file name to which VecTor2 appends the *A2E and/or *A2R extension when storing analysis results.

- **Starting Load Stage Number**

Enter an integer greater than or equal to 1. This defines the number of the first *A2E or *A2R file that is stored by VecTor2. When resuming an analysis, enter an integer greater than the last completed load stage to avoid overwriting previously generated output files.

- **No. of Load Stages**

Enter an integer greater than or equal to 1. This defines the number of load stages analyzed by VecTor2. The total number of required stages is defined by equation 8.1.1.3.1.

To create a load case, complete the following steps:

1. Check the load **Case** box to activate the load case. Only active load cases can be modified.
2. Complete the following entry fields for the activated load case.

- **Load File Name**

Enter an alpha-numeric file name up to 8 characters long without spaces. This defines the file name to which FormWorks appends the *L2R extension when generating the Load Case Data files.

- **Load Case Title**

Enter a descriptive identifier up to 30 characters long to differentiate the load case.

- **Initial Factor**

Enter the load factor of the first load stage.

- **Final Factor**

For monotonic loading, enter the load factor of the last load stage. For cyclic and reversed loading, enter the maximum load factor of the first set of repetitions.

- **Inc. Factor**

Enter the change in load factor from one load stage to the next.

- **Load Type**

Select the desired loading type from the drop-list.

- **Repetitions**

Enter the number of cycles per set. (For cyclic and reversed cyclic loading only.)

- **Cyclic Inc.Factor**

Enter the change in final load factor from one set of repetitions to the next. For uniformity in load stage increments, the value should be a multiple of the load stage load factor increment. (For cyclic and reversed cyclic loading only.)

Having specified the load factors and load factor increments, the number of load stages required to analyze all load stages can be computed as follows:

$$\text{No. Stages} = \begin{cases} \frac{LF_f - LF_i}{LS_{inc}} + 1 & \text{for monotonic loading} \\ 2(R \cdot S) \left(\frac{LF_f - LF_i}{LS_{inc}} \right) + \left(\frac{R \cdot C_{inc}}{LS_{inc}} \right) [S(S-1)] + 1 & \text{for cyclic loading} \\ 4(R \cdot S) \left(\frac{LF_f - LF_i}{LS_{inc}} \right) + \left(\frac{2R \cdot C_{inc}}{LS_{inc}} \right) [S(S-1)] + 1 & \text{for reversed cyclic loading} \end{cases} \quad (9.1.3.1)$$

where LF_i is the initial load factor, LF_f is the final load factor, LS_{inc} is the load factor increment for each load stage, R is the number of repetitions, S is the number of sets of full repetitions and C_{inc} is the cyclic load factor increment.

9.1.3.2 Dynamic Analysis

To create a load case for a dynamic analysis:

The time-step size for the analysis is specified in the first load case. Therefore, the first load case should contain the dynamic mass information.

1. Check the load **Case** box to activate the load case, as in a typical analysis. Note that the dynamic information must be contained in the first load case.
2. Fill in the following fields:
 - **Load File Name**
 - **Load Case Title**

- **Initial Factor:** the initial factor coefficient is ignored for the first load case in dynamic analysis (enter it as 1)
- **Final Factor:** the final factor is also ignored in the first load case (enter it as 1)
- **Inc. Factor:** this is the time increment between two recorded output files
- **Load Type:** The load type must be set to *Cyclic* in order to activate the *Repetitions* input
- **Repetitions:** Specify the number of time divisions between two output files. The time-step that is actually used in the numerical integration for dynamic analysis is the *Inc. Factor/Repetitions*

As mentioned above, the initial and final load factors are ignored for the first load case in dynamic analyses. However, if static loads are also present in the first load case file, the load factor for those static loads is taken as 1.0.

In addition, selecting the proper time-step size for the analysis is very important, as it affects both the accuracy and the stability of the solution. One way to determine if the time-step is sufficiently small is to perform the analysis with a smaller time-step size and compare the two results. If the results are the same, then the time-step size is appropriately small. If not, then a smaller time-step size should be used.

9.1.4 Analysis Parameters Group

This group controls the progress of the iterative solution procedure and the analysis output:

- **Analysis Mode**

There are five options for the analysis mode. The **Linear Elastic** option is the most basic analysis mode. The **Static Nonlinear-Load Step** option is chosen for most static analyses where the load is increasing in stages. The **Static Nonlinear-Time Step** option is used when modeling time-varying loads such as surface thermal loads. The **Dynamic Nonlinear-General** option is used for impact and impulse load analyses, including ground acceleration. Note that if this option is used, the ground acceleration must be applied by selecting the “Considered” option in the *Apply Ground Acceleration* field of the Auxiliary tab of the *Define Job* window. The **Dynamic Nonlinear-EQ Record** option is used when the ground acceleration is specified by an earthquake record, in the form of a VECTOR.EQR file.

- **Seed File Name**

Enter **NULL** if no seed file is used. Otherwise, enter the file name of the *A2R file.

- **Max. No. of Iterations**

Enter the maximum number of iterations VecTor2 performs for each load stage. Regardless of the convergence quality, VecTor2 proceeds to the next load stage when this limit is reached.

- **Averaging Factor**

Enter the weighting factor between 0 and 1 used to update the value of the material stiffness coefficients between iterations. Structures exhibiting less stability such as lightly reinforced structures require values closer to zero. Alternatively, check the **dynamic averaging factor** to allow VecTor2 to automatically choose a value based on response of the structure.

- **Convergence Limit**

Enter a value greater than 1 for the maximum ratio of the convergence criteria that must be satisfied before the VecTor2 proceeds from one load stage to the next. As the value approaches 1, the more stringent the convergence criterion becomes.

- **Convergence Criteria**

Select the parameter by which the solution convergence is judged against the convergence limit before VecTor2 proceeds to the next load step.

- **Results Files**

Select the file type of the analysis output. ASCII files are extended analysis files that can be read by text editors. Binary files are reduced analysis files that may be used as seed files.

- **Output Format**

Select **To Computer**.

9.2 The Model Page

1. Select the **Models** property page as shown in Figure 90.
2. Select the desired material and behavioral models. The following sections provide abbreviated descriptions of the models.



3. When done, click **Ok** to store changes to the Job Data.

For the majority of analyses, it is advisable to select the VecTor2 default models. Ultimately, however, it remains the responsibility of the analyst to exercise his or her discretion regarding the appropriateness of the models and the reliability of the results.

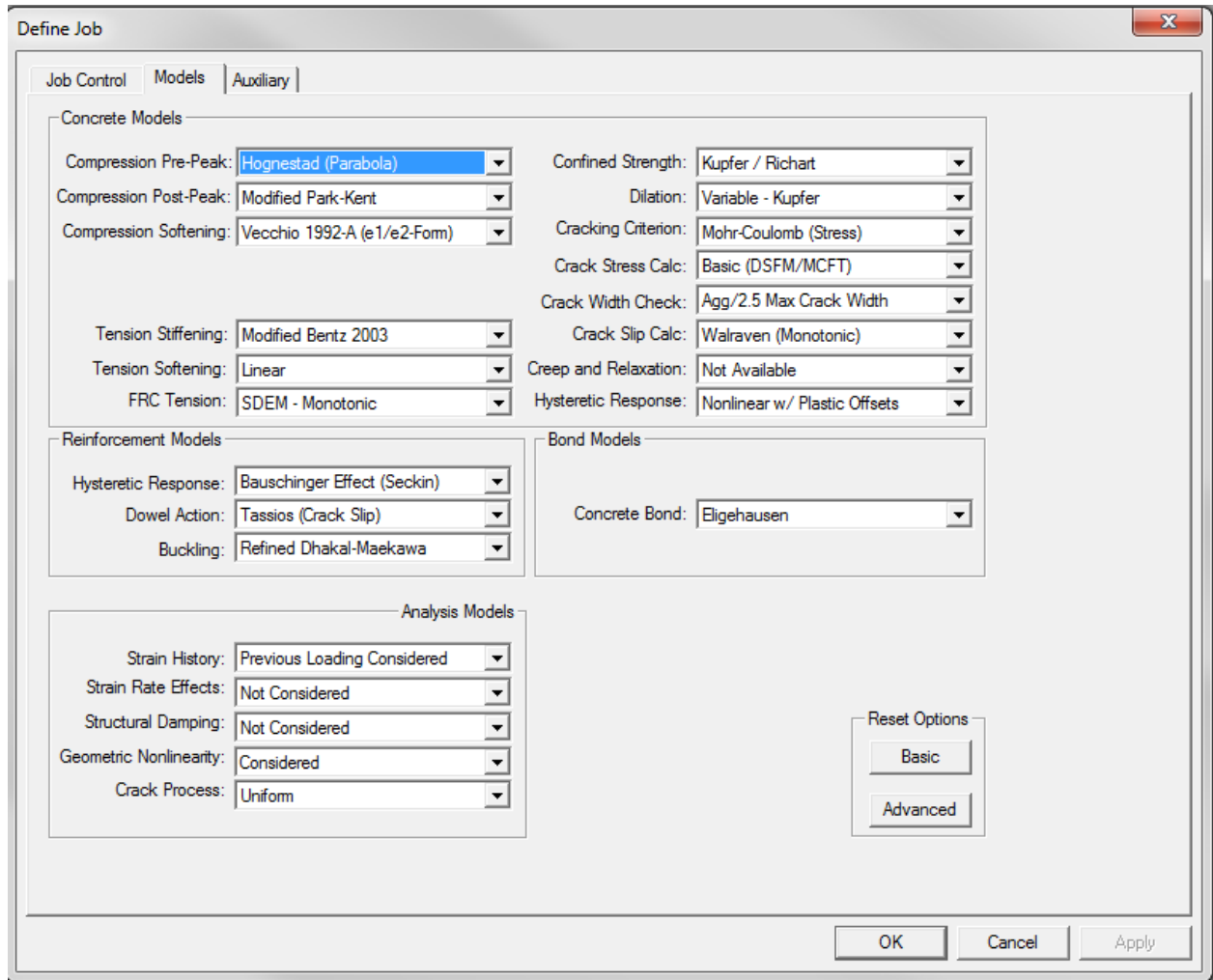


Figure 90: The Models page

9.2.1 Concrete Models

- **Compression Pre-Peak Response**

Select the ascending branch of the average concrete compression stress-strain response.

- **Compression Post-Peak Response**

Select the descending branch of the average concrete compression stress-strain response.

- **Compression Softening**

Select the model for reducing the concrete compressive strength and stiffness relative due to the presence of coexisting transverse tensile strains.

- **Tension Stiffening**

Select the post-cracking average tensile stress-strain response of reinforced concrete.

- **Tension Softening**

Select the post-cracking average tensile stress-strain response of plain concrete.

- **FRC Tension**

Select the FRC Tension model, if applicable.

- **Confined Strength**

Select the model for strength and ductility enhancement of concrete subject to biaxial or triaxial compressive stress states.

- **Dilation**

Select the model for computing the post-cracking Poisson's effect for expansion in the direction transverse to compressive stresses..

- **Cracking Criterion**

Select the model for determining the concrete cracking strength based on the stress or strain state of an assumed failure condition.

- **Crack Stress Calc**

Select the model for calculating the shear stress at a crack.

- **Crack Width Check**

Select the crack width beyond which the average concrete compressive stress is reduced to effect the inability of the concrete to transmit compressive stresses across large crack widths.

- **Crack Slip Calc**

Select the model for determining the crack slip strains as a component of the total strains. If **Not Considered** is selected, VecTor2 conducts the analysis based on Modified Compression Field

Theory. If any other option is selected, VecTor2 conducts the analysis based on the Disturbed Stress Field Model.

- **Creep and Relaxation** (currently not available)

- **Hysteretic Response**

Select the model for the average stress-strain response of concrete when subjected to unloading and unloading, and the resulting plastic strain offsets.

9.2.2 Reinforcement Models

- **Hysteretic Response**

Select the model for the average stress-strain response of reinforcement when subjected to unloading and unloading, and the resulting plastic strain offsets.

- **Dowel Action**

Select the model for determining the contribution to shear resistance of reinforcing bars crossing cracks.

- **Buckling**

Select the model for determining the failure of the failure of truss bar elements in compression due to buckling and associated splitting of the concrete cover. (Note that the truss bar elements must be connected to the concrete with bond elements to use the Asatsu model.)

9.2.3 Bond Models

- **Concrete Bond**

Select the bond stress-slip relationship of between concrete and embedded reinforcing bars.

9.2.4 Analysis Models

- **Strain History:**

The previous loading should be considered for analyses involving cyclic and reversed cyclic loading to include the hysteretic response models.

- **Strain Rate Effects:**

Strain rate effects may be considered when performing dynamic analyses. Strain rate effects increase the dynamic strength of materials, and are discussed in the VecTor2 section of this manual.

- **Structural Damping**

Damping is used for dynamic analyses; VecTor2 offers two types of damping, Rayleigh and Alternative.

- **Geometric Nonlinearity**

- **Crack Process**

Two different crack allocation models are available. Uniform crack allocation is suitable for most modeling purposes; the variable crack allocation model may be used where members are reinforced with FRP sheets.

9.3 The Auxiliary Input Page

1. Select the **Auxiliary** input page as shown in Figure 91.

The screenshot shows the 'Define Job' dialog box with the 'Auxiliary' tab selected. The dialog is organized into several sections:

- General:**
 - Stiffness Matrix Solver: Solver 1
 - Quadrilateral Element Type: Isoparametric
 - Concrete Aggregate Type: Carbonate
 - Concrete Conductivity (W/mK): 2.19
 - Concrete Fracture Energy (kJ/m): 0
 - Prestressing Friction Coefficient (r): 0.3
 - Prestressing Wobble Coefficient (r/m): 0.0025
 - Thermal Time Stepping Factor: 0.666667
- Dynamic Analysis:**
 - Newmark Beta Factor: 0.25
 - Newmark Gamma Factor: 0.5
 - Reference Mode #1: 1
 - Reference Mode #2: 2
 - Damping Factor #1: 0
 - Damping Factor #2: 0
 - Ground Acceleration in x-direction: Not Considered
 - Ground Acceleration in y-direction: Not Considered
- Tension Softening:**
 - Tension Softening Pt 1: Strain (me): 0
 - Tension Softening Pt 1: Stress (MPa): 0
 - Tension Softening Pt 2: Strain (me): 0.5
 - Tension Softening Pt 2: Stress (MPa): 2
 - Tension Softening Pt 3: Strain (me): 1
 - Tension Softening Pt 3: Stress (MPa): 1
 - Tension Softening Pt 4: Strain (me): 2
 - Tension Softening Pt 4: Stress (MPa): 0.1
- Masonry Structures:**
 - Principal Direction wrt x-axis (deg): 0
 - Masonry Joint 1: Thickness (mm): 10
 - Masonry Joint 2: Thickness (mm): 10
 - Joint Shear Strength Ratio: 0.01
 - Masonry Strength Ratio f_{my}/f_{mx} : 0.5
 - Elastic Modulus Ratio E_{my}/E_{mx} : 0.5
 - Friction Angle (deg): 37
 - Brick Strength Ratio: 0.1
 - Strength Reduction Factor: 1
- Material Resistance / Creep Factors:**
 - Concrete Resistance Factor: 1
 - Rebar Steel Resistance Factor: 1
 - P/S Steel Resistance Factor: 1
 - Structural Steel Resistance Factor: 1
 - Masonry/Mortar Resistance Factor: 1
 - Wood/Ortho Resistance Factor: 1
 - Concrete Creep Coefficient: 0
 - P/S Relaxation Coefficient: 0

At the bottom right of the dialog, there is a 'Reset Default' button and three buttons: 'OK', 'Cancel', and 'Apply'.

Figure 91: The Auxiliary Input Page

2. Enter applicable analysis parameters.
3. When done, click **Ok** to store changes to the Job Data.

For the majority of analyses, it is advisable to select the VecTor 2 default models. Ultimately, however, it remains the responsibility of the analyst to exercise his or her discretion regarding the appropriateness of the models and the reliability of the results.

9.3.1 General

- **Stiffness Matrix Solver**

Select the solver to use, Solver 1 or Solver 2.

Default value: Solver 1

- **Quadrilateral Element Type**

Select which type of quadrilateral element to use in the mesh. The two options for quadrilateral element type are isoparametric and degenerate. Degenerate elements allow for a mixture of both quadrilateral and triangular elements and are convenient for structures with complex geometries.

Default value: Isoparametric

- **Concrete Aggregate Type**

Select the concrete aggregate type. The two options are carbonate and siliceous; the difference between the two aggregate types is their response to thermal loading.

Default value: Carbonate

- **Concrete Conductivity**

Enter the concrete conductivity.

Default value: 2.19 W/mK.

- **Concrete Fracture Energy**

Enter the concrete fracture energy.

Default value: 0.75 kN/m.

- **Pre-stressing Friction Coefficient**

Enter the pre-stressing friction coefficient.

Default value: 0.30

- **Pre-stressing Wobble Coefficient**

Enter the pre-stressing wobble coefficient.

Default value: 0.0025/m.

- **Thermal Time Stepping Factor**

Enter the thermal time stepping factor. This factor determines the time step used in the Crank-Nicolson Method. In general, the accuracy of the result will decrease with increasing time step size.

Default value: $2/3$ or 0.666667.

9.3.2 Dynamic Analysis Options

- **Newmark Beta Factor**

Enter the Newmark Beta Factor to be used in the analysis. As described before, the default value in VecTor2 of $\beta = 0.25$ defines the constant acceleration method for Newmark's method of direct integration. For the linear acceleration method, $\beta = 1/6$ can be used, and caution is advised when using any other value for β .

Default value: 0.25

- **Newmark Gamma Factor**

Enter the Newmark Gamma Factor.

Default value: $\gamma = 0.5$.

- **Reference Mode #1**

Enter reference mode #1, to be used in Rayleigh damping.

Default value: 1

- **Reference Mode #2**

Enter reference mode #2, for Rayleigh damping.

Default value: 2

- **Damping Factor #1**

Enter the damping factor assigned to Reference Mode #1.

Default value: 0 (no damping)

- **Damping Factor #2**

Enter the damping factor assigned to Reference Mode#2.

Default value: 0 (no damping)

- **Ground Acceleration in x-direction**

Choose to Consider or Not Consider the ground acceleration in the x-direction. The *Considered* option is to be chosen when the *Analysis Mode* on the Job Control page is set to *Dynamic Nonlinear—General*.

- **Ground Acceleration in y-direction**

Choose to *Consider* or *Not Consider* the ground acceleration in the y-direction. The *Considered* option is to be chosen when the *Analysis Mode* on the Job Control page is set to *Dynamic Nonlinear—General*.

9.3.3 Tension Softening Options

By specifying tension softening points, a custom tension softening curve can be developed.

- **Tension Softening Pt 1: Strain**

Enter the strain, expressed in units of millistrain, for the first tension softening point

Default value: 0

- **Tension Softening Pt 1: Stress**

Enter the stress, expressed in MPa, for the first tension softening point.

Default value: 0

- **Tension Softening Pt 2: Strain**

Enter the strain for the second point on the tension softening curve.

Default value: 0.5

- **Tension Softening Pt2: Stress**

Enter the stress for the second point on the tension softening curve.

Default value: 2 MPa.

- **Tension Softening Pt 3: Strain**

Enter the strain for the third point on the tension softening curve.

Default value: 1

- **Tension Softening Pt 3: Stress**

Enter the stress for the third point on the tension softening curve.

Default value: 1 MPa

- **Tension Softening Pt 4: Strain**

Enter the strain for the fourth point on the tension softening curve.

Default value: 2

- **Tension Softening Pt 4: Stress**

Enter the stress for the fourth point on the tension softening curve.

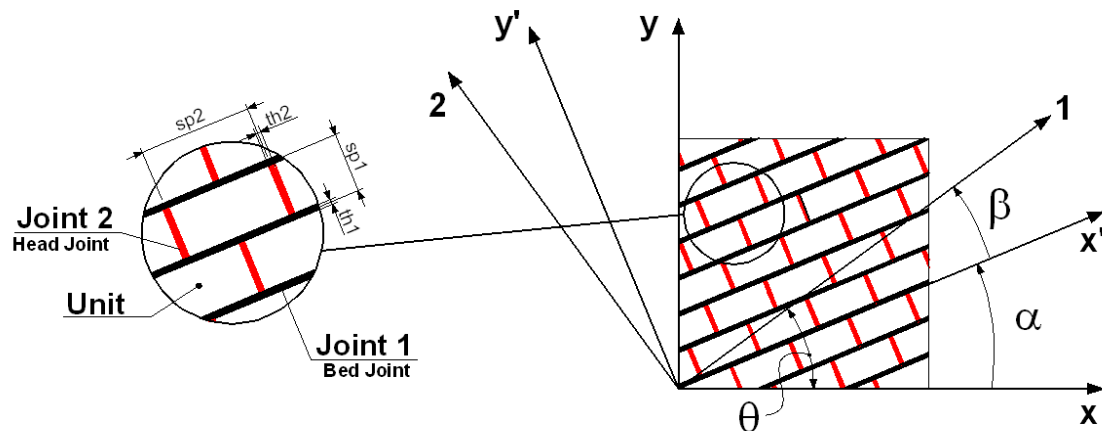
Default value: 0.1 MPa

9.3.4 Masonry Structures Data

- **Principal direction wrt x-axis**

In degrees, enter the direction of Joint 1, as shown on the figure below. Once the direction of Joint 1 is set, Joint 2 is considered to be perpendicular to it. The default value of the principal direction in VecTor2 is 0 degrees, meaning that it is assumed to be aligned with the x-axis.

Default value: 0 degrees



x-y = global axes

x'-y' = orthotropy axes

1-2 = principal stress axes

β = angle between the axes x' and 1

θ = angle between the axes x and 1

α = direction of the bed joints with respect to x

Figure 92: Masonry joints

- **Masonry Joint 1: Thickness**

Enter the thickness of Joint 1, th_1 , in millimeters.

Default value: 10 mm.

- **Masonry Joint 2: Thickness**

Enter the thickness of Joint 2, th_2 , in millimeters.

Default value: 10 mm.

- **Joint Shear Strength Ratio**

Enter the Joint Shear Strength Ratio, c/f_{my} , for the masonry. This is the ratio between the shear strength of the joints, c , and the maximum compressive strength, f_{my} .

Default value: 0.01

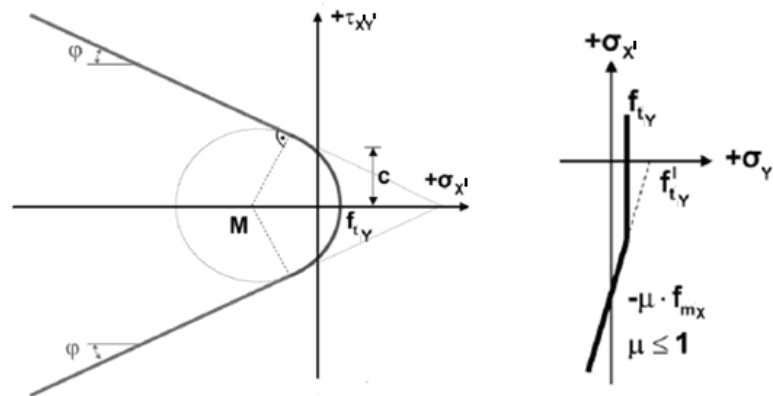


Figure 93: Masonry joint shear strength ratio

- **Masonry Strength Ratio**

Enter the masonry strength ratio, f_{mx}/f_{my} . This defines the ratio between the minimum compressive strength of masonry, f_{mx} , and the maximum compressive strength of masonry, f_{my} .

Default value: 0.5

- **Elastic Modulus Ratio**

Enter the elastic modulus ratio, E_{my}/E_{mx} . This defines the ratio between maximum initial elastic modulus, E_{my} , and the minimum initial elastic modulus, E_{mx} in each direction of orthotropy. As
Default value: 0.5

- **Friction Angle**

Enter the friction angle, φ , of the joints in degrees. The friction angle is illustrated in the Joint Shear Strength Ratio subsection.

Default value: 37 degrees

- **Brick Strength Ratio**

Enter the brick strength ratio. This defines the ratio between the tensile strength of masonry in the x-direction, evaluated when $\alpha = 0$, and the compressive strength, f_{my} .

Default value: 0.1

- **Strength Reduction Factor**

Enter the shear strength reduction factor, μ . This is the reduction factor for the f_{mx} strength, applicable in cases of uniaxial compression. The reduction factor, μ , accounts for the decrease in stress parallel to the bed joints under uniaxial compression.

Default value: 1

9.3.5 Material Resistance/Creep Factors

- **Concrete Resistance Factor**

Enter the concrete resistance factor.

Default value: 1

- **Rebar Steel Resistance Factor**

Enter the rebar steel resistance factor.

Default value: 1

- **P/S Steel Resistance Factor**

Enter the pre-stressing steel resistance factor.

Default value: 1

- **Structural Steel Resistance Factor**

Enter the structural steel resistance factor.

Default value: 1

- **Masonry/Mortar Resistance Factor**

Enter the masonry/mortar resistance factor.

Default value: 1

- **Wood/Ortho Resistance Factor**

Enter the wood resistance factor.

Default value: 1

- **Concrete Creep Coefficient**

Enter the creep coefficient of concrete.

Default value: 0 (no creep)

- **P/S Relaxation Coefficient**

Enter the relaxation coefficient for the pre-stressing steel.

Default value: 0 (no relaxation)

10 The Structure Data

The second step in creating the input is to define the Structure Data, which describes the finite element model itself. The following sections describe how to define material properties, create nodes and elements, restraint the structure and assign material types.

10.1 Preliminary considerations

At this stage, a sketch is useful to map out the proposed finite element mesh. Often, a practical mesh requires some simplification of the actual structure. Nonetheless, the sketch should delineate geometric features, changes in concrete thickness and mechanical properties, changes in distributed reinforcement amounts and properties, the locations of concentrated reinforcement, and essential boundary conditions.

An appropriate mesh topology depends on several factors including the required degree of accuracy, anticipated stress gradients, selected element types, changes in material types, placement of loads, and computational limits. Considering the low-power of elements and the formulation of the Modified Compression Field Theory, elements should be sized so that assumptions of uniform stress and crack distributions are passable within elements. Analysis results indicating abrupt stress variations in adjacent elements may suggest the need for mesh refinement.

FormWorks provides two methods for defining the nodes and elements of the finite element mesh: the **Manual Method** and the **Automatic Method**. In the Manual Method, the recommended sequence of steps for creating the mesh is to specify material properties, specify the numbering and location of nodes, specify elements, assign nodal restraints, and assign material types to elements. This method offers complete control over the mesh topology and its computational characteristics, but may be more time consuming for complicated geometries. In the Automatic Method, the structure is described by a series of mesh boundaries and reinforcement locations. A mesh generation facility automatically creates and numbers the nodes, elements, and restraints and assigns material types. This method allows easier redefinition or refinement of the mesh, but sacrifices some control over the mesh topology.

When utilizing the Manual Method, the nodes should be systematically numbered to minimize the **bandwidth** of the structure stiffness matrix $[K]$. The computation time required by VecTor2 is approximately proportional to the square of the bandwidth. The bandwidth may be approximated as:

$$Bandwidth \approx \max\{2[2(i - j) - R] - 1\} \quad (9.1.1.1)$$

where, i is largest node number of an element, j is the smallest node number of the same element, R is the number restrained degrees of freedom for nodes with numbers between i and j inclusive. Therefore, smaller bandwidths result when the nodes of the elements have numbers that are as similar as possible. For simply connected meshes, this can typically be achieved by consecutive node numbering along the shortest dimension of the structure. FormWorks includes a bandwidth reduction algorithm. While it is no substitute for well planned node numbering, this feature is useful for geometrically complicated meshes where an efficient node numbering is either non-obvious or impractical to input. It is also useful if the structure is subsequently altered.

10.2 Structure Limits

VecTor2 limits the number of material types, nodes, elements and a maximum bandwidth permitted for any finite element mesh. These limits vary with the version of VecTor2. To view these limits, select the **Structure/Structure Limits** menu item. The **Structure Limits** dialog box appears as shown in Figure 94.

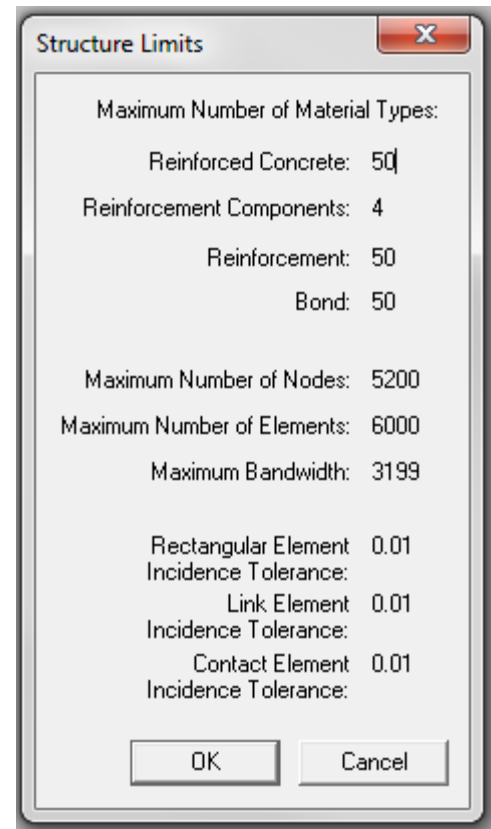


Figure 94: Structure Limits dialog box

10.3 Structure Information



Select the **Structure/Structure Information** menu item or click the **Structure Information** toolbar button to determine the number of defined materials types, nodes and elements currently defined in the model. The **Structure Information** dialog appears as shown in Figure 95. These values are updated as the model is constructed.

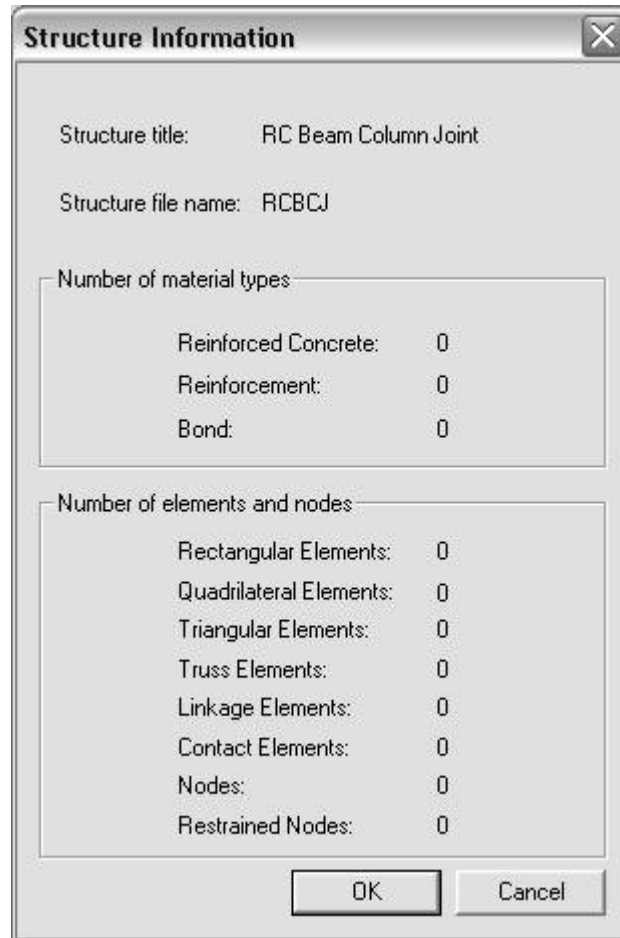


Figure 95: Structure Information dialog box

10.4 Specifying Material Types

VecTor2 includes three types of materials: reinforced concrete, reinforcement, and bond materials. Their uses and description are described in the following sections.

10.4.1 Reinforced Concrete Material Types

In VecTor2 and FormWorks, reinforced concrete materials encompass reinforced concrete, as well as other materials that are modeled with or without smeared reinforcement components or laminate components. Reinforced concrete materials are applied to rectangular, quadrilateral, or triangular elements.

Although referred to as Reinforced Concrete, a wide variety of materials can be analyzed in VecTor2 and modeled in FormWorks. The Reinforced Concrete materials are:

- Reinforced concrete
- Structural steel
- Masonry
- Wood (fixed orthotropic)

With those four reinforced concrete materials, by choosing the appropriate type of smeared reinforcement, the user is able to model the following composite materials:

- Concrete-Steel Laminate
- Concrete-SFRC Laminate
- Masonry-SFRC Laminate
- Concrete-Ortho Laminate

The reinforcement components that are available to be used with the reinforced concrete materials are:

- Ductile steel reinforcement
- Prestressing steel
- Tension only reinforcement
- Compression only reinforcement
- External bonded FRP Fabric
- Steel-fibre—hooked
- Steel-fibre—straight
- Steel skin plate
- SFRC laminate—hooked fibre

- SFRC laminate—straight fibre
- Orthotropic laminate
- Shape Memory Alloy Type 1 and Type 2

Brief descriptions of how to model the above concrete materials and reinforcement components in FormWorks are included in the sections 10.4.1.1-10.4.1.5.

10.4.1.1 Reinforced Concrete

To add, modify or delete concrete material types, click the **Structure/Define Reinforced Concrete Materials** menu item or click the **Define Reinforced Concrete Materials** toolbar button. The **Define Reinforced Concrete Materials** dialog box appears as shown in Figure 96.



Define Reinforced Concrete Properties

Concrete Types

Type:

Concrete 1 [Add] [Update] [Delete]

Reinforcement Components

Component:

Reinforcement 1 [Add] [Update] [Delete]

Concrete Properties

Reference Type: Reinforced Concrete

Thickness, T: 0 mm

Cylinder Compressive Strength, f_c : 0 MPa

Tensile Strength, f_t : * 0 MPa

Initial Tangent Elastic Modulus, E_c : * 0 MPa

Cylinder Strain at f_c , ϵ_c : * 0 me

Poisson's Ratio, μ_c : * 0

Thermal Expansion Coefficient, C_c : * 0 /°C

Maximum Aggregate Size, a : * 0 mm

Density: * 0 kg/m³

Thermal Diffusivity, K_c : * 0 mm²/s

Average Crack Spacing...

perpendicular to x-reinforcement, S_x : * 0 mm

perpendicular to y-reinforcement, S_y : * 0 mm

Color [Color] [Color]

Reinforcement Component Properties

Reference Type: Ductile Steel Reinforcement

Out of Plane Reinforcement:

Reinforcement Direction from X-Axis: 0 °

Reinforcement Ratio, A_s : 0 %

Reinforcement Diameter, D_b : 0 mm

Yield Strength, F_y : 0 MPa

Ultimate Strength, F_u : 0 MPa

Elastic Modulus, E_s : 0 MPa

Strain Hardening Strain, ϵ_{sh} : 0 me

Ultimate Strain, ϵ_u : 0 me

Thermal Expansion Coefficient, C_s : * 0 /°C

Prestrain, $\Delta\epsilon_p$: 0 me

Unsupported Length Ratio, b/t : 0

Reinforced concrete material types to be used for rectangular, quadrilateral and triangular elements only. * Enter '0' for VT2 default value. [OK] [Cancel]

Figure 96: Reinforced Concrete Materials Properties Dialog Box

To **Add Concrete Material Types**, complete the following steps:

1. Enter the following properties in the **Concrete Properties** group. Properties marked by * are assigned default values when '0' are entered in their fields.

- **Thickness, T**

Enter the out of plane thickness of the concrete in millimeters.

- **Cylinder Compressive Strength, f'_c :**

Enter the peak compressive stress of a standard concrete test cylinder, in MPa.

- **Tensile Strength, f'_t :**

Enter the uniaxial cracking strength of concrete in MPa.

Default value: $f'_t = 0.33\sqrt{f'_c}$ MPa.

- **Initial Tangent Modulus, E_c :**

Enter the tangent stiffness of the concrete stress-strain response at zero-strain, in MPa.

Default value: $E_c = 5500\sqrt{f'_c}$ MPa.

- **Cylinder Strain at f'_c , ϵ_o :**

Enter the compressive strain, ϵ_o , corresponding to f'_c , as a positive value in millistrain.

Default value: $\epsilon_o = 1.8 + 0.0075f'_c$ millistrain.

- **Poisson's Ratio, μ :**

Enter the initial Poisson's ratio, ν_o , of the concrete as a positive value.

Default value: 0.15.

- **Thermal Expansion Coefficient, C_c :**

Enter the concrete strain increase per temperature increase of 1°C.

Default value: 10×10^{-6} /°C.

- **Maximum Aggregate Size, a :**

Enter the maximum aggregate size, in millimeters.

Default value: 10 mm.

- **Density:**

Enter the mass density of the concrete in kg/m³.

Default value: 2400 kg/m³.

- **Thermal Diffusivity, Kc:**

Default value: 1.20 s/mm².

- **Average Crack Spacing:**

Enter the crack control parameter indicating the spacing of cracks parallel to the y-axis for **S_x**, and parallel to the x-axis for **S_y**, in millimeters. If “0” is specified, the maximum crack spacing is taken as 1000 mm. If the evaluated crack spacing is larger than 1000 mm, 1000 mm is used to calculate the crack width. This value can be reduced by specifying a negative number for crack spacing “-NUM”; in this case, the maximum crack spacing is NUM.

Default value: computed by the CEB-FIP model, unless the Tension Chord (Kauffmann) model is selected for tension stiffening.

- **Color:**

Select the display color of the concrete material type in the FormWorks Workspace.

2. Click **Add** in the **Concrete Types** group. The newly added concrete type appears in the Concrete Types list box and the reinforcement component properties fields are enabled.

To **Modify Concrete Material Types**, complete the following steps:

1. In the **Concrete Types** list box, select the concrete type to be modified.
2. Re-enter the properties in the **Concrete Properties** group as desired.
3. Click **Update** in the Concrete Types group to store the modified concrete properties.

To **Delete Concrete Material Types**, complete the following steps:

1. In the **Concrete Types** list box, select the concrete type to be deleted.
2. Click **Delete** in the Concrete Types group. The concrete material type is deleted from the list box and the remaining concrete types are renumbered.

To **Add Reinforcement Components** to a concrete material type, complete the following steps.

1. In the **Concrete Types** list box, select the concrete type to which the reinforcement component will belong. The selected concrete type appears highlighted in the list box.
2. Enter the following properties in the **Reinforcement Component Properties** group.
 - **Reference Type**

Refer to Section 5.1 for the stress-strain response of different reinforcement types.
 - **Out of Plane Reinforcement**

Check this box to orient the reinforcement perpendicularly to the x,y plane.
 - **Direction from X-Axis**

For in plane reinforcement, enter the inclination of the reinforcement axis, measured counterclockwise from the positive x-axis in degrees. Enter a value between 0° and 360° .
 - **Reinforcement Ratio, A_s**

Enter the ratio of cross-sectional area of the reinforcement to the area of concrete over which it is smeared, expressed as a percentage.
 - **Reinforcement Diameter, D_b**

Enter the size of the reinforcing bar, in millimeters.
 - **Yield Strength, F_y**

Enter the stress of the yield plateau.
 - **Ultimate Strength, F_u**

Enter the maximum stress the reinforcement can attain before rupturing, in MPa. The ultimate strength must be greater than or equal to the yield strength.
 - **Elastic Modulus, E_s**

Enter the stiffness of the initial linear-elastic branch of the stress-strain response, in MPa.
 - **Strain Hardening Modulus, E_{sh}**

Enter the stiffness of the hardening branch of the stress-strain response, in MPa.
 - **Strain Hardening Strain, esh**

Enter the strain at which the reinforcement stress-strain response begins to ascend from the yield plateau to the ultimate strength, in millistrain. The value must be greater than or equal to the yield strain, F_y/E_s .

- **Thermal Expansion Coefficient, Cs**

Enter the reinforcement strain increase per temperature increase of 1°C.

Default value: 10×10^{-6} /°C.

- **Prestrain, $\Delta\epsilon_p$**

Enter the elastic strain offset of the reinforcement relative to the unstrained concrete, in millistrain.

3. Click **Add** in the **Reinforcement Components** group. The newly added reinforcement component type appears in the Reinforcement Component Types list box.

To **Modify Reinforcement Components** of a concrete material type, complete the following steps:

1. In the **Concrete Types** list box, select the concrete type to which the reinforcement component belongs. The selected concrete type appears highlighted.
2. In the **Reinforcement Components** list box, select the component to be modified. The selected reinforcement component appears highlighted.
3. Re-enter the properties in the **Reinforcement Component Properties** group as desired.
4. Click **Update** in the Reinforcement Components group to store the modified reinforcement component properties.

To **Delete Reinforcement Components** of a concrete material type, complete the following steps:

1. In the **Concrete Types** list box, select the concrete type to which the reinforcement component belongs. The selected concrete type appears highlighted.
2. In the **Reinforcement Components** list box, select the component to be deleted. The selected reinforcement component appears highlighted.

3. Click **Delete** in the Reinforcement Components group. The reinforcement component is deleted from the list box and the remaining reinforcement components are renumbered.

When modeling SFRC in FormWorks the selections that options that need to be selected in the *Define Reinforced Concrete Properties* tab are **Reinforced Concrete** as the reference type in the *Concrete Properties* section, and either **Steel Fibre-Hooked** or **Steel Fibre-Straight** as the reference type in the *Reinforcement Component Properties* section. In FormWorks, the required inputs in the *Reinforcement Component Properties* section of the *Define Reinforced Concrete Properties* tab are the same for both the straight and hooked fibres.

10.4.1.2 Structural Steel

The **Define Reinforced Concrete Properties** dialog box appears as shown in Figure 97 when structural steel is selected as the main material type.

Define Reinforced Concrete Properties

Concrete Types

Type:

Add

Update

Delete

Reinforcement Components

Component:

Add

Update

Delete

Concrete Properties

Reference Type: Structural Steel

Thickness, T: 0 mm

Yield Strength, F_y: 0 MPa

Ultimate Strength, F_u: 0 MPa

Elastic Modulus, E_s: 0 MPa

Strain-Hardening Strain, esh: 0 me

Ultimate Strain, eu: 0

Thermal Expansion Coefficient, C_s: 0 /°C

Poisson's Ratio, Mu: 0

Density: * 0 kg/m³

Thermal Diffusivity, K_s: 0 mm²/s

Average Crack Spacing...

Unsupported Length Ratio, b/t: 0

perpendicular to y-reinforcement, S_y: * 0 mm

Color

Reinforcement Component Properties

Reference Type: Ductile Steel Reinforcement

Out of Plane Reinforcement:

Reinforcement Direction from X-Axis: 0 °

Reinforcement Ratio, A_s: 0 %

Reinforcement Diameter, D_b: 0 mm

Yield Strength, F_y: 0 MPa

Ultimate Strength, F_u: 0 MPa

Elastic Modulus, E_s: 0 MPa

Strain Hardening Strain, esh: 0 me

Ultimate Strain, eu: 0 me

Thermal Expansion Coefficient, C_s: * 0 /°C

Prestrain, Dep: 0 me

Unsupported Length Ratio, b/t: 0

Reinforced concrete material types to be used for rectangular, quadrilateral and triangular elements only. * Enter '0' for VT2 default value.

OK Cancel

Figure 97: Define Reinforced Concrete Properties Dialog Box: Structural Steel

Enter the following properties in the **Concrete Properties** group. Any default values that are assigned when a “0” is entered in FormWorks are noted.

- **Thickness, T**

Enter the out of plane thickness of the steel in millimetres.

- **Yield Strength, F_y**

Enter the stress of the yield plateau in MPa.

- **Ultimate Strength, F_u**

Enter the maximum stress the steel can attain before rupturing, in MPa. The ultimate strength must be greater than or equal to the yield strength.

Default value: $F_u = 1.5F_y$ MPa

- **Elastic Modulus, E_s**

Enter the stiffness of the initial linear-elastic branch of the stress-strain response, in MPa.

Default value: $E_s = 200\,000$ MPa

- **Strain Hardening Strain, ϵ_{sh}**

Enter the strain at which the steel stress-strain response begins to ascend from the yield plateau to the ultimate strength, in millistrain. The value must be greater than or equal to the yield strain, F_y/E_s .

Default value: $e_{sh} = 5$ me

- **Ultimate Strain, ϵ_u**

Enter the strain at which the steel ruptures in millistrain.

Default value: $e_u = 150$ me

- **Thermal Expansion Coefficient, C_c**

Enter the steel strain increase per temperature increase of 1 °C.

Default value: $C_c = 10 \times 10^{-6}$ /°C

- **Poisson's Ratio, ν**

Enter the initial Poisson's ratio, ν_o , of the steel as a positive value.

Default value: $\nu = 0.30$

- **Density**

Enter the mass density of the steel in kg/m³.

Default value: $\rho = 7850 \text{ kg/m}^3$

- **Thermal Diffusivity, K_s**

Enter the thermal diffusivity of the steel in mm²/s.

- **Unsupported Length Ratio, b/t**

Enter the unsupported length ratio of the steel.

10.4.1.3 Masonry

The **Define Reinforced Concrete Properties** dialog box appears as shown in Figure 98 when masonry is selected as the main material type.

Define Reinforced Concrete Properties

Concrete Types

Type:

Reinforcement Components

Component:

Concrete Properties

Reference Type:

Thickness, T: mm

Cylinder Compressive Strength, f_c : MPa

Tensile Strength, f_t : * MPa

Initial Tangent Elastic Modulus, E_c : * MPa

Cylinder Strain at f_c , ϵ_c : * me

Poisson's Ratio, μ_c : *

Thermal Expansion Coefficient, C_c : * /°C

Maximum Aggregate Size, a : * mm

Density: * kg/m³

Thermal Diffusivity, K_c : * mm²/s

Joint Spacing...

perpendicular to x direction, S_x : * mm

perpendicular to y direction, S_y : * mm

Reinforcement Component Properties

Reference Type:

Out of Plane Reinforcement:

Reinforcement Direction from X-Axis: °

Reinforcement Ratio, A_s : %

Reinforcement Diameter, D_b : mm

Yield Strength, F_y : MPa

Ultimate Strength, F_u : MPa

Elastic Modulus, E_s : MPa

Strain Hardening Strain, ϵ_{sh} : me

Ultimate Strain, ϵ_u : me

Thermal Expansion Coefficient, C_s : * /°C

Prestrain, Dep : me

Unsupported Length Ratio, b/t :

Reinforced concrete material types to be used for rectangular, quadrilateral and triangular elements only. * Enter '0' for VT2 default value.

Figure 98: Define Reinforced Concrete Properties: Masonry

Enter the following properties in the **Concrete Properties** group. Properties marked by * are assigned default values when '0' are entered in their fields.

- **Thickness, T**

Enter the out of plane thickness of the masonry in millimetres.

- **Cylinder Compressive Strength, f'_c**

Enter the peak compressive stress in MPa. As explained in section 5.2.2, the maximum compressive masonry strength, f_{my} , is entered as the cylinder compressive strength, f'_c .

- **Tensile Strength, f'_t**

Enter the uniaxial cracking strength of the masonry in MPa.

Default value: $f_t = 0.33\sqrt{f'_c}$ MPa

- **Initial Tangent Elastic Modulus, E_c**

Enter the tangent stiffness of the masonry stress-strain response at zero-strain in MPa.

Default value: $E_c = \frac{2000f'_c}{\epsilon_o}$ MPa (if $\epsilon_o > 0$); $E_c = 3320\sqrt{f'_c} + 6900$ MPa

- **Cylinder Strain at f'_c , ϵ_o**

Enter the compressive strain, ϵ_o , corresponding to f'_c , as a positive value in millistrain.

Default value: $\epsilon_o = \frac{2000f'_c}{E_c}$ if $E_c > 0$; $\epsilon_o = 1.8 + 0.0075f'_c$ me

- **Poisson's Ratio, ν**

Enter the initial Poisson's ratio, ν_o , of the masonry as a positive value.

Default value: $\nu = 0.15$

- **Thermal Expansion Coefficient, C_c**

Enter the masonry strain increase per temperature increase of 1 °C.

Default value: $C_c = 10 \times 10^{-6} / ^\circ\text{C}$

- **Maximum Aggregate Size, a**

Enter the maximum aggregate size in millimetres.

Default value: $a = 20$ mm

- **Density**

Enter the mass density of the masonry in kg/m³.

Default value: $\rho = 2400$ kg/m³

- **Thermal Diffusivity, K_c**

Enter the thermal diffusivity of the masonry in mm²/s.

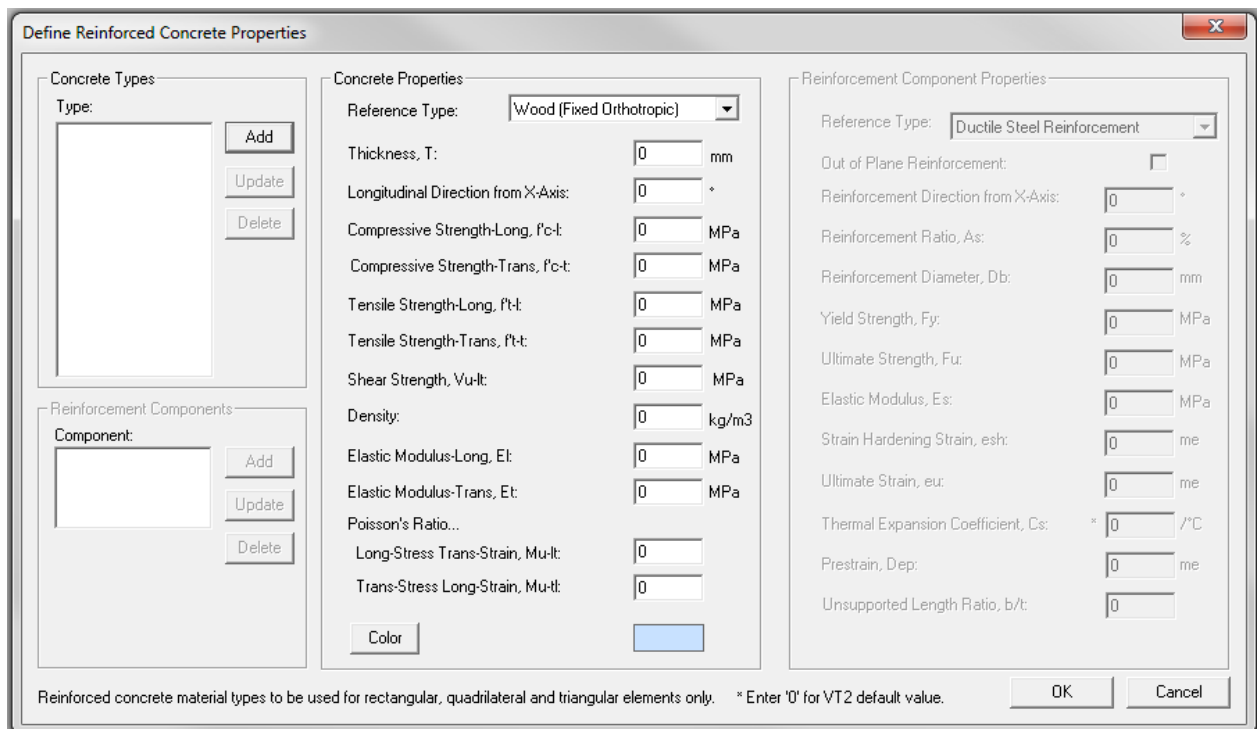
Default value: $K_c = 1.20$ mm²/s

- **Joint Spacing**

Enter the joint spacing parallel to the y-axis for S_x and parallel to the x-axis for S_y . S_x and S_y are defined as the spacings between the head joints and bed joints. See section 5.2.1 for a description and diagram.

10.4.1.4 Wood-Orthotropic

The **Define Reinforced Concrete Properties** dialog box appears as shown in Figure 99 when wood is selected as the main material type.



Define Reinforced Concrete Properties

Concrete Types

Type:

Concrete Properties

Reference Type:

Thickness, T: mm

Longitudinal Direction from X-Axis: °

Compressive Strength-Long, f_c-l : MPa

Compressive Strength-Trans, f_c-t : MPa

Tensile Strength-Long, f_t-l : MPa

Tensile Strength-Trans, f_t-t : MPa

Shear Strength, V_u-lt : MPa

Density: kg/m³

Elastic Modulus-Long, E_l : MPa

Elastic Modulus-Trans, E_t : MPa

Poisson's Ratio...

Long-Stress Trans-Strain, μ_{l-t} :

Trans-Stress Long-Strain, μ_{t-l} :

Reinforcement Component Properties

Reference Type:

Out of Plane Reinforcement:

Reinforcement Direction from X-Axis: °

Reinforcement Ratio, A_s : %

Reinforcement Diameter, D_b : mm

Yield Strength, F_y : MPa

Ultimate Strength, F_u : MPa

Elastic Modulus, E_s : MPa

Strain Hardening Strain, ϵ_{sh} : me

Ultimate Strain, ϵ_u : me

Thermal Expansion Coefficient, C_s : /°C

Prestrain, Dep : me

Unsupported Length Ratio, b/t :

Reinforced concrete material types to be used for rectangular, quadrilateral and triangular elements only. * Enter '0' for VT2 default value.

Figure 99: Define Reinforced Concrete Properties: Wood-Orthotropic

Enter the following properties in the **Concrete Properties** group. There are no VecTor2 default properties for this material type.

- **Thickness, T**

Enter the thickness of the wood in the out of plane direction in millimetres.

- **Longitudinal Direction from x-axis**

Enter the longitudinal direction of the wood from the x-axis in degrees. In wood material models, the longitudinal direction is the direction of the grain of the wood.

- **Compressive Strength—Longitudinal, f'_{c-l}**

Enter the compressive strength in the longitudinal direction in MPa.

- **Compressive Strength—Transverse, f'_{c-t}**

Enter the compressive strength in the transverse direction, perpendicular to the direction of the grain, in MPa.

- **Tensile Strength—Longitudinal, f'_{t-l}**

Enter the tensile strength in the longitudinal direction in MPa.

- **Tensile Strength—Transverse, f'_{t-t}**

Enter the tensile strength in the transverse direction, perpendicular to the direction of the grain, in MPa.

- **Shear Strength**

Enter the shear strength, v_{lt} , in MPa. This is the wood shear strength parallel to the grain, the longitudinal shear strength of the wood. Shear strength, v_{lt} v_{lt} , varies depending on the type of wood, and the water content of the wood.

- **Density**

Enter the density of the wood in kg/m³.

- **Elastic Modulus—Longitudinal, E_l**

Enter the elastic modulus for the longitudinal direction in MPa.

- **Elastic Modulus—Transverse, E_t**

Enter the elastic modulus for the transverse direction in MPa.

- **Poisson's Ratio—Longitudinal stress-transverse strain, ν_{lt}**

Specify the initial Poisson's ratio for longitudinal stress-transverse strain.

- **Poisson's Ratio—Transverse stress-longitudinal strain, ν_{tl}**

Specify the initial Poisson's ratio for transverse stress-longitudinal strain.

10.4.1.5 Modeling Composite Materials

As mentioned previously, composite materials can be modeled in VecTor2 using the four main reinforced concrete materials and the appropriate type of smeared reinforcement. This section outlines how to model each type of composite. The four composites that can be modeled are: concrete-steel laminate, concrete-SFRC laminate, masonry-SFRC laminate, and concrete-ortho laminate.

10.4.1.5.1 Concrete-Steel Laminate

To model concrete-steel laminate the material type selected must be reinforced concrete. The **Define Reinforced Concrete Properties** dialog box appears as shown in Figure 100.

Define Material Properties

Material Types

Type:

Material 1 [Add] [Update] [Delete]

Reinforcement Components

Component:

Reinforcement 1 [Add] [Update] [Delete]

Material Properties

Reference Type: Reinforced Concrete

Thickness, T: 0 mm

Cylinder Compressive Strength, f_c : 0 MPa

Tensile Strength, f_t : * 0 MPa

Initial Tangent Elastic Modulus, E_c : * 0 MPa

Cylinder Strain at f_c , ϵ_c : * 0 me

Poisson's Ratio, μ_c : * 0

Thermal Expansion Coefficient, C_c : * 0 /°C

Maximum Aggregate Size, a : * 0 mm

Density: * 0 kg/m³

Thermal Diffusivity, K_c : * 0 mm²/s

Average Crack Spacing...

perpendicular to x-reinforcement, S_x : * 0 mm

perpendicular to y-reinforcement, S_y : * 0 mm

[Color]

Smeared Reinforcement Properties

Reference Type: Steel Skin Plate

Out of Plane Reinforcement:

Reinforcement Direction from X-Axis: 0 °

Laminate Thickness, T_s : 0 mm

Poisson's Ratio, μ_s : 0

Yield Strength, F_y : 0 MPa

Ultimate Strength, F_u : 0 MPa

Elastic Modulus, E_s : 0 MPa

Strain Hardening Strain, ϵ_{sh} : 0 me

Ultimate Strain, ϵ_u : 0 me

Thermal Expansion Coefficient, C_s : * 0 /°C

Prestrain, Dep : 0 me

Unsupported Length Ratio, b/t : 0

Material types to be used for rectangular, quadrilateral and triangular elements only. * Enter '0' for VT2 default value.

[OK] [Cancel]

Figure 100: Define Reinforced Concrete Properties: Concrete-Steel Laminate

After the two materials, the concrete and reinforcement, are defined in FormWorks, VecTor2 creates a combined material stiffness which is used for the analysis, as discussed previously in section 5.4. Regular ductile steel reinforcement can also be specified as a reinforcement component for the concrete in the concrete-steel laminate, although this is not required. If specified, the ductile steel reinforcing bars will also be incorporated into the combined material stiffness matrix.

Concrete Properties

See section 10.4.1.1 for the required concrete inputs. Note that that the thickness entered in the **Concrete Properties** section is the thickness of the concrete core only and does not include the steel skin plate, the thickness of which is specified in the **Reinforcement Component Properties** section.

Reinforcement (Steel Skin Plate) Properties

For the most part, the input properties required for the steel skin plate are similar to the input requirements for the other steel reinforcement types. The input parameters unique to the steel skin plate reinforcement are:

- **Laminate Thickness, T_s**

Enter the sum of the thicknesses of the steel plates in millimetres.

- **Poisson's Ratio, ν**

Enter the initial Poisson's ratio, ν_0 , for the steel plate.

The other parameters that must be entered are:

- Yield Strength, F_y
- Ultimate Strength, F_u
- Elastic Modulus, E_s
- Strain Hardening Strain, ϵ_{sh}
- Ultimate Strain, ϵ_u
- Thermal Expansion Coefficient, C_s (default value assigned if left as "0")

- Prestrain (if applicable)
- Unsupported Length Ratio, b/t

For further instruction on how to enter these parameters, see section 10.4.1.1.

10.4.1.5.2 Concrete-SFRC Laminate

Defining the concrete-SFRC laminate properly in FormWorks is important. In the *Define Reinforced Concrete Properties* tab, in the *Concrete Properties* subgroup, the reference type must be set to **Reinforced Concrete**. In the *Reinforcement Component Properties* subgroup, the reference type must be set to either **SFRC Laminate-Hooked Fibre** or **SFRC Laminate-Straight Fibre**. The difference between the two fibre types is discussed briefly in the reinforcement materials section of this user manual. The user can also choose to include normal ductile reinforcing steel in the concrete, although this is not required.

The **Define Reinforced Concrete Properties** dialog box appears as shown in Figure 101.

Define Material Properties

Material Types

Type:

Material 1 [Add] [Update] [Delete]

Reinforcement Components

Component:

Reinforcement 1 [Add] [Update] [Delete]

Material Properties

Reference Type: Reinforced Concrete

Thickness, T: 0 mm

Cylinder Compressive Strength, f_c : 0 MPa

Tensile Strength, f_t : * 0 MPa

Initial Tangent Elastic Modulus, E_c : * 0 MPa

Cylinder Strain at f_c , ϵ_c : * 0 me

Poisson's Ratio, μ_u : * 0

Thermal Expansion Coefficient, C_c : * 0 /°C

Maximum Aggregate Size, a : * 0 mm

Density: * 0 kg/m³

Thermal Diffusivity, K_c : * 0 mm²/s

Average Crack Spacing...

perpendicular to x-reinforcement, S_x : * 0 mm

perpendicular to y-reinforcement, S_y : * 0 mm

[Color]

Smearred Reinforcement Properties

Reference Type: Steel Fibre - Hooked

Out of Plane Reinforcement:

Fibre Volume Fraction, V_f : 0 %

Fibre Length, L_f : 0 mm

Fibre Diameter, D_f : 0 mm

Fibre Tensile Strength, F_u : 0 MPa

Fibre Bond Strength, T_u : * 0 MPa

Elastic Modulus, E_s : 0 MPa

Strain Hardening Strain, ϵ_{sh} : 0 me

Ultimate Strain, ϵ_u : 0 me

Thermal Expansion Coefficient, C_s : * 0 /°C

Residual Flexural Strength, F_{r1k} : *** 0 MPa

Residual Flexural Strength, F_{r3k} : *** 0 MPa

*** Required for MC 2010 option only

Material types to be used for rectangular, quadrilateral and triangular elements only. * Enter '0' for VT2 default value. [OK] [Cancel]

Figure 101: Define Reinforced Concrete Properties: Concrete-SFRC Laminate

Concrete Properties

See section 10.4.1.1 for the required concrete inputs.

SFRC Laminate Reinforcement Properties

Enter the following properties in the **Reinforcement Component Properties** group. Properties marked by * are assigned default values when '0' are entered in their fields. The same properties must be entered regardless of whether the hooked fibre or straight fibre laminate is used.

- **Fibre Volume Fraction, V_f**

Enter the fibre volume fraction in %.

- **Fibre Length, L_f**

Enter the fibre length used in the SFRC in millimetres.

- **Fibre Diameter, D_f**

Enter the fibre diameter in millimetres.

- **Fibre Tensile Strength, F_u**

Enter the fibre tensile strength in MPa.

Default value: $F_u = 1100$ MPa

- **Fibre Bond Strength, T_u**

Enter the fibre bond strength in MPa.

- **Cylinder Compressive Strength, f'_c**

Enter the peak compressive stress in MPa.

- **Tensile Strength, f'_t**

Enter the uniaxial cracking strength of the SFRC in MPa.

Default value: $f'_t = 0.33\sqrt{f'_c}$ MPa

- **Initial Tangent Elastic Modulus, E_c**

Enter the tangent stiffness of the SFRC stress-strain response at zero-strain in MPa.

Default value: $E_c = 3320\sqrt{f'_c} + 6900$ MPa

- **Cylinder Strain at f'_c , ϵ_o**

Enter the compressive strain, ϵ_0 , corresponding to f'_c , as a positive value in millistrain.

Default value: $\epsilon_0 = 1.8 + 0.0075f'_c$ me

- **Maximum Aggregate Size, a**

Enter the maximum aggregate size in millimetres.

Default value: $a = 20$ mm

- **Laminate Thickness, T**

Enter the SFRC laminate total thickness in millimetres.

10.4.1.5.3 Masonry-SFRC Laminate

The masonry-SFRC laminate is defined in FormWorks in basically the same way as the concrete-SFRC laminate. In the *Define Reinforced Concrete Properties* tab, in the *Concrete Properties* subgroup, the reference type must be set to **Reinforced Concrete**. In the *Reinforcement Component Properties* subgroup, the reference type must be set to either **SFRC Laminate-Hooked Fibre** or **SFRC Laminate-Straight Fibre**.

The **Define Reinforced Concrete Properties** dialog box appears as shown in Figure 102.

Define Material Properties

Material Types

Type:

Material 1 Add Update Delete

Reinforcement Components

Component:

Reinforcement 1 Add Update Delete

Material Properties

Reference Type: Reinforced Concrete

Thickness, T: 0 mm

Cylinder Compressive Strength, f'_c : 0 MPa

Tensile Strength, f_t : * 0 MPa

Initial Tangent Elastic Modulus, E_c : * 0 MPa

Cylinder Strain at f'_c , ϵ_0 : * 0 me

Poisson's Ratio, μ : * 0

Thermal Expansion Coefficient, C_c : * 0 /°C

Maximum Aggregate Size, a : * 0 mm

Density: * 0 kg/m³

Thermal Diffusivity, K_c : * 0 mm²/s

Average Crack Spacing...

perpendicular to x-reinforcement, S_x : * 0 mm

perpendicular to y-reinforcement, S_y : * 0 mm

Color

Smeared Reinforcement Properties

Reference Type: SFRC Laminate - Hooked Fibre

Out of Plane Reinforcement:

Fibre Volume Fraction, V_f : 0 %

Fibre Length, L_f : 0 mm

Fibre Diameter, D_f : 0 mm

Fibre Tensile Strength, F_u : 0 MPa

Fibre Bond Strength, T_u : * 0 MPa

Concrete Compressive Strength, f'_c : 0 MPa

Concrete Tensile Strength, f_t : * 0 MPa

Initial Tangent Elastic Modulus, E_c : * 0 MPa

Concrete Strain at f'_c , ϵ_0 : * 0 me

Maximum Aggregate Size, a : * 0 mm

Laminate Thickness, T : 0 mm

Material types to be used for rectangular, quadrilateral and triangular elements only. * Enter '0' for VT2 default value.

OK Cancel

Figure 102: Define Reinforced Concrete Properties: Masonry-SFRC Laminate

Masonry Properties

The same masonry properties must be entered as are required to define regular reinforced or unreinforced masonry. See section 10.4.1.3 for the required concrete inputs.

SFRC Laminate Reinforcement Properties

The SFRC laminate properties are entered as they are entered for concrete-SFRC laminate. See section 10.4.1.5.2 for details on the required inputs.

10.4.1.5.4 Concrete-Ortho Laminate

The Concrete-Ortho Laminate is a combination of a concrete core and wood (orthotropic) faceplates. In the *Define Reinforced Concrete Properties* tab, in the *Concrete Properties* subgroup, the reference type must be set to **Concrete-Ortho Laminate**. In the *Reinforcement Component Properties* subgroup, the reference type must be set to **Orthotropic Laminate**.

The **Define Reinforced Concrete Properties** dialog box appears as shown in Figure 103.

Define Material Properties

Material Types

Type:

Material 1 [Add] [Update] [Delete]

Reinforcement Components

Component:

Reinforcement 1 [Add] [Update] [Delete]

Material Properties

Reference Type: Reinforced Concrete

Thickness, T: 0 mm

Cylinder Compressive Strength, f_c : 0 MPa

Tensile Strength, f_t : * 0 MPa

Initial Tangent Elastic Modulus, E_c : * 0 MPa

Cylinder Strain at f_c , ϵ_c : * 0 me

Poisson's Ratio, μ_u : * 0

Thermal Expansion Coefficient, C_c : * 0 /°C

Maximum Aggregate Size, a : * 0 mm

Density: * 0 kg/m³

Thermal Diffusivity, K_c : * 0 mm²/s

Average Crack Spacing...

perpendicular to x-reinforcement, S_x : * 0 mm

perpendicular to y-reinforcement, S_y : * 0 mm

Color [Color]

Smeared Reinforcement Properties

Reference Type: Orthotropic Laminate

Out of Plane Reinforcement:

Longitudinal Direction from X-Axis: 0 °

Compressive Strength-Long, f_{c-l} : 0 MPa

Compressive Strength-Trans, f_{c-t} : 0 MPa

Tensile Strength-Long, f_{t-l} : 0 MPa

Tensile Strength-Trans, f_{t-t} : 0 MPa

Shear Strength, V_u -lt: 0 MPa

Elastic Modulus-Long, E_l : 0 MPa

Elastic Modulus-Trans, E_t : 0 MPa

Poisson's Ratio-LT, μ_{lt} : 0

Poisson's Ratio-TL, μ_{tl} : 0

Thickness, T: 0 mm

Material types to be used for rectangular, quadrilateral and triangular elements only. * Enter '0' for VT2 default value.

[OK] [Cancel]

Figure 103: Define Reinforced Concrete Properties: Concrete-Ortho Laminate

Concrete Properties

The same concrete properties must be entered as are required to define regular reinforced concrete. See section 10.4.1.1 for the required concrete inputs.

Orthotropic Laminate Properties

The inputs required are the same as for the wood (fixed orthotropic) material type, with the exception of density. The wood density is not a required input for orthotropic laminate. The required inputs are specified in section 10.4.1.4.

10.4.2 Reinforcement Material Types

Reinforcement materials types describe steel or FRP reinforcement materials for truss bar elements. To add, modify or delete reinforcement material types, click the **Structure/Define Reinforcement Materials** menu item or click the **Define Reinforcement Materials** toolbar button. The **Define Reinforcement Materials** dialog box appears as shown in Figure 104.



Figure 104: Reinforcement Materials Properties Dialog Box

The procedures for adding, modifying and deleting reinforcement material types are similar to those for reinforced concrete materials. The properties for reinforcement materials are similar to those for reinforcement components. Only the unique values are described below.

- **Cross-Sectional Area**
Enter the cross-sectional area of reinforcement assigned to truss elements, in mm².
- **Color**

Enter the display color of the reinforcement material type in the FormWorks Workspace.

10.4.2.1 Bond Types

Bond types describe bond stress-slip relationships between concrete and discrete reinforcement, and are applied to link and contact elements. To add, modify or delete bond types, click the **Structure/Define Bond Properties** menu item or click the **Define Bond Properties** toolbar button. The **Define Bond Properties** dialog box appears as shown in Figure 105.



Figure 105: Bond Properties Dialog Box

The procedures for adding, modifying and deleting bond types are similar to those for reinforced concrete materials. The properties for bond materials are described below.

- **Reference Type**

As described in Chapter 7, VecTor2 determines bond stress-slip relationships for **Embedded Deformed Bars** and **Embedded Smooth Bars** based on the selected concrete bond model.

For **Externally Bonded Plates and Sheets**, the bond stress-slip relationship is explicitly specified by a series of reference bond stress and corresponding slips.

- **Color**

Select the display color of the bond type in the FormWorks Workspace.

If **Embedded Deformed Bars** or **Embedded Deformed Bars** is selected:

- **Confinement Pressure Factor**

The confinement pressure factor is used to interpolate the bond stress-slip relationship between unconfined splitting failure and confined pull-out failure. Compute the confinement pressure factor, β , as follows:

$$\beta = \frac{\sigma}{7.5}, \quad (\text{in MPa}) \quad 0 \leq \beta \leq 1, \quad (10.4.2.1.1)$$

where σ is the anticipated confining pressure on the embedded bar in MPa.

- **Min (Bar Clear Cover, Spacing), Cmin**

Enter the lesser of the clear cover of the embedded bar and half of the spacing between the embedded bars, in millimeters.

- **No. of Reinforcement Layers thru Depth**

Enter the number of layers of reinforcing bars represented by truss elements to be attached to the bond element.

If **Externally Bonded Plates or Sheets** is selected:

- **Bonded Surface Area, Ao**

Enter the area of the external plate or sheet that is adherent to the concrete, in mm^2 , per element.

- **Bond Stress-Slip Curve Reference Points**

Enter three reference bond stresses, U_i , and corresponding slips, S_i , to define a multilinear bond stress-slip relationship. Enter bond stresses, U_i , in MPa and corresponding slips, S_i , in millimeters.

10.4.3 Defining Nodes

The following section describes how to add and delete nodes by the **Manual Method**.

The rules for defining nodes in VecTor2 are as follows:

- A finite element mesh having 'n' nodes must contain all nodes numbered consecutively from 1 to 'n.'
- All nodes must be attached to at least one element.

FormWorks, circumvents the first rule and allows nodes to be arbitrarily numbered. If the rule is violated or if the bandwidth reduction algorithm is used, FormWorks renumbers the nodes when generating the input files. This feature may be useful when it is more convenient to edit a mesh in progress or modify an existing mesh than to define a new one. Still, it is advisable to number nodes according to the rule as the renumbering may appear disorderly.

To **Create Nodes**, complete the following steps.

1. Select the **Structure/Create Nodes** menu item or click the **Create Nodes** toolbar button. The Create Nodes dialog box appears as shown in Figure 106.



| Create Nodes | | | | | | | | | | | | |
|--------------|------|------|--------|--------|------|-----|--------|--------|-----|------|--------------------------------------------------------------------------------------------------------------|--|
| node | x | y | #nodes | d node | d x | d y | #nodes | d node | d x | d y | Total | |
| 13 | 100. | 200. | 6 | 1 | 125. | 0. | 5 | 6 | 0. | 100. | 0 | |
| | | | | | | | | | | | <input type="button" value="Add"/> <input type="button" value="Delete"/> <input type="button" value="Done"/> | |

Figure 106: Create Nodes Dialog Box

2. Complete the fields to create a lattice of nodes separated by constant spacing and node number. Refer to Figure 107 as an example corresponding to the values shown in Figure 106.

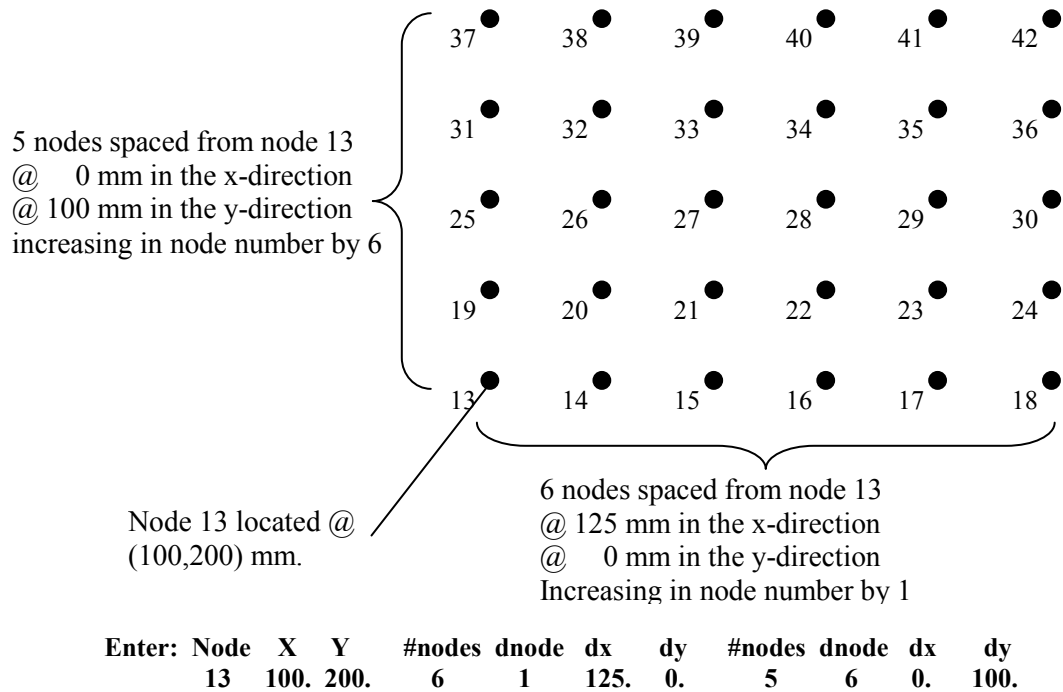


Figure 107: Example of node creation entry

3. Click **Add** or type **Enter**. The generated nodes are drawn in the Workspace, the total number of nodes is updated, and the last node entry is added to the drop list in the dialog box.

To **Delete Nodes** complete the following steps.

1. In the drop list, select the nodes to be deleted. The selected node entry appears highlighted. Note that only nodes that are unattached to elements may be deleted.
2. Click **Delete**. The deleted nodes disappear from the Workspace, the total number of nodes is updated, and the node entry is deleted from the drop list in the dialog box. Also any nodal loads or support displacements assigned to these nodes are also deleted.

10.4.4 Defining Elements

The following section describes how to create and delete elements by the **Manual Method**.

Element types may be categorized by their function in the finite element model. **Rectangular**, **Quadrilateral** and **Triangular** elements are used in conjunction with Reinforced Concrete material types to model reinforced concrete regions. **Truss Bar** elements are used in conjunction with Reinforcement

material types to model reinforcement in a discrete manner. **Link** and **Contact** elements are used to model the interface between rectangular, quadrilateral or triangular elements and truss bar elements.

In VecTor2, the following rules exist for defining elements:

- A finite element mesh having 'n' elements must contain all elements numbered from 1 to 'n.'
- Elements numbers must be ordered by element type from lowest to highest: rectangular, quadrilateral, triangular, truss, link and contact.

FormWorks circumvents these two rules and allows elements to be arbitrarily numbered. If either rule is violated, FormWorks automatically renumbers the elements when generating input files. This feature may be useful when it is more convenient to edit a mesh in progress or modify an existing mesh than to define a new one. Nevertheless, it is advisable to obey the rules, as renumbering may be disorderly and make result interpretation difficult.

The procedure for creating and deleting elements is similar for all six element types. A generic procedure follows, with necessary rules for each element type.

To **Create Elements**, complete the following procedure.

1. Select the **Structure/Create [Type] Elements...**

menu item or click the **Create [Type] Elements**



toolbar button for the desired element type. As an example the Create Rectangular Elements dialog box is shown in Figure 108.

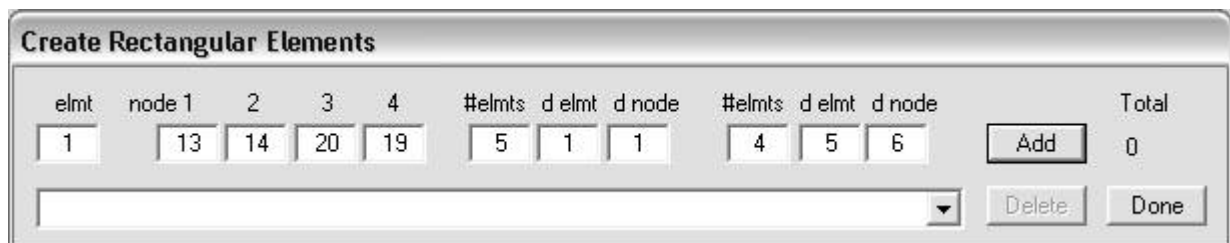
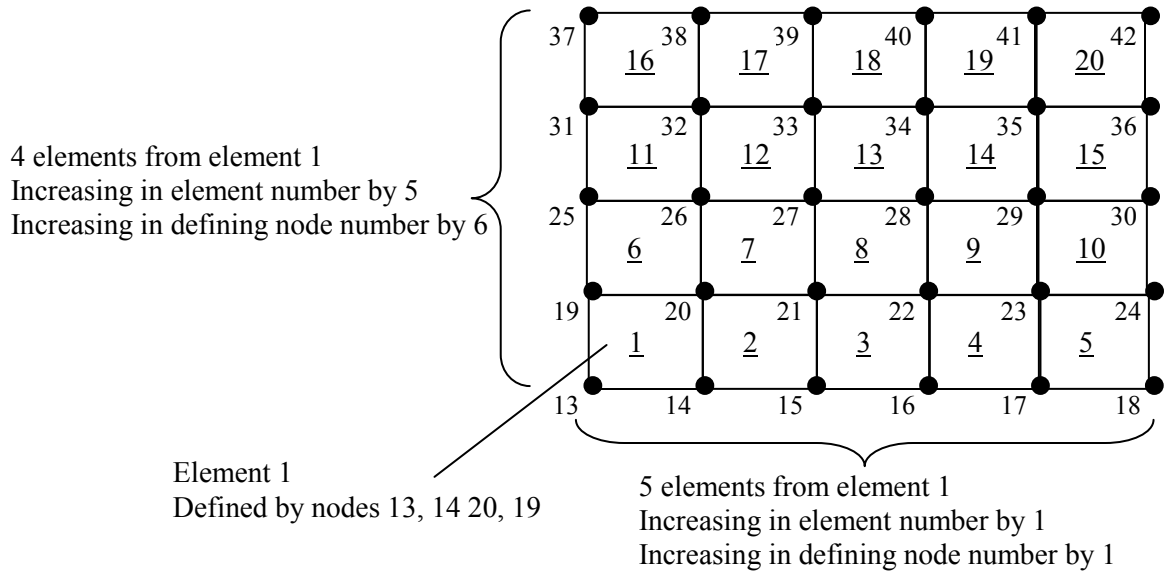


Figure 108: Create Rectangular Elements Dialog Box

- Complete the fields to create a lattice of elements with constant change in element numbering and defining nodes. Refer to Figure 109 as an example for creating rectangular elements. The rules for different element types are subsequently discussed.



```
Enter: Elmt node 1 2 3 4 #elmts delmt dnode #elmts delmt dnode
       1      13 14 20 19 5 1 1 4 5 6
```

Figure 109: Example of rectangular element creation entry

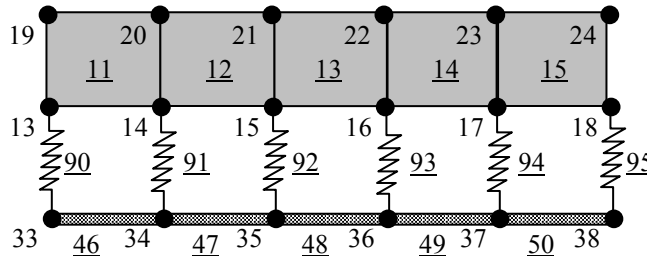
For **Rectangular** elements, enter four node numbers that define the corner nodes of the source element. The four nodes must be predefined and form the corners of an isothetic rectangle in cyclic counter-clockwise order.

For **Quadrilateral** elements, enter the four node numbers that define the vertex nodes of the source element. The four nodes must be predefined and form the corners of a quadrilateral in cyclic counter-clockwise order. Note that quadrilateral elements that are rectangular in shape are not analytically equivalent to rectangular elements.

For **Triangular** elements, enter the three node numbers that define the vertex nodes of the source element. The three nodes must be predefined and may be in either cyclic clockwise or cyclic counterclockwise order.

For **Truss** elements, enter the two node numbers that define the end nodes of the source element. The two nodes must be predefined.

For **Link** elements, enter the two node numbers that define the nodes of the source element. The two nodes must be predefined with the same coordinates so that the link is non-dimensional. As shown in the example of Figure 110, defining link elements requires creating layers of nodes. One node must be an incident node of a rectangular, quadrilateral or triangular element. The other node must be an incident node of a truss bar element. Further, if two or more truss bars intersect at a common node and each truss bar is connected to the concrete by a link element, it is necessary to define separate nodes and link elements for each truss bar at the intersection location.



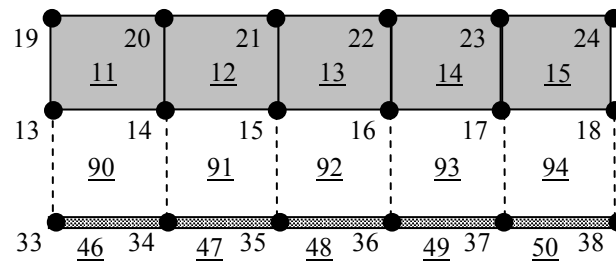
| | |
|-----------------------|-----------------------------------|
| Elements: | Node Pairs with same coordinates: |
| Rectangular: 12 to 15 | 13 & 33 |
| Truss: 46 to 50 | 14 & 34 |
| Link: 90 to 95 | 15 & 35 |
| | 16 & 36 |
| | 17 & 37 |
| | 18 & 38 |

| | | | | | | | | | |
|-------------|-------|---|---|--------|-------|-------|--------|-------|-------|
| Enter: Elmt | node | 1 | 2 | #elmts | delmt | dnode | #elmts | delmt | dnode |
| 90 | 13 33 | 6 | 1 | 1 | 1 | 1 | 1 | 1 | 1 |

Figure 110: Example of link element creation entry

For **Contact** elements, enter the four node numbers that define the nodes of the source element.

As shown in the example of Figure 111, nodes 1 and 2 must have the same coordinate, and nodes 3 and 4 must have the same coordinate. Of each node pair, one node must be an incident node of a rectangular, quadrilateral or triangular elements, while the other node must be an incident node of a truss bar element. Further, if two or more truss bars intersect at a common node and each truss bar is connected to the concrete by a contact element, it is necessary to define separate nodes and contact elements for each truss bar at the intersection location.



| | |
|-----------------------|-----------------------------------|
| Elements: | Node Pairs with same coordinates: |
| Rectangular: 12 to 15 | 13 & 33 |
| Truss: 46 to 40 | 14 & 34 |
| Contact: 90 to 94 | 15 & 35 |
| | 16 & 36 |
| | 17 & 37 |
| | 18 & 38 |

```
Enter: Elmt node 1 2 3 4 #elmts delmt dnode #elmts delmt dnode
90      13 33 14 34 5 1 1 1 1 1
```

Figure 111: Example of contact element creation entry

- Click **Add** or type **Enter**. The generated elements are drawn in the Workspace, the total number of elements is updated, and the last element entry is added to the drop list in the dialog box. At this stage, the elements have no material types assigned to them, and are assigned the following default colors:

- Rectangular, Quadrilateral and Triangular: White
- Truss Bar: Magenta
- Link: Blue
- Contact: Cyan

To **Delete Elements**, complete the following steps.

1. In the drop list, select the elements to be deleted. The selected element entry appears highlighted.
2. Click **Delete**. The deleted elements disappear from the Workspace, the total number of elements is updated and the element entry is deleted from the drop list in the dialog box. Any associated material type assignments and loads for these elements are also deleted.

10.4.4.1 Viewing Elements Attributes

To view a summary of the attributes of an element, position the mouse cross-hairs within the boundaries of the desired element and click the **left** mouse button. The selected element appears highlighted in green and the **Element Attributes** dialog box appears as shown in Figure 112. The element number, element type, incident nodes and their coordinates, material types and assigned loads are shown.

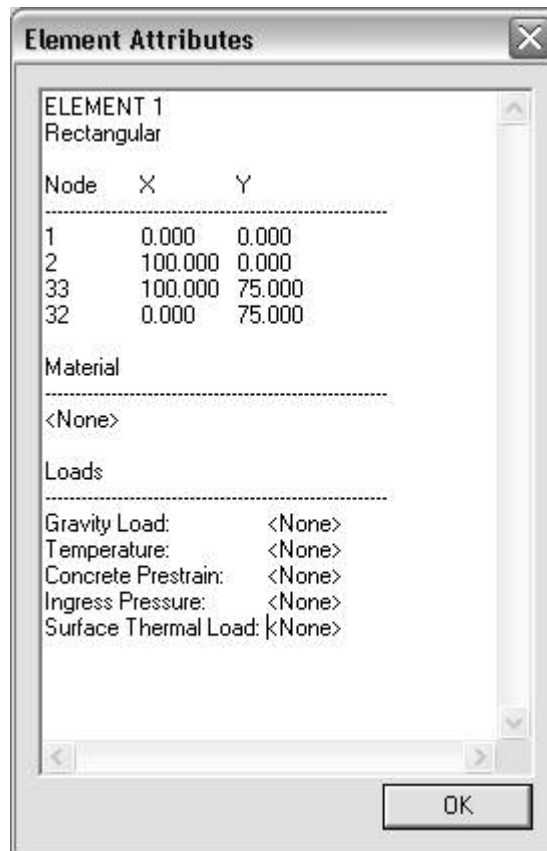


Figure 112: Element attributes dialog

10.4.4.2 Viewing Multiple Element Layers

Occasionally, it is necessary to create layers of elements that occupy the same space. In the Workspace, only the top layer is visible and conceals the elements beneath it. To view concealed element layers, it is necessary to send the topmost layer backwards.

To **send one element backwards**:

1. Position the mouse cross-hairs within the boundary of the element.
2. Click the **right** mouse button. The context menu appears below the mouse cross-hairs.
3. Select **Send This Element Back**. The element beneath the mouse cross-hairs is sent to the back, revealing the element beneath it.

To **send multiple elements backwards**:

1. Position the mouse cross-hairs within the boundary of any element.
2. Click the **right** mouse button. The context menu appears below the mouse cross-hairs.
3. Select **Send Multiple Elements Back**. The **Send Elements Back** dialog box appears.
4. Click the **Send** button. The mouse cross-hair becomes a pick arrow.
5. Click the **left** mouse button and drag pick arrow over the elements to be sent backwards. The selected elements appear highlighted in bright green.
6. Click **Send**. The selected elements are sent to the back, revealing the elements beneath them.
7. Click **Done**.

10.4.5 **Assigning Material Types**

Having defined elements and material types, the following section describes how to assign the material types to the elements.

In VecTor2, the following rules exist for assigning material types:

- All Rectangular, Quadrilateral and Triangular elements must be assigned a Reinforced Concrete material type.

- All Truss Bar elements must be assigned a Reinforcement material type.
- All Link and Contact elements must be assigned a Bond type.

To **Assign Material Types**, complete the following procedure.

1. Select the **Structure/Assign Material Type** menu item or click the **Assign Material Types** toolbar button. The Assign Material Types dialog box appears as shown in Figure 113.

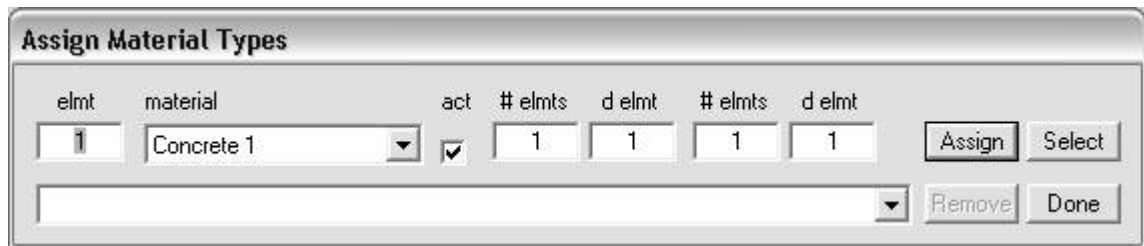


Figure 113: Assign Material types dialog box

2. Specify the material types and select elements by one of the following two methods.

To Select Elements by Element Number

Complete the entry fields to select the desired elements. The element selection method is similar to the specification of element numbers. Select a compatible material type from the drop list.

Check the **Active** box if the selected elements are engaged, so that they contribute to the stiffness and strength of the structure. Uncheck the box if the selected elements are disengaged, so that they do not contribute to the strength and stiffness of the structure. In the latter case, all element strains are computed as plastic strain offsets. Use this feature to disengage and engage elements for repair applications.

Alternatively, to Select Elements with the Mouse:

Select the material type from the drop list. Click **Select**. The mouse cross-hairs become a pick arrow. Click the **left** mouse button and the drag pick arrow over the elements to be selected. The selected elements appear highlighted in bright green, as shown in Figure 114. Only elements compatible with material type may be selected.

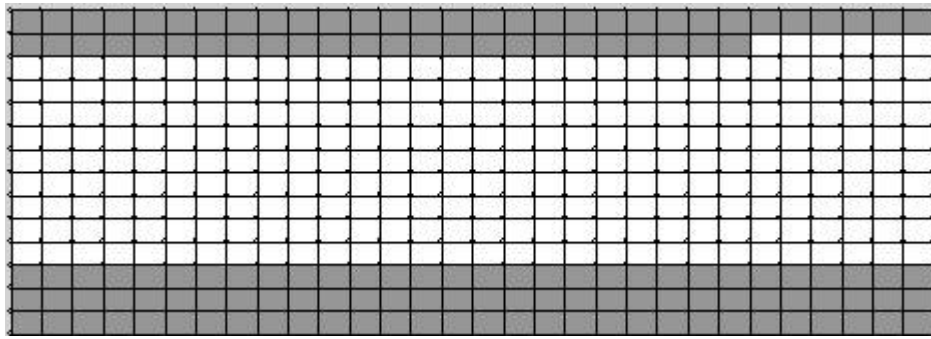


Figure 114: Selecting elements for material type assignment with the mouse

3. Click **Assign** or type **Enter**. The assigned material types are drawn in the Workspace, and the material type assignments are added to the drop list in the dialog box. Active concrete elements are filled with solid colors, while inactive concrete elements are filled with hatched colors. Active truss, link and contact elements are drawn as thicker lines than inactive elements.

Material type assignments can be modified by repeating the above procedure. Previous material assignments will be overwritten.

10.4.6 Restraining the Structure

Having defined the nodes, the following section describes how to add support restraints.

To **Add Support Restraints**, complete the following procedure.



1. Select the **Structure/Create Support Restraints** menu item or click the **Create Support Restraints** toolbar button. The **Create Support Restraints** dialog box appears, as shown in Figure 115.

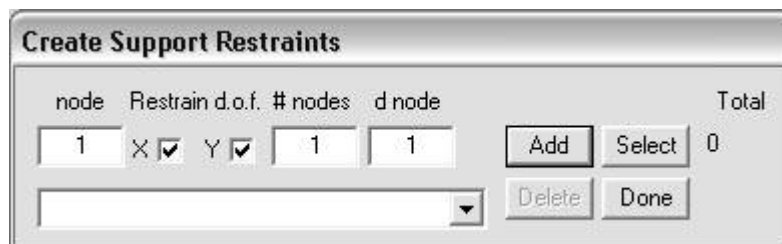


Figure 115: Create Support Restraints Dialog Box

2. Specify the restraints and select nodes by one of the following two methods.

To Select Nodes by Node Number

Complete the entry fields to select the desired nodes. The node selection method is similar to the specification of node numbers. Check the **X** and/or **Y** box to restrain the selected nodes against displacements in the x and Y directions, respectively.

Alternatively, to Select Nodes with the Mouse:

Click **Select**. The mouse cross-hairs become a pick arrow. Position the pick arrow over desired nodes to restrain and click the **left** mouse button. The selected nodes appear highlighted in bright green, as shown in Figure 116. Check the **X** and/or **Y** box to restrain the selected nodes against displacements in the x and Y directions, respectively.

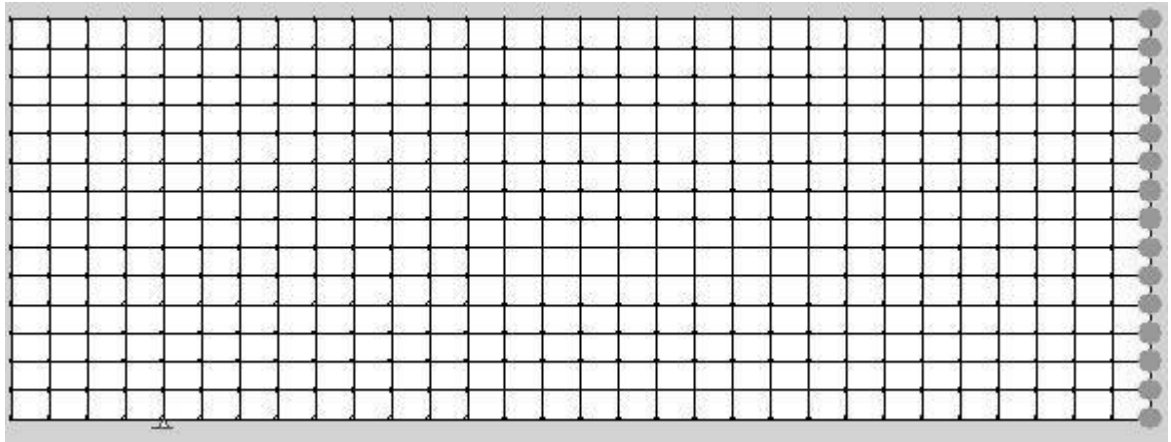


Figure 116: Selecting nodes for restraints with the mouse

3. Click **Add** or type **Enter**. The restraints are drawn in the Workspace and the restraint entries are added to the drop list in the dialog box.

Restraints may be removed by selecting the restraint entry in the drop list and clicking **Remove**, or selecting nodes with the mouse and clicking **Remove**.

10.4.7 Automatic Method

The **Automatic Method** provides a method to define nodes, elements, restraints, and assign material types without having to manually create and number the nodes and elements. Instead, concrete regions are defined by one or more polygonal regions. These regions may contain voids, and linear and point constraints for the mesh. Truss bars elements are defined by linear paths. Link and contact elements can be created for segments of the discrete reinforcement. Several automatic discretization and meshing options are provided to accommodate different structure geometries, meshing needs, element types and the extent of manual control. Material types should be defined before proceeding to the subsequent sections.

10.4.7.1 Reinforced Concrete Regions

The first step is to define one or more **Reinforced Concrete Regions**. Each region is defined as a polygon that will be meshed with rectangular, quadrilateral, and/or triangular elements. Each region can have different meshing parameters, concrete material type assignments, and numbers of layers. The guidelines for defining reinforced concrete regions are as follows:

- The region is defined by a nontrivial closed polygon.
- The vertices defining the region are entered in cyclic counter-clockwise order.
- The edges of a region must be simple and not self-intersecting.
- Regions can be attached along common edges, but cannot overlap. Care should be taken to define the common vertices of regions with exactly the same coordinates.

Legal and illegal polygon regions are shown in Figure 117.

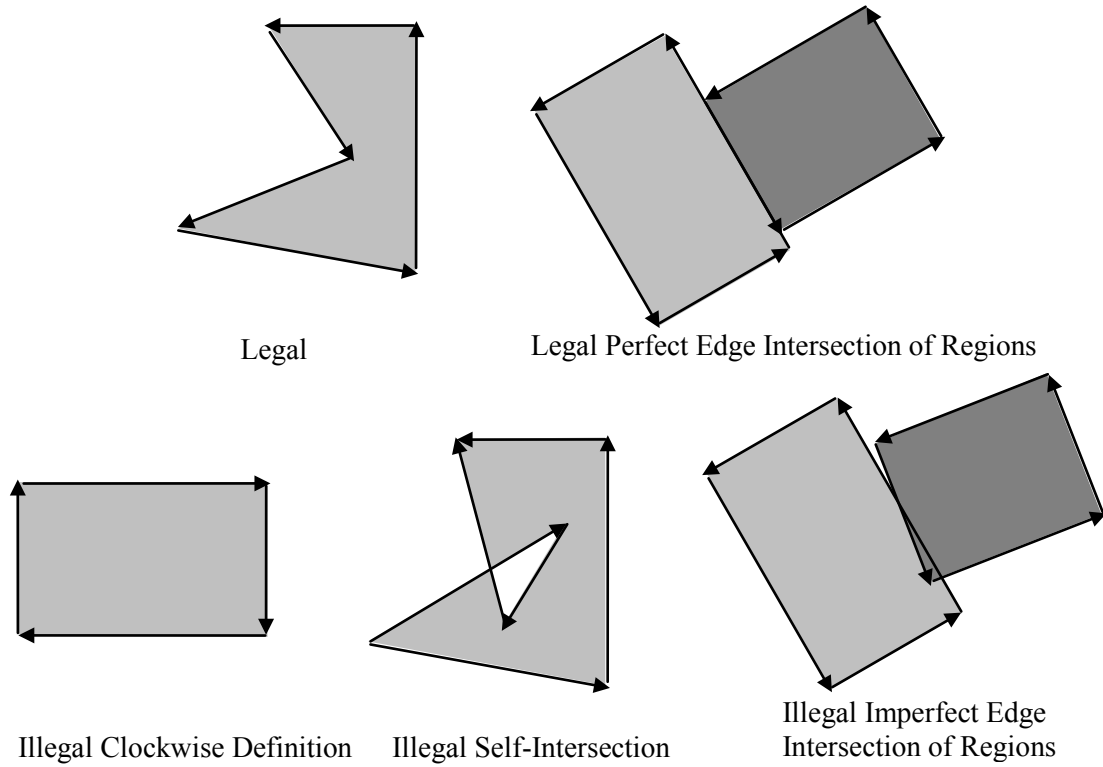


Figure 117: Examples of legal and illegal region definitions and intersections

To **Define a Concrete Region**, complete the following steps.

1. Select the **Structure / Define and Mesh Structure** menu item or select the **Define and Mesh Structure** toolbar button. The **Define and Mesh Structure** property sheet appears as shown in Figure 115, with the **RC regions** property page as the active page.



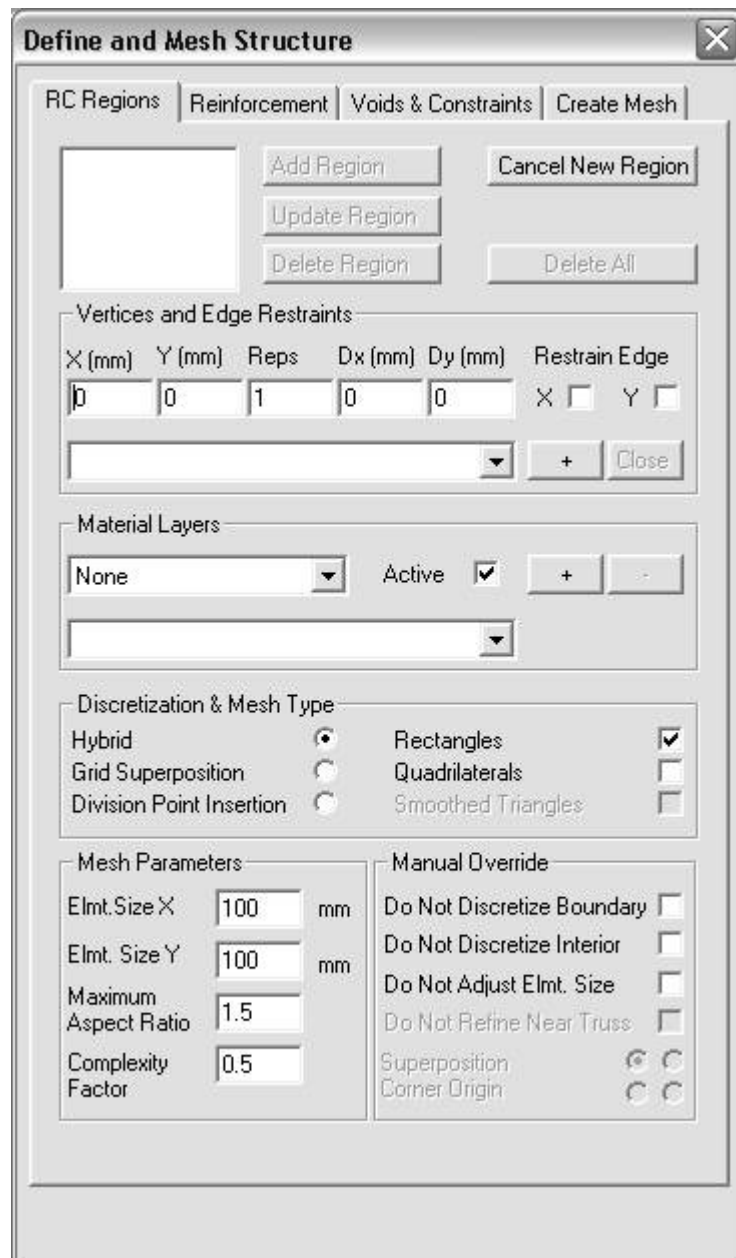


Figure 118: RC Regions Property Page

2. Click **Create New Region** to start a new region. To abort the region at any time, click the same button, which is now labeled as **Cancel New Region**.
3. In the **Vertices and Restraints** group, complete the following procedure to define the region. An example is shown in Figure 119 to create a rectangle with one restrained edge.
 - i) Enter the following fields to define a vertice of the region. It is necessary to define only the vertices at the ends of edges of the region. If desired, one can also define intermediate vertices to enforce the location of boundary nodes. By doing so, and selecting the Do Not

Discretize Boundary manual override option, it is possible to designate the location of all boundary nodes.

- **X**

Enter the x-coordinate of a vertice, in millimeters.

- **Y**

Enter the y-coordinate of a vertice, in millimeters.

- **Reps**

Enter the number of vertices to create along a line.

- **Dx**

Enter the spacing of vertices in the x-direction from X, in millimeters.

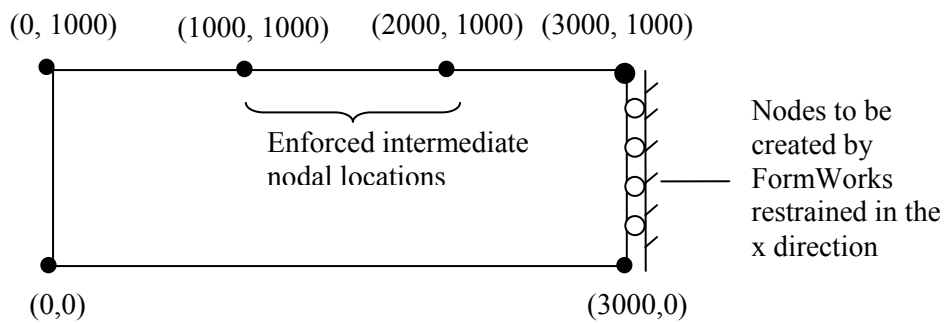
- **Dy**

Enter the spacing of vertices in the y-direction from Y, in millimeters.

- **Restrain Edge X,Y**

Check the appropriate degree of freedom to restrain all nodes on the edge defined by the current vertice and the next vertice against displacements in the x and/or y directions.

ii) Click + after each vertice entry, except the last vertice. After the last vertice, click **Close**. The region is drawn in the Workspace as vertices are added.



| Entry: | X | Y | Reps | Dx | Dy | Restrain Edge | |
|--------|-------|-------|------|--------|----|------------------|-------|
| | 0. | 0. | 1 | 0. | 0. | X Y | + |
| | 3000. | 0. | 1 | 0. | 0. | X [✓] Y | + |
| | 3000. | 1000. | 3 | -1000. | 0. | X Y | + |
| | 0. | 1000. | 1 | 0. | 0. | X Y | Close |

Figure 119: Example of reinforced concrete region creation

4. In the **Material Layers** group, complete the following procedure to add a layer of concrete elements. In general, only one layer of elements is necessary. More than one layer may be added to double-meshed a region. Each layer of the region may be assigned different reinforced concrete material types. If **None** is selected, FormWorks creates a layer of elements without any material type assignments. If no layers are added, FormWorks creates no elements, whatsoever.
 - i) In the drop list, select the reinforced concrete material type to assign the elements of the region.
 - ii) Check or uncheck **Active** if the layer of elements is to be engaged or disengaged, respectively.
 - iii) Click + to add the layer of elements with the selected material type. (Click – to delete defined layers from the drop list).
 - iv) Repeat steps i) to iii) to add additional layers of elements, if desired.
5. In the **Discretization and Mesh Type** group, select from the following options.

(Note that each region can have different discretization and mesh types.)

The following options determine the manner in which the FormWorks discretizes the region.

- **Hybrid**

This option is recommended for structures comprised primarily by one or more rectangular regions, as is encountered in the elevation of common reinforced concrete beams, columns and walls. The discretization is shown for a simple region in Figure 120. Like the Grid Superposition algorithm, FormWorks attempts to discretize the

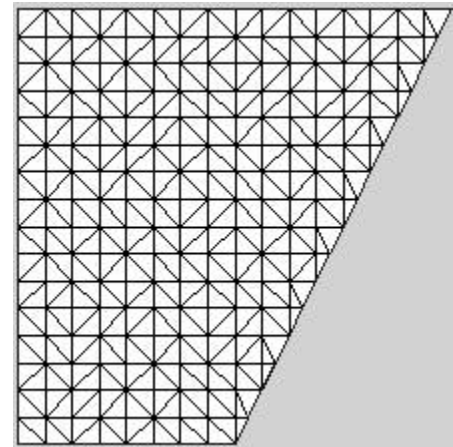


Figure 120: Hybrid Discretization

region with a highly regular grid of nodes. Like the Point Insertion Algorithm, it accommodates nonlinearity of the region boundary and interfering features with local variations in node spacing. A constrained Delaunay algorithm triangulates the inserted nodes.

- **Grid Superposition**

This option is recommended for polygons of arbitrary shape, having relatively coarse boundary features. The discretization for a simple region is shown in Figure 121. FormWorks superimposes the region with a regular grid of rectangular elements, and then removes elements that are too close to the boundary or other interfering features within the polygon. The boundary nodes of the rectangular grid are then triangulated with a constrained Delaunay algorithm. This meshing procedure was liberally adapted from the concepts described by Petersen, Rodrigues and Martins (2000).

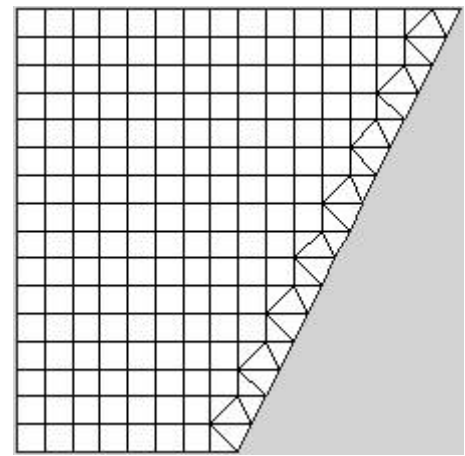


Figure 121: Grid Superposition Discretization

- **Division Point Insertion**

This option is recommended for polygons of arbitrary shape, having several nonlinear edges. The discretization for a simple region is shown in Figure 122. FormWorks discretizes the region by inserting nodes at approximately equal intervals in the x and y direction. Nonlinearity of the region boundary and interfering features within the polygon are accommodated by local variations the node spacing. A constrained Delaunay algorithm triangulates the inserted nodes.

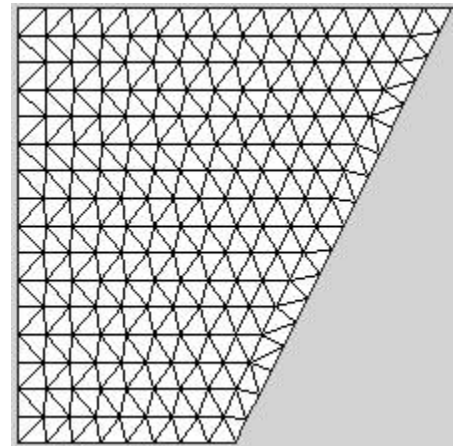


Figure 122: Division Point Insertion Discretization

The following options determine how FormWorks treats the triangular elements created by the Delaunay triangulation.

- **Rectangles**

If checked, FormWorks merges adjacent pairs of triangles to create as many rectangular elements of suitable quality. If the Quadrilaterals option is also selected, rectangular elements are formed preferentially over quadrilateral elements. Figure 123 shows the Hybrid discretization of Figure 120 with the rectangle option

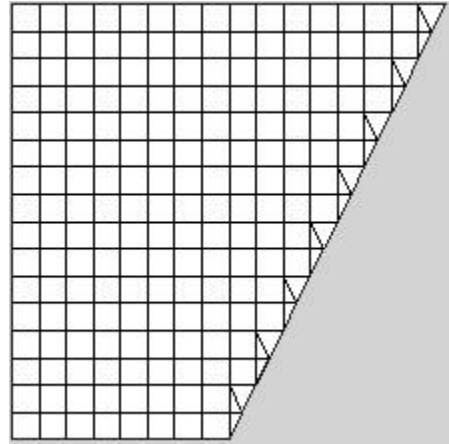


Figure 123: Hybrid Discretization with Rectangle Option

- **Quadrilaterals**

If checked, FormWorks merges adjacent pairs of triangular elements to form quadrilateral elements. FormWorks selects the best quality quadrilaterals based upon the resulting aspect ratio and internal angles. As many quadrilateral elements as possible are created to minimize the number of residual triangular elements. If the Rectangles option is also selected, rectangular elements are created preferentially over quadrilateral elements. Figure 124 shows the Division point insertion discretization of Figure 122 with the quadrilateral option.

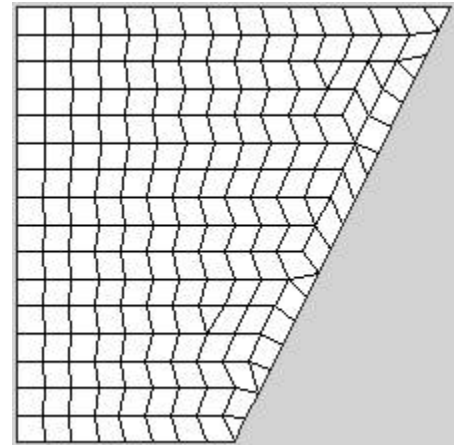


Figure 124: Division Point Insertion Discretization with Quadrilateral Option

- **Smoothed Triangles**

If checked, the shape of the triangular elements are optimized by adjusting the position of free nodes by iterative Lagrangian averaging, such that final position of each node is approximately an average of the position of its contiguous nodes. Figure 125 shows the Division point insertion discretization of Figure 122 with the smoothed triangles option.

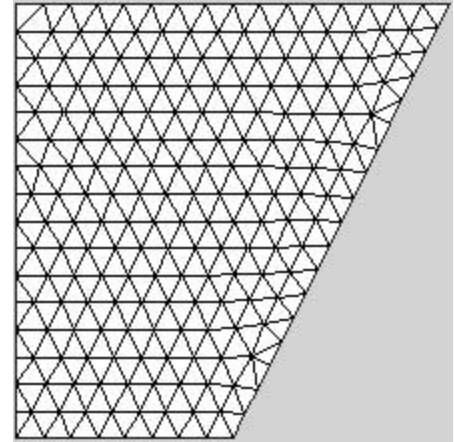


Figure 125: Division Point Insertion Discretization with Smoothed Triangles Option

6. In the **Mesh Parameters** group, specify the parameters.

- **Elmt Size X and Elmt Size Y**

For grid superposition and hybrid discretization types, enter the average length of elements in the x and y directions, respectively, in millimeters.

- **Tri Elmt. Size**

For the division point insertion discretization type, enter the average side length of triangular elements, in millimeters.

- **Max. Aspect Ratio**

For grid superposition and hybrid discretization types, enter the maximum permitted ratio of the rectangular element height to width, or *vice versa*. If the maximum aspect ratio is exceeded, Elmt Size X and Elmt Size Y are automatically adjusted to the largest possible dimensions that satisfy the maximum aspect ratio.

- **Complexity Factor**

Enter the decimal fraction of the element size used for the minimum permissible distance between nodes created by the FormWorks discretization. As the complexity factor decreases, nodes may be created close the boundary region and other interfering features within the region. A smaller value may result in higher mesh quality for regions having fine boundary

features, such as tight re-entrant corners or small internal angles, or for regions having a layout of reinforcement lines that is congested relative to the element size.

7. In the **Manual Overrides** group, specify the following overrides.

- **Do Not Discretize Boundary**

Check this option to prevent FormWorks from creating additional nodes on the region boundary, other than those specified as intermediate vertices. Use this option to control the boundary discretization.

- **Do Not Discretize Interior**

Check this option to prevent FormWorks from discretizing the interior of the region with additional nodes, other than those specified by reinforcement lines, voids, and line and point constraints. Use this option to control the interior discretization.

- **Do Not Adjust Elmt Size**

Check this option to prevent FormWorks from adjusting the Elmt Size X and Y, regardless of the maximum aspect ratio specified. When using the grid superposition discretization type, utilize this option with the Superposition Corner Origin override to control the placement of the grid.

- **Do Not Refine Near Truss**

For the grid superposition discretization type, check this option to prevent FormWorks from creating nodes offset from vertical and horizontal segments of reinforcement lines. The purpose of the offsetting is to create more regularly spaced rectangular elements near truss elements.

- **Superposition Corner Origin**

For the grid superposition discretization type, specify the corner of the bounding rectangle of the region from which the superposition grid originates. This option has no effect unless the Do Not Adjust Elmt Size option is checked.

8. Click **Add Region** to store the region. The region is added to the list.

To **Modify a Region**, complete the following steps.

1. Select the region in the list box. The selected region appears highlighted and its current attributes are displayed in the entry fields.
2. Modify the attributes of the region. Note that the vertices of the region cannot be changed.
3. Click **Update Region** to store the changes.

To **Delete a Region**, complete the following steps.

1. Select the region in the list box. The selected region appears highlighted and its current attributes are displayed in the entry fields.
2. Click **Delete Region**. The selected region is removed from the list box and disappears from the Workspace. The remaining regions are renumbered. Alternatively, click **Delete All** to remove all defined regions.

10.4.7.2 Reinforcement

The second step is to define **Reinforcement Paths**, if any. Each reinforcement path is defined by a series of line segments, which will be meshed with truss bar elements. If desired, segments of the path can be attached with link or bond elements to the concrete elements. Each reinforcement path can have several layers of truss bar and bond elements, with different material type assignments. The reinforcement path assumes the meshing parameters of the surrounding concrete and the mesh will be constrained to the reinforcement path. The guidelines for defining reinforcement paths are as follows:

- The reinforcement path cannot intersect itself.
- The reinforcement path may traverse boundaries of regions and voids. Reinforcement paths may intersect each other. It is not necessary to define the points of intersection.
- Only segments of paths that are contained inside or on a reinforced concrete region are meshed. To create a bare bar, it is necessary to surround the bar with a region having no material layers.

To **Define a Reinforcement Path**, complete the following steps.

1. Select the **Reinforcement** property page of the **Define and Mesh Structure** property sheet, as shown in Figure 126.

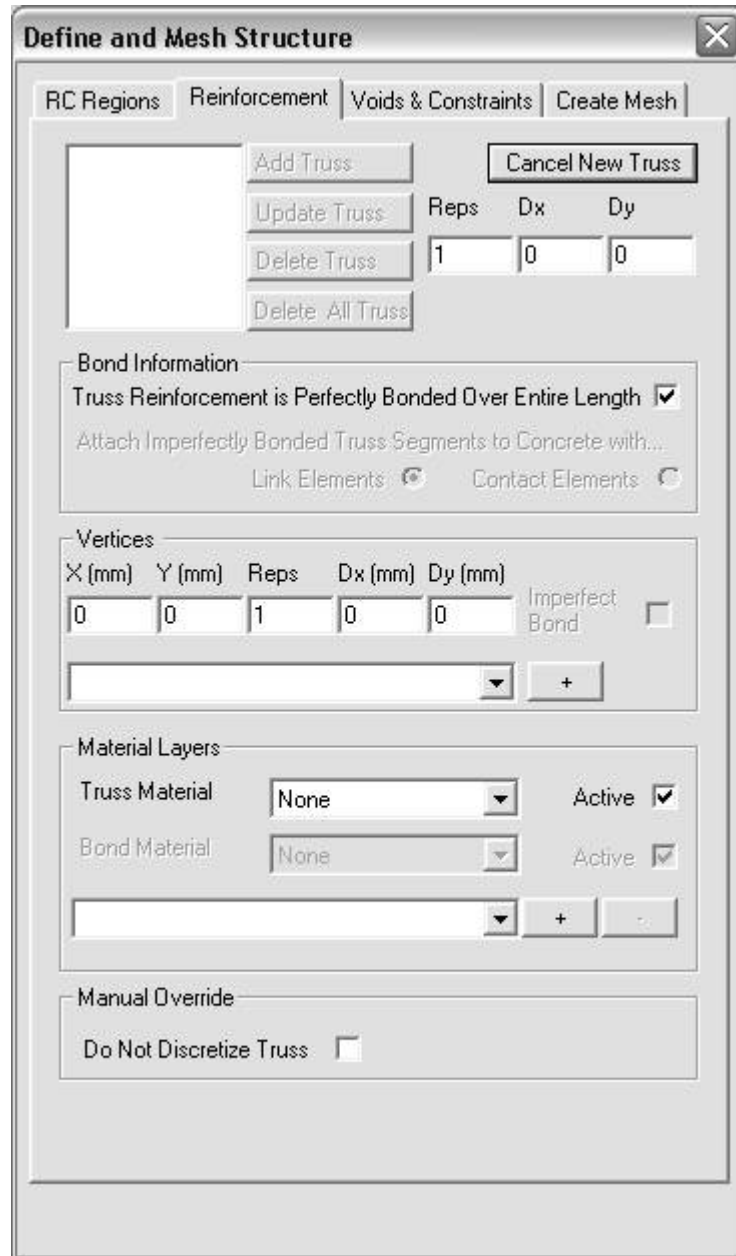


Figure 126: Reinforcement Page

2. Click **Create New Truss** to start a new reinforcement path. To abort the path at any time, click the same button, which is now labeled as **Cancel New Truss**.
3. In the **Bond Information** group, specify the following options.
 - **Truss Reinforcement Is Perfectly Bonded Over Entire Length**

Check this option if the truss bar elements created over the whole reinforcement path are to be connected directly to the nodes of the concrete elements. Uncheck this option if any segment of the path is to be connected with bond elements.

- **Attach Imperfectly Bonded Truss Segments to Concrete with...**

If the above selection is unchecked, select either **Link** or **Contact** elements as the type of bond element for this reinforcement path.

4. In the **Vertices** group, complete the following procedure to define the reinforcement path. An example is shown in Figure 127 to create a rectangle with one restrained edge.
 - i) Enter the following fields to define a vertice of the reinforcement path. It is necessary to define only the vertices at the ends of the path segments. If desired, one can also define intermediate vertices to enforce the location of nodes defining the truss bar elements. Indeed by doing so, and selecting the Do Not Discretize Truss manual override option, it is possible to designate the discretization of all truss bar elements on the path.
 - The **X**, **Y**, **Reps**, **Dx** and **Dy** fields have the same meaning as for defining regions.
 - **Imperfect Bond**

If checked, all truss elements between the current vertice and the next vertice will be connected with bond elements. Only segments between two successive perfectly bonded vertices are attached directly to the concrete elements.
 - ii) Click + after each entry. The reinforcement path is drawn in the Workspace.

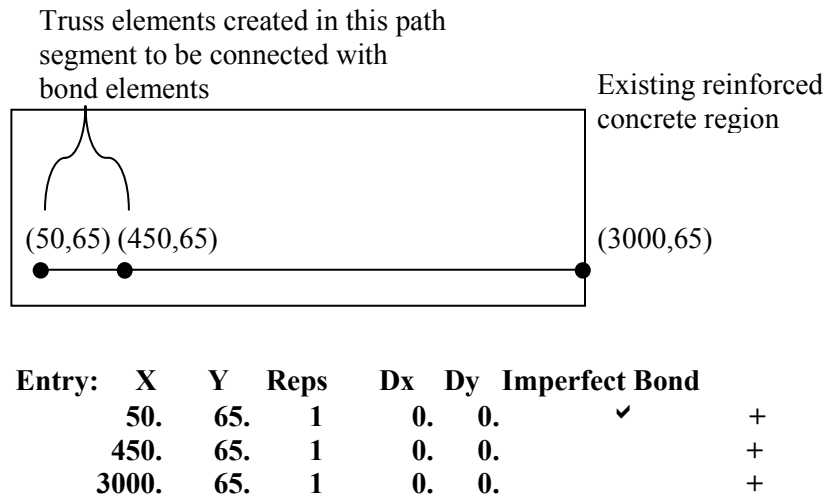


Figure 127: Example of reinforcement path creation

5. In the **Material Layers** group complete the following procedure to add layers of truss bars elements and contact elements (if imperfectly bonded). More than one layer may be added to double mesh the path. Each layer of the reinforcement path may be assigned different reinforcement and bond material types. If **None** is selected, FormWorks creates a layer of elements without any material type assignments. If no layers are added, FormWorks creates no elements, whatsoever.
 - i) In the **Truss Material** drop list, select the reinforcement material type to assign to the truss elements.
 - ii) In the **Bond Material** drop list, select the bond material type to assign to the link or contact elements, if the reinforcement path is not perfectly bonded along its entire length.
 - iii) Click + to add a layer of elements to the reinforcement path with the currently selected material type. (Click – to delete the defined layers from the drop list.)
 - iv) Repeat steps i) to iii) to add additional layers of elements (e.g. double-meshing).
6. In the **Manual Overrides** group, specify the following overrides.
 - **Do Not Discretize Truss**

Check this option to prevent FormWorks from creating additional nodes on the reinforcement path, other than those specified as vertices. Use this option to control the path discretization.

7. Near the top of the page, complete the following entry fields to create multiple reinforcement paths, offset by constant displacements. This is a convenient way to define repetitive reinforcement details, such as beam stirrups and column ties, without having to separately enter the vertices of each reinforcement path.
 - **Reps**
Enter the number of repetitions of the reinforcement path.
 - **Dx**
Enter the translation in the x direction between successive paths, from the defined vertices.
 - **Dy**
Enter the translation in the y direction between successive paths, from the defined vertices.
8. Click **Add Truss** to store the reinforcement path(s). The reinforcement path(s) are added to the list and appear in the Workspace as red lines.

To **Modify a Reinforcement Path**, complete the following steps.

1. Select the reinforcement path in the list box. The selected path appears highlighted and its current attributes are displayed in the entry fields.
2. Modify the attributes of the region. With regard to the path itself, vertices can only be added.
3. Click **Update Truss** to store the changes.

To **Delete a Reinforcement Path**, complete the following steps.

1. Select the reinforcement path in the list box. The selected reinforcement path appears highlighted and its current attributes are displayed in the entry fields.
2. Click **Delete Truss**. The selected reinforcement path is removed from the list box and disappears from the Workspace. The remaining reinforcement paths are renumbered. Alternatively, click **Delete All Truss** to remove all defined reinforcement paths.

10.4.7.3 Voids

The third step is to define **Voids**, if any, in the reinforced concrete regions, if any. As examples, voids may represent an opening such as a window, the space between framing members, or the cavities of cellular structures. Like Concrete Regions, each void is defined as a polygon. No elements of any type are created within the void. The void boundary assumes the meshing parameters of the surrounding concrete.

The guidelines for defining voids are as follows:

- The void is defined by a nontrivial closed polygon.
- The vertices defining the voids are defined in cyclic clockwise order.
- The edges of the void must be simple and not self-intersecting.
- Voids can transverse reinforced concrete regions and reinforcement paths. It is not necessary to define intersection points.

To **Define a Void**, complete the following steps.

1. Select the **Voids & Constraints** property page of the **Define and Mesh Structure** property sheet, as shown in Figure 128.
2. In the **Voids** group, click **Create New Void** to start a new void. To abort the void at any time, click the same button, which is now labeled as **Cancel New Void**.
3. Complete the following procedure to define the void.
 - i) Enter the fields defining the location of the void vertices, in clockwise order. It is necessary to define only the vertices at the ends of the void segments. If desired, one can also define intermediate vertices to enforce the location of nodes on the void boundary. Indeed, by doing so, and selecting the Do Not Discretize manual override option, it is possible to designate the location of all nodes on the void boundary.
 - The **X**, **Y**, **Reps**, **Dx** and **Dy** fields have the same meaning as for defining regions.
 - ii) Click **+** after each vertice entry, except the last. After the last vertice, click **Close**.

Define and Mesh Structure [X]

RC Regions | Reinforcement | Voids & Constraints | Create Mesh

Voids

Add Void Cancel New Void

Update Void

Delete Void Repts Dx Dy

Delete All Voids 1 0 0

X (mm) Y (mm) Repts Dx (mm) Dy (mm)

0 0 1 0 0 + Close

Do Not Discretize

Line Constraints

Add Line Cancel New Line

Update Line

Delete Line Repts Dx Dy

Delete All Lines 1 0 0

X (mm) Y (mm) Repts Dx (mm) Dy (mm)

0 0 1 0 0 +

Do Not Discretize

Point Constraints

Restrain X Y

X (mm) Y (mm) Repts Dx (mm) Dy (mm) Repts Dx (mm) Dy (mm)

0 0 1 0 0 1 0 0

+ - -All

Figure 128: Voids and Constraints

4. Click the **Do Not Discretize** option to prevent FormWorks from creating additional nodes on the void boundary other than those specified as vertices. Use this option to control the void boundary discretization.
5. Near the top of the Void group, complete the following entry fields to create multiple voids, offset by constant displacements. This is a convenient way to define repetitive voids, such as

evenly spaced equal-sized openings in frame structures, without having to separately enter the vertices of each void.

- **Reps**

Enter the number of repetitions of the void.

- **Dx**

Enter the translation in the x direction between successive voids, from the defined vertices.

- **Dy**

Enter the translation in the y direction between successive voids, from the defined vertices.

6. Click **Add Void** to store the void(s). The void(s) are added to the list and appear in the Workspace as polygons composed of dashed blue lines.

To **Delete a Void**, complete the following steps.

1. Select the void in the list box. The selected void appears highlighted and its current attributes are displayed in the entry fields.
2. Click **Delete Void**. The selected void is removed from the list and disappears from the Workspace. The remaining voids are renumbered. Alternatively, click **Delete All Voids** to remove all defined voids.

10.4.7.4 Line Constraints

The fourth step is to define **Line Constraints**, if any, in the reinforced concrete regions. Line constraints are used to create material type boundaries or any other type of conformal edge inside within the reinforced concrete region. FormWorks constrains element edges to line-up with line constraints. As such, it is not necessary to define reinforced concrete regions for every localized change in material type. Instead, larger regions containing several regions can be defined and different material types can be assigned within the region after the mesh is created. Line constraints assume the meshing parameters of the surrounding concrete. The guidelines for creating line constraints are the same as those for reinforcement paths.

To **Define a Line Constraint**, complete the following steps.

1. Select the **Voids & Constraints** property page of the **Define and Mesh Structure** property sheet, as shown in Figure 128.
2. In the **Line Constraints** group, click **Create New Line** to start a new line constraint. To abort the constraint at any time, click the same button, which is now labeled as **Cancel New Line**.
3. Define a line constraint in the same manner that reinforcement paths are created, by entering the location of vertices and clicking +.
4. Click the **Do Not Discretize** box to prevent FormWorks from creating nodes along the line constraint, other than those specified as vertices. Use this option to control the line constraint discretization.
5. Near the top of the Line Constraints group, complete the **Reps**, **Dx**, and **Dy** entry fields to create multiple line constraints, offset by constant displacements. This is a convenient way to define repetitive line constraints, without having to separately enter the vertices of each line constraint.
6. Click **Add Line** to store the line constraint(s). The line constraint(s) are added to the list and appear in the Workspace as dashed green lines.

To **Delete a Line Constraint**, complete the following steps.

1. Select the line in the list box. The selected line appears highlighted and its current attributes are displayed in the entry fields.
2. Click **Delete Line**. The selected line is removed from the list and disappears from the Workspace. The remaining lines are renumbered. Alternatively, click **Delete All Lines** to remove all defined line constraints.

10.4.7.5 Point Constraints

The fifth step is to define **Point Constraints**, if any, in the reinforced concrete regions. A node is always created at the location of a point constraint. Point constraints have three possible uses. First, point constraints can be used to specify the exact locations of restraints, nodal loads or support displacements

acting on the structure. Second, point constraints can be used to locally refine a mesh by placing nodes at a finer resolution than the specified element sizes for enclosing reinforced concrete region. Finally, it is possible to fully control the mesh discretization by specifying the location of all nodes with point constraints and selecting the Do Not Discretize override options in the preceding sections. This technique would resemble the Manual Method for creating nodes and elements, except that neither the nodes nor elements need to be manually numbered. The guidelines for creating point constraints are as follows:

- Point Constraints may be placed anywhere, including a reinforced concrete region, on region boundaries, on reinforcement paths, on void boundaries, or on line constraints.
- Point constraints that are not inside a reinforced concrete region are ignored.

To **Define Point Constraints**, complete the following steps.

1. In the **Point Constraints** group, complete the following fields. Figure 129 shows an example.

- **X**

Enter the x coordinate of the point constraint, in millimeters.

- **Y**

Enter the y coordinate of the point constraint, in millimeters.

- **Reps**

Enter the number of points in the row/column.

- **Dx**

Enter the spacing of successive points of a row/column in the x direction, in millimeters.

- **Dy**

Enter the spacing of successive points of a row/column, in the y direction, in millimeters.

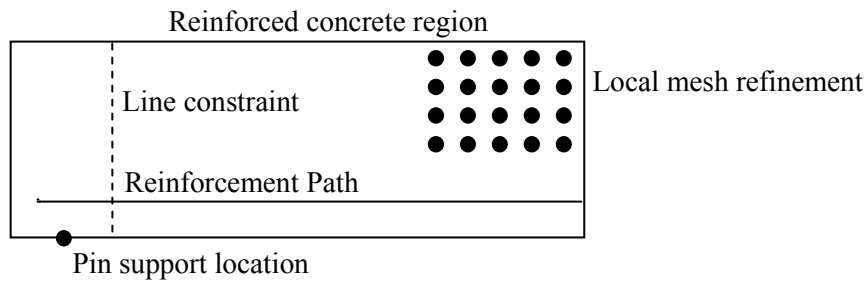
- **Restrain X**

Check this option to create a support restraint in the x direction for the point constraint(s).

- **Restrain Y**

Check this option to create a support restraint in the y direction for the point constraint(s).

2. Click + to store the point constraint(s). Point constraints appear in the Workspace as green dots.



| Entry: | X | Y | Reps | Dx | Dy | Reps | Dx | Dy | Restrain |
|--------|-------|------|------|-----|----|------|----|-----|-----------|
| | 100. | 0. | 1 | 0. | 0. | 1 | 0. | 0. | X ✓ Y ✓ + |
| | 2750. | 800. | 5 | 50. | 0. | 4 | 0. | 50. | X Y + |

Figure 129: Example of point constraint creation

To **Delete a Point Constraint**, complete the following steps.

1. Select the point constraint in the drop list. The selected point constraint appears highlighted.
2. Click **-**. The selected point is removed from the list and disappears from the Workspace. Clicking **-** will remove point constraints one at a time. Alternatively, click **-All**, to remove all the point constraints at once.

10.4.7.6 Generating the Mesh

Once the concrete regions, reinforcement paths, voids, line constraints and point constraints have been defined, the mesh can be generated.

To **Generate the Mesh**, complete the following steps.

1. Select the **Create Mesh** property page of the **Define and Mesh Structure** property sheet, as shown in Figure 130.

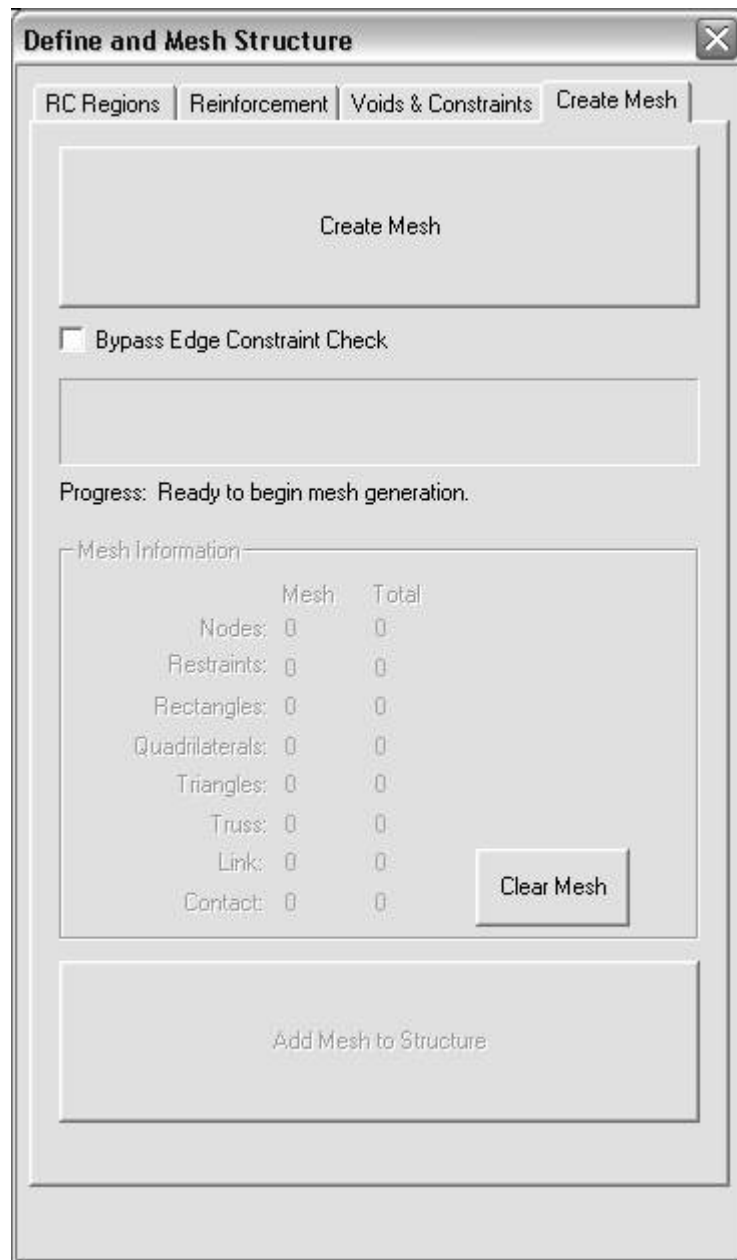


Figure 130: Mesh Creation Page

2. Check the **Bypass Edge Constraint Check** to speed-up the meshing process by not explicitly checking the conformity of element edges with the various boundaries and constraints. Generally, this option should not be checked, especially for regions that are not strictly convex.
3. Click **Create Mesh**. The meshing generation proceeds until complete as indicated by the status bar. In the **Mesh Information** group, the **Mesh** column indicates the number of nodes, elements and restraints required by the meshed region. The **Total** column indicates these values plus the

- number of nodes, elements and restraints already defined in the Structure Data. The **Limit Check** indicates whether the Structure Limits have been exceeded.
4. Inspect the resulting mesh in the Workspace view. If the Structure Limits have been exceeded or elements are misshapen, modify the meshing parameters or redefine the regions, reinforcement paths, voids, and constraints as necessary. Then, repeat Steps 1 to 3. When using the Grid Superposition method or Division Point Insertion discretization types, judiciously adding point constraints often provides a simple correction.
 5. If the mesh is acceptable, click **Add Mesh to Structure** and close the **Define and Mesh Structure** property sheet. The nodes, elements and restraints are then stored in the Structure Data. The regions, reinforcement paths, voids and constraints are stored for future revision whenever the Define and Mesh Structure property sheet is reopened.
 6. If necessary, refine material type assignments and add support restraints to the new mesh using the **Manual Method** to complete the Structure Data.

11 The Load Case Data

The third step in creating the input is to define the data for one or more load cases. As previously described, all the loads belonging to a load case are multiplied by the load factors defined for that load case in the Job Data.

11.1 Load Limits

VecTor2 limits the number of loads acting on nodes and elements in each load case. These limits vary with the version of VecTor2. To view these limits, select the **Load/Load Limits** menu item. The **Load Limits** dialog box appears as shown in Figure 131.

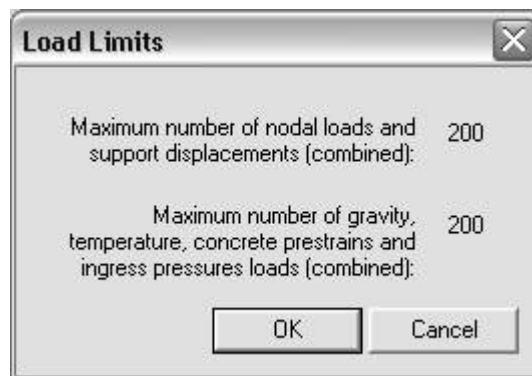


Figure 131: Load Limits Dialog Box

11.2 Selecting the Load Case



Before assigning any loads, select the **Load/Select**

Load Case [n] menu item or click the **Load Case [n]** tool bar button to choose the load case to which the loads will be added. Only the load cases that are active in the Job Data may be selected.

11.3 Load Information

Select the **Load/Load Information** menu item or click the **Load Information** toolbar button to view the number of defined loads of each type for the current load case. The **Load**



Information dialog appears as shown in Figure 132.

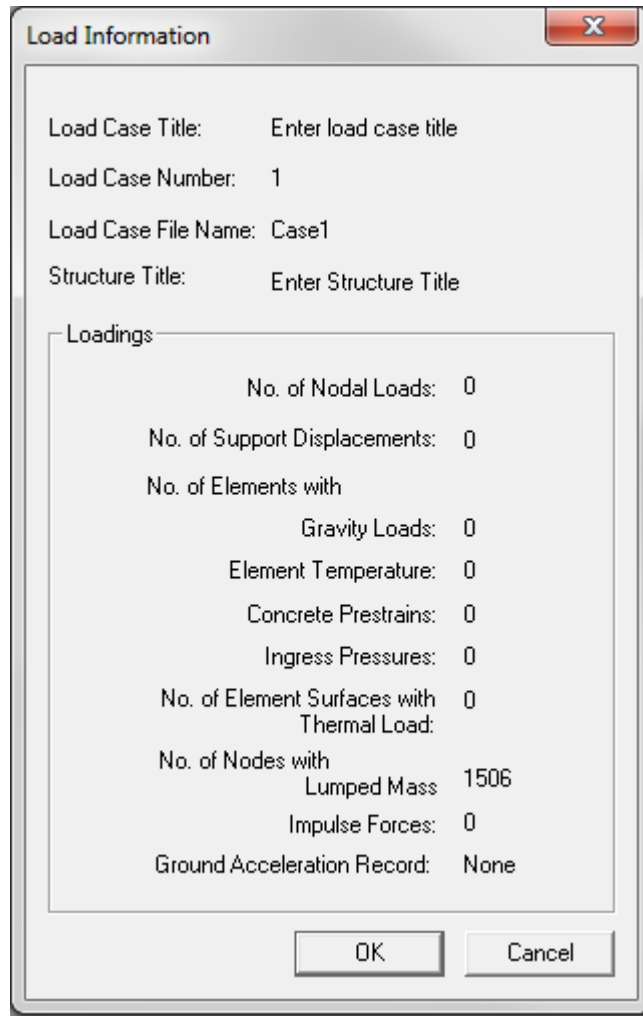


Figure 132: Load Information Dialog Box

11.4 Nodal Loads



These loads are concentrated forces acting in either the x or y directions, on individual nodes.

To **Add Nodal Loads**, complete the following procedure.

1. Select the **Load/Apply Nodal Loads** menu item or click the **Nodal Loads** toolbar button. The **Apply Nodal Loads** dialog box appears as shown in Figure 133.

| Case | node | Fx | Fy | # nodes | d node | d Fx | d Fy | Total |
|------|------|----|----|---------|--------|------|------|-------|
| 1 | 1 | 0 | 0 | 1 | 1 | 0 | 0 | 0 |

Figure 133: Apply Nodal Loads Dialog Box

- Specify the nodes and nodal loads by one of the following two methods.

To Select Nodes by Node Number

Complete the **Node**, **#nodes** and **dnode** entry fields to select the desired nodes. The node selection method is similar to specifying node numbers when creating nodes. Specify the loads.

- **Fx**

Enter the force acting on **Node** in the x direction, in kN. Positive values act in the direction of the positive x axis, while negative values act towards the negative x axis.

- **Fy**

Enter the force acting on **Node** in the y direction, in kN. Positive values act in the direction of the positive y axis, while negative values act towards the negative y axis.

- **dFx**

Enter the increment of the force **Fx**, acting on successively selected nodes, in kN.

- **dFy**

Enter the increment of the force **Fy**, acting on successively selected nodes, in kN.

Alternatively, to Select Nodes with the Mouse:

Click **Select**. The mouse cross-hairs become a pick arrow. Position the pick arrow over nodes to be selected and click the **left** mouse button. The selected nodes are highlighted in bright green.

Enter the values for **Fx** and **Fy**, as described above. The same force is applied to all selected nodes.

- Click **Apply** or type **Enter**. The applied nodal loads are drawn in the Workspace and added to the drop list in the dialog box.

Nodal loads can be modified by repeating the above procedure. Previously applied nodal loads will be overwritten. Nodal loads can be deleted by selecting them either from the drop list or by using the mouse, then clicking **Delete**.

11.5 Support Displacements



These loads are imposed displacements of nodes of the structure.

Select the **Load/Apply Support Displacements** menu item or click the **Support Displacements** toolbar button. The **Apply Support Displacements** dialog box appears as shown in Figure 134.

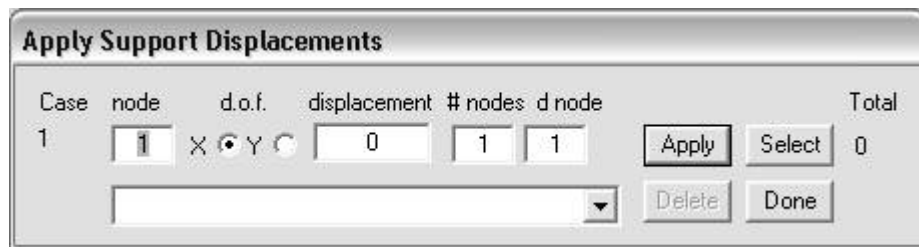


Figure 134: Apply Support Displacements Dialog Box

The procedure for adding support displacements is similar to that for adding nodal loads. The unique entry fields are described as follows.

- **D.O.F. X,Y**

Select either the X or Y direction for the nodal displacement. Separate entries must be made to displace the node in both degrees of freedom.

- **Displacement**

Enter the imposed displacement of the nodes, in millimeters. Enter positive values for displacements in the direction of the positive X or Y axis, and negative values for displacements in the direction of the negative X or Y axis.

11.6 Gravity Loads



Gravity loads are applied to rectangular, quadrilateral and triangular elements to include the weight, W , of the element, as follows.

$$W_x = +GX \cdot 9.81 \cdot \rho \cdot V \quad (11.6.1a)$$

$$W_y = -GY \cdot 9.81 \cdot \rho \cdot V \quad (11.6.1b)$$

where, W_x and W_y are the components of the weight acting in the X and Y directions, respectively, GX and GY are the G-forces acting in the X and Y directions, respectively, ρ is the mass density of the reinforced concrete, and V is the volume of the element. The weight components are then evenly distributed as nodal loads among the nodes of the element.

To **Apply Gravity Loads**, complete the following procedure.

1. Select the **Load/Apply Gravity Loads** menu item or click the **Gravity Loads** toolbar button.

The **Apply Gravity Loads** dialog box appears as shown in Figure 135.

| Case | elmt | DENS (kg/m3) | GX | GY | # elmts | d elmt | # elmts | d elmt | Total |
|------|------|--------------|----|----|---------|--------|---------|--------|-------|
| 1 | 1 | 0 | 0 | 1 | 1 | 1 | 1 | 1 | 0 |

Figure 135: Apply Gravity Loads Dialog Box

2. Specify the elements and gravity loads by one of the following methods:

To Select Elements by Element Number

Complete **Elmt**, **#elmts** and **delmt** entry fields to select the desired concrete elements. The element selection method is similar to specifying element numbers when creating elements.

Specify the loads.

- **Dens**

Enter the mass density of the reinforced concrete element, in kg/m^3 .

- **Gx**

Enter the G-force acting in the x direction. Enter positive values for gravity forces acting in the direction of the positive x-axis. (If the x-axis of the Workspace is parallel to the ground, this value is typically zero. Otherwise, if the coordinate axis has been rotated so that the x-axis is not parallel to the ground, a nonzero value can be used to specify a component of the gravitational force.)

- **Gy**

Enter the G-force acting in the y direction. Enter positive values for gravity forces in the direction of the *negative* Y-axis. (If the y-axis is perpendicular to the ground, this value is typically positive one. Otherwise, if the coordinate axis has been rotated so that the y-axis is not perpendicular to the ground, a nonzero value can be used to specify a component of the gravitational force.)

Alternatively, to Select Elements with the Mouse:

Click **Select**. The mouse cross-hairs become a pick arrow. Click the **left** mouse button and drag the pick arrow over the elements to be selected. The selected elements are highlighted in bright green. Enter the values for **Gx**, **Gy** and **Dens** as described above.

3. Click **Apply** or type **Enter**. The applied gravity loads are drawn in the Workspace and added to the drop list in the dialog box.

Gravity loads can be modified by repeating the above procedure. Previously defined gravity loads will be overwritten. Gravity loads are deleted by selecting them either from the drop list or by using the mouse, then clicking **Delete**.

11.7 Temperature Loads



Temperature loads are applied to rectangular, quadrilateral, and triangular elements and truss bar elements. The applied temperature loads model only expansion and contraction effects of temperature gradients. VecTor2 incorporates temperature loads by converting them to elastic strain offsets, as follows:

$$\begin{bmatrix} \varepsilon_{cx}^o & \varepsilon_{cy}^o & \gamma_{cxy}^o \end{bmatrix}^T + = [\alpha_c \cdot \Delta T \quad \alpha_c \cdot \Delta T \quad 0]^T \quad (11.7.1)$$

$$\varepsilon_s^o = \alpha_s \cdot \Delta T \quad (11.7.2)$$

where ε_c^o and ε_s^o are elastic strain offsets for the concrete and reinforcement, respectively, α_c and α_s are the coefficients of thermal expansion for concrete and reinforcement (defined as material properties) and ΔT is the temperature load acting on the element.

Select the **Load/Apply Temperature Loads** menu item or click the **Element Temperature** toolbar button. The **Apply Temperature Loads** dialog box appears as shown in Figure 136.

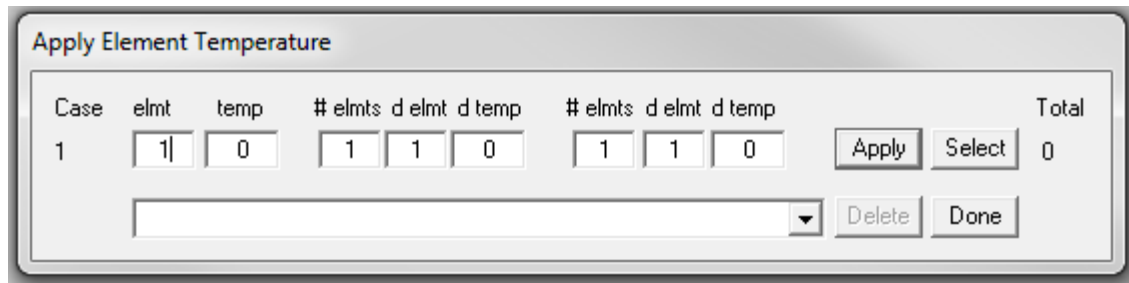


Figure 136: Apply Temperature Loads Dialog

The procedure for adding temperature loads is similar to that for adding gravity loads. The unique entry fields are described as follows.

- **Temp**

Enter the temperature, ΔT , of the source element with respect to the temperature of unloaded elements, in °C.

- **dtemp**

Enter the increment in temperature, in °C, between successive elements in the row/column.

Temperature loads can be modified by repeating the above procedure. Previously defined temperature loads will be overwritten. Temperature loads are deleted by selecting them either from the drop list or by using the mouse, then clicking **Delete**.

11.8 Concrete Prestrains



Concrete prestrain loads are applied to rectangular, quadrilateral and triangular elements. Example applications of concrete prestrains include negative shrinkage strains or positive expansive strains due to alkali-aggregate reactivity. VecTor2 directly incorporates the prestrain load as an elastic strain offset as follows:

$$\begin{bmatrix} \varepsilon_{cx}^o & \varepsilon_{cy}^o & \gamma_{cxy}^o \end{bmatrix}^T + = \begin{bmatrix} \varepsilon_{ps} & \varepsilon_{ps} & 0 \end{bmatrix}^T \quad (11.8.1)$$

where ε_c^o is elastic strain offsets of the concrete, and ε_{ps} is the applied prestrain load. As such, the load translates the concrete stress-strain response by a strain amount equal to the specified prestrain.

Select the **Load/Apply Concrete Prestrains** menu item or click the apply **Concrete Prestrains** toolbar button. The **Apply Concrete Prestrains** dialog box appears as shown in Figure 137.

| Case | elmt | strain | # elmts | d elmt | d strain | # elmts | d elmt | d strain | Total |
|------|------|--------|---------|--------|----------|---------|--------|----------|-------|
| 1 | 1 | 0 | 1 | 1 | 0 | 1 | 1 | 0 | 0 |

Figure 137: Apply Concrete Prestrains Dialog Box

The procedure for applying, modifying and deleting concrete prestrain loads is similar to that for applying temperature loads. The unique entry fields are described as follows:

- **Strain**

Enter the prestrain value, in millistrain. For instance, enter a negative value for shrinkage strains.

- **d strain**

Enter the increment in prestrain between successive elements in a row/column.

11.9 Ingress Pressures



Ingress pressure loads are applied to rectangular, quadrilateral and triangular elements.

When the element is cracked, the pressure acts on the out-of-plane dimension in a hydrostatic state.

VecTor2 multiplies the specified pressure by the out-of-plane area of each edge of the membrane element to determine equivalent nodal loads in the x and y directions.

Select the **Load/Apply Ingress Pressures** menu item or click the Ingress Pressures toolbar button. The **Apply Ingress Pressures** dialog box appears as shown in Figure 138.

| Case | elmt | pressure | # elmts | d elmt | d pressure | # elmts | d elmt | d pressure | Total |
|------|------|----------|---------|--------|------------|---------|--------|------------|-------|
| 1 | 1 | 0 | 1 | 1 | 0 | 1 | 1 | 0 | 0 |

Buttons: Apply, Select, Delete, Done

Figure 138: Apply Ingress Pressures Dialog Box

The procedure for applying, modifying and deleting ingress pressures is similar to that for applying temperature loads. The unique entry fields are described as follows:

- **Pressure**

Enter the ingress pressure acting on the element, in MPa.

- **dPressure**

Enter the increment in ingress pressure between successive elements selected in a row/column.

11.10 Nodal Thermal Loads



Nodal thermal loads are time varying temperature loads applied to the surface of rectangular,

quadrilateral, and triangular elements. These loads are to be used with the **time step** analysis mode.

Types of Thermal Loads

In VecTor2, there are 5 types of thermal loads, specified in FormWorks by entering type number 1-5 in the **Apply Nodal Thermal Loads** dialog box. The different thermal profiles are outlined in Figure 139.

| Load Type | Entry Fields in Load File | | | | | | | | Load Plots |
|-----------|--------------------------------------------------------------------------------------------------------------------------------------------------------------------------------------------------------------------------------------------------------------------------------------------------------------------------------------------------------------------------------------------------------------------------------------------------------------|------|-----|-----|-----|-----|-----|-----|------------------------------------------------------------------------------------------------------------------------------------------------------------------------|
| | Node | Type | Tm1 | Tp1 | Tm2 | Tp2 | Tm3 | Tp3 | |
| 1 | + | 1 | | + | | | | | <p><u>Steady-State</u> Constant Tp1</p> |
| 2 | + | 2 | + | + | + | + | + | + | <p><u>Three-Key-Node Linear Model</u> (Tm1, Tp1) (Tm2, Tp2) Constant (Tm3, Tp3)</p> |
| 3 | + | 3 | + | + | + | + | | | <p><u>Compartment Simplified Fire Model</u> Horizontal growth Symmetrical decay (Tm2, Tp2) = (3h, 1064C) Full development (Tm1, Tp1) = (30s, 255C)</p> |
| 4 | + | 4 | | | | | | | <p><u>ASTM-E119 Fire Model</u> $T = 20 + 750(1 - e^{-3.79553\sqrt{t}}) + 170.41\sqrt{t}$</p> |
| 5 | + | 5 | | | | | | | <p><u>ISO-834 Fire Model</u> $T = 20 + 345 \log_{10}(480t + 1)$</p> |
| Notes: | <ol style="list-style-type: none"> 1. "+" indicates the field that is used in load definition; 2. Load types 2-5 are transient analyses while type 1 is steady-state one. 3. Full development curve in load type 3 is based on ASTM-E119 during the range of 255C-1064C; and the decay curve is symmetrical with development one about the peak point. 4. Standard fire curves in load types 4 and 5 have no ends. | | | | | | | | |

Figure 139: Thermal profiles in VecTor2 (Zhou, 2004)

To apply **Nodal Thermal Loads**, complete the following steps.

1. Click the **Nodal Thermal Loads** toolbar button. The **Apply Nodal Thermal Loads** dialog box appears as shown in Figure 140.
2. Specify the nodal thermal loads by one of the following methods.

| Case | node | type | Tm1 | Tp1 | Tm2 | Tp2 | Tm3 | Tp3 | # nodes | d node | # nodes | d node | Total |
|------|------|------|-----|-----|-----|-----|-----|-----|---------|--------|---------|--------|-------|
| 1 | 1 | 1 | 0 | 0 | 0 | 0 | 0 | 0 | 1 | 1 | 1 | 1 | |

Figure 140: Apply Nodal Thermal Loads Dialog Box

To Select Surfaces by Node Number

Complete the **Node**, **#Nodes**, and **dNode** inputs to select the desired concrete elements. Specify the **Type** of thermal load, and the applicable **Tmi** and **Tpi**.

Alternatively, to Select Surfaces with the Mouse:

Click **Select**. The mouse cross-hairs become a pick arrow. Position the pick arrow over the free surfaces of the structure to be selected and click the left mouse button. The selected free-surfaces are highlighted in bright green. Enter the **Type** of thermal load, and required **Tmi** and **Tpi**.

Note that for thermal load types 4 and 5, the standard fire models, require no user input of time-temperature data.

3. Click **Apply** or type **Enter**. The applied nodal thermal loads are drawn in the Workspace and added to the drop list in the dialog box.

Nodal thermal loads can be modified by repeating the above procedure. Previously defined nodal thermal loads will be overwritten. Nodal thermal loads are deleted by selecting them either from the drop list or by using the mouse, then clicking **Delete**.

11.11 Lumped Masses

Impact loads can be modeled with lumped masses when the structural mass is known; this is typically the case where dropped weights are used. When modeling lumped masses, the structural mass is lumped at the nodes, and is specified using the *Apply Lumped Masses* option in FormWorks. The most general way to calculate the nodal masses is to calculate the mass of an element and divide it by the number of nodes; more than one element can contribute to an individual nodal mass. Currently in VecTor2, the density entered in the *Concrete Material Properties* section is not converted to nodal mass automatically, but is included as static self-weight loads. If a non-zero GF-X or GF-Y is specified for the lumped mass, and the default concrete density is assumed, the self-weight will have been double counted. It is recommended that when using non-zero static load multipliers with lumped masses, that a very small positive density be used to avoid double counting.

To **Apply Lumped Masses**, complete the following procedure.

1. Select the **Load/Apply Lumped Masses** menu item or click the **Lumped Masses** toolbar button. The **Apply Lumped Masses** dialog box appears as shown in Figure 141.

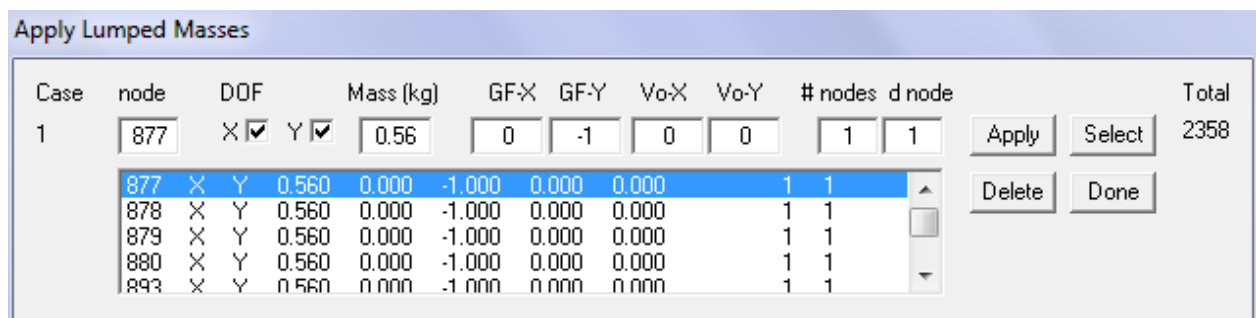


Figure 141: Apply Lumped Masses Dialog Box

2. Specify the nodes and lumped masses by one of the following methods:

To select nodes by node number

Complete **Node**, **#Nodes**, and **dNodes** entry fields to select the desired nodes. Specify the loads.

- **DOF-X**

If the mass is activated in the x-direction, check this box. Otherwise, leave it unchecked.

- **DOF-Y**

If the mass is activated in the y-direction, check this box. Otherwise, leave it unchecked.

- **Mass (kg)**

Enter the nodal mass in kg.

- **GF-X**

Enter the multiplier for the static load in the x-direction. This converts the nodal mass to a force and applies it as a static load in the x-direction. Typically, values of +1 or -1 are used to consider self-weight. For the conversion into a force, $g=9.81 \text{ m/s}^2$ is used.

- **GF-Y**

Enter the multiplier for the static load in the y-direction. In order to specify a gravity load downward, the direction must be specified as -1.

- **V₀-X**

Enter the contact velocity (the initial velocity) of the lumped mass in the x-direction.

- **V₀-Y**

Enter the contact velocity of the lumped mass in the y-direction. A downward velocity is specified with a negative.

Alternatively, to Select Nodes with the Mouse:

Click **Select**. The mouse cross-hairs become a pick arrow. Click the **left** mouse button and drag the pick arrow over the elements to be selected. The selected elements are highlighted in bright green. Enter the values for **DOF-X**, **DOF-Y**, **Mass (kg)**, **GF-X**, **GF-Y**, **V₀-X**, and **V₀-Y** as described above.

Lumped masses can be modified by repeating the above procedure. Previously defined lumped masses will be overwritten. Lumped masses can be deleted by selecting tem from the drop list or by using the mouse, then clicking **Delete**.



11.12 Impulse Forces

Impulse loads are time varying nodal forces. In VecTor2, up to 20 impulse forces can be input for a given node, and VecTor2 does not make any assumptions about the force returning to zero. VecTor2 does assume that the impulse starts at $t=0$ at $F=0$ kN, and will connect the origin to the first point with a straight line. After defining the impulse in FormWorks, there is the option to display the impulse force for a given node, as shown below.

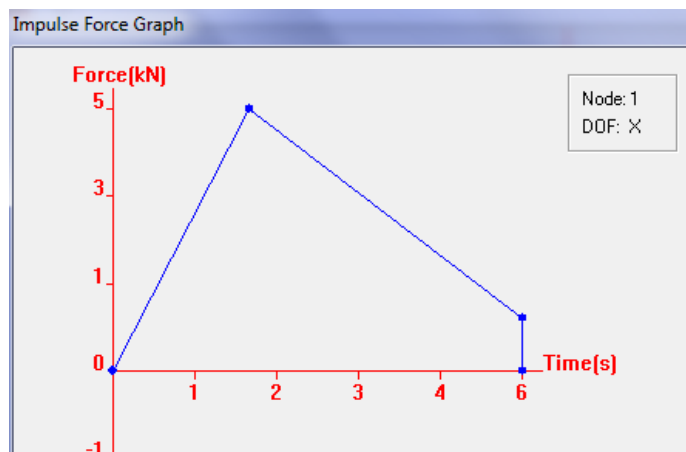


Figure 142: Impulse forces in VecTor2

When modeling the impulse from a blast, if the impact load-time history is not previously known, VecTorBlast can be used to determine the impulse forces at different locations of the structure.

Note that for impulse loads, nodal/lumped masses must be specified in order for a dynamic analysis to occur. The lumped masses do not need to be assigned any initial speed or acceleration, however, masses only need to be assigned to the required nodes.

Select the **Load/Apply Impulse Loads** menu item or click the **Impulse Loads** toolbar button.

The **Apply Impulse Loads** dialog box appears as shown in Figure 143. The figure shows the points that must be input to produce the graph shown in Figure 142.

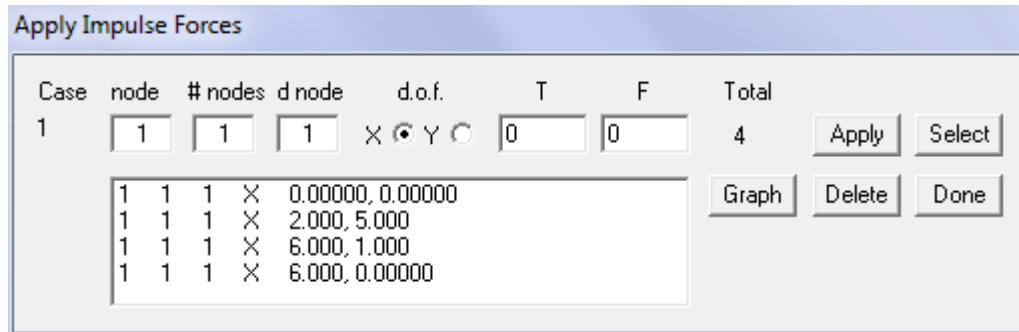


Figure 143: Apply Impulse Forces Dialog Box

The procedure for applying impulse loads is similar to that for applying nodal loads and support displacements. The unique entry fields are described as follows.

- **dof**

Select either the x or y direction in which the impulse force acts.

- **Ti**

Enter the time, in seconds, corresponding **Fi**.

- **Fi**

Enter the force, in kN, corresponding **Ti**. Positive forces act in the direction of the positive axes.

Impulse loads can be modified by repeating the above procedure. Previously defined impulse loads will be overwritten. Impulse loads are deleted by selecting them either from the drop list or by using the mouse, then clicking **Delete**.

Note: A total of 20 points can be defined for each node.



11.13 Ground Acceleration Loads

Ground acceleration loads may be specified to subject the structure to seismic-type loads. As mentioned previously, there are two methods for specifying the ground acceleration in VecTor2. Ground acceleration in terms of time and x- and y-accelerations can be input through FormWorks using the *Apply Ground Acceleration Load* window. Alternatively, ground acceleration can be input using a VECTOR.EQR file.

To specify user-defined **Ground Acceleration Loads**, complete the following steps.

1. Select the **Load/Apply Ground Acceleration** menu item or click the **Ground Acceleration** toolbar button. The **Apply Ground Acceleration** dialog box appears as shown in Figure 144.

| Case | Time [s] | Acc X [m/s ²] | Acc Y [m/s ²] |
|------|----------|---------------------------|---------------------------|
| 1 | 0 | 0 | 0 |

Buttons: Apply, Delete, Done

Figure 144: Apply Ground Acceleration Load Dialog

2. Specify the ground acceleration record by completing the following fields.
 - **Time**
Enter the time, in seconds.
 - **Acc X, Y**
Enter the ground acceleration in the x and y directions, in m/s², occurring at the above time.
3. Click **Add** or type **Enter**.
4. Repeat Steps 2 to 4 to enter the remainder of the ground acceleration record. The acceleration record should conclude with a final entry with a time of 99 999 seconds.

Ground accelerations can also be specified using the **VECTOR.EQR file**.

The earthquake record should be available online as a text file. Online earthquake record databases include:

Pacific Earthquake Engineering Research Center-Ground Motion Database

<http://peer.berkeley.edu/smcat/>

Pacific Earthquake Engineering Research Center: NGA Database

<http://peer.berkeley.edu/nga/>

Incorporated Research Institutions for Seismology

<http://www.iris.edu/>

Cosmos Virtual Data Center

<http://db.cosmos-eq.org>

After downloading the earthquake record, it must be renamed as VECTOR.EQR and put in the same folder as the other input files. The VECTOR.EQR file must be of the following format (Saatci and Vecchio, 2007):

```

VECTOR.EQR - Notepad
File Edit Format View Help
1 4
2 "NORTHRIDGE EARTHQUAKE - SANTA MONICA, CITY HALL GROUNDS"
3 "JANUARY 17, 1994, 04:31 PST"
4 "CORRECTED ACCELEROGRAM, CHANNEL 1, 90 DEGREES, CDMG QN94A538"
5 "SOURCE: NISEE, U.C. BERKELEY, CALIFORNIA"
6 3000 0.02 8 CM
7 3000 0.02 8 CM
8 3000 0.02 8 CM
9 3000 POINTS OF ACCEL DATA EQUALLY SPACED AT .020 SEC. (UNITS: CM/SEC/SEC)
10 2.321 1.647 .854 -.188 -1.492 -.155 1.559 1.468
11 1.468 .234 -1.725 -.507 .331 .014 1.031 1.911

```

Figure 145: input file format of VECTOR.EQR file

1. Number of lines to be skipped containing supplementary information.
2. Lines containing supplementary information.
3. Information: total number of data points, time increment, number of data points/row, data unit

4. Three lines to be skipped. (contain supplementary info)
5. Acceleration data for earthquake event in row-wise order.

Note that when the ground acceleration is entered using the VECTOR.EQR file, the *Ground Acceleration* option in the *Auxiliary* tab of the *Define Job* window must be set to “Considered”. Further, no Ground Acceleration Record should be specified in FormWorks when using a VECTOR.EQR file.

12 Running VecTor2

Once the Job, Structure and Load Case Data have been properly defined, it is possible to start the VecTor2 analysis. Complete the following steps to proceed with the VecTor2 analysis.

12.1 Starting the Analysis

1. As described in Section 8.4.3, save the FormWorks Workspace file by selecting the **File/Save** menu item or clicking the **Save** toolbar item. It is recommended that **.FWK** file be saved in the directory containing the FormWorks application.
2. Select the **Analysis/Run VecTor2 Processor** menu item or click the **Run VecTor2 Processor** toolbar button.
3. FormWorks presents the option to attempt to reduce the bandwidth. A reduced bandwidth decreases the computation time by renumbering the nodes in a more computationally efficient manner. If **No** is selected, proceed to Step 4. If **Yes** is selected the **Bandwidth Reduction** dialog appears as shown in Figure 146. Complete the following procedure.

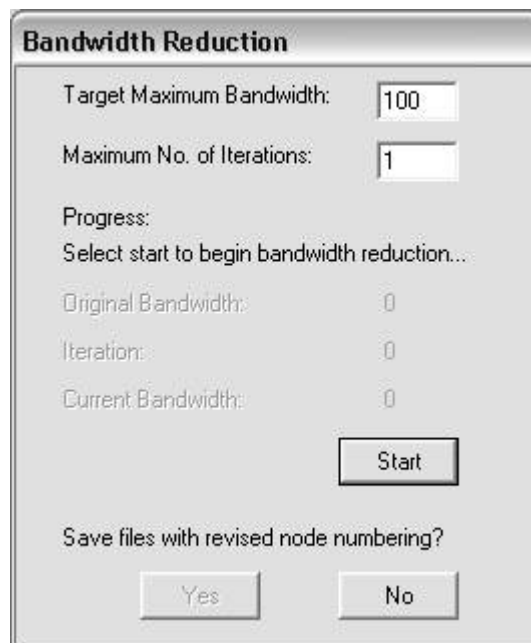


Figure 146: Bandwidth Reduction Dialog Box

- i) Click **Start**. FormWorks determines the bandwidth of the mesh and displays it as **Original Bandwidth**.
 - ii) Enter a value for the **Target Maximum Bandwidth**. Choose a trial value less than the original bandwidth.
 - iii) Enter a value for the **Maximum No. of Iterations**. This controls how many iterations FormWorks attempts before pausing the bandwidth reduction algorithm. Begin with a value approximately equal to one tenth of the number of nodes in the structure.
 - iv) Click **Resume**. The bandwidth reduction proceeds and stops when either the bandwidth is less than the Target Maximum Bandwidth, or the Maximum Number of Iterations is reached.
 - v) Inspect the **Current Bandwidth** of the structure. The iterative bandwidth reduction algorithm used by FormWorks may converge slowly for some numbering schemes, resulting in an initial increase of bandwidth followed by substantial reductions. In this case, additional iteration is required. For some numbering schemes, it may actually increase the bandwidth. In this case, click **No** and proceed to Step 4.
 - vi) Repeat steps ii to v, and until an acceptable bandwidth is achieved or further iterations do not reduce the bandwidth.
 - vii) If the bandwidth reduction is acceptable, click **Yes**. Otherwise, click **No** to proceed with the original node numbering.
4. The **Save Job File** dialog appears. The job file must be saved as **Vector.job** for analysis. Select the directory corresponding to that containing the FormWorks and VecTor2 program and click **Save**.
 5. The **Save Structure File** dialog appears. Accept the structure file name, as assigned in the Job Data. Click **Save**.
 6. For each load case, the Save Load Case File dialog appears. Accept the load case file name, as assigned in the Job Data. Click **Save**.

The VecTor2 analysis proceeds as shown in Figure 147. Providing there are no errors in the input, the analysis proceeds until all specified load steps are performed, or until the stiffness matrix is no longer invertible.

```

C:\PROGRA~1\VecTor2\WT2.EXE
*
*          LOAD STAGE No.: 1
*          Load case          Factor
*          BM100              0.000
*
*
*          Iteration          Convergence
*          1                  1.000000
*          2                  1.000000
*
* STORING LOAD STAGE RESULTS IN ASCII FILE:  BM_01.A2E
*
*
*          LOAD STAGE No.: 2
*          Load case          Factor
*          BM100              0.100
*
*
*          Iteration          Convergence
*          1                  1.046236

```

Figure 147: VecTor2 Analysis Proceeding

12.2 Example 1: Simply Supported Beam

A simple example is presented in this section for the FormWorks modeling procedure. This example is not intended to rigorously analyze and interpret the results, but rather to illustrate a possible means of discretization and model selection.

It is proposed to determine the ultimate load and corresponding deflection of the reinforced concrete beam shown in Figure 148 subject to center point loading, as tested by Shim (2002). VecTor2 input files, which are equivalent to those used in this example, are provided in Appendix A.

The Hognestad model was selected for both the pre and post-peak compression response, with the Vecchio 1992-A compression softening model. The Bentz 2003 model was selected for tension stiffening. A crack width limit of 2 mm was imposed and element slip-distortions were included with the Hybrid II Vecchio-Lai model.

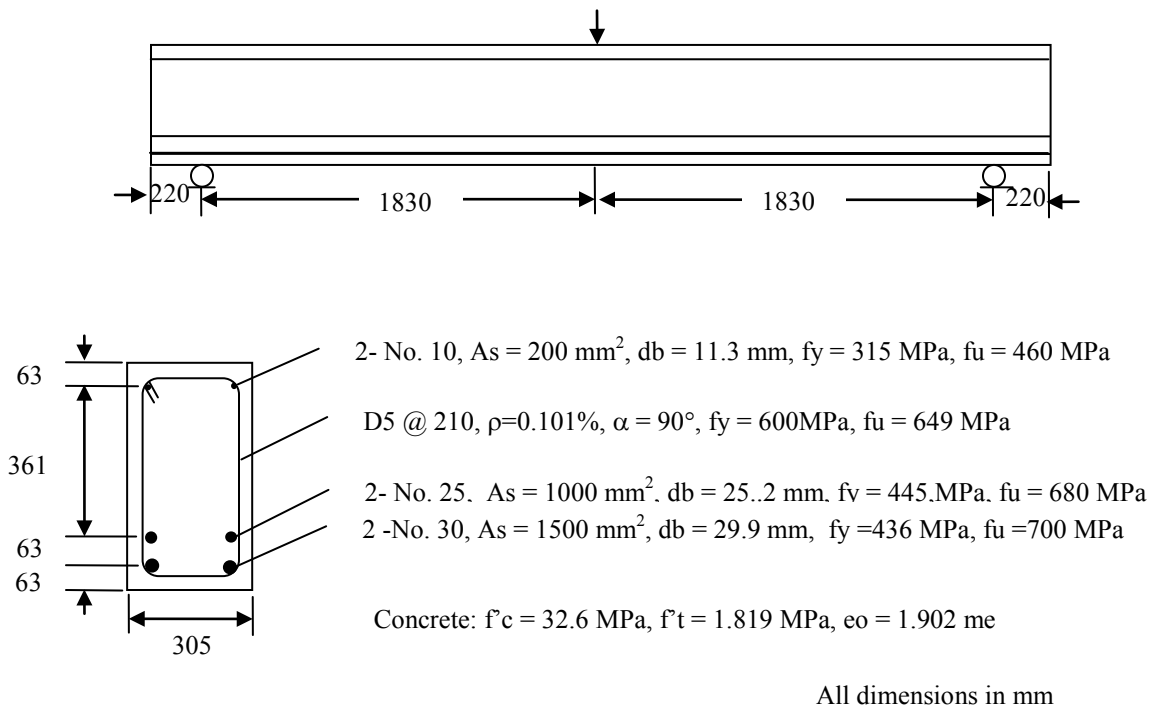


Figure 148: Reinforced Concrete Beam

It is decided to model the beam with rectangular elements for the concrete, and truss bar elements for the longitudinal reinforcing bars. Two reinforced concrete material types are utilized. One type represents the plain concrete cover. The other type models the web region of the beam with one smeared reinforcement component, which represents the stirrup reinforcement. Three ductile steel reinforcement material types are utilized; one each for the pair of No. 10 bars, the pair of No. 25 bars, and the pair of No. 30 bars.

As both the beam and the loading conditions are symmetrical about the midspan, only half of the beam needs to be modeled. The automatic mesh generation facility with the hybrid discretization type was used to create the mesh shown in Figure 149. Each pair of longitudinal reinforcing bars was entered as a separate reinforcement path with its corresponding material type. Nodes at the midspan of the beam are restrained from displacements in the longitudinal direction. The node at the support is restrained from displacements in the transverse direction.

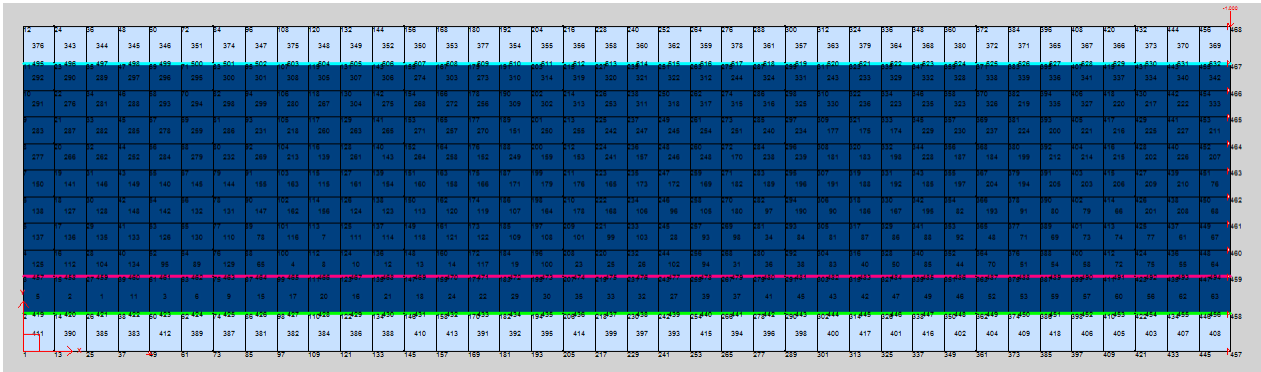


Figure 149: FormWorks Model

One load case was utilized to impose a support displacement of 1 mm at the midspan. The load factor was increased monotonically from zero to failure in increments of 0.25 mm. The self-weight of the beam is not included.

VecTor2 determines the load vs. midspan deflection response as shown in Figure 150.

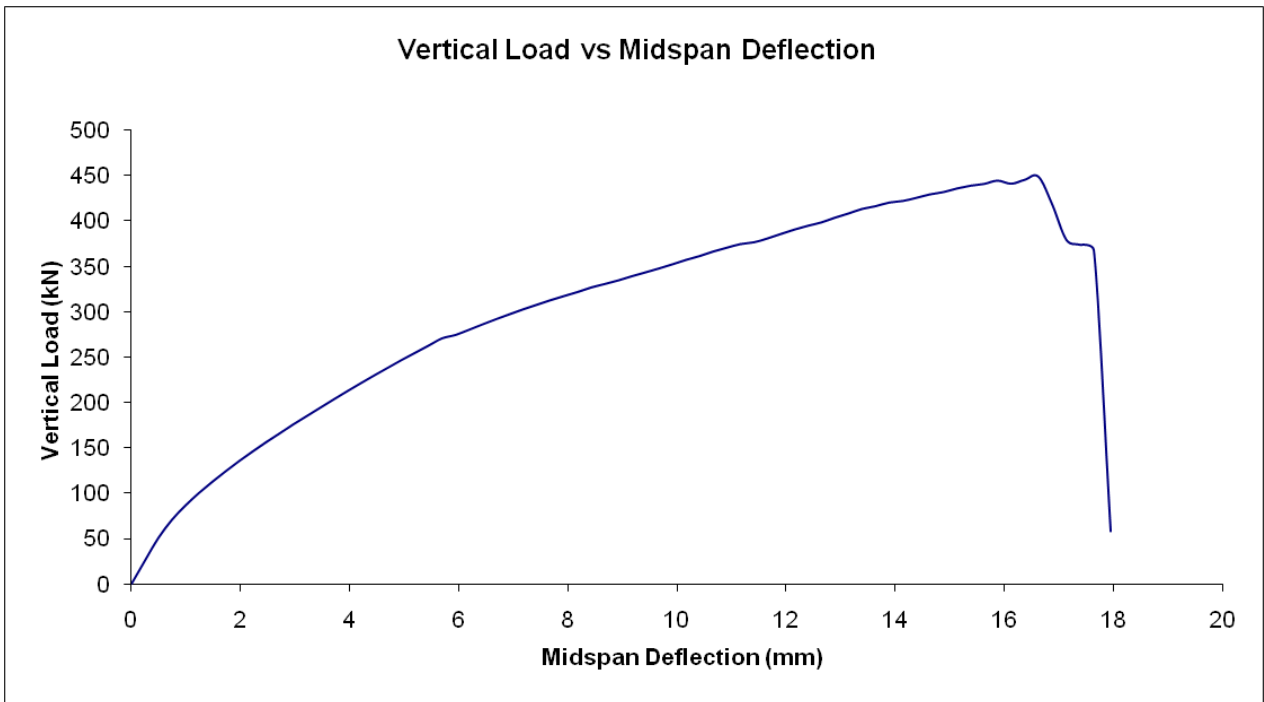


Figure 150: Load versus midspan deflection of reinforced concrete beam

At the ultimate load corresponding deflection of 450 kN and 17 mm, respectively, VecTor2 determines the cracking pattern as shown in Figure 151.

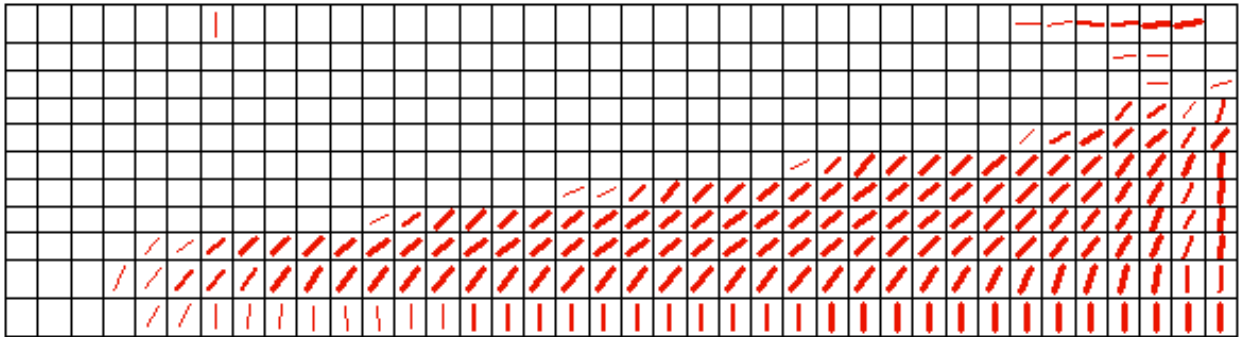


Figure 151: Crack pattern of reinforced concrete beam at ultimate load

12.3 Example 2: SW22

This second example shows the FormWorks modeling and VecTor2 calculation of load-deflection response for a shear wall. The shear wall, SW22, in this example was one of 13 shear walls tested under axial load and monotonically increasing lateral load by Lefas et al in 1990 and modeled in Vecchio (1992). The shear wall dimensions and reinforcement properties are illustrated in Figure 152.

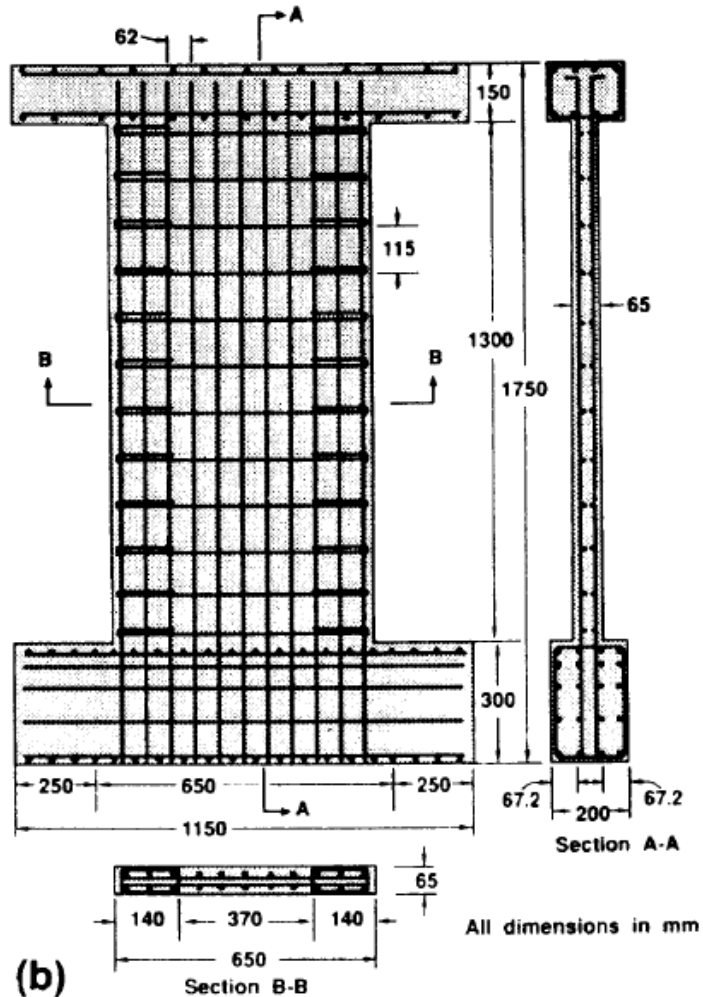


Figure 152: SW22

The vertical reinforcement consists of two layers of 8 mm-diameter bars at 62 mm spacing; horizontal reinforcement consists of 6.25 mm-diameter bars at 115 mm spacing. A 140 mm wide internal column was formed at the end of each wall. The yield strengths for the 8 mm and 6.25 mm bars were taken as 470 MPa and 520 MPa, respectively. The modulus of elasticity for the reinforcement was 210,000 MPa,

with a strain hardening modulus of approximately 10,000 MPa, The concrete cylinder compressive strength used in the model was 36.6 MPa; the tensile strength used was 2.16 MPa, with an initial tangent elastic modulus of 32800 MPa. Poisson's ratio was assumed to be 0.15. An axial load of 182 kN was applied to the wall.

All reinforcement for SW22 was modeled as smeared reinforcement in VecTor2; there are no discrete reinforcing bars in the model. The mesh for SW22 is shown in Figure 153.

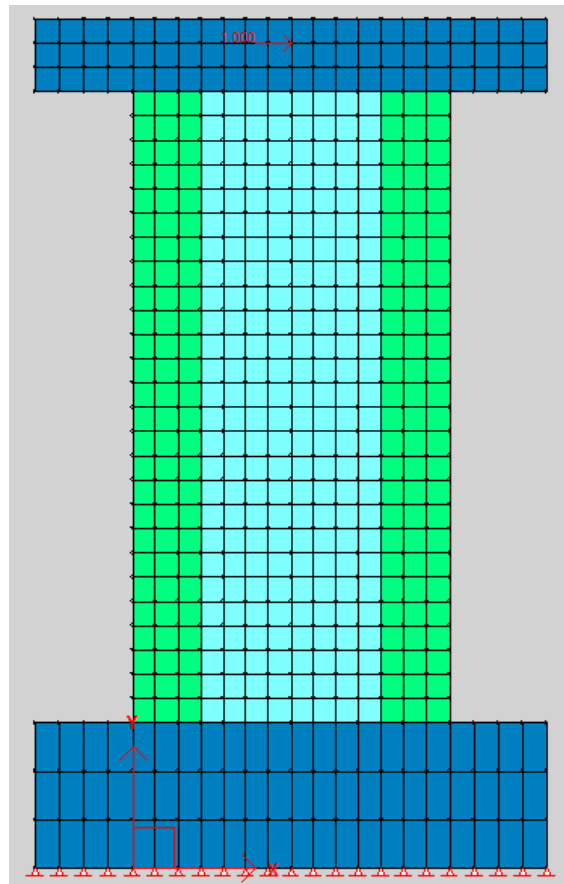


Figure 153: FormWorks Model for SW22

As shown in the mesh, there are three concrete types. Type 1 is used in the centre of the shear wall, type 2 is used for the exterior columns, Type 3 is used for the base and top. The specific properties used for each concrete material type can be found in the excerpt from the SW22 structure file.

The models used in the analysis of SW22 are summarized in Figure 154:

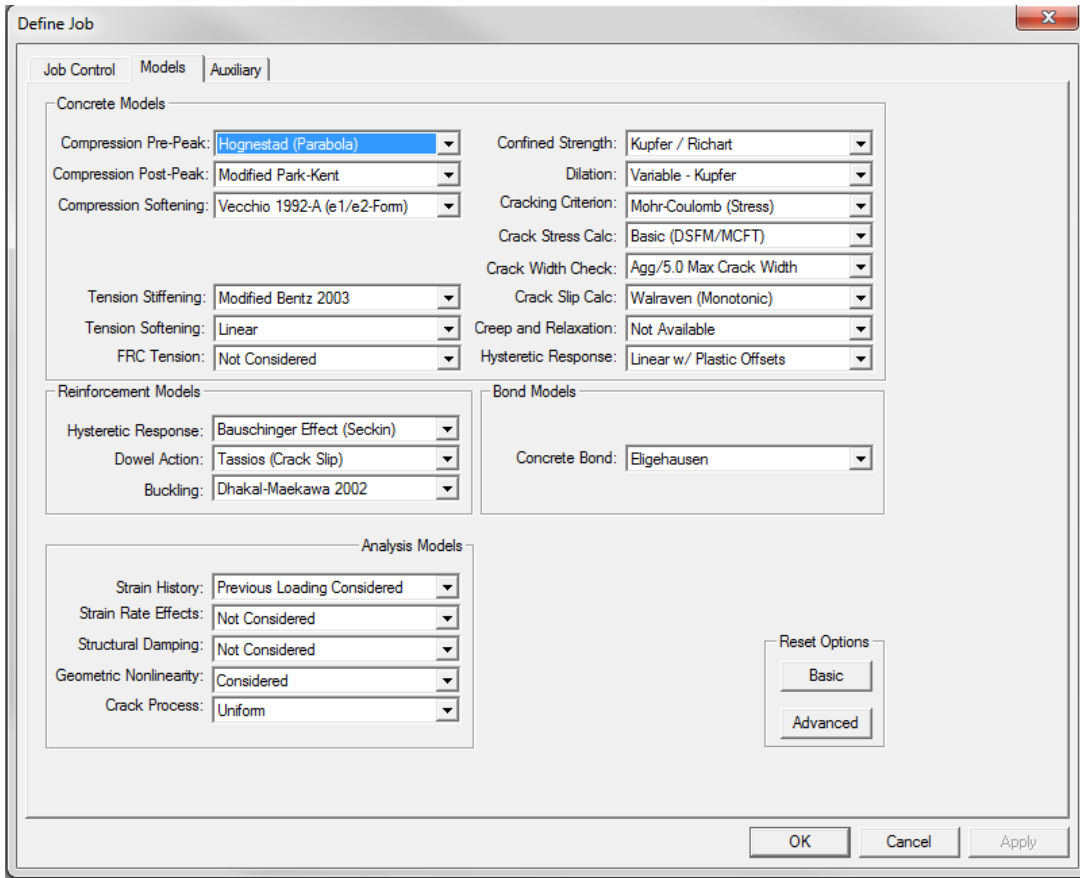


Figure 154: Models used for SW22

The load-deflection response for SW22 as calculated by VecTor2 is shown in Figure 155.

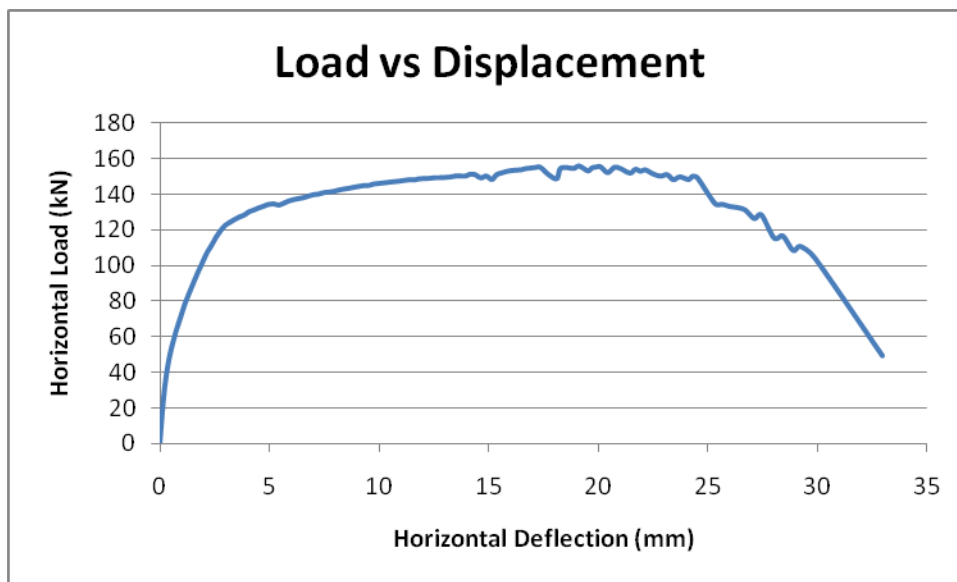


Figure 155: Load-displacement response for SW22

At the ultimate load condition of 20mm and 154kN, the crack pattern and deflected shape of SW22 are shown in Figure 156.

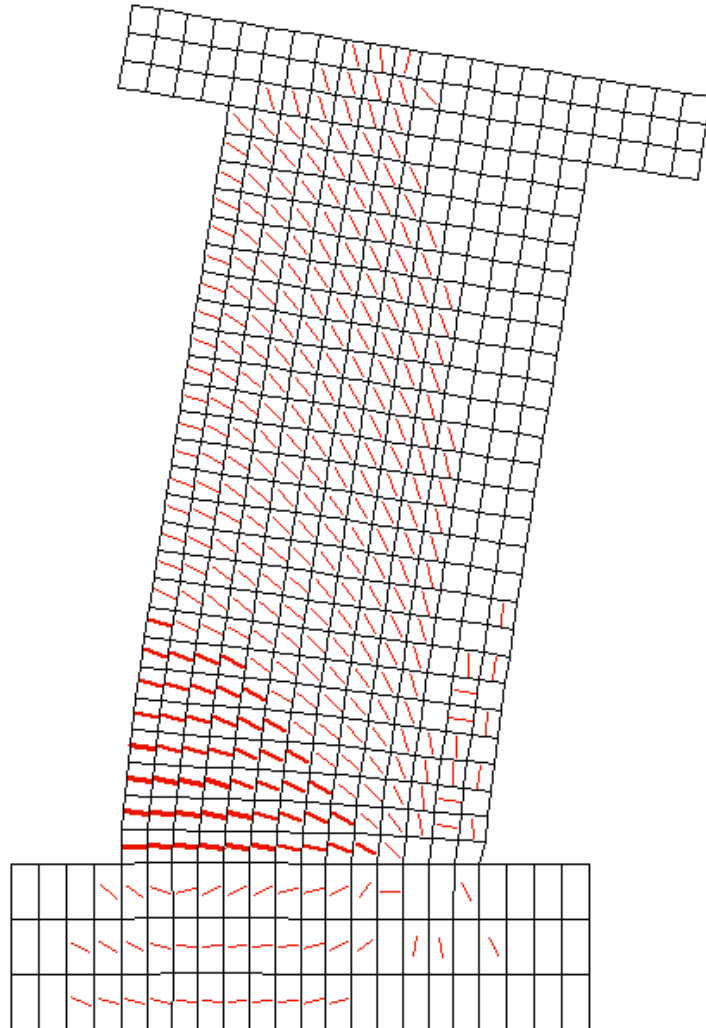


Figure 156: Deflected Shape and Final Crack Pattern for SW22

13 Summary & Recommendations

13.1 Summary

User facilities have been presented for the two-dimensional nonlinear finite element analysis program, VecTor2. These user facilities consist of program documentation for VecTor2 and a newly developed preprocessor program called FormWorks. With the purpose of providing a basis for rational usage, the program documentation has addressed the formulation and implementation of the VecTor2 program, its element library and its numerous constitutive models. The FormWorks program has been developed to expedite the modeling process by providing a graphical interface for data visualization and input, data checking procedures, a two-dimensional automatic mesh generator, and a bandwidth reduction algorithm. In order to provide a high degree of user control, the automatic mesh generator is capable of producing mixed element meshes and accommodating arbitrary material delineations, constraints, and local variations in element size.

13.2 Recommendations

It is apparent that one of the fundamental challenges facing a user of a nonlinear finite element program such as VecTor2 is the modeling process itself. Unless a generalized NLFEARC program exists, it remains necessary to extract a portion of the structure to analyze, determine appropriate boundary and loading conditions, and select appropriate analysis models. In this regard, the automatic mesh generator provides convenience utility, but does not provide context to the analysis. This may be achieved by implementing a catalog of common structural members in a preprocessor program with familiar boundary conditions and recommended analysis models. Alternatively, it may be beneficial to implement procedures that harmonize or automatically prescribe material models. Possibly, different material models could be applied to different mesh regions depending on the predicted stress state.

With regards to NLFEARC as a design tool, it would be beneficial to integrate NLFEARC into the iterative design process. In this regard, the importance of graphical preprocessor facilities to efficiency should not be discounted, particularly for NLFEARC programs that conduct three-dimensional analyses or utilize more geometrically complex elements. Conceivably, the input interface could be CAD-based and include mesh generators dedicated for finite element analysis. Other analysis procedures could also be integrated to provide a means of verifying results against more conventional analysis methods or accepted design standards.

References

- Akkaya, Y., Guner, S. and Vecchio, F. J., 2013, "Modeling inelastic buckling behavior of reinforcing bars in compression"
- Akkaya, Y., Guner, S. and Vecchio, F. J., 2013, "Modeling hysteretic response of reinforcing bars including buckling in reinforced concrete members"
- Akkaya, Y., Guner, S. and Vecchio, F. J., 2012, "Modeling cyclic behavior of reinforcing steel bars including buckling,"
- Bazant, Z.P., 2002. "Concrete fracture models: testing and practice". Engineering Fracture Mechanics. Vol. 69, pp. 165-205
- Bentz, E.C., 2000. "Sectional Analysis of Reinforced Concrete Members", Ph.D. Thesis, Department of Civil Engineering, University of Toronto, 310 pp.
- Chopra, A., 2007. "Dynamics of Structures". Prentice Hall. New Jersey.
- Collins, M.P., and Mitchell, D., 1997. "Prestressed Concrete Structures", Response Publications, Canada, 766 pp.
- Comite Euro-International du Beton. 1990. "CEB-FIP Model Code 1990". Thomas Telford. London.
- Cornelissen, H.A., Hordijk, D.A., Reinhardt, H.W. 1986. "Experimental determination of crack softening characteristics of normal weight and lightweight concrete". HERON Vol. 31, No. 2

- Deluce, J.D., Lee, S.-C., and Vecchio, F.J. 2012. "Crack Model for SFRC Members Containing Conventional Reinforcement," *ACI Structural Journal*, under review.
- Dhakal, R.P. and Maekawa, K., 2002a, "Modeling for post-yield buckling of reinforcement," *Journal of Structural Engineering*, ASCE, Vol. 128, No. 9, pp. 1139-1147.
- Dhakal, R.P., and Maekawa, K., 2002b, "Reinforcement Stability and Fracture of Cover Concrete in Reinforced Concrete Members," *Journal of Structural Engineering*, ASCE, Vol. 128, No.10, pp. 1253-1262.
- Dhakal, R.P., and Maekawa, K., 2002c, "Path-dependent Cyclic Stress-Strain Relationship of Reinforcing bar including buckling," *Engineering Structures*, Vol. 24, No. 11, pp. 1383-1396.
- Eligehausen, R., Popov, E., and Bertero, V. 1983. "Local Bond Stress-Slip relationship of Deformed Bars under Generalized Excitations", Report No. UCB/EERC-83/23, Earthquake Engineering Center, University of California, Berkeley.
- fib. 2010. "First complete draft: bulletin 55". Vol 1
- Gan, Y., 2000. "Bond Stress and Slip Modeling in Nonlinear Finite Element Analysis of Reinforced Concrete Structures", M.A.Sc Thesis, University of Toronto, 251 pp.
- Ganz, H.R., 1985. "Mauerwerksscheiben unter Normalkraft und Schub". Dissertation 7849, Institute of Structural Engineering (IBK), Swiss Federal Institute of Technology (ETH). Zurich, Switzerland
- Gupta, P.R., 1998. "Shear Design of Reinforced Concrete Members under Axial Compression", Ph.D. Thesis, Department of Civil Engineering, University of Toronto, 189 pp.

- Harajli, M.H. and Mukaddam, M.A., 1988. "Slip of Steel Bars in Concrete Joints under Cyclic Loading", ASCE Journal of Structural Engineering, Vol. 114, No. 9, pp. 2017-2035.
- He, X.G., and Kwan, A.K.H., 2001. "Modeling Dowel Action of Reinforcement Bars for Finite Element Analysis of Concrete Structures", Computers and Structures, Vol. 79, No.6, pp. 595-604.
- Hoshikuma, J., Kawashima, K., Nagaya, K. and Taylor, A.W., 1997. "Stress-Strain Model for Confined Reinforced Concrete in Bridge Piers", ASCE Journal of Structural Engineering, Vol. 123, No. 5, pp. 624-633.
- Hsieh, S.S., Ting, E.C., and Chen, W.F., 1979. "An Elastic-Fracture Model for Concrete." Proc. 3rd Eng. Mech. Div. Spec. Conf., ASCE, Austin, Texas, pp. 437-440.
- Izumo, J., Shin. H., Maeakawa, K., Okamura, H., 1992. "An Analytical Model for RC Panels Subjected to In-Plane Stresses", Concrete Shear in Earthquake, Elsevier Applied Science, London and New York, pp. 206-215.
- Kaufmann, W. and Marti, P., 1998. "Structural Concrete: Cracked Membrane Model", ASCE Journal of Structural Engineering, Vol. 124, No. 12, pp. 1467-1475.
- Kent, D.C., and Park, R., 1971. "Flexural Members with Confined Concrete", ASCE Journal of the Structural Division, Vol. 97, No. ST7, Proc. Paper 8243, pp. 1341-1360.
- Keuser, M. and Mehlhorn, G., 1987. "Finite Element Models for Bond Problems", ASCE Journal of Structural Engineering, Vol. 113, No. 10, pp. 2160-2173.

Kupfer, H.B., and Gerstle, K.H., 1973. "Behaviour of Concrete under Biaxial Stresses", ASCE Journal of Engineering Mechanics, Vol. 99, EM4, pp. 853-866.

Kupfer, H., Hilsdorf, H.K. and Rusch, H., 1969. "Behavior of Concrete under Biaxial Stress", ACI Journal, Vol. 87, No. 2, pp. 656-666.

Kwon, M. and Spacone, E., 2002. "Three-Dimensional Finite Element Analyses of Reinforced Concrete Columns", Computers and Structures. Vol. 80, No. 2, pp.199-212.

Lai, D. 2001. "Crack Shear-Slip in Reinforced Concrete Elements", M.A.Sc. Thesis, Department of Civil Engineering, University of Toronto, 154 pp.

Lee, S.-C., Cho, J.-Y., and Vecchio, F.J. 2011a. "Diverse Embedment Model for Steel Fiber-Reinforced Concrete in Tension: Model Development". ACI Materials Journal, Vol. 108, No. 5, pp.516-525

Lee, S.-C., Cho, J.-Y., and Vecchio, F.J. 2011b. "Diverse Embedment Model for Steel Fiber-Reinforced Concrete in Tension: Model Verification". ACI Materials Journal, Vol. 108, No. 5, pp.526-535

Lee, S.-C., Cho, J.-Y., and Vecchio, F.J. 2011c. "Model for Post-Yield Tension Stiffening and Rebar Rupture in Concrete Members". Engineering Structures, Vol. 33, No. 5, pp.1723-1733

Lee, S.-C., Cho, J.-Y., and Vecchio, F.J. 2012a. "Simplified Diverse Embedment Model for SFRC Elements in Tension". ACI Materials Journal, under review

Lee, S.-C., Cho, J.-Y., and Vecchio, F.J. 2012b. "Tension Stiffening Model for Steel Fiber Reinforced Concrete Containing Conventional Reinforcement". ACI Structural Journal, under review

- Lee, S.-C., Oh, J.-H., and Cho, J.-Y. 2012. "Compressive Behavior of Normal and High Strength Concrete with End-Hooked Steel Fibers". in progress
- Li, L., Han, X., and Xu, S. 2004. "Study on the degeneration of quadrilateral element to triangular element". *Communications in Numerical methods in Engineering*. pp 671-679.
- Mander, J.B., Priestley, M.J.N., and Park. R., 1988. "Theoretical Stress-Strain Model for Confined Concrete", *ASCE Journal of Structural Engineering*, Vol. 114, No. 8, pp. 1804-1826.
- Minelli, F., and Vecchio, F.J. 2006. "Compression Field Modeling of Fiber Reinforced Concrete Members Under Shear Loading". *ACI Structural Journal*, Vol. 103, No. 2, pp. 244-252
- Montoya, E. 2003. "Behaviour and Analysis of Confined Concrete". PhD Thesis. Department of Civil Engineering. University of Toronto. 321 pp.
- Montoya, E., Vecchio, F.J., and Sheikh, S.A. 2004. "Numerical evaluation of the behavior of steel- and FRP-confined concrete columns using compression field modeling". *Engineering Structures*, Vol. 26, pp. 1535-1545
- Montoya, E., Vecchio, F.J., and Sheikh S.A. 2006. "Compression Field Modeling of Confined Concrete: Constitutive Models". *ASCE Journal of Materials in Civil Engineering*, Vol. 18, No. 4, pp. 1-8
- Ngo, D. and Scordelis, A.C., 1967. "Finite Element Analysis of Reinforced Concrete Beams", *ACI Journal*, Vol. 64, No. 3 , pp. 152-163.
- Okamura, H., and Maekawa, K. 1991. "Nonlinear Analysis and Constitutive Models of Reinforced Concrete", University of Tokyo, ISBN 7655-1506-0, 182 pp.

Ottosen, N.S. 1977. "A Failure Criterion for Concrete", ASCE Journal of Engineering Mechanics Division, Vol. 103, No. 4, pp. 527-535.

Palermo, D., and Vecchio, F.J., 2002, "Behaviour and Analysis of Reinforced Concrete Walls Subjected to Reversed Cyclic Loading", Publication No. 2002-01, Department of Civil Engineering, University of Toronto, 351 pp.

Petersen, S.B., Rodrigues, J.M.C, and Martins, P.A.F., 1993. "Automatic Generation of Quadrilateral Meshes for the Finite Element Analysis of Metal Forming Processes", Finite Elements in Analysis and Design, Vol. 35, pp. 157-168.

Popovics, S., 1973. "A Numerical Approach to the Complete Stress-Strain Curve of Concrete", Cement and Concrete Research, Vol. 3, No.5, pp. 583-599.

Richart, F.E., Brandtzaeg, A., and Brown, R.L., 1928. "A Study of the Failure of Concrete under Combined Compressive Stresses", Bulletin No.185, University of Illinois Engineering Experimental Station, Urbana, Illinois, 104 pp.

Saatci, S. 2007. "Behaviour and Modeling of Reinforced Concrete Structures Subjected to Impact Loads", PhD Thesis, Department of Civil Engineering, University of Toronto, 316 pp.

Saatci, S. and Vecchio, F.J. 2007. "Dynamic Analysis with VecTor2". FormWorks Bulletin

Saenz, L.P., 1973. Discussion of "Equation for the Stress-Strain Relation for Concrete", Cement and Concrete Research. Vol. 3, No. 5, pp. 583-599.

- Sato, Y. and Vecchio, F.J., 2003. "Tension Stiffening and Crack Formation in RC Members with FRP Sheets", ASCE Journal of Structural Engineering, Vol. 129, No 6, pp. 717-724
- Scott, B.D., Park, R., and Priestley, M.J.N. 1982. "Stress-Strain Behavior of Concrete Confined by Overlapping Hoops at Low and High Strain Rates", ACI Journal, Vol. 79, No. 1, pp.13-27.
- Seckin, M., 1981. "Hysteretic Behaviour of Cast-in-Place Exterior Beam-Column-Slab Subassemblies", Ph.D. Thesis, Department of Civil Engineering, University of Toronto, 266 pp.
- Selby, R.G. 1993. "Three-Dimensional Constitutive Relations for Reinforced Concrete", Publication No. 93-02, Department of Civil Engineering, University of Toronto, 147 pp.
- Shim, W., 2002. "Analysis of Beams with Low Shear Reinforcement", M.A.Sc. Thesis, Department of Civil Engineering, University of Toronto, 358 pp.
- Smith, G.M., and Young, L.E. 1956. "Ultimate Flexural Analysis Based on Stress-Strain Curve of Cylinder". ACI Journal. Vol. 53, No. 6, pp. 597-609
- Susetyo, J. 2009. "Fibre Reinforcement for Shrinkage Crack Control in Prestressed, Precast Segmental Bridges". PhD Thesis. Department of Civil Engineering. University of Toronto. 532 pp.
- Thorenfeldt, E., Tomaszewicz, A., and Jensen, J.J., 1987. "Mechanical Properties of High-Strength Concrete and Application in Design", Proceedings of the Symposium "Utilization of High Strength Concrete," Stavanger, Norway, June 1987, Tapir, Trondheim, pp. 149-159.
- Vecchio, F.J., 1992. "Finite Element Modeling of Concrete Expansion and Confinement", ASCE Journal of Structural Engineering, Vol. 118, No. 9, pp. 2390-2406.

- Vecchio, F.J. 1999. "Towards Cyclic Load Modeling of Reinforced Concrete", ACI Structural Journal, Vol. 96, No. 2, pp.193-202.
- Vecchio, F.J., 2000. "Analysis of Shear-Critical Reinforced Concrete Beams", ACI Structural Journal, Vol. 97, No.1 pp. 102-110.
- Vecchio, F.J., 2000. "Disturbed Stress Field Model for Reinforced Concrete: Formulation", ASCE Journal of Structural Engineering, Vol. 126, No. 9, pp. 1070-1077.
- Vecchio, F.J. and Collins, M.P., 1982. "Response of Reinforced Concrete to In-Plane Shear and Normal Stresses", Publication No. 82-03, Department of Civil Engineering, University of Toronto, 332 pp.
- Vecchio, F.J. and Collins, M.P., 1986. "The Modified Compression Field Theory for Reinforced Concrete Elements Subject to Shear", ACI Journal Vol. 83, No. 2, pp. 219-231.
- Vecchio, F.J. and Collins, M.P., 1993. "Compression Response of Cracked Reinforced Concrete", ASCE Journal of Structural Engineering, Vol. 119, No. 12, pp. 3590-3610.
- Vecchio, F.J. and DeRoo, A., 1995. "Smearred-Crack Modeling of Concrete Tension Splitting", ASCE Journal of Engineering Mechanics, Vol. 121, No. 6 pp. 702-708.
- Vecchio, F.J. and Lai, D., 2004. "Crack Shear-Slip in Reinforced Concrete Elements", Journal of Advanced Concrete Technology, Vol. 2, No. 3, pp. 289-300
- Vecchio, F.J. and McQuade, I., 2011. "Towards improved modeling of steel-concrete composite wall elements", Journal of Nuclear Engineering and Design, Vol. 241, No. 8, pp. 2629-2642

- Walraven, J.C., 1981. "Fundamental Analysis of Aggregate Interlock", ASCE Journal of the Structural Division, Vol. 107, No. 11, pp. 2245-2270.
- Walraven, J.C., and Reinhardt, H.W., 1981. "Theory and Experiments on the Mechanical Behaviour of Cracks in Plain and Reinforced Concrete Subjected to Shear Loading", Concrete Mechanics – Part A, Heron, Vol. 26, No. 4, 65 pp.
- Wilson, E., 2002. "Three-Dimensional Static and Dynamic Analysis of Structures". Computers and Structures, Berkeley.
- Wittmann, F. H. 2002. "Crack formation and fracture energy of normal and high strength concrete". Qingdao: Centre for Durability, Maintenance, and Repair
- Wong, R., 2001. "Towards Modelling of Reinforced Concrete Members with Externally-Bonded Fibre Reinforced Polymer (FRP) Composites," M.A.Sc. Thesis, Department of Civil Engineering, University of Toronto, 298 pp.
- Yamamoto, T., 1999. "Nonlinear Finite Element Analysis of Transverse Shear and Torsional Problems in Reinforced Concrete Shells," M.A.Sc. Thesis, Department of Civil Engineering, University of Toronto, 112 pp.
- Zhou, C.E. 2004. "Nonlinear Finite Element Analysis of Reinforced Concrete Structures Subjected to Transient Thermal Loads". M.A.Sc. Thesis. Department of Civil Engineering. University of Toronto. 153 pp.

Zhou, C. E. and Vecchio, F. J., 2005. "Nonlinear Finite Element analysis of Reinforced Concrete Structures Subjected to Transient Thermal Loads", *Computers and Structures*, Vol. 2, No. 6, pp. 455-480.

Appendix A – VecTor2 Input Files for Sample Problem 1

VecTor.JOB

VER 3.5

```

* * * * *
*   V E C T O R   *
*   J O B   D A T A   *
* * * * *

```

```

Job Title      (30 char. max.)      : Enter Job Title
Job File Name  ( 8 char. max.)      : VecTor
Date          (30 char. max.)      : Enter Date

```

STRUCTURE DATA

```

Structure Type      : 2
File Name          ( 8 char. max.) : Struct

```

LOADING DATA

```

No. of Load Stages      : 201
Starting Load Stage No. : 1
Load Series ID ( 5 char. max.) : ID

```

| Load Case | File Name (8 char. max.) | Initial | Final | Factors LS-Inc | Type | Reps | C-Inc |
|-----------|--------------------------|---------|---------|----------------|------|------|--------|
| 1 | Case1 | 0.0000 | 50.0000 | 0.2500 | 1 | 1 | 0.0000 |
| 2 | NULL | 0.0000 | 0.0000 | 0.0000 | 1 | 1 | 0.0000 |
| 3 | NULL | 0.0000 | 0.0000 | 0.0000 | 1 | 1 | 0.0000 |
| 4 | NULL | 0.0000 | 0.0000 | 0.0000 | 1 | 1 | 0.0000 |
| 5 | NULL | 0.0000 | 0.0000 | 0.0000 | 1 | 1 | 0.0000 |

ANALYSIS PARAMETERS

```

Analysis Mode      (1-2) : 1
Seed File Name    (8 char. max.) : NULL
Convergence Limit (>1.0) : 1.000010
Averaging Factor  (<1.0) : 0.600
Maximum No. of Iterations : 60
Convergence Criteria (1-5) : 2
Results Files     (1-4) : 2
Output Format      (1-3) : 1

```

MATERIAL BEHAVIOUR MODELS

```

Concrete Compression Base Curve (0-3) : 1
Concrete Compression Post-Peak (0-3) : 1
Concrete Compression Softening (0-8) : 1
Concrete Tension Stiffening (0-6) : 1
Concrete Tension Softening (0-3) : 1
Concrete Tension Splitting (0-1) : 0
Concrete Confined Strength (0-2) : 1
Concrete Dilation (0-1) : 1
Concrete Cracking Criterion (0-4) : 1
Concrete Crack Stress Calculation (0-2) : 1
Concrete Crack Width Check (0-2) : 1
Concrete Bond or Adhesion (0-3) : 1
Concrete Creep and Relaxation (0-1) : 1
Concrete Hysteresis (0-2) : 1
Reinforcement Hysteresis (0-2) : 1
Reinforcement Dowel Action (0-1) : 1
Reinforcement Buckling (0-1) : 1
Element Strain Histories (0-1) : 1
Element Slip Distortions (0-4) : 1
Strain Rate Effects (0-1) : 1
Structural Damping (0-1) : 1
Geometric Nonlinearity (0-1) : 1
Crack Allocation Process (0-1) : 1

```

<<< JOB FILE NOTES>>>

Struct.S2R

```

* * * * *
*           V e c T o r 2           *
*   S T R U C T U R E   D A T A   *
* * * * *

```

STRUCTURAL PARAMETERS

```

Structure Title      (30 char. max.)   : Enter Structure Title
Structure File Name  ( 8 char. max.)   : Struct
No. of R.C. Material Types           : 2
No. of Steel Material Types          : 3
No. of Bond Material Types           : 0
No. of Rectangular Elements          : 418
No. of Quadrilateral Elements        : 0
No. of Triangular Elements           : 0
No. of Truss Bar Elements            : 114
No. of Linkage Elements              : 0
No. of Contact Elements              : 0
No. of Joints                    : 468
No. of Restraints                  : 13

```

MATERIAL SPECIFICATIONS

(A) REINFORCED CONCRETE

<NOTE:> TO BE USED IN RECTANGULAR AND TRIANGULAR ELEMENTS ONLY

CONCRETE

| MAT | REF | Ns | T | f'c | [f't | Ec | e0 | Mu | Cc | Agg | Dens | Kc] | [Sx | Sy] |
|-----|-----|----|---------|--------|-------|-----------|-------|-------|-------|--------|----------|-------|-------|-----|
| TYP | TYP | # | mm | MPa | MPa | MPa | me | /C | mm | kg/m3 | mm2/s | mm | mm | |
| 1 | 1 | 0 | 305.000 | 22.600 | 1.819 | 23770.000 | 1.902 | 0.150 | 0.000 | 20.000 | 2400.000 | 0.000 | 0.000 | |
| 2 | 1 | 1 | 305.000 | 22.600 | 1.819 | 23770.000 | 1.902 | 0.150 | 0.000 | 20.000 | 2400.000 | 0.000 | 0.000 | |

/

REINFORCEMENT COMPONENTS

| MAT | REF | DIR | As | Db | Fy | Fu | Es | esh | eu | Cs | Dep | b/t |
|-----|-----|--------|-------|-------|---------|---------|------------|----------|-------|-------|-----|-----|
| TYP | TYP | deg | % | mm | MPa | MPa | MPa | me | me | /C | me | |
| 2 | 1 | 90.000 | 0.101 | 6.400 | 600.000 | 649.000 | 200000.000 | 4900.000 | 0.000 | 0.000 | | |

/

(B) STEEL

<NOTE:> TO BE USED FOR TRUSS ELEMENTS ONLY

| MAT | REF | AREA | Db | Fy | Fu | Es | esh | eu | Cs | Dep | b/t |
|-----|-----|----------|--------|---------|---------|------------|--------|-------|-------|-------|-----|
| TYP | TYP | mm2 | mm | MPa | MPa | MPa | me | me | /C | me | |
| 1 | 1 | 200.600 | 11.300 | 315.000 | 460.000 | 200000.000 | 10.000 | 0.000 | 0.000 | 0.000 | |
| 2 | 1 | 997.600 | 25.200 | 445.000 | 680.000 | 200000.000 | 10.000 | 0.000 | 0.000 | 0.000 | |
| 3 | 1 | 1404.400 | 29.900 | 436.000 | 700.000 | 200000.000 | 10.000 | 0.000 | 0.000 | 0.000 | |

/

(C) BOND

<NOTE:> TO BE USED FOR EXTERIOR/INTERIOR BONDED ELEMENTS

| MAT | REF | { Ao | U1 | U2 | U3 | S1 | S2 | S3 } | { CPF | Cmin | No. | HOOK } |
|-----|-----|------|-----|-----|-----|----|----|------|-------|------|-----|--------|
| TYP | TYP | mm^2 | MPa | MPa | MPa | mm | mm | mm | 0-1 | mm | LYR | 0/1 |
| | | | | | | | | | | | | |

/

ELEMENT INCIDENCES

(A) RECTANGULAR ELEMENTS

<<<<< FORMAT >>>>>

| ELMT | INC1 | INC2 | INC3 | INC4 | [#ELMT | d(ELMT) | d(INC)] | [#ELMT | d(ELMT) | d(INC)]/ |
|------|------|------|------|------|--------|---------|---------|--------|---------|----------|
| 1 | 38 | 39 | 27 | 26 | 1 | 1 | 1 | 1 | 1 | / |
| 2 | 14 | 26 | 27 | 15 | 1 | 1 | 1 | 1 | 1 | / |

(B) QUADRILATERAL ELEMENTS

```

<<<<< FORMAT >>>>>
ELMT INC1 INC2 INC3 INC4 [#ELMT d(ELMT) d(INC)] [#ELMT d(ELMT) d(INC)] /
/

```

(C) TRIANGULAR ELEMENTS

```

<<<<< FORMAT >>>>>
ELMT INC1 INC2 INC3 [ #ELMT d(ELMT) d(INC) ] [ #ELMT d(ELMT) d(INC) ] /
/

```

(D) TRUSS ELEMENTS

```

<<<<< FORMAT >>>>>
ELMT INC1 INC2 [ #ELMT d(ELMT) d(INC) ] [#ELMT d(ELMT) d(INC) ] /
419 2 14 1 1 1 1 1 1 /
420 14 26 1 1 1 1 1 1 /
421 26 38 1 1 1 1 1 1 /

```

(E) LINKAGE ELEMENTS

```

<<<<< FORMAT >>>>>
ELMT INC1 INC2 [ #ELMT d(ELMT) d(INC) ] [ #ELMT d(ELMT) d(INC) ]
/

```

(F) CONTACT ELEMENTS

```

<<<<< FORMAT >>>>>
ELMT INC1 INC2 INC3 INC4 [ #ELMT d(ELMT) d(INC) ] [ #ELMT d(ELMT) d(INC) ]
/

```

MATERIAL TYPE ASSIGNMENT

```

<<<<< FORMAT >>>>>
ELMT MAT ACT [ #ELMT d(ELMT) ] [ #ELMT d(ELMT) ] /
1 2 1 1 1 1 1 /
2 2 1 1 1 1 1 /
3 2 1 1 1 1 1 /
/

```

COORDINATES

<NOTE:> UNITS: in OR mm

```

<<<<< FORMAT >>>>>
NODE X Y [ #NODES d(NODES) d(X) d(Y) ] [ #NODES d(NODES) d(X) d(Y) ] /
1 0.000 0.000 1 1 0.000 0.000 1 1 0.000 0.000 /
2 0.000 63.000 1 1 0.000 0.000 1 1 0.000 0.000 /
3 0.000 126.000 1 1 0.000 0.000 1 1 0.000 0.000 /
/

```

SUPPORT RESTRAINTS

<NOTE:> CODE: '0' FOR NOT RESTRAINED NODES AND '1' FOR RESTRAINED ONES

```

<<<<< FORMAT >>>>>
NODE X-RST Y-RST [ #NODE d(NODE) ] /
49 0 1 1 1 /
457 1 0 1 1 /
458 1 0 1 1 /
/

```

<<< STRUCTURE FILE NOTES >>>

Case1.L2R

```

* * * * *
*   V e c T o r 2   *
*   L O A D   D A T A   *
* * * * *

```

```

LOAD CASE PARAMETERS
*****

```

```

Structure Title      (30 char. max.)      : Enter Structure Title
Load Case Title      (30 char. max.)      : Enter load case title
Load Case File Name  (8 char. max.)       : Casel
No. of Loaded Joints : 0
No. of Prescribed Support Displacements : 1
No. of Elements with Gravity Loads      : 0
No. of Elements with Temperature Loads  : 0
No. of Elements with Concrete Prestrain : 0
No. of Elements with Ingress Pressure   : 0
No. of Nodes with Thermal Load          : 0
No. of Nodes with Lumped Masses        : 0
No. of Nodes with Impulse Forces       : 0
Ground Acceleration Record (0-1)       : 0

```

```

JOINT LOADS
*****

```

```

<NOTE:> UNITS: KIPS OR KN
<<<<< FORMAT >>>>>
NODE   Fx   Fy   [ #NODE d(NODE) d(Fx) d(Fy) ] /
/

```

```

SUPPORT DISPLACEMENTS
*****

```

```

<NOTE:> UNITS: MM OR IN
<<<<< FORMAT >>>>>
JNT DOF DISPL [ #JNT d(JNT) ] /
  468  2  -1.000  1  1/
/

```

```

GRAVITY LOADS
*****

```

```

<NOTE:> UNITS: KG/M3
<<<<< FORMAT >>>>>
ELMT DENS GX GY [ #ELMT d(ELMT) ] [ #ELMT d(ELMT) ] /
/

```

```

ELEMENT TEMPERATURE
*****

```

```

<NOTE:> UNITS: F OR C
<<<<< FORMAT >>>>>
ELMT TEMP [ #ELMT d(ELMT) d(TEMP) ] [ #ELMT d(ELMT) d(TEMP) ] /
/

```

```

CONCRETE PRESTRAINS
*****

```

```

<NOTE:> UNITS: me
<<<<< FORMAT >>>>>
ELMT STRAIN [ #ELMT d(ELMT) d(STRAIN) ] [ #ELMT d(ELMT) d(STRAIN) ] /
/

```

```

INGRESS PRESSURES
*****

```

```

<NOTE:> UNITS: MPa
<<<<< FORMAT >>>>>
ELMT PRESSURE [ #ELMT d(ELMT) d(PRS) ] [ #ELMT d(ELMT) d(PRS) ] /
/

```

```

NODAL THERMAL LOADS
*****

```

```

<NOTE:>
<<<<< FORMAT >>>>>
NODE TYPE Tm1 Tp1 Tm2 Tp2 Tm3 Tp3 [ #NODE d(NODE) ] [ #NODE d(NODE) ] /
/

```

```

LUMPED MASSES
*****

```

```

<NOTE:> UNITS: kg, m/s
<<<<< FORMAT >>>>>
NODE DOF-X DOF-Y MASS GF-X GF-Y Vo-X Vo-Y [ #NODE d(NODE) ] /
/

```

```

IMPULSE FORCES

```

```
*****  
<NOTE:> UNITS: Sec, kN  
<<<<< FORMAT >>>>>  
NODE DOF T1 F1 T2 F2 T3 F3 T4 F4 [ #NODE d(NODE) ] /  
/  
GROUND ACCELERATION  
*****  
<NOTE:> UNITS: Sec, G  
<<<<< FORMAT >>>>>  
TIME ACC-X ACC-Y  
/  
  
<<< LOAD FILE NOTES >>>
```

Appendix B – VecTor2 Input Files for Sample Problem 2

VecTor.JOB

VER 3.5

```

* * * * *
*   V E C T O R   *
*   J O B   D A T A   *
* * * * *

```

```

Job Title      (30 char. max.)      : Shear Wall SW22
Job File Name  ( 8 char. max.)      : SW22
Date          (30 char. max.)      : May 2011

```

STRUCTURE DATA

```

Structure Type      : 2
File Name          ( 8 char. max.) : SW22

```

LOADING DATA

```

No. of Load Stages      : 201
Starting Load Stage No. : 1
Load Series ID  ( 5 char. max.) : SW22

```

| Load Case | File Name (8 char. max.) | Initial | Final | Factors LS-Inc | Type | Reps | C-Inc |
|-----------|--------------------------|---------|----------|----------------|------|------|--------|
| 1 | SW22DL | 0.0000 | 100.0000 | 0.5000 | 1 | 1 | 0.0000 |
| 2 | SW22VL | 1.8200 | 1.8200 | 0.0000 | 1 | 1 | 0.0000 |
| 3 | NULL | 0.0000 | 0.0000 | 0.0000 | 1 | 1 | 0.0000 |
| 4 | NULL | 0.0000 | 0.0000 | 0.0000 | 1 | 1 | 0.0000 |
| 5 | NULL | 0.0000 | 0.0000 | 0.0000 | 1 | 1 | 0.0000 |

ANALYSIS PARAMETERS

```

Analysis Mode      (1-2) : 1
Seed File Name    (8 char. max.) : NULL
Convergence Limit (>1.0) : 1.000010
Averaging Factor  (<1.0) : 0.500
Maximum No. of Iterations : 100
Convergence Criteria (1-5) : 2
Results Files     (1-4) : 2
Output Format      (1-3) : 1

```

MATERIAL BEHAVIOUR MODELS

```

Concrete Compression Base Curve      (0-3) : 1
Concrete Compression Post-Peak       (0-3) : 1
Concrete Compression Softening       (0-8) : 1
Concrete Tension Stiffening          (0-6) : 1
Concrete Tension Softening           (0-3) : 1
Concrete Tension Splitting           (0-1) : 1
Concrete Confined Strength            (0-2) : 1
Concrete Dilation                     (0-1) : 1
Concrete Cracking Criterion           (0-4) : 1
Concrete Crack Stress Calculation     (0-2) : 1
Concrete Crack Width Check            (0-2) : 2
Concrete Bond or Adhesion             (0-3) : 1
Concrete Creep and Relaxation         (0-1) : 1
Concrete Hysteresis                   (0-2) : 1
Reinforcement Hysteresis              (0-2) : 1
Reinforcement Dowel Action            (0-1) : 1
Reinforcement Buckling                (0-1) : 1
Element Strain Histories              (0-1) : 1
Element Slip Distortions              (0-4) : 1
Strain Rate Effects                   (0-1) : 1
Structural Damping                    (0-1) : 1
Geometric Nonlinearity                (0-1) : 1
Crack Allocation Process              (0-1) : 1

```

<<< JOB FILE NOTES>>>

SW22.S2R

 * V e c T o r 2 *
 * S T R U C T U R E D A T A *

STRUCTURAL PARAMETERS

Structure Title (30 char. max.) : Shear Wall SW22
 Structure File Name (8 char. max.) : SW22
 No. of R.C. Material Types : 3
 No. of Steel Material Types : 0
 No. of Bond Material Types : 0
 No. of Rectangular Elements : 496
 No. of Quadrilateral Elements : 0
 No. of Triangular Elements : 0
 No. of Truss Bar Elements : 0
 No. of Linkage Elements : 0
 No. of Contact Elements : 0
 No. of Joints : 559
 No. of Restraints : 46

MATERIAL SPECIFICATIONS

(A) REINFORCED CONCRETE

<NOTE:> TO BE USED IN RECTANGULAR AND TRIANGULAR ELEMENTS ONLY

CONCRETE

| MAT TYP | REF TYP | Ns # | T mm | f'c MPa | [f't MPa | Ec MPa | e0 me | Mu | Cc /C | Agg mm | Dens kg/m3 | Kc] mm2/s | [Sx mm | Sy mm |
|---------|---------|------|---------|---------|-----------|-----------|-------|-------|-------|--------|------------|------------|--------|-------|
| 1 | 1 | 2 | 65.000 | 36.600 | 2.160 | 32800.000 | 2.000 | 0.150 | 0.000 | 10.000 | 2400.000 | 0.000 | 0.000 | 0.000 |
| 2 | 1 | 4 | 65.000 | 36.600 | 2.160 | 32800.000 | 2.000 | 0.150 | 0.000 | 10.000 | 2400.000 | 0.000 | 0.000 | 0.000 |
| 3 | 1 | 3 | 200.000 | 36.600 | 2.160 | 32800.000 | 2.000 | 0.150 | 0.000 | 10.000 | 2400.000 | 0.000 | 0.000 | 0.000 |

/
 REINFORCEMENT COMPONENTS

| MAT TYP | REF TYP | DIR deg | As % | Db mm | Fy MPa | Fu MPa | Es MPa | esh me | eu me | Cs /C | Dep me | b/t |
|---------|---------|---------|-------|-------|---------|---------|------------|--------|---------|-------|--------|-------|
| 1 | 1 | 0.000 | 0.820 | 6.000 | 520.000 | 650.000 | 200000.000 | 10.000 | 150.000 | 0.000 | 0.000 | 0.000 |
| 1 | 1 | 90.000 | 2.090 | 6.000 | 470.000 | 650.000 | 200000.000 | 10.000 | 150.000 | 0.000 | 0.000 | 0.000 |
| 2 | 1 | 0.000 | 0.820 | 6.000 | 520.000 | 650.000 | 200000.000 | 10.000 | 150.000 | 0.000 | 0.000 | 0.000 |
| 2 | 1 | 0.000 | 0.336 | 6.000 | 420.000 | 650.000 | 200000.000 | 10.000 | 150.000 | 0.000 | 0.000 | 0.000 |
| 2 | 1 | 90.000 | 3.312 | 8.000 | 470.000 | 650.000 | 200000.000 | 10.000 | 150.000 | 0.000 | 0.000 | 0.000 |
| 2 | 1 | 361.000 | 0.900 | 6.000 | 420.000 | 650.000 | 200000.000 | 10.000 | 150.000 | 0.000 | 0.000 | 0.000 |
| 3 | 1 | 0.000 | 2.500 | 6.000 | 420.000 | 650.000 | 200000.000 | 10.000 | 150.000 | 0.000 | 0.000 | 0.000 |
| 3 | 1 | 90.000 | 2.500 | 6.000 | 420.000 | 650.000 | 200000.000 | 10.000 | 150.000 | 0.000 | 0.000 | 0.000 |
| 3 | 1 | 361.000 | 2.500 | 6.000 | 420.000 | 650.000 | 200000.000 | 10.000 | 150.000 | 0.000 | 0.000 | 0.000 |

(B) STEEL

<NOTE:> TO BE USED FOR TRUSS ELEMENTS ONLY

| MAT TYP | REF TYP | AREA mm2 | Db mm | Fy MPa | Fu MPa | Es MPa | esh me | eu me | Cs /C | Dep me | b/t |
|---------|---------|----------|-------|--------|--------|--------|--------|-------|-------|--------|-----|
|---------|---------|----------|-------|--------|--------|--------|--------|-------|-------|--------|-----|

(C) BOND

<NOTE:> TO BE USED FOR EXTERIOR/INTERIOR BONDED ELEMENTS

```

MAT REF { Ao U1 U2 U3 S1 S2 S3 }/{ CPF Cmin No. HOOK }
TYP TYP mm^2 MPa MPa MPa mm mm mm 0-1 mm LYR 0/1
/

ELEMENT INCIDENCES
*****

(A) RECTANGULAR ELEMENTS
-----
<<<<< FORMAT >>>>>
ELMT INC1 INC2 INC3 INC4 [#ELMT d(ELMT) d(INC)] [#ELMT d(ELMT) d(INC)]/
1 9 10 33 32 1 1 1 1 1 1 /
2 11 12 35 34 1 1 1 1 1 1 /
3 10 11 34 33 1 1 1 1 1 1 /
4 35 12 13 36 1 1 1 1 1 1 /
/

(B) QUADRILATERAL ELEMENTS
-----
<<<<< FORMAT >>>>>
ELMT INC1 INC2 INC3 INC4 [#ELMT d(ELMT) d(INC)] [#ELMT d(ELMT) d(INC)]/
/

(C) TRIANGULAR ELEMENTS
-----
<<<<< FORMAT >>>>>
ELMT INC1 INC2 INC3 [ #ELMT d(ELMT) d(INC) ] [ #ELMT d(ELMT) d(INC) ] /
/

(D) TRUSS ELEMENTS
-----
<<<<< FORMAT >>>>>
ELMT INC1 INC2 [ #ELMT d(ELMT) d(INC) ] [#ELMT d(ELMT) d(INC) ]/
/

(E) LINKAGE ELEMENTS
-----
<<<<< FORMAT >>>>>
ELMT INC1 INC2 [ #ELMT d(ELMT) d(INC) ] [ #ELMT d(ELMT) d(INC) ]
/

(F) CONTACT ELEMENTS
-----
<<<<< FORMAT >>>>>
ELMT INC1 INC2 INC3 INC4 [ #ELMT d(ELMT) d(INC) ] [ #ELMT d(ELMT) d(INC) ]
/

MATERIAL TYPE ASSIGNMENT
*****

<<<<< FORMAT >>>>>
ELMT MAT ACT [ #ELMT d(ELMT) ] [ #ELMT d(ELMT) ] /
1 3 1 1 1 1 1 /
2 3 1 1 1 1 1 /
3 3 1 1 1 1 1 /
/

COORDINATES
*****

<NOTE:> UNITS: in OR mm
<<<<< FORMAT >>>>>
NODE X Y [ #NODES d(NODES) d(X) d(Y) ] [ #NODES d(NODES) d(X) d(Y) ] /
1 -200.000 0.000 1 1 0.000 0.000 1 1 0.000 0.000 /
2 -150.000 0.000 1 1 0.000 0.000 1 1 0.000 0.000 /
3 -100.000 0.000 1 1 0.000 0.000 1 1 0.000 0.000 /
4 -50.000 0.000 1 1 0.000 0.000 1 1 0.000 0.000 /
/

SUPPORT RESTRAINTS
*****

<NOTE:> CODE: '0' FOR NOT RESTRAINED NODES AND '1' FOR RESTRAINED ONES
<<<<< FORMAT >>>>>
NODE X-RST Y-RST [ #NODE d(NODE) ] /
1 1 1 1 1 /
2 1 1 1 1 /
3 1 1 1 1 /
4 1 1 1 1 /

<<< STRUCTURE FILE NOTES >>>

```

SW22VL.L2R

```

* * * * *
*   V e c T o r 2   *
*   L O A D   D A T A   *
* * * * *

```

```

LOAD CASE PARAMETERS
*****

```

```

Structure Title      (30 char. max.)   : Shear Wall SW22
Load Case Title     (30 char. max.)   : Axial Ld (100 kN)
Load Case File Name (8 char. max.)    : SW22VL
No. of Loaded Joints      : 13
No. of Prescribed Support Displacements : 0
No. of Elements with Gravity Loads     : 0
No. of Elements with Temperature Loads : 0
No. of Elements with Concrete Prestrain : 0
No. of Elements with Ingress Pressure  : 0
No. of Nodes with Thermal Load         : 0
No. of Nodes with Lumped Masses       : 0
No. of Nodes with Impulse Forces      : 0
Ground Acceleration Record (0-1)      : 0

```

```

JOINT LOADS
*****

```

```

<NOTE:> UNITS: KIPS OR KN

```

```

<<<<< FORMAT >>>>>

```

```

NODE   Fx   Fy   [ #NODE d(NODE) d(Fx) d(Fy) ] /
 519  0.000 -7.692 1 1 0.000 0.000/
 520  0.000 -7.692 1 1 0.000 0.000/
 521  0.000 -7.692 1 1 0.000 0.000/
 522  0.000 -7.692 1 1 0.000 0.000/
 523  0.000 -7.692 1 1 0.000 0.000/
 524  0.000 -7.692 1 1 0.000 0.000/
 525  0.000 -7.692 1 1 0.000 0.000/
 526  0.000 -7.692 1 1 0.000 0.000/
 527  0.000 -7.692 1 1 0.000 0.000/
 528  0.000 -7.692 1 1 0.000 0.000/
 529  0.000 -7.692 1 1 0.000 0.000/
 530  0.000 -7.692 1 1 0.000 0.000/
 531  0.000 -7.692 1 1 0.000 0.000/
/

```

```

SUPPORT DISPLACEMENTS
*****

```

```

<NOTE:> UNITS: MM OR IN

```

```

<<<<< FORMAT >>>>>

```

```

JNT DOF DISPL [ #JNT d(JNT) ] /
/

```

```

GRAVITY LOADS
*****

```

```

<NOTE:> UNITS: KG/M3

```

```

<<<<< FORMAT >>>>>

```

```

ELMT DENS GX GY [ #ELMT d(ELMT) ] [ #ELMT d(ELMT) ] /
/

```

```

ELEMENT TEMPERATURE
*****

```

```

<NOTE:> UNITS: F OR C

```

```

<<<<< FORMAT >>>>>

```

```

ELMT TEMP [ #ELMT d(ELMT) d(TEMP) ] [ #ELMT d(ELMT) d(TEMP) ] /
/

```

```

CONCRETE PRESTRAINS
*****

```

```

<NOTE:> UNITS: me

```

```

<<<<< FORMAT >>>>>

```

```

ELMT STRAIN [ #ELMT d(ELMT) d(STRAIN) ] [ #ELMT d(ELMT) d(STRAIN) ] /
/

```

```

INGRESS PRESSURES
*****

```

```

<NOTE:> UNITS: MPa

```

```

<<<<< FORMAT >>>>>

```

```

ELMT PRESSURE [ #ELMT d(ELMT) d(PRS) ] [ #ELMT d(ELMT) d(PRS) ] /
/

```

```

NODAL THERMAL LOADS
*****

```

```

<NOTE:>
<<<<< FORMAT >>>>>
NODE   TYPE   Tm1   Tp1   Tm2   Tp2   Tm3   Tp3   [ #NODE d(NODE) ] [ #NODE d(NODE) ] /
/
                                LUMPED MASSES
                                *****

<NOTE:> UNITS: kg, m/s
<<<<< FORMAT >>>>>
NODE   DOF-X  DOF-Y  MASS  GF-X  GF-Y  Vo-X  Vo-Y  [ #NODE d(NODE) ] /
/
                                IMPULSE FORCES
                                *****

<NOTE:> UNITS: Sec, kN
<<<<< FORMAT >>>>>
NODE   DOF  T1   F1   T2   F2   T3   F3   T4   F4  [ #NODE d(NODE) ] /
/
                                GROUND ACCELERATION
                                *****

<NOTE:> UNITS: Sec, G
<<<<< FORMAT >>>>>
TIME   ACC-X  ACC-Y
/

<<< LOAD FILE NOTES >>>

```

SW22DL.L2R

```

* * * * *
*   V e c T o r 2   *
*   L O A D   D A T A   *
* * * * *

```

```

LOAD CASE PARAMETERS
*****

```

```

Structure Title      (30 char. max.)   : Shear Wall SW22
Load Case Title     (30 char. max.)   : Horiz Disp (1 mm)
Load Case File Name (8 char. max.)    : SW22DL
No. of Loaded Joints      : 0
No. of Prescribed Support Displacements : 1
No. of Elements with Gravity Loads     : 0
No. of Elements with Temperature Loads : 0
No. of Elements with Concrete Prestrain : 0
No. of Elements with Ingress Pressure  : 0
No. of Nodes with Thermal Load         : 0
No. of Nodes with Lumped Masses       : 0
No. of Nodes with Impulse Forces      : 0
Ground Acceleration Record (0-1)      : 0

```

```

JOINT LOADS
*****

```

```

<NOTE:> UNITS: KIPS OR KN
<<<<< FORMAT >>>>>
NODE   Fx   Fy   [ #NODE d(NODE) d(Fx) d(Fy) ] /
/

```

```

SUPPORT DISPLACEMENTS
*****

```

```

<NOTE:> UNITS: MM OR IN
<<<<< FORMAT >>>>>
JNT   DOF   DISPL [ #JNT d(JNT) ] /
      525   1   1.000 1 1/
/

```

```

GRAVITY LOADS
*****

```

```

<NOTE:> UNITS: KG/M3
<<<<< FORMAT >>>>>
ELMT  DENS  GX  GY  [ #ELMT d(ELMT) ] [ #ELMT d(ELMT) ] /
/

```

```

ELEMENT TEMPERATURE
*****

```

```

<NOTE:> UNITS: F OR C
<<<<< FORMAT >>>>>
ELMT  TEMP  [ #ELMT d(ELMT) d(TEMP) ] [ #ELMT d(ELMT) d(TEMP) ] /
/

```

```

CONCRETE PRESTRAINS
*****

```

```

<NOTE:> UNITS: me
<<<<< FORMAT >>>>>
ELMT  STRAIN [ #ELMT d(ELMT) d(STRAIN) ] [ #ELMT d(ELMT) d(STRAIN) ] /
/

```

```

INGRESS PRESSURES
*****

```

```

<NOTE:> UNITS: MPa
<<<<< FORMAT >>>>>
ELMT  PRESSURE [ #ELMT d(ELMT) d(PRS) ] [ #ELMT d(ELMT) d(PRS) ] /
/

```

```

NODAL THERMAL LOADS
*****

```

```

<NOTE:>
<<<<< FORMAT >>>>>
NODE   TYPE   Tm1  Tp1  Tm2  Tp2  Tm3  Tp3  [ #NODE d(NODE) ] [ #NODE d(NODE) ] /
/

```

```

LUMPED MASSES
*****

```

```

<NOTE:> UNITS: kg, m/s
<<<<< FORMAT >>>>>
NODE  DOF-X  DOF-Y  MASS  GF-X  GF-Y  Vo-X  Vo-Y  [ #NODE d(NODE) ] /
/

```

```

IMPULSE FORCES

```

```
*****
<NOTE:> UNITS: Sec, kN
<<<<< FORMAT >>>>>
NODE DOF T1 F1 T2 F2 T3 F3 T4 F4 [ #NODE d(NODE) ] /
/
GROUND ACCELERATION
*****
<NOTE:> UNITS: Sec, G
<<<<< FORMAT >>>>>
TIME ACC-X ACC-Y
/

<<< LOAD FILE NOTES >>>
```